

**THE FEASIBILITY OF USING A VEGETABLE  
OIL-BASED FLUID AS ELECTRICAL INSULATING OIL**

**Thesis submitted for the degree of  
Doctor of Philosophy  
at the University of Leicester**

**by**

**Abdelghaffar Amoka Abdelmalik  
Department of Engineering  
University of Leicester**

**2012**

# THE FEASIBILITY OF USING A VEGETABLE OIL-BASED FLUID AS ELECTRICAL INSULATING OIL

by  
Abdelghaffar Amoka Abdelmalik

## Abstract

Esters of palm kernel oil have been synthesized and characterized for application as electrical insulating oil. Since such fluids serve both as insulants and coolants, tests were performed to characterize the chemical, physical and dielectric properties. Accelerated ageing tests were carried out to mimic conditions in a power transformer.

Alkyl esters were synthesized from laboratory purified palm kernel oil: methyl ester was prepared through a transesterification reaction; an epoxidation reaction involving the methyl ester produced with insitu per-acetic acid in the presence of a catalyst to produce corresponding epoxy alkyl ester. This was then reacted with acid anhydrides under nitrogen in the presence of catalyst. This opened the epoxy rings of the epoxy alkyl oleate and linoleate components to attach side hydrocarbon chains. The characteristics and composition of the products were monitored using GC-MS and FTIR spectroscopy. The synthesized ester possessed a flash point that satisfied the specified minimum flash point for mineral oil, higher thermo-oxidative stability, and high and reliable breakdown strength from the distribution of breakdown data (43 kV/mm). It has a melting point of about  $-7^{\circ}\text{C}$  which is higher than mineral oil.

An ester-paper sample which was aged in a pressure vessel under nitrogen and metal catalysts exhibited improved performance compared with the mineral oil-paper system. The rate of decrease in the tensile strength of alkyl ester-paper within the ageing condition was significantly lower than mineral oil-paper. Impregnation of cellulose paper with ester increased the charge storage capacity of the insulating paper. A strong low frequency dielectric dispersion (LFD) was observed which became more pronounced with ageing. Quasi-DC conduction was deduced to have dominated the low frequency response of alkyl ester-paper. The characteristic breakdown strength of the aged paper samples in comparison with the unaged sample did not show any significant difference.

It is suggested that the synthesized ester is as good as mineral oil in many ways and a viable alternative fluid for cooling and insulating power transformers.

## **Acknowledgements**

I wish to express my sincere appreciation to my supervisors; Prof John Fothergill and Dr Stephen Dodd for giving me the opportunity to work under their supervision and guidance. They have being source of inspiration to me. I couldn't have gotten to this point without their excellent guidance, encouragement, sincere criticism, and the valuable suggestions. They have greatly influenced my academic and personal life.

Andy Willby have being of great help to me. I appreciate his prompt response to my queries. To my colleagues; Nikola Chalashkanov and Tong Liu, thanks for those fruitful discussions, they were very helpful. I wish to express my appreciation to Prof Len Dissado for his attention and suggestions. I am grateful to Julie Hage, Paul Williams and the staff in the mechanical work for their assistance. To Prof Andy Abbott, Rob Harris, and the research workers in Scionix Laboratory, Chemistry Department; thanks for having me in the laboratory. I appreciate your assistance during my sample synthesis in that lab. I wish to acknowledge Late Prof N. Hariharan who introduced me into the field of dielectrics. He was a source of inspiration.

Coming here for this project would not have been possible without the Merit Scholarship Award from Islamic Development Bank. My sincere appreciation to the organization for finding the work worthy of the grant. The National Grid UK support for the project is acknowledged. I also want to acknowledge IEEE Dielectrics and Electrical Insulation Society (DEIS) for the 2010 DEIS Graduate Fellowship Award.

I wish to express my appreciation to my family and friends for their untiring support all through the study period.

And finally, my gratitude goes to Allah for seeing me through the course of this work. I could not have achieved this without His infinite mercy and grace.

## Table of Contents

Abstract.....	ii
Acknowledgements.....	iii
Chapter 1. Introduction.....	1
1.1 Research Background.....	1
1.2 Palm Kernel Oil.....	7
1.3 Objectives.....	9
1.4 Organization of the Thesis .....	10
Chapter 2. Background Theory .....	12
2.1 Thermo-Chemical Properties of Liquid .....	12
2.2 Electrical Response of Materials.....	15
2.2.1 Charge Transport .....	15
2.2.2 Low Frequency Dispersion (LFD).....	19
2.2.3 Dielectric Polarization .....	20
2.3 Dielectric Breakdown Theory .....	24
2.4 Summary .....	27
Chapter 3. Materials .....	28
3.1 Introduction .....	28
3.2 Background .....	28
3.3 Oil Purification.....	32
3.3.1 Review of Purification Method.....	32
3.3.2 Purification Process .....	32
3.4 Initial Chemical Modification Trials.....	33
3.5 Palm Kernel Oil Ester Synthesis .....	34
3.5.1 Palm Kernel Oil Alkyl Ester.....	34
3.5.2 Epoxy Alkyl Ester of Palm Kernel oil .....	35
3.5.3 Palm Kernel Oil Side Branched Alkyl Ester .....	36
3.6 Electrical Insulation Paper .....	38
3.7 Summary .....	39
Chapter 4. Experimental Methods.....	40
4.1 Introduction .....	40
4.2 Structural Identification .....	40
4.2.1 Gas Chromatography-Mass Spectrometry (GC-MS) .....	40
4.2.2 Fourier Transform Infrared (FT-IR) Spectrometry.....	41
4.3 Thermo-Physical Characterization.....	41
4.3.1 Viscosity and Density .....	41
4.3.2 Differential Scanning Calorimetry (DSC) .....	44

4.3.3	Pour Point Temperature .....	44
4.3.4	Flash Point .....	45
4.3.5	Acidity .....	45
4.3.6	Water Content .....	45
4.4	Dielectric Response.....	45
4.4.1	Dielectric Response Measurement Technique.....	46
4.4.2	Dielectric Liquid Test Cell .....	47
4.4.3	Dielectric Measurement Set-up .....	50
4.4.4	DC Conductivity Measurement Set-up.....	51
4.5	Dielectric Breakdown.....	52
4.5.1	Breakdown Test Cell .....	52
4.5.2	Experimental Setup.....	53
4.6	Laboratory Ageing System .....	54
4.6.1	Ageing Vessel .....	56
4.6.2	Experimental Setup.....	57
4.7	Tensile Strength Measurement.....	59
4.8	Summary .....	60
Chapter 5.	Results and Analysis of PKO and Synthesized Esters.....	61
5.1	Introduction .....	61
5.2	Spectrometry Identification of Ester Molecules .....	61
5.3	Gas Chromatography-Mass Spectrometry (GC-MS) of the Esters.....	61
5.3.1	Fourier Transform Infrared (FT-IR) Spectrometry of the Esters.....	66
5.4	Thermo-Physical Properties of Ester Fluids .....	70
5.4.1	Dynamic Viscosity.....	70
5.4.2	Low Temperature Thermal Analysis .....	74
5.4.3	High Temperature Thermal Analysis .....	76
5.4.4	Effect of Additive on Thermo-Oxidative Stability.....	80
5.5	Moisture and Acidity.....	83
5.6	Dielectric Response of PKO Ester Fluids .....	84
5.6.1	DC Conductivity .....	84
5.6.2	Frequency Response Analysis .....	85
5.6.3	Arrhenius Behaviour of Frequency Response .....	93
5.7	Dielectric Breakdown Characteristics of Ester Fluids .....	96
5.8	Summary .....	101
Chapter 6.	Effect of Ageing on the Alkyl Ester-Paper System .....	103
6.1	Physical Appearance of the Aged Oil Samples.....	104
6.2	Identification of the Aged Ester Molecules .....	105

6.3	Thermo-Chemical Properties of Aged Ester Fluids .....	107
6.4	Dielectric Response of Aged PKO Ester Fluid .....	109
6.5	Dielectric Breakdown Characteristics .....	111
6.6	Characteristics of Ester Impregnated Paper .....	114
6.6.1	Tensile Strength .....	115
6.6.2	Dielectric Response of Aged Oil-Impregnated Paper.....	117
6.6.3	Breakdown Field Strength .....	124
6.7	Summary .....	126
Chapter 7.	Discussion .....	127
7.1	Alkyl Ester Fluid .....	127
7.1.1	Thermo-physical Behaviour of Alkyl Esters .....	127
7.1.2	Dielectric Response of Palm kernel Oil and Alkyl Esters .....	130
7.1.3	Ester Breakdown Strength .....	138
7.1.4	Dielectric Response of Ester-Paper System.....	139
Chapter 8.	Conclusions and Further Research Work .....	145
8.1	Summary of Major Findings .....	145
8.2	Contributions and Limitations.....	148
8.2.1	Contributions .....	148
8.2.2	Limitations .....	148
8.3	Areas for Further Research Work .....	149
Appendix A	Properties of Typical Insulating Fluids .....	152
Appendix B	Design Drawing of Dielectric Test Cell.....	153
Appendix C	Design Drawing of Ageing Vessel.....	154
Appendix D	Pressure Vessel Calculation .....	155
Appendix E	Appendix A: Mass Spectra of Oil Samples.....	158
Appendix F	FTIR Spectra of Oil Sample.....	164
Appendix G	Dielectric Spectra of Paper Samples .....	168
Appendix H	Equivalent Circuit fit for Ester-Paper .....	170
Appendix I	Publications.....	172
References.....		173

## **Chapter 1. Introduction**

Firstly, this chapter gives a description of the research background; throwing light on the historical background of insulating fluids and the efforts put into research and development for viable alternative transformer oils. This section of the chapter also gives an overview of the commercially available natural ester insulating fluids. Secondly, brief information on the availability of palm kernel oil and the chemical composition is given. Thirdly, the objective and justification for this study is discussed and finally, the structure and organisation of the thesis is presented in Section 1.4.

### **1.1 Research Background**

Electrical insulation materials, whether solid, liquid or gas, play an important role in electrical distribution networks [Berberich, 1954]. Liquids provide electrical insulation and cooling in power transformers. Adequate knowledge of the dielectric behaviour of these insulating materials when in service in an electrical network could enhance network reliability and minimize the probability of failure. This makes the field of electrical insulation and dielectrics important in the electrical generation, transmission and distribution industries. The materials used for insulation in liquid-filled transformers are mineral oil, pressboard and cellulose papers. Electrical insulating liquids are used either alone or as impregnates in cellulose papers to insulate electrical conductors in a network from each other or from ground. Generally, mineral oil that has been purified to transformer oil grade, for example Nynas 10GBN, is the commonly used transformer fluid. Its popularity is not just because of its excellent insulating and heat dissipation properties, but also because of its availability, and its resistance to electrical and thermal ageing.

The main requirements of oil in transformers are to increase the dielectric strength between conductors by replacing air with a high dielectric strength fluid, and filling the pores of the cellulose paper and pressboard, to prevent discharges. The oil should also have adequate thermal and viscosity properties to be able to dissipate, by convection, heat generated due to losses in the transformer and it must flow freely under all operating temperatures. According to Berberich, (1954) and later on Heathcote, (2007), a good insulating fluid should:

- have high breakdown strength to withstand the applied stresses while in service,
- have low viscosity so that its heat dissipation function is maintained at all time,
- have adequate low temperature properties under severe climatic conditions such as weather temperature of about  $-10^{\circ}\text{C}$  expected at the installation site during winter,
- have adequate high temperature properties to survive total losses at rated current which can raise the temperature of the oil-filled electric equipment up to  $85^{\circ}\text{C}$ ,
- have excellent chemical stability to ensure long time service performance as oil-filled electric equipment such as power transformers should be able to survive for at least 40 years without explosion,
- be free from materials that could cause corrosion of metal parts and insulation or that could accelerate the production of sludge,
- have low water content; 25 mg/kg for mineral oil and 200 mg/kg for ester fluid, as sufficient water in transformer oil can lead to hydrolytic degradation of insulation paper. It can also initiate electrical breakdown of the equipment.

Mineral-based insulation oil has performed well over the years. However, in a situation where there is accidental leakage in a transformer, the oil could constitute an environmental hazard because it is toxic and non-biodegradable. This has shifted attention towards new insulating materials that are biodegradable and sustainable, and hence mitigate environmental issues. Such new fluids should be suitable for retro-filling of existing transformers as well as being suitable for new designs.

Towards this end, attempts have been made in the past for the development of alternative transformer oils. *Askarel*, a generic name for a number of synthetic halogenated hydrocarbon dielectric fluids was developed for use in transformers where fireproof liquids are required [Berberich, 1954]. They were used between 1930 and the mid seventies. This is a mixture of polychlorinated biphenyls (PCBs) and trichlorobenzene, typically containing 40-50% trichlorobenzene. This is more stable to oxidation than petroleum oil and it is not prone to form an acid or sludge under normal transformer operating conditions. Neither do they emit flammable or explosive gases under arcing conditions. It was later found that in case of fire, incomplete combustion of PCBs can form dioxins after undergoing chemical modification. Dioxin is said to be more toxic to human than the PCBs themselves [Fofana *et al*, 2001]. To reduce the

toxicity of insulating fluids on environment, silicone oil was later developed and was quite useful in utility network and rectifier transformers. Subsequent tests have shown that silicone oil is essentially non-biodegradable [McShane, 2002]. It was reported that quick degradation of silicone oil in the environment is possible only under certain conditions such as oven-dried soils, a condition that is unlikely to be obtained in the real world. In a quest for high performance transformer fluids, High Molecular Weight Hydrocarbon (*HMWH*) fluids, a class of less-flammable fluids than mineral oil, were developed and were widely used particularly in electrical unit substations, pad-mounted transformers, and oil retro-fills. They achieved a very good operating performance due to their stability even at high-temperature operation, and their superior resistance to fast front impulse electrical breakdown. HMWH fluids were used in high-temperature transformers (HTTs) due to their proven compatibility with aramid insulation materials; such transformers are used in mobile substations. HMWH oils are mineral-based just like conventional mineral transformer oils, and as a result, are not free from the negative environmental impact of mineral oil [McShane, 2002]. Perchloroethylene ( $C_2Cl_4$ ) also known as *Perc*, was proposed for cleaning and refilling PCB-filled transformers. It possesses excellent dielectric and thermal properties; but it is toxic. An accidental spill in a transformer substation with *Perc* could lead to serious health problems or even death for exposed workers [Fofana *et al*, 2001].

Synthetic ester dielectric fluids of polyolesters, with suitable dielectric properties and significantly more biodegradability than mineral oil were developed as alternative insulating fluids [Heathcote, 2007]. Their advent and usage greatly decreased the rate of failure of traction transformers after the *askarels* were replaced [McShane, 2002]. *Midel 7131* was developed in 1978 as a substitute to replace the fire-resistant but toxic *askarels*. It has a high fire point and can sustain conductor temperatures well above those acceptable for Kraft paper [Wasserberg *et al*, 2005]. The report on the comparative study of the insulating properties of transformer oil and *Midel 7131* shows that the electrical breakdown characteristics of conventional transformer oil and *Midel* are similar for short gaps between sphere electrodes. Although *Midel* displayed an inferior impulse breakdown property in more sharply diverging fields for longer gap lengths, the report indicated that *Midel* could replace transformer oil for impregnating Kraft paper or Nomex without problems [Binns, 1982]. A newly developed synthetic ester liquid with commercial name *Proeco TR20* was reported to be suitable for use in

every kind of transformer. According to the report, it demonstrates good electric and dielectric properties in new and aged conditions. It has high thermal and ageing stability and its low viscosity allows efficient cooling, and accelerates the impregnation of a new transformer [Wasserberg *et al*, 2005]. Moeny of Tetra Corporation, U.S.A. [Moeny, 2005], reported the development of new high dielectric constant insulating oil, *Tetra High Energy Storage Oil* (THESO), for pulsed power applications with an unusual property in its ability to absorb water without apparent effect on the dielectric properties of the oil, but no information was found concerning the constitution of the oil. However, there is only limited use of these synthetic ester fluids due to their high cost.

Insulating liquids of mostly synthetic origin could still not serve as a replacement for insulating mineral oils either because they have some inferior characteristics or their prices are on the high side. The need to develop insulating oil that is affordable, with an appropriate degree of biodegradability, essentially non-toxic and derived from renewable sources is very important for ecological sustainability. In a quest for an economically viable and renewable raw material for alternative transformer fluid, natural plant-based oils appear to be the class of material with the potential of serving as a dielectric fluid. They may also satisfy affordable cost, health and ecological considerations. Several research papers have reported the tremendous progress made in the search for less flammable and non-toxic ecological insulating. However, the basic challenge in using a natural ester as a dielectric fluid is in synthesizing a fluid with low pour point and high thermo-oxidative stability.

There have been several reports on the potential of using vegetable oil as an alternative to transformer oil. The properties of coconut oil were investigated in Sri Lanka for its suitability as a dielectric fluid in transformers. Abeyesundara *et al* [Abeyesundara *et al*, 2001] in Malaysia used purified coconut oil as an insulant/coolant in an experimental 5 kVA transformer. They reported that the oil possessed the necessary electrical properties to serve as insulating fluid and was environmentally friendly. The pour point of the oil was quite high, 20°C. An effort to reduce the pour point was not successful, though they reported that solidification does not appear to have an adverse effect on the dielectric strength as the oil solidified without forming voids which could trigger partial discharge (P.D.).

A study on the suitability of refined, bleached and deodorized (RBD) palm oil for insulation in transformers indicated that it possessed physical and electrical breakdown properties that made it a potential alternative dielectric fluid, but further investigations on ageing and long-term performance needed to be performed [Thomas *et al*, 1995; Suwarmo *et al*, 2003; Abdullah *et al*, 2004]. However, the low temperature behaviour of the oil was not investigated. Studies on the dielectric properties of fatty acid methyl ester of palm oil called *PFAE* (Palm Fatty Acid Ester) by a Japanese research group was reported to have excellent properties that is comparable to mineral oil [Kanoh *et al*, 2008; Saito *et al*, 2011; Suzuki *et al*, 2011].

Research groups such as Bertrand *et al*, Duy *et al*, Jian *et al* [Bertrand *et al*, 2003; Duy *et al*, 2007; Jian *et al*, 2007] have studied the behaviour of purified rapeseed oil as an alternative insulating fluid. The report of Bertrand *et al*'s [Bertrand *et al*, 2003] investigation on castor oil, sunflower oil, rapeseed oil and esters prepared from the refined oils with different alcohol content showed that the matrix based on refined rapeseed oil and its ester derivative is the most promising choice and that it will be most suitable for hermetically sealed transformers because of its oxidative stability. Streamer propagation in rapeseed oil was studied by Duy *et al* [Duy *et al*, 2007] using a point-plane electrode system to produce highly divergent electric fields. From the results, it appears that the properties of streamers in rapeseed oil are less favourable for high voltage insulation than mineral oil. In a study of purified rapeseed oil-paper insulation in comparison with mineral oil by Jian *et al* [Jian *et al*, 2007], the paper samples were dried for 24 hours and vacuum impregnation of the paper took place in an oil tank with 200 Pa of pressure for 48 hours. According to the report, there appear no obvious differences between the dissipation factors of the two systems up till 100°C. Beyond 100°C, the dissipation factor of mineral oil system became greater. The breakdown voltage of the rapeseed oil-paper system was greater than the mineral oil-paper system for the same electrode gap. Also, the breakdown voltage of an arrangement of oil-paper and oil-gap showed that the rapeseed oil-paper-oil-gap had greater breakdown strength than the mineral oil-paper-oil-gap in the same model insulation structure. They concluded that the greater breakdown strength of rapeseed oil-paper oil-gap system makes the rapeseed oil-paper insulation system better than mineral oil-paper system.

A report on the analysis of the electro-chemical and physical characteristics of a group of vegetable oils by Amanullah *et al* suggests that proper research to improve the non-favourable properties of some oils by using appropriate processing techniques and blending additives would lead to a highly biodegradable and environmental friendly vegetable-based dielectric fluid that could be used in power and distribution transformers [Amanullah et al, 2005].

Oommen *et al* of ABB Inc, U.S.A. [Oommen *et al*, 2000], introduced a newly developed environmentally friendly bio-based dielectric fluid called *BIOTEMP* fluid. It was the first commercial bio-based dielectric product to be available [Oommen, 2002]. The fluid was high oleic oil-based and was reported to have excellent dielectric characteristics with high temperature stability and superior flash and fire resistance, excellent compatibility with solid insulating materials and short time biodegradability. Long time ageing of this fluid shows that the life of the paper insulation was considerably prolonged than mineral oil when used in transformers.

Waverly Light and Power (WLP) conceived the idea of developing soybean-based transformer oil in the early 1990s. WLP's research on this project included laboratory tests carried out with the University of Northern Iowa's Ag-Based Industrial Lubricants (ABIL) Research facility which was later renamed National Ag-Based Lubricant Center (NABL). The soybean-based insulating fluid produced was used to retrofill transformer units in 1997. Later, Cargill, Inc. after purchasing the patents and trademark rights, began manufacturing of *BioTrans* transformers based on the Soybean-based transformer oil in conjunction with Electric Research and Manufacturing Cooperative, Inc. (ERMCO), United States of America [Waverly Light and Power, 2011]. Cooper Power Systems (CPS), a division of Houston (U.S.A)-based Cooper Industries, also began the development of vegetable based transformer oil in the early 1990s. An optimum balance was selected from food-grade-based oil and blended with various percentages of free fatty acid. The oxidative stability and pour point temperature of the oil was improved with anti-oxidants and pour point depressants respectively. The formulated food-grade materials possessed excellent key characteristics. The natural ester fluid had the highest fire resistance. It had a superior dielectric breakdown compared to mineral oil, both in new condition and after multiple-load break-switching operations compared to mineral oil. It had a viscosity close to either silicone or HMWH fluids at operating temperatures.

However, the pour point temperature is relatively high ( $-21^{\circ}\text{C}$ ) compared to mineral oil, although not higher than the HMWH, whose performance was excellent in transformers installed in cold and hot climates [McShane *et al*, 2001]. In 2004 Cargill and CPS formed an alliance to produce, market, and distribute *Envirotemp FR3* fluid [Waverly Light and Power, 2011]. *FR3* is the most popular commercially available natural ester insulating fluid.

Although the existing bio-based transformer fluid has excellent key properties, the high viscosity (33 - 45 cSt at  $40^{\circ}\text{C}$ ) of the existing ester fluid is a drawback. The use of the fluid in EHV power transformers may require design changes related to heat transfer properties, and modifications to the pumping system due to the fluid being of higher viscosity than conventional transformer oil (9.2 cSt at  $40^{\circ}\text{C}$ ) [Oommen, 2002; Tenbohlen *et al*, 2008]. The commercially available bio-based transformer fluids are also designed specifically for sealed transformers where air contact of the fluid is necessarily restricted because of the instability of the dominant carbon-carbon double bonds present in the fatty acids structure to oxidation [Stockton *et al*, 2009]. This limited their use in existing power transformers which are mostly of a free-breathing system type. Free-breathing system is a system, for example transformer, with vents above the oil that allow air to enter and exit as the oil expands and contracts in response to variations in the operating temperature.

In summary, the above bio-based insulating fluids have significant limitations preventing them from being used as a direct replacement for mineral oil. These include high viscosity and poor thermo-oxidative stability, making further research on new alternative, like palm kernel oil, justifiable. If a bio-based alternative insulating fluid is desired for use in free breathing transformers, then research into a cost effective, sustainable and all purpose ester-based insulating fluid is still open.

## **1.2 Palm Kernel Oil**

Palm kernel oil (PKO) is one of the processed products of oil palm. The world production of palm kernel oil was estimated to be over 3.84 million tonnes [Gunstone, 2005] in 2004/05 with Nigeria, accounting for 0.21 million tonnes, being the third largest producer after Malaysia and Indonesia. The world production of this oil has increased to 5.39 million tonnes in 2009/10. This increase was linked to an increase in

the area under oil palm cultivation [Gunstone, 2011]. According to the World Bank and IMF commodity price data [The World Bank, 2011; International Monetary Fund, 2011], the average price of palm kernel oil between July and December 2011 as shown in *Table 1.1* is comparable to the vegetable oils used for the existing natural ester dielectric fluids. However, the price of vegetable oils is about 70% higher than crude oil (petroleum). With the continuous increase in the demand for petroleum products, the prices may become comparable. The production of palm kernel oil in Nigeria is from oil palm that grows naturally in a tract of wild grooves in West Africa estimated to be 2.3 million hectares and from a species cultivated in plantations and small holdings estimated to be 214,090 hectares. This brings the total hectareage of oil palm in Nigeria to above 2.5 million hectares. There are indications that the production capacity in Nigeria could be improved if the available resources are fully utilized and more industrial applications of the oil are developed [RMRDC, 2004].

**Table 1.1: Average Price of a Range of Oils between July and December 2011**

<b>Oil</b>	<b>Palm kernel Oil</b>	<b>Sunflower Oil</b>	<b>Soybean Oil</b>	<b>Rapeseed Oil</b>	<b>Crude Petroleum</b>
<b>Price/tonne (GBP)</b>	813.28	1,012.73	736.52	822.53	474.34 (64.7/b)

Palm kernel oil is known to have a high percentage of saturated fatty acids. The limited concentration of C-C double bonds within its chemical structure whose site is prone to thermo-oxidation makes it more resistant to oxidation and classified as chemically stable vegetable oil. This makes it a good choice for consideration as a dielectric in oil-filled electric equipment (OFEE) where oxidation stability is a key factor. It has 83% saturated acids, the major fatty acid being lauric acid. Among this saturated fatty acids, are the low molecular weights fatty acids; caprylic and capric acid. It has 15% mono-unsaturated acids (oleic) and 2% poly-unsaturated acids (linoleic) [Gunstone, 2005]. A problem with palm kernel oil is its high freezing point (26°C) resulting from the high percentage of straight long-chain carboxylic acid. The fatty acid chains have a “tuning fork” conformation which undergoes molecular stacking during the cooling process [Gunstone *et al*, 2007]. Chemical modification and blend additives may improve this low temperature performance of palm kernel oil [Erhan *et al*, 2002].

### 1.3 Objectives

The research carried out in this thesis is to test the hypothesis that “A natural ester-based dielectric fluid can be developed by synthesis and chemical modification of esters of PKO”. The structural modification is envisioned to add value to the desirable properties which may make it suitable as alternative insulating oil in oil-filled electric equipment such as electric transformers. The fluid may be useful as insulating oil in free breathing power transformers due to its envisaged high oxidative stability of this class of natural ester fluid.

To achieve this;

- Alkyl esters of palm kernel oil were synthesized by chemical modification of the crude oil focussing on utilization of the reactive C=C bond. The chemical modification was to achieve improved thermo-chemical properties that are comparable to characteristics of Nynas 10GBN as tabulated in Appendix A .
- The structural, chemical and physical parameters of the synthesized fluids were characterized to identify how the chemical modification affects the viscosity, pour point, flash point and thermo-oxidative stability.
- The dielectric response of the synthesized ester samples and ester impregnated insulating paper samples were investigated under varying temperature conditions as thermally activated processes can influence dielectric loss.
- The charge transport mechanism in the fluid and impregnated paper samples under varying temperature were studied as charge transport can lead to high dielectric loss at power frequency.
- The breakdown strength of the synthesized fluid was studied since a fluid with high breakdown field is required for optimum performance.
- A system was developed for accelerated thermal ageing of the oil-paper combination to understand long time performance of the synthesized fluid since ageing reduced heat transfer, electrical properties and life time of high voltage (HV) plant.
- The behaviour of the aged ester samples was studied by performing viscometric and dielectric characterization over a wide spectrum of temperature to study the thermo-chemical properties of the aged fluid.

- The mechanical, dielectric, breakdown characterization of the aged ester-paper samples was also studied to understand if the composite material can provide the necessary mechanical and insulation support to the conductors with ageing.
- The measured characteristics were related to the chemical properties of the fluids since the properties are inter-related.
- The results of the performed tests were used to assess which of the synthesized ester of palm kernel oil that is most suitable as insulating fluid and hence a replacement for mineral oil.

The overall goal of the research is targeted at utilizing the abundantly available but less utilized Nigerian palm kernel oil as the base oil. Apart from its application in soap making, the success of this research may increase the economic value of this raw material (Palm Kernel Oil).

#### **1.4 Organization of the Thesis**

Chapter 2 reviews the theory of the thermo-chemical properties of dielectric fluids that are important for controlling heat transfer and dissipation. It also describes dielectric loss theory, origin of dielectric relaxation in dielectrics, low frequency dispersion (LFD), and the theory of dielectric breakdown in dielectric materials.

Chapter 3 presents in detail, the procedures used in the purification of the crude palm kernel oil. It also describes the procedures involved in the synthesis of esters to create more complex chemical structures that enhance some of the desired properties of the oil, which include improved pour point, viscosity and thermo-oxidative stability.

Chapter 4 describes the various methodologies and the experimental setup used in the characterization of the synthesized natural ester-based dielectric liquid developed using the procedures described in chapter 3. A detailed description of bespoke test cells and a pressure vessel designed for the ester characterization is also presented in this chapter.

Chapter 5 deals with the results and interpretation of the thermo-chemical and electrical measurements performed on palm kernel oil and its synthesized esters.

Chapter 6 presents the results of ageing on the ester-paper system. The chemical change that occurred in the ester fluid after accelerated ageing was identified. The effect of

ageing on the dynamic viscosity of the oil, dielectric loss of aged oil, and breakdown field of the oil is presented. The dielectric response of aged alkyl ester impregnated paper and electrical and tensile strength of aged alkyl ester impregnated paper is also presented in this chapter.

A general discussion of the entire results from the laboratory measurements is presented in Chapter 7, with Chapter 8 binding together the key results that emerged from the thesis. The limitations of the research and suggestions for future work on the research are contained in this chapter.

## **Chapter 2. Background Theory**

Solid and liquid dielectrics are used for insulation in oil-filled electric equipment. The dielectric liquid and a combination of oil and solid (paper insulation) serve a dual purpose in the equipment. The paper insulation protects the live from the grounded parts and provides mechanical support. The liquid acts as insulant to protect the live and grounded parts, and also as coolant to absorb, transport and dissipate heat generated in the transformer. The solid is expected to provide the mechanical and electrical support even as the equipment ages. The fluid in operation is expected to be able to flow for example, in extremely cold weather, retain its cooling properties at extremely high temperatures and be stable to oxidation for a long period of time at working temperature. There are quite a number of properties used in the characterization of insulation materials. They are thermo-oxidative stability, heat capacity, thermal (volume) expansion, dynamic viscosity, viscosity temperature dependence, pour point, flash point, volume resistivity, breakdown strength, as well as the ageing characteristics. This chapter is a brief presentation of the theory behind thermo-chemical and electrical behaviour of the dielectrics.

### **2.1 Thermo-Chemical Properties of Liquid**

Energy loss takes place in transformers while in operation. Two types of losses occurred in a transformer and two parts are responsible for most of the energy loss. No load losses occur at the magnetic core due to variation of alternating flux (hysteresis losses), the core's eddy-current loss, and dielectric losses. The dielectric loss results from leakage flux that took a path outside the winding when intercepted by a nearby conducting part of the transformer. The load losses take place at the windings. The primary and secondary windings in most transformers are either copper, aluminium, or one of them may be aluminium and the other copper. Application of load current on the windings leads to interactions between the moving current carrying particles and the atomic ions that make up the conductor. This interaction leads to ohmic heating ( $Q \propto I^2 R$ ) [Degeneff, 2004]. These energy losses are converted to heat losses at the respective parts.

If the heat is left in the transformer unit without any attention, it may lead to overheating of the equipment. Insulating oil absorbs, and dissipates the heat to the

surroundings using the cooling system. Heat transfer by liquid in a transformer is through both convection and conduction, even though convection dominates the rate of heat transfer. Convection heat transfer strongly depends on the thermal properties of the liquid. The thermal characteristics of insulating oil are temperature dependent. Some of the thermal properties of the oil are dynamic viscosity, thermal conductivity, density, thermal expansion coefficient, and specific heat capacity. Although all the properties are temperature dependent, temperature change has a stronger influence on the viscosity of the oil.

For free convection, where thermal expansion, reduced density and viscosity are responsible for fluid motion, heat transfer correlation of the form  $N_u = f(G_r, P_r)$  is expected [Incropera *et al*, 2007]. Where  $N_u$ , the Nusselt number, is a measure of the convection heat transfer that takes place at the surface, and it is a function of Grashof number ( $G_r$ ) and Prandtl number ( $P_r$ ). The Grashof number is a measure of the ratio of buoyancy forces to the viscous forces acting on the fluid. The Prandtl number is a measure of the ratio of momentum diffusivity to the thermal diffusivity. It evaluates the relative effectiveness of momentum and energy transport by diffusion in the velocity and thermal boundary layers, respectively.  $N_u$ ,  $G_r$ , and  $P_r$  are related with the relation [Iskender, 2011];

$$N_u = C_1 \times (G_r \times P_r)^n, \quad 2.1$$

where  $C_1$  and  $n$  are empirical constants that depends on the oil circulation type, i.e. laminar or turbulent flow. The Nusselt number, Grashof number, and Prandtl number are expressed as:

$$N_u = \frac{h \times L}{k} \quad 2.2$$

$$P_r = \frac{C_{oil} \times \mu}{k} \quad 2.3$$

$$G_r = \frac{L^3 \times g \times \beta \times \rho_{oil}^2 \times \Delta T_{oil}}{\mu^2} \quad 2.4$$

Where  $L$  is the characteristic dimension,  $h$  is the heat transfer coefficient,  $k$  is the thermal conductivity of the oil,  $C_{oil}$  is the heat capacity of the oil,  $\mu$  is the dynamic

viscosity of the oil,  $g$  is gravitational constant,  $\beta$  is the thermal expansion coefficient of the oil,  $\rho_{oil}$  is the oil density, and  $\Delta T_{oil}$  is the oil temperature difference.

After substituting equations 2.2, 2.3, and 2.4 in 2.1, the heat transfer coefficient is related to the oil viscosity by the expression;

$$h = C \times \left( \frac{\Delta T_{oil}}{\mu(T)} \right)^n \quad 2.5$$

where  $T$  is temperature in Kelvin, and  $C$  is dependent on the thermal conductivity, density, thermal expansion coefficient, and specific heat of the oil. The temperature change for an individual oil does not have much influence on these parameters as a result;  $C$  is taken to be a constant. For different oil samples, these parameters cannot be treated as a constant. The constant,  $C$ , for a particular oil sample is expressed as;

$$C = C_1 \times \left( \rho^2 \times g \times \beta_{oil} \times k^{\left(\frac{1-n}{n}\right)} \times L^{\left(\frac{3n-1}{n}\right)} \times C_{oil} \right)^n \quad 2.6$$

Equation 2.5 indicates that the heat transfer coefficient is strongly dependent on the viscosity of the oil and viscosity is temperature dependent. The dependence of viscosity on temperature can be determined using the Arrhenius relation for a thermally activated process. It is given by the equation;

$$\mu(T) = A \exp \left[ \frac{E_a}{kT} \right] \quad 2.7$$

where

$$A = \left( \frac{Nk}{V} \right) \exp[-\Delta S], \quad 2.8$$

The dynamic viscosity,  $\mu$  is in *Pa.s*,  $E_a$  is the activation energy for viscosity in *eV*,  $N$  is the number of molecules in *moles*,  $V$  is the molar volume of the liquid in  $m^3$  and  $\Delta S$ , the conductor entropy, can be used to determine the response of the viscosity of oil to temperature change. The activation energy of the viscosity phenomenon can be determined if the viscosity-temperature relation follows simple Arrhenius process, i.e. equation 2.7, else a tangent values of activation energies at each temperature can be determined graphically for the oil [Bartnikas, 1999].

## 2.2 Electrical Response of Materials

Electrical insulating liquid and solid insulating material impregnated with liquid are used to insulate the live and grounded parts of oil-filled electrical equipment. The behaviour of the materials is associated with their molecular structure, operating temperature, and applied field. Although, electric equipment operate at frequency of either 50 Hz or 60 Hz, characterization of dielectrics over wide ranges of frequency enable the understanding of the behaviour of the material since the response of the material varies with frequency variation. For example, information on the behaviour of charged particles in dielectrics and the molecular behaviour of the dielectric can be obtained at very low and higher frequencies. The dielectric response at very low frequencies in the range between  $10^{-5}$  and  $10^{-1}$  Hz can reveal useful information about the behaviour of free charges and this can be used to identify the character of the conduction ions [Bartnikas, 1987].

### 2.2.1 Charge Transport

For a nearly perfect dielectric material, application of a sufficiently low alternative field produces no detectable phase difference ( $\delta$ ) between the voltage gradient ( $\bar{E}$ ) and displacement vector ( $\bar{D}$ ). The ratio of the two vectors gives a real value constant referred to as the dielectric constant. An ideal dielectric material has finite dielectric loss and in simple terms can be said to behave like parallel  $RC$  circuit (*Figure 2.1a*). The values of  $R$  and  $C$  may be frequency dependent and the permittivity of the material becomes a complex quantity. The resistance  $R$  represents the lossy part of the dielectric which may result from electronic and/or ionic conductivity, dipole orientation, and space charge accumulation on the application of electric field. The storage capacity of the dielectric may be visualized as the action of dipole chains which forms under the influence of the applied field and bind counter-charges with their free ends on the surfaces of the plates [Von Hippel, 1954].

If a parallel plate with a vacuum in between is considered, the stored charges when an alternating sinusoidal voltage source,  $\bar{V} = \bar{V}_0 e^{i\omega t}$  is applied is expressed as:

$$Q = C_0 \bar{V} \quad 2.9$$

Where  $\omega = 2\pi\nu$ , is the angular frequency,  $\nu$  is the driving frequency in Hz and  $C_0$  is the vacuum capacitance of the capacitor, i.e. when vacuum is the dielectric between the two parallel plates. The charging current drawn by the capacitor is:

$$\bar{I}_C = \frac{dq}{dt} = i\omega C_0 \bar{V} \quad 2.10$$

and leads the voltage by a phase angle of  $90^\circ$ .

When the space between the parallel plates is filled with the dielectric material, the capacitance increases to

$$C = \frac{C_0 \epsilon}{\epsilon_0} = C_0 \epsilon_r \quad 2.11$$

Where,  $\epsilon_r$  is the relative dielectric constant of the dielectric,  $\epsilon$  is the permittivity of the material and  $\epsilon_0$  is the permittivity of free space. The charging current becomes;

$$\bar{I}_C = i\omega C \bar{V} \quad 2.12$$

According to equations 2.9 and 2.11, the voltage of the capacitor filled with a dielectric can be written as

$$V = \frac{Q}{\epsilon_r} \cdot \frac{1}{C_0} \quad 2.13$$

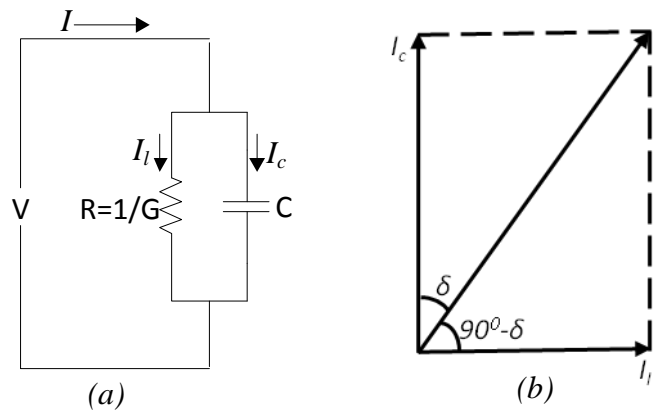


**Figure 2.1:** (a) Parallel equivalent circuit of a dielectric and (b) corresponding phasor diagram

Phasor diagram as shown in *Figure 2.1b* can be used to represent the complex permittivity of the dielectric material represented as RC in *Figure 2.1a*. The charging current and loss current are 90° out of phase and cannot be added directly. The total current will depend upon the resistance,  $R$  and the reactance of the capacitor,  $X_C$ , and the phase difference ( $90^\circ - \delta$ ) with the applied voltage.

The loss current in the dielectric material resulting from drifting of charges is characterized by DC conductivity of the material. This is often referred to as volume conductivity. The loss current component ( $I_l$ ) is in phase with the voltage (*Figure 2.1*) and is expressed in terms of  $G$ , the conductance of the dielectric as:

$$\bar{I}_l = G\bar{V} \quad 2.14$$

The total current can be expressed as

$$\bar{I} = (G + i\omega C)\bar{V} \quad 2.15$$

For a real dielectric, the current phasor will not be in phase with the voltage but by an angle ( $90^\circ - \delta$ ) where  $\delta$  is refer to as the loss angle. The complex permittivity is defined as [Bartnikas, 1987]:

$$\varepsilon^* = \varepsilon' - i\varepsilon'' \quad 2.17$$

Where  $\varepsilon'$  is real permittivity and  $\varepsilon''$  is the imaginary permittivity. The total current through dielectric material can be completely defined using the geometry of the capacitor;

$$\bar{I} = i \frac{\omega \varepsilon^* A \bar{V}}{d} = i \omega \varepsilon^* A \bar{E} \quad 2.18$$

The total current density is

$$\bar{J} = \frac{\bar{I}}{A} = i \omega \varepsilon^* \bar{E} \quad 2.19$$

Substitution of equation (2.17) in equation (2.19) gives

$$\bar{J} = (i\omega\varepsilon' + \omega\varepsilon'')\bar{E} = \bar{J}_c + \bar{J}_l \quad 2.20$$

Where,  $\bar{J}_c$  and  $\bar{J}_l$  are the capacitive and leakage current density of the total current density respectively. The frequency response can be expressed in terms of the ratio of the leakage current to capacitive current. It is referred to as loss tangent,  $\tan \delta$ . i.e.

$$\tan \delta = \frac{\bar{J}_l}{\bar{J}_c} = \frac{\varepsilon''}{\varepsilon'} = \frac{\varepsilon_r''}{\varepsilon_r'} = \frac{1}{\omega RC} \quad 2.21$$

Where  $\varepsilon'' = \varepsilon_0\varepsilon_r''$ ,  $\varepsilon' = \varepsilon_0\varepsilon_r'$ ,  $\varepsilon_0$  is permittivity of free space, and  $\omega$  is the radial frequency in *radian s<sup>-1</sup>*.

The conductivity of the dielectric, defined as the ratio of the leakage current density to the electric field, and from equation 2.20, conductivity can be expressed as;

$$\sigma = \frac{\bar{J}_l}{E} = \omega\varepsilon'' \quad 2.22$$

Conductivity can also be expressed as;

$$\sigma = \sum (q_i N_i \mu_i) \quad 2.23$$

Where  $q_i$  is the charge of ions of types  $i$  in *Coulomb*,  $N_i$  is the concentration of mobile ionic impurities in  $m^{-3}$ , and  $\mu_i$  is the ionic mobility in  $m^2 \cdot V^{-1} \cdot s^{-1}$ , the charge mobility is dependent on viscosity, temperature and molecular collision. With the assumption that the impurity ions are spheres of radii  $r_0$ , using Stoke's law, the ionic mobility of the ionic impurities in dielectric liquid can be approximated as [Bartinikas 1994];

$$\mu_m = \frac{q}{6\pi\eta r_0} \quad 2.24$$

where  $\eta$  is the dynamic viscosity and from equations 2.23 and 2.24,

$$\sigma = \frac{q^2 N}{6\pi\eta r_0} \quad 2.25$$

As these impurity charges drift through the liquid, they may undergo electrode polarization and the charges accumulate at the interfaces between the bulk liquid and the electrodes. This results in the formation of a thin layer of charges with high capacitance at the electrode-liquid interface. This layer is known as electric double layer (EDL).

### 2.2.2 Low Frequency Dispersion (LFD)

For a pure DC conduction in condensed matter, the real part of the relative permittivity,  $\varepsilon'$ , is close to zero and independent of frequency. Acquisition of slope by  $\varepsilon'$  at low frequency due to polarizing species that is dominated by slowly mobile charge carriers and the slope of the imaginary part,  $\varepsilon''$ , close to -1 is an indication of a low frequency dispersion. Low frequency dispersion can be volume or interfacial processes. While the presence of interfacial barrier layer at the electrode-sample interface is sometimes referred to as interfacial LFD, volume LFD is distributed throughout the thickness of the material. The loss in the material in this case is more than just a mere DC conduction. This type of response seems to be the lowest-frequency process observed in frequency response of dielectric material and has been termed the anomalous low-frequency dispersion (LFD) [Dissado *et al*, 1984]. The strong rise of  $\varepsilon'$  at low frequencies has a physical significance which indicates a finite and reversible storage of charge in the bulk material or at the material-electrode interface [Jonscher, 1996]. The curves of  $\varepsilon'$  and  $\varepsilon''$  cross over at  $\omega_c$ . At a frequency below threshold frequency,  $\omega_c$ , ( $\omega < \omega_c$ ), this response follows a fractional power law which is expressed as:

$$\varepsilon^*(\omega) = A(i\omega)^{n_2-1} = A[\sin(n_2\pi/2) - i\cos(n_2\pi/2)]\omega^{n_2-1} \quad 2.26$$

In this low frequency region  $\varepsilon'' > \varepsilon'$ , the frequency response is due to highly lossy “drift-like” processes. The high frequency response, ( $\omega > \omega_c$ ) may follow a similar power law but with the exponent equal to  $n_1$  as expressed below. This is due to a low-loss “polarization like” process.

$$\varepsilon^*(\omega) = A(i\omega)^{n_1-1} = A[\sin(n_1\pi/2) - i\cos(n_1\pi/2)]\omega^{n_1-1} \quad 2.27$$

Where constant  $A$  is an empirical constant and  $n_1$  and  $n_2$  have value between 0 and 1 [Jonscher, 1996]. The characteristic of Quasi-DC conduction process is [Raju, 2003]:

$$\varepsilon'(\omega) \propto \varepsilon''(\omega) \propto \omega^{n_2-1}; \quad \text{for } \omega < \omega_c \quad 2.28$$

$$\varepsilon'(\omega) \propto \varepsilon''(\omega) \propto \omega^{n_1-1}; \quad \text{for } \omega > \omega_c \quad 2.29$$

### 2.2.3 Dielectric Polarization

In addition to DC conductivity which results from charge transport in dielectric materials, there is additional polarization contribution due to displacements. The dipole moment induced in molecules on the application of electric field result from a slight displacement of its electron cloud with respect to the nuclei. This is known as electronic polarization. The applied field also leads to relative displacement of polyatomic molecules to each other. This is referred to as atomic or ionic polarization. Molecules carrying a permanent dipole moment in the liquid in addition to electronic and atomic polarization suffer a torque in an electric field  $E$  that tends to orient the dipole in the field direction leading to orientation polarization [Von Hippel, 1957]. Thermal agitation, on the other hand, tends to maintain a random distribution as a result there will be a time averaged orientation in the direction of electric field,  $E$ . Increase in temperature decreases the reorientation process leading to decrease in orientation polarization.

The application of a step DC field across a dielectric material results in a build up of polarization which attains a maximum value instantaneously or after short time interval. The applied field  $\bar{E}(t)$  generates a total current density  $\bar{J}(t)$ , which is the sum of conduction and displacement currents;

$$\bar{J}(t) = \sigma_0 \bar{E}(t) + \frac{d\bar{D}}{dt} \quad 2.30$$

where  $\sigma_0$  is the DC conductivity. The flux density due to polarization  $P(t)$  is:

$$\bar{D}(t) = \varepsilon_\infty \bar{E} + P(t) \quad 2.31$$

The instantaneous response of the material to the applied electric field is represented by  $\varepsilon_\infty$ , the “high frequency” permittivity, in equation 2.31.

The charges,  $Q$ , stored by the dielectric material which is attributed to the charges at the surfaces of the dielectric when an electric field,  $E$ , is applied is expressed as

$$Q = A\bar{E}\varepsilon_0(\varepsilon - 1) \quad 2.32$$

Where  $A$  is the area of the plate,  $\varepsilon_0$  is permittivity of free space,  $\varepsilon$ , is the dielectric constant of the material [Von Hippel, 1954]. The total charge  $Q$ , concentrated in the capacitor is distributed over the surface of the metal electrodes and the dielectric constant can be defined as the ratio of charge per unit area to force per unit area. The polarization vector  $P$  corresponds to the surface charge density bound at the electrodes by the polarized dielectric, and it points in the direction of the applied field. The polarization  $P$  is identical with the electric dipole moment per unit volume of the dielectric material. Since the volume of the dielectric is,  $V = Ad$ , where  $d$  is the separation between the parallel plates, the polarization is:

$$\bar{P} = \frac{Qd}{V} = \varepsilon_0(\varepsilon - 1)\bar{E} \quad 2.33$$

Sudden removal of the applied field results in the decay of polarization to zero value. The decay does not happen instantaneously but takes a finite time. This is the time required for the relaxation of the dipoles and the free charge carrier migration from a field oriented alignment to a random distribution, in equilibrium with temperature and the chemical and physical properties of the medium.

The idealized polarization curve for a typical dielectric material is shown in Figure 2.2. The equation for the time dependent polarization,  $\{P(t)\}$ , for Figure 2.2 on the application of electric field can be represented as

$$P(t) = P_s \left\{ 1 - \exp\left(-\frac{t}{\tau}\right) \right\} \quad 2.34$$

Where  $\tau$  is the relaxation time, and is a function of temperature and independent of the time.

Differentiating equation 2.34 gives

$$\frac{dP(t)}{dt} = -\frac{P_s}{\tau} \left\{ \exp\left(-\frac{t}{\tau}\right) \right\} \quad 2.35$$

$$\frac{dP(t)}{dt} = -\frac{1}{\tau} \{P_s(t) - P(t)\} \quad 2.36$$

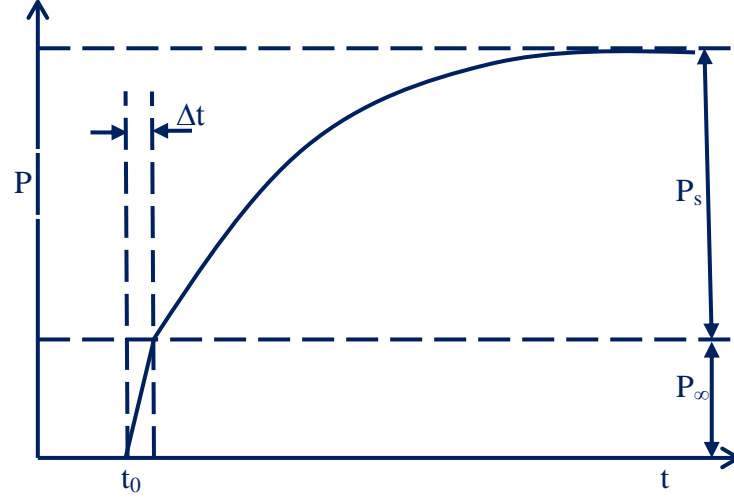


**Figure 2.2: Polarization-time characteristic of a dielectric material.**

Assuming that electronic polarization dominates at optical frequency, neglecting the atomic polarization, the final polarization  $P_T(t)$  can be expressed as the sum of the static polarization at that instant,  $P_s(t)$ , and electronic polarization,  $P_e$  which is assumed to attain its final value instantaneously because the time required for it to attain saturation value is in the optical frequency range.

$$P_T(t) = P_s(t) + P_e \quad 2.37$$

If equation 2.33 expressed the polarization at optical frequency, then the total polarization attained by the dielectric is express as:

$$P_T = \epsilon_0 (\epsilon_s - 1) \bar{E} \quad 2.38$$

And equation 2.37 can be written as

$$P_s = \epsilon_0 (\epsilon_s - \epsilon_\infty) \bar{E} \quad 2.39$$

Expressing equation 2.39 in complex form gives:

$$P_s^* = \varepsilon_0 (\varepsilon_s - \varepsilon_\infty) \bar{E}_0 \exp(i\omega t) \quad 2.40$$

Substitution of equation 2.40 into 2.36 will give:

$$\frac{dP^*(t)}{dt} = -\frac{1}{\tau} \left\{ \varepsilon_0 (\varepsilon_s - \varepsilon_\infty) \bar{E}_0 \exp(i\omega t) - P^*(t) \right\} \quad 2.41$$

The general solution to equation 2.41 is:

$$P_s^*(t) = \varepsilon_0 \left\{ \frac{(\varepsilon_s - \varepsilon_\infty)}{1 + i\omega\tau} \right\} \bar{E}_0 \exp(i\omega t) \quad 2.42$$

Substitution of equation 2.42 into 2.37 yields:

$$P_T^*(t) = \left\{ \varepsilon_\infty - 1 + \left[ \frac{(\varepsilon_s - \varepsilon_\infty)}{1 + i\omega\tau} \right] \right\} \varepsilon_0 \bar{E}_0 \exp(i\omega t) \quad 2.43$$

The electric displacement which describes the influence of the applied electric field,  $E$ , on the distribution of charge particle motion and electric dipole reorientation in a given medium is expressed as:

$$D(t) = \varepsilon_0 \varepsilon^* E_0 \exp(i\omega t) \quad 2.44$$

Expressing the flux density in equation 2.31 in complex form gives:

$$D(t) = \varepsilon_0 E_0 \exp(i\omega t) + P_T^*(t) \quad 2.45$$

Equating equations 2.44 and 2.45 gives:

$$\varepsilon_0 \varepsilon^* E_0 \exp(i\omega t) = \varepsilon_0 E_0 \exp(i\omega t) + P_T^*(t) \quad 2.46$$

Substitution of equation 2.43 in 2.46 will give:

$$\varepsilon^* = \varepsilon_\infty + \frac{(\varepsilon_s - \varepsilon_\infty)}{1 + i\omega\tau} = (\varepsilon' - i\varepsilon'') \quad 2.47$$

Separating the real and imaginary parts leads to the Pellat-Debye equation:

$$\varepsilon' = \varepsilon_\infty + \frac{(\varepsilon_s - \varepsilon_\infty)}{1 + \omega^2 \tau^2} \quad 2.48$$

and

$$\varepsilon'' = \frac{(\varepsilon_s - \varepsilon_\infty)\omega\tau}{1 + \omega^2 \tau^2} \quad 2.49$$

The motion of the charged particles in the dielectric material, besides causing conduction current, gives rise to polarization of the dielectric material. If the total loss in the dielectric is visualized as a combination of DC conductivity and loss due to polarization, the measured dielectric loss can be express as:

$$\frac{\sigma(\omega)}{\omega\varepsilon_0} = \varepsilon''(\omega) + \frac{\sigma_0}{\omega\varepsilon_0} \quad 2.50$$

where  $\varepsilon''$  in this context is the loss due to polarization, and is related to conductivity as as:

$$\sigma'(\omega) = \omega\varepsilon_0\varepsilon''(\omega) \quad 2.51$$

Substituting equation 2.49 in 2.51 gives:

$$\sigma'(\omega) = \varepsilon_0 \frac{(\varepsilon_s - \varepsilon_\infty)\omega^2\tau}{1 + \omega^2\tau^2} \quad 2.52$$

If DC conductivity is involved in the loss mechanism, the total loss will be:

$$\sigma(\omega) = \sigma_0 + \varepsilon_0 \frac{(\varepsilon_s - \varepsilon_\infty)\omega^2\tau}{1 + \omega^2\tau^2} \quad 2.53$$

### 2.3 Dielectric Breakdown Theory

The processes of electrical breakdown in dielectric liquids are not fully understood. However a number of processes have been identified that may contribute to electrical breakdown in a liquid. Some researchers extend the gaseous breakdown model to explain breakdown in insulating liquid. This process is considered to be applicable to homogeneous liquids of extreme purity. Application of high field rapidly increases the

conduction of impurity charges due to electron emission at the cathode or field aided dissociation of the molecules in the molecule. A possible return of positively charged particles to the cathode may cause local field enhancement and results in local electron emission. Intrinsic breakdown may occur if the injected electrons into the liquid gains energy from the applied field as they drift through the liquid; some of the energy is lost as a result of collisions with the liquid molecules. Some of the electrons may gain more energy than they lose in collisions with molecules. The electrons are accelerated until they acquire sufficient energy that can cause ionization of molecules on collisions. The energy gained by the liquid molecules may lead to excitation of C–H and C–C bonds and could result in some of the bonds being broken thereby producing extra ions and an avalanche is initiated. [Kuffel *et al*, 2000; Forster, 1999].

Some other researchers identified that the breakdown field strength of an insulating liquid is affected by impurities present in the liquid. The types of breakdown process depend on the existence or otherwise of regions of field non-uniformity. Since insulating liquids are known to contain impurities such as particles and water, a model based on suspended particles may be more appropriate in the explanation of breakdown processes in insulating liquid. Dielectrophoresis may cause uncharged particles to move to regions of high electric field causing inhomogeneity and additional electric field enhancement. If the particles have a higher relative permittivity than the oil then the particles will move towards the higher field region with a force;

$$F = r^3 \frac{\epsilon_p \times \epsilon_{liq}}{\epsilon_p \times 2\epsilon_{liq}} E \cdot \frac{dE}{dx} \quad 2.54$$

where the particle was assumed to be sphere of radius  $r$ , otherwise they will move away [Wadhwa, 2007]. The force makes the particles to align themselves to bridge the electrode gap in order to bring about a breakdown. If the number of particles is not enough to form such a bridge across the electrode, formation of gas bubbles may result from local breakdown near the particles. The electrical field of a gas bubble with the assumption that it is spherical in a dielectric liquid was reported to be more accurately expressed by the expression;

$$E_b = \frac{1}{\varepsilon_{liq} - \varepsilon_b} \left[ \frac{2\pi\sigma(2\varepsilon_{oil} + \varepsilon_b)}{r} \left( \frac{\pi}{4} \sqrt{\left( \frac{V_b}{2rE_0} \right)^2 - 1} \right) \right]^{1/2} \quad 2.55$$

where  $E_0$  is the field in the liquid in the absent of bubble,  $\sigma$  is the surface tension,  $V_b$  is the voltage drop in the bubble. Discharges may take place when the electric field in a spherical gas bubble becomes equal to the gaseous ionization field, which will lead to decomposition of the liquid and breakdown may follow [Kuffel *et al*, 2000].

As ionic charge carriers, responsible for the DC electrical conductivity, drift and collide with liquid molecules, momentum is lost and energy is transferred to the fluid. When the applied voltage increases, there may be onset of instability at a critical voltage leading to electro-hydrodynamic (EHD) motion of the liquid near breakdown [Arora, 1995]. This is a mechanical effect of electric fields acting on a dielectric liquid. At a voltage close to breakdown, the speed of EHD motion approaches a value close to  $\left\{ (\varepsilon_{liq} / \rho)^{1/2} / E \right\}$ , where  $\rho$  is the specific mass and  $E$  is the electric field strength. This turbulent motion in oil between the electrodes causes the temperature of the liquid to rise locally. It also significantly affects the local pressure [Butcher *et al*, 2006]. The injected energy could also result in a phase change in the oil or liberation of simpler molecules from the dissociation of part of the oil molecule. The liberated vapour influences the formation of bubbles [Forster, 1999]. Discharges may take place when the electric field in a spherical gas bubble becomes equal to the gaseous ionization field, which will lead to decomposition of the liquid and breakdown may follow [Kuffel *et al*, 2000].

Although the intrinsic breakdown strength of a dielectric liquid has determinable value in principle, but in practice the measurement of breakdown field strength is subject to random or uncontrollable variations in the experimental procedure. In addition, the process of electrical breakdown is sensitive to material impurities. The variation in the measurement for each specimen is due to the random distribution of the weakest paths and the mean value is usually interpreted as the most probable breakdown value for the material. This can be analyzed using a suitable statistical tool.

## **2.4 Summary**

This chapter provided theoretical background on the relationship between heat transfer coefficient and thermo-physical properties of liquids using empirical relation. The mathematical relation established that the viscosity of liquid play a major role in the heat transfer and dissipation. Dielectric loss in material results from polarization due to displacement of dipoles, and conductivity due to charge transport in the material. Breakdown model based on suspended particles fits the description of the breakdown processes in practical insulating fluids. The next chapter described the processes involved in the preparation of the samples and experimental test will be performed on the samples to study the properties described in this chapter.

## Chapter 3. Materials

### 3.1 Introduction

Vegetable oil is a combination of fatty acids and glycerine. The fatty acids may be saturated or unsaturated. The degree of unsaturation of these acids depends on the class of the vegetable oil. A higher proportion of saturated fatty acids in palm kernel oil lead to a higher melting point and greater oxidative stability. Unsaturated fatty acids in vegetable oil are more chemically active and can undergo chemical modification to yield saturated fatty acids, thereby altering some of the thermo-chemical properties of the oil. This chapter describes the procedure used in the purification of the crude palm kernel oil. It also describes the procedures involved in the synthesis of esters to create complex structures that may improve some of the desired properties of the oil. Four different types of alkyl esters were synthesized for analysis.

### 3.2 Background

Transformer-grade natural esters have displayed promising results in serving as alternatives to the existing mineral based transformer oils [Oommen, 2002; Mcshane, 2002]. Useful properties of natural esters include: fire safety, environmental biodegradability and slower ageing rate of cellulose insulation when impregnated with the esters. One of the challenges of natural ester as a dielectric material is synthesizing a fluid with favourable low temperature properties (e.g. pour point), whilst maintaining a high thermo-oxidative stability. The base oils for natural ester fluid are extracted from oil seeds; they are renewable resources. They are triglycerides or esters of glycerol and fatty acids. The fatty acids have carbon chain lengths between 8 and 24 carbon atoms with double bonds ranging from zero to three. The physical and chemical properties of the oils are dependent on the structure of the triglyceride. These are affected by the position of the fatty acid linkage to the glycerol, and whether the three fatty acids  $R^1$ ,  $R^2$ ,  $R^3$  shown in *Figure 3.1* are the same or different. These properties are also dependent on the degree of saturation of the fatty acids. The crude vegetable oil also contains about 2% or more nonglyceride substances consisting of phospholipids, trace metals, oxidation products, pigments, undesirable flavourings etc. These minor components are also referred to as the unsaponifiable fraction [Stockton *et al* 2009].

Hydrocarbon compounds containing carbon-carbon double bonds are referred to as unsaturated hydrocarbons because the number of hydrogen atoms they contain is less than the maximum possible number. The thermal stability of vegetable oil is a function of the degree of saturation. It becomes more susceptible to oxidation as the degree of unsaturation progresses from monounsaturated to polyunsaturated. The relative instability of fatty acids to oxidation is roughly estimated as 1:10:100 for saturated, mono-, and poly-unsaturated C-18 triglycerides [Oommen, 2002]. On the other hand, the melting temperature of the oil increases with the degree of saturation. Therefore, improving the oxidative stability by increasing the degree of saturation tends to have the undesirable effect of increasing the melting point. The unsaturated fatty acids generally have a lower melting point compared with saturated fatty acids. The high melting point of saturated fatty acids results from their uniform shapes which enables them to pack themselves efficiently together in a crystal lattice. Crystal formation is difficult in esters with carbon-carbon double bonds because of the bends and kinks introduced into the hydrocarbon chain. This is because the bends limit the ability of the fatty acids to be closely packed. As a result, the higher the concentration of double bonds, the harder it becomes for the molecules to crystallize and consequently, the lower the melting point of the oil [O'Brien, 2004].

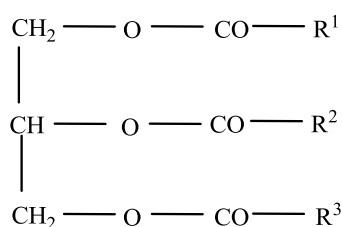


*Figure 3.1: Structure of Triglyceride*

Vegetable oils are known to have inadequate oxidative stability and poor low temperature properties such as melting point, pour point and viscosity. These properties could be improved by modifying the oil through the double bond sites. The active nature of the double bonds, which makes them susceptible to chemical reactions in the presence of oxygen, is linked to the poor oxidative stability of the oil. The modification of vegetable oil ester by the elimination of the double carbon bonds may lead to improved oxidative stability. The complex structure obtained from this modification may also lead to improved pour point temperature and viscosity [McMurry, 2000; Hwang, 2001].

The double bond is a combination of a  $\sigma$  bond and  $\pi$  bond as shown in *Figure 2.1*. These are formed as a result of  $sp^2$  hybridization.  $sp^2$  orbitals of the two carbon atoms overlap to form the  $\sigma$  bond which contains two of the four electrons of the double bond. The  $\pi$  bond, which is formed by a “side-by-side” overlap of singly occupied p orbitals of the two  $sp^2$  carbons, contributes the other two electrons. The total numbers of  $\pi$  bonds is used to determine the degree of unsaturation. The  $sp^2$  carbons are called vinylic carbons [Bruice, 2003].

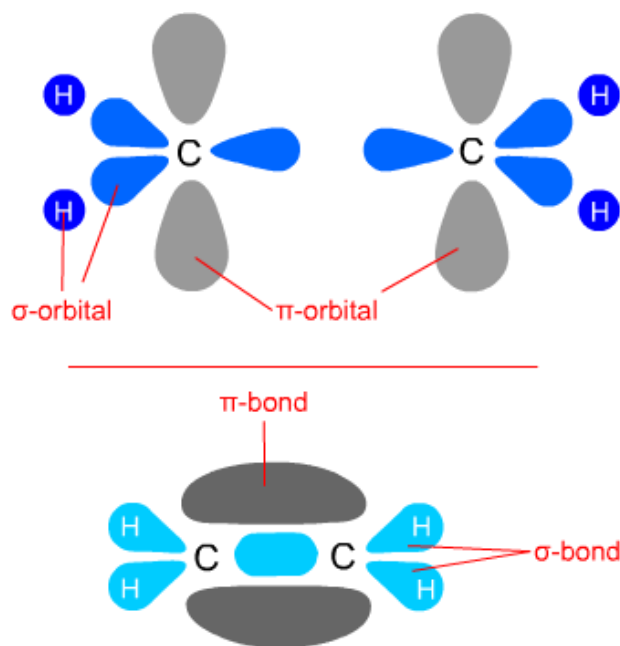


Figure 3.2: Ethene Orbital [biochem.co]

Alkenes have the ability to undergo addition reactions [Carey, 2000]. The  $\pi$  bond is easily broken whenever unsaturated hydrocarbons undergo such reactions. This is because the  $\pi$  bond is weaker than the  $\sigma$  bond requiring less energy to break. A reaction between an alkene and a reagent with a partially positively charged ion, results in the attraction of the loosely held  $\pi$  electron of the carbon–carbon double bond to an electrophile resulting in the addition of an electrophile to one of the  $sp^2$  carbons. The negatively charged ion of the reagent (nucleophile) is then added to the other  $sp^2$  carbon to conclude the reaction. Some of the reactions form carbocation (electrophile) intermediates whilst some form other intermediates, and others do not form any intermediates [Bruice, 2003]. The reactivity of alkenes makes them an important class of organic compound as a variety of industrial products can be synthesized using them.

Attaching molecular side chains to vegetable oils can be achieved by first transforming the double bonds to epoxides through an epoxidation reaction. An epoxide is a three-membered ring containing oxygen. The epoxy ring is a highly reactive site. They are very reactive in nucleophilic substitution reactions because the ring opening relieves the strain in the ring. Its reaction with the appropriate reagent and catalyst opens the ring and simultaneously grafts the side hydrocarbon chains. The grafting of side chains can influence the ability of the fatty acids to be closely packed [McMurray, 2000; Hwang *et al*, 2001].

Several research groups have worked on the epoxidation of various vegetable oils to optimize the product's yield [Goud *et al*, 2006; 2007; Park *et al*, 2004; Cai *et al*, 2008; Mungroo *et al*, 2008]. Their reports show that the epoxidation reaction can be achieved using acidic ion exchange resin (AIER) as a catalyst. Epoxy methyl esters of some natural oils, which can equally serve as a starting material for bio-based products, can be prepared either by the epoxidation of fatty acid methyl esters [Ikhuoria *et al*, 2007; Campanella *et al*, 2008] or the transesterification of epoxidized vegetable oils. The transesterification of epoxidized soybean oil by Holser [Holser, 2008] converted the oil to the corresponding methyl ester without degradation of the epoxy functional group.

This chemical structure modification can be achieved using a two-step process. The first stage, which involves the reaction of the double bonds with peracid to convert them to epoxides, is widely exploited for the modification of the properties of fatty acids [Sharma *et al*, 2006]. The second stage involves the grafting of molecular side chains to the epoxy group [Sharma *et al*, 2008]. This approach may be found useful in the development of vegetable oil-based electrical insulation liquids to improve their oxidative stability and/or the pour point.

The chemicals used in the synthesis process are listed below. Most of the chemicals were obtained from Fisher Scientific and Sigma Chemicals. The chemicals include: Citric acid of 99.5% purity, sodium hydroxide of 97.5% purity, potassium hydroxide of 85.9% purity, acetic acid, 30 % hydrogen peroxide, amberlite IR-120, diethyl ether of >99.5% purity, sodium bicarbonate of 99% purity, sodium chloride of 99.5% purity, sodium sulphate of 99% purity, methanol of 99.9%, phosphoric acid of >85%, ethyl acetate of >99% purity, propionic anhydride of 99%, butyric anhydride of  $\geq 97\%$ , boron trifluoro diethyl etherate, and tert butyl hydroquinone of 97% purity. Crude palm kernel

oil was purchased from Jarmac Ltd. The oil has 10 % free fatty acid, iodine value of 14-23 and 0.5% of moisture and impurities. Tonsil supreme 110 FF was obtained from Sud-Chemie Ltd. Trysil 300 was obtained from Grace Davison.

### **3.3 Oil Purification**

#### **3.3.1 Review of Purification Method**

The quality of oil used for electrical insulation in transformers is very important. Highly purified oil is required for electrical insulation as impurities may contribute to breakdown at high temperature. Crude palm kernel oil contained high level of impurities which make it not suitable for electrical insulation in high voltage electrical equipment. Elemental analysis of palm kernel oil by Obi *et al* [Obi *et al*, 2001] shows the presence of trace elements such as aluminium, calcium, chlorine, copper, magnesium, manganese and sodium. The impurities in the oil include trace metals, lecithin, colour, water, gas, free fatty acids, and conducting and non-conducting particles. It is therefore necessary to subject it to further refining to remove Lecithin (phosphoric acid derivatives) from phospholipids, and the other impurities. A modified Dijkstra and Opstal purification method [Dijkstra *et al*, 1987] was adopted. Phosphatides (phospholipids) foul bleaching earth and impart dark colour when heated at elevated temperatures (90°C) [Lusas, 2007]. The process of removing phosphatides is referred to as degumming. The free fatty acid makes the oil corrosive and it may be removed through alkali neutralization. Silica gel adsorption has been used to remove the metal ions and residual phosphatides and soaps [Lusas, 2007]. This will also eliminate water washing of the sample after alkali refining. The bleaching process is intended to remove the saponifiable matter, colouring pigments, oxidation-degraded compounds and it scavenges the remaining soaps, phosphatides and minerals. Activated clay provides a catalytic surface for breaking down peroxides. The cationic exchange property of the activated clay removes magnesium from the centre of the chlorophyll complex, rendering the phenophytin adsorbable to the clay. It also removes heavy trace metals pro-oxidants such as iron and copper and nickel [Lusas, 2007] some of which have been reported to have high concentrations in palm kernel oil [Obi *et al*, 2001].

#### **3.3.2 Purification Process**

The purification process used in this work is as follows:

- 200 ml of crude palm kernel oil (CPKO) was heated in a conical flask to 70°C and 1.5 ml of aqueous citric acid solution (0.8 vol.% of 64%) was added gently and mixed thoroughly with a magnetic stirrer for 15 minutes.
- This was followed by addition of 4 ml of aqueous NaOH solution (vol.% of 8%) and mixed at 70°C with magnetic stirrer for 15 minutes. The mixture was dried in a vacuum oven at 85 °C for 30 minutes to reduce the water content.
- 2 g of Trysil 300 was added to the mixture at 70°C and stirred for about 30 minutes to prevent the silica settling out.
- Bleaching clay (Tonsil supreme 110 FF) was then added and stirred well with a magnetic stirrer at 85°C for 30 minutes. The amount of bleaching clay was varied from 4 g to 20 g.
- The sample was then filtered in a vacuum oven at 85°C. Whatman No.5 filter paper which is capable of limiting the size of particles in the filtrate to 2.5 microns was used to filter out the bleaching clay.

### **3.4 Initial Chemical Modification Trials**

There was initial trial of chemical modification of the palm kernel oil where the reaction was observed not to have occurred. The purified oils sample was made to undergo epoxidation reaction and esterification for an attempted synthesis of diester derivatives.

Epoxidation reaction was carried out by placing 50g of PPKO in a three-necked flask. 7g of Acetic acid was equally placed in a round bottom flask to satisfy the 0.5:1 molar ratio of carboxylic acid - ethylenic unsaturation that gave maximum yield followed by the addition of 8g (16 wt%) of Amberlite IR-120. The mixture was stirred continuously and followed by the addition of 1.5 moles of hydrogen peroxide per mole of ethylenic unsaturation to the mixture to produce PAA (peracetic acid). The PPKO in the three necked flask was heated to 70°C followed by the addition of the mixture that produced PPA. The reaction time started at the completion of the addition of PPA. The mixture was allowed to react at 70°C for 7 hours with continuous stirring at 1,200 rpm. Aliquot samples were taking out every 1 hour for FTIR analysis and maximum epoxy yield was obtained after a reaction time of 4 hours. When the reaction was completed, the sample was extracted with diethyl ether, purified with 5% NaHCO<sub>3</sub> three times to neutralize the remnant acid present, then with brine solution. The sample was dried over anhydrous

sodium sulphate, and then the solvent removed under reduced pressure of about 10 mbar.

An attempt was made to prepare diester derivative of the epoxidized palm kernel oil product by esterification of the epoxidized oil with carboxylic acid anhydride. 22.6 g of the epoxidized PKO sample was dissolved in ethyl acetate in a three-necked flask. 20 g hexanoic anhydride was added followed by 10 drops of boron trifluoride etherate as catalyst. The mixture was stirred under nitrogen at 100°C for 9 hours. The mixture was cooled down and the product was purified by washing it three times with 5% NaHCO<sub>3</sub> solution followed by brine solution. The ethyl acetate layer was dried over anhydrous sodium sulphate, then filtered and the solvent and the excess anhydride were removed under reduced pressure of about 10 mbar.

The spectra of the new product still displayed the epoxy group peak around 837cm<sup>-1</sup>. This suggests that the reaction of the epoxide with the anhydride was not completed. The reaction was suspected to be slow possibly because the epoxides which are the active sites are buried within the triglyceride structure and the epoxy ring opening was difficult for the esterification reaction to occur.

Alkyl ester route was later adopted for the chemical modification of the oil and *Figure 3.3* shows the block diagram of the adopted processing sequence.



*Figure 3.3: Processing Sequence*

### **3.5 Palm Kernel Oil Ester Synthesis**

#### **3.5.1 Palm Kernel Oil Alkyl Ester**

100 g of purified oil sample (PPKO) was placed in a round bottom flask and heated to 70°C. 33 wt% of methanol was added under moderate stirring (1,200 rpm) and followed by 1.5 wt% anhydrous NaOH as a catalyst. The reaction continued for 2 hours. The mixture was transferred into a separating funnel and kept in an oven for 30 minutes. The bottom layer containing the glycerol was discarded while the top layer containing alkyl ester (PKOAE1) was washed with 0.015 M H<sub>3</sub>PO<sub>4</sub> three times. The emulsion was kept in an oven at 45°C for one hour for separation. The bottom layer which contains remnant glycerol and NaOH was discarded, while the top layer containing purified alkyl

ester and methanol was dried over anhydrous magnesium sulphate. It was then placed in a rotary evaporator under reduced pressure of about 10 mbar and temperature of 60°C to remove the excess methanol. The reaction scheme is shown in *Figure 3.4*.

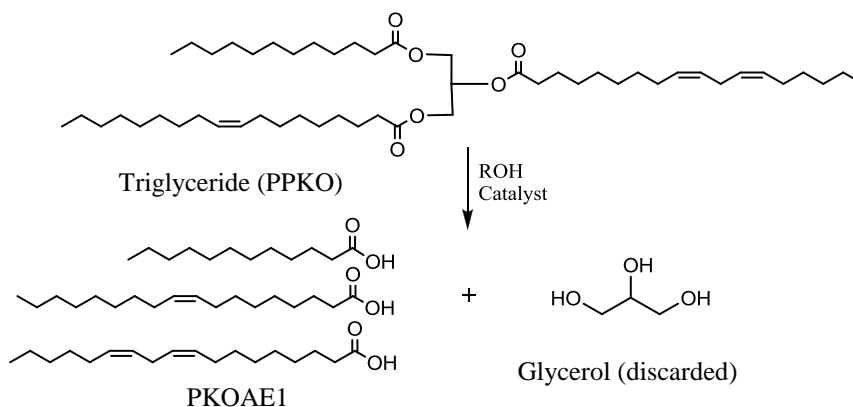


*Figure 3.4: Reaction Scheme for Transesterification Reaction*

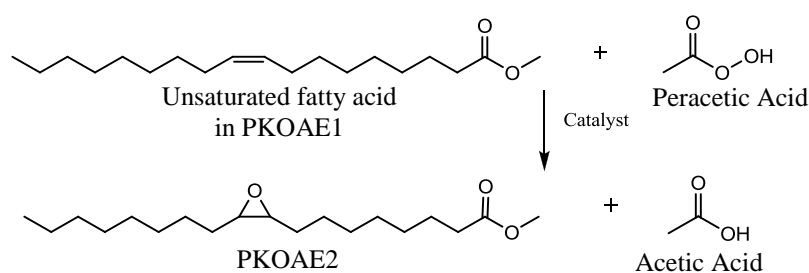


*Figure 3.5: Reaction scheme for epoxidation reaction [Sharma et al, 2008]*

### 3.5.2 Epoxy Alkyl Ester of Palm Kernel oil

100 g of palm kernel oil methyl ester (PKOAE1) was placed in a three-necked flask. Acetic acid (14 wt%) was placed in a round bottom flask followed by the addition of Amberlite IR-120 (16 wt%). The mixture was stirred continuously and followed by the addition of 1.5 moles of hydrogen peroxide per mole of ethylenic unsaturation to the mixture to produce peracetic acid (PAA). Palm kernel oil methyl ester in the three-necked flask was then heated to 70°C followed by the addition of the PAA mixture. This was allowed to react at 70°C for 7 hours with continuous stirring at 1,200 rpm. Aliquots were taken out every 1 hour for FTIR analysis to determine the effect of reaction time on the yield at 70°C. The sample was then extracted with diethyl ether in separating funnel, purified with 5% NaHCO<sub>3</sub> three times to neutralize the unreacted acid present and then a saturated solution of NaCl was added. The sample was dried over anhydrous magnesium sulphate, and the solvent was then removed under reduced pressure using a rotary evaporator. The reaction scheme is shown in *Figure 3.5*.

### 3.5.3 Palm Kernel Oil Side Branched Alkyl Ester

20 g of epoxy alkyl ester was placed in a three necked round bottom flask and followed with the addition of 10 ml of ethyl acetate. The mixture was stirred continuously and followed by the addition of 4 g of acid anhydride. The flask was purged with nitrogen and followed by the addition of 1 ml boron trifluoro diethyl etherate. It was heated to 70°C. The mixture was left to react at this temperature for 7 hours under nitrogen with continuous stirring. The sample was purified with 5% NaHCO<sub>3</sub> three times and then a saturated solution of 10 % NaCl was added. The sample was dried over anhydrous magnesium sulphate, and the solvent was then removed under reduced pressure using rotary evaporator. The unreacted anhydride was removed using Kugelrohr's distillation under reduced pressure (0.5 mbar) at about 80°C. The distillation unit can only process about 20 ml of sample each time, limiting the amount of sample that can be processed. The reaction scheme is shown in *Figure 3.6*. The ester with three hydrocarbon side chains (C-3) was synthesized using propionic anhydride, while the ester with four hydrocarbon side chains (C-4) was synthesized using butyric anhydride. The grafting of side chain was limited to C-4 because the boiling point of anhydrides with longer chain length is close to the boiling point of some of the fatty acids in the synthesized alkyl ester. This will make difficult the removal of the unreacted anhydride without destroying some of the fatty acids using the available distillation system.

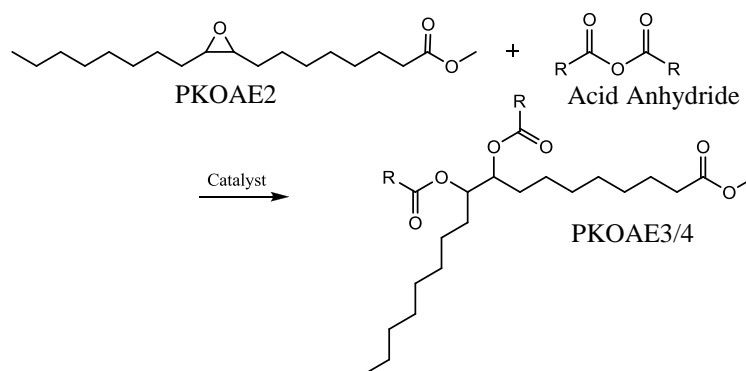


*Figure 3.6: Reaction Scheme for esterification of epoxide*

The flow chart in *Figure 3.7* summarized the steps taken in the synthesis of the chemically modified ester samples. The picture of an ongoing synthesis, samples, and table of description of the samples, are shown in *Figure 3.8*, *Figure 3.9*, and *Table 3.1* respectively.

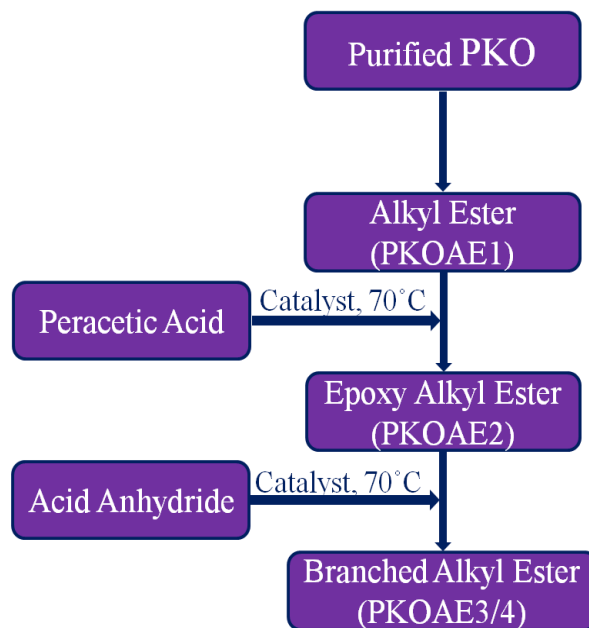


Figure 3.7: Flowchart of the Ester Synthesis

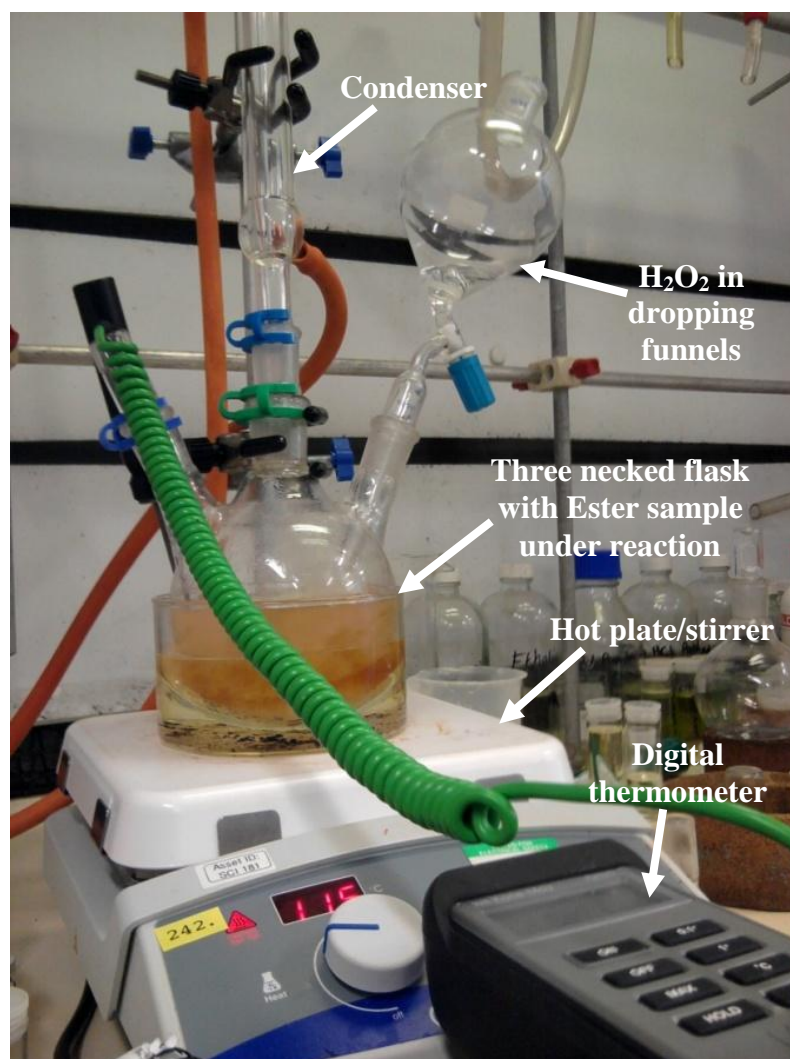


Figure 3.8: Ongoing Ester Synthesis

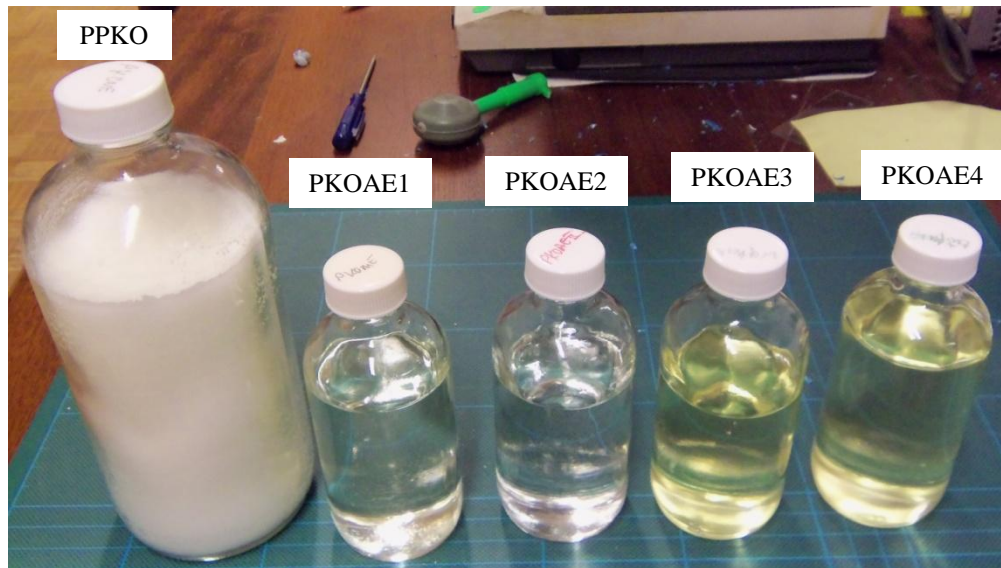


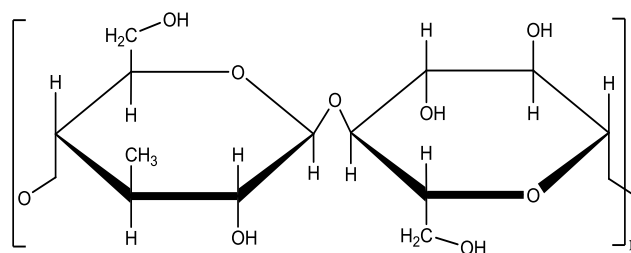
Figure 3.9: Samples

Table 3.1: Sample description

Sample	Description
CPKO	As received crude palm kernel oil
PPKO	Purified palm kernel oil
PKOAE1	Palm kernel oil methyl ester
PKOAE2	Palm kernel oil epoxy methyl ester
PKOAE3	Palm kernel oil methyl ester with C-3 carbon side chain
PKOAE4	Palm kernel oil methyl ester with C-4 carbon side chain

### 3.6 Electrical Insulation Paper

The solid insulation materials in electric power transformers are made from cellulose. Ageing of paper insulation is one of the major factors that determine the ultimate life of transformers [McNutt, 1992]. Cellulose is an organic polymeric material whose molecule is made of glucose rings that are linked to each other as shown in *Figure 3.10* [McShane, 2001; 2002]. They provide both electrical and mechanical support in transformers. Immersion of the paper in oil improves its electrical insulation strength. Thermal stress, oxidation and hydrolysis of the paper while in service may lead to degradation of the paper insulation and a reduction of its life time. This may lead to reduction in its mechanical properties and could influence the ageing performance of the paper insulation.



*Figure 3.10: Cellulose Structure*

The electrical insulation paper under study is an elephantide Grade K thermally upgraded presspaper produced from 100% electrical grade kraft wood pulp. Thermally upgraded presspaper has an improved thermal capacity which was achieved by impregnating the paper with chemicals that increase nitrogen content and decrease paper degradation under prolonged high temperature conditions [Weidmann, 2011]. The presspaper under study was obtained from Weidman Whiteley Ltd and has a thickness of 0.255 mm. The dried and degassed paper will be identified as DKP.

### **3.7 Summary**

The chemistry of alkenes has provided an insight on how fatty acids containing carbon-carbon double bonds can be modified to enhance the properties of vegetable oils. The adopted Dijkstra and Opstal purification methodology was used to produce a purified version of palm kernel oil. Ester of palm kernel oil was synthesized by the separation of glycerol from the oil. This was followed by the production of epoxy-ester of palm kernel oil. Side branched hydrocarbon chains were then attached to the ester by the opening of the epoxy ring to synthesize the side-branched alkyl esters. This modification involves changes in the chemical structure of some of the fatty acids' chains. This change was monitored with spectrometric methods discussed in the next chapter. The suitability of these esters as insulating and cooling fluid will be studied using the measurement methods described in the next chapter.

## **Chapter 4. Experimental Methods**

### **4.1 Introduction**

Characterization of materials for electrical insulation involved studying various properties of the materials. The study of dielectric liquid as insulant and coolant in transformers required some sets of methods of measurement as no single methodology can completely characterize the material. The properties to be studied include thermal, physical, chemical and electrical properties and their variation with thermal degradation. This chapter presents the description of the various methodologies and the experimental setups used in the characterization of the synthesized natural ester-based dielectric liquid.

### **4.2 Structural Identification**

Natural ester was earlier mentioned in chapter three as consisting of fatty acids of various chain lengths. The synthesis involves a change in the chemical structure through modification of some of the fatty acids' chains in the ester. It is necessary to monitor the chemical reaction to know if the required products are obtained and identify the functional groups in the synthesized esters. This section describes the Gas Chromatography-Mass Spectrometry (GC-MS) and Fourier Transform Infrared (FT-IR) Spectrometry that was used for this purpose.

#### **4.2.1 Gas Chromatography-Mass Spectrometry (GC-MS)**

The composition of the alkyl ester was analyzed with GC-MS. The analysis was carried out using Perkin Elmer AutoSystem XL Gas Chromatograph and TurboMass Mass spectrometer (GC-MS). The instrument detects the components as well as determining the molecular mass of each component in a sample. The sample was dissolved in chloroform as solvent in a vial, sealed and was thoroughly mixed. It was placed in the sample holder of the instrument and the sample was injected onto a heated injection block by syringe. The injection volumes were 1.0  $\mu\text{l}$ . Volatilization of the samples occurred in the injection block. Helium was introduced into the injection block as the carrier gas with a flow rate of 50 ml/min to transfer the sample from the injector through the column packed with stationary phase to the detector. The components in the sample passed through the column at different rates due to their different retention time. The effluents from the gas chromatograph passed through flame ionization detector (FID)

for the detection of any substance that is different from the carrier gas. The detector interacts with the eluted solutes to produce a current that varies in proportion to the amount of solute. The identified substances are the components of the sample. The total run time for the GC was 30 minutes. These effluents were transferred from GC to MS to analyse the substance. On arrival at MS, the effluents were scanned between  $m/z$  100 - 500 kg/C for a total run time of 35 minutes to determine mass to charge ratio ( $m/z$ ) of the components of the samples.

#### **4.2.2 Fourier Transform Infrared (FT-IR) Spectrometry**

The FTIR spectra analysis was carried out using Perkin Elmer Spectrum One FT-IR spectrometer. The spectrometer sample holder and the cap were cleaned with methanol and acetone thoroughly. The cap was fixed and a background scan was carried out. A drop of the sample was placed on the spectrometer measurement cell. The sample was scanned with infrared radiation through frequency of  $4000 - 650 \text{ cm}^{-1}$  to obtain the spectrum. The amount of radiation absorbed by the sample was plotted as a function of the wave number of the absorbed radiation by a detector. Each spike (absorption bands) in the IR spectrum represents absorption of energy. The functional groups of the samples were identified from the spectra.

### **4.3 Thermo-physical Characterization**

Fluids intended for electrical insulation are often expected to be able to flow under extremely cold weather conditions as well as being able to act as an effective coolant at all times. The coils and the iron core of a transformer exchanged the generated heat while in operation with the oil which is transferred and dissipated at the cooling unit. The cooling system may utilize natural convection (no pump, no fan), or forced convection for the transfer of the generated heat. For a natural convection, the cooling capability depends on the viscosity of the oil. The oil flow speed in the transformer and the heat transfer coefficient of the oil has a direct link with the dynamic viscosity of the oil. This section presents the description of the experimental methods used in the study of low and high temperature thermo-physical properties of the ester fluids.

#### **4.3.1 Viscosity and Density**

A study of the viscosity-temperature dependence and flow properties of the alkyl ester is essential for its consideration as a potential choice as a bio-based insulating fluid.

There are various viscosity measurement techniques that have been developed over the years. The most commonly used for liquid with negligible non-Newtonian effect are capillary viscometers. Capillary viscometers are based on the principle that a specific volume of fluid will flow through the capillary under gravity and the time necessary for this volume of fluid to flow is proportional to the ‘kinematic viscosity’. Flow through the capillary must be laminar and the deductions are based on Poiseuille’s law for steady viscous flow in a pipe. With an assumption that the fluids are Newtonian, the kinematic viscosity can be calculated from the formula:

$$\nu = \frac{\pi r^4 g l t}{8 L V} = k(t_2 - t_1) \quad 4.1$$

Where  $\nu$  is the Kinematic viscosity ( $m^2 s^{-1}$ ),  $r$  is the capillary radius ( $m$ ),  $l$  is the mean hydrostatic head ( $m$ ),  $g$  is the acceleration due to gravity ( $ms^{-2}$ ),  $L$  is the capillary length ( $m$ ),  $V$  is the flow volume of the fluid ( $m^3$ ),  $t$  is the flow time through the tube,  $t = t_2 - t_1$ , ( $s$ ) and  $k$  is the capillary constant in  $m^2 s^{-2}$  [Stachowiak *et al.*, 2001].



*Figure 4.1: Glass capillary kinematic viscometer*

A suspended-level capillary viscometer and a Paar DMA 40 digital density meter were used to determine the kinematic viscosity and the density of the products respectively. The viscometer is a U-shaped piece of glassware (*Figure 4.1*). It has a reservoir on one side and a measuring bulb with a capillary on the other. It has an additional arm extending from the end of the capillary. This arm is to ensure that the pressure head is only dependent on a fixed height and not on the total volume of the liquid in the viscometer. The viscometer was immersed in a water bath equipped with a thermostatic temperature controller (*Figure 4.2*). The controller controls the temperature of the

system within accuracy of  $0.5^{\circ}\text{C}$ . The sample was introduced into the reservoir of the viscometer. The temperature was set to  $20^{\circ}\text{C}$  and the system was allowed to attain thermal equilibrium. The sample was sucked through the capillary and measuring bulb with a syringe and allowed to travel back through the measuring bulb. The time it takes the sample to travel back through the two calibrated marks was used along with the calibration constant to calculate the kinematic viscosity of the sample. Duplicate measurements were performed and an average value taken. Measurements were performed at temperature intervals of  $10^{\circ}\text{C}$ .

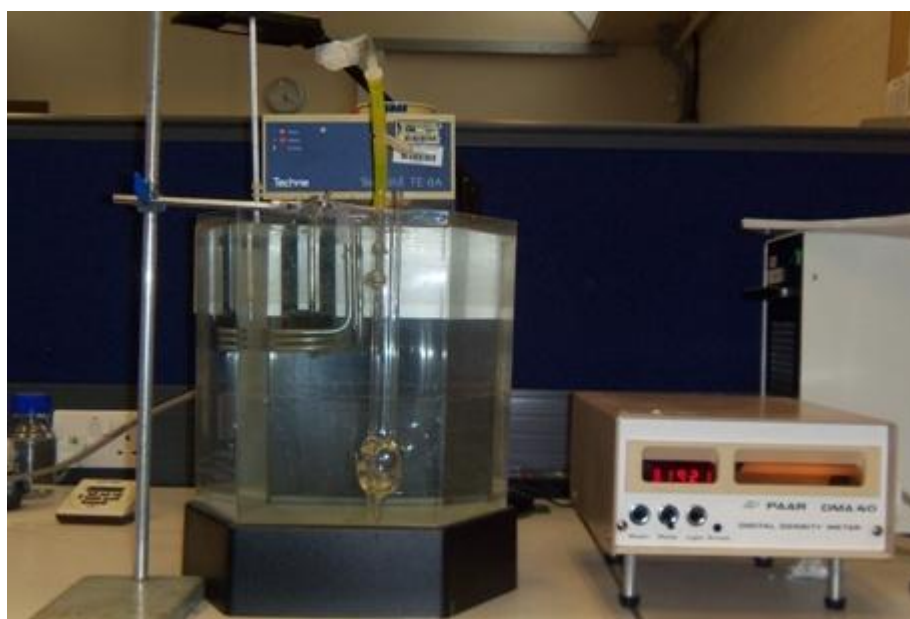


*Figure 4.2: Viscosity and Density Measurement Setup*

The Paar DMA 40 digital density meter shown in *Figure 4.2* has a U-tube glass capillary oscillator as sample tube. The tube is mounted in the centre of a double walled cylinder filled with a gas of high thermal conductivity and fused at both ends. The U-tube was completely filled with the sample without the presence of bubbles, and thermostatically controlled water was allowed to flow between the outer and the inner wall of the cylinder to control the temperature of the sample. The temperature was set to  $20^{\circ}\text{C}$  and the system was allowed to attain thermal equilibrium. The power was switched on to set the sample tube in oscillation and the period of oscillation was taken from the readout on the instrument. The density of the sample was evaluated from the oscillation period. The coefficient of thermal expansion of the samples was evaluated from the obtained data on density in line with ASTM D1903 standard test method.

### **4.3.2 Differential Scanning Calorimetry (DSC)**

The melting behaviour of the oil samples were analyzed using DSC technique. This was carried out using Mettler Toledo DSC1 instrument. A sample of known mass was placed in the aluminium crucible and sealed with the crucible sealing press. The sealed crucible was then placed in the furnace of the DSC and was thermally treated to equilibrate the sample at a starting temperature sufficiently below the onset of crystallization [Hinz *et al*, 2001]. The following procedure was used to stabilize the sample under nitrogen. The sample was heated from 25°C to 50°C at a rate of 50°C/min. It was held at that temperature for 1 minute, cooled to -100°C at a rate -50°C/min and held for 2 minutes. It was then heated to 50°C at a rate 50°C/min and held for 4 minutes. The heat flow through the sample was then measured while cooling the sample from 50°C to -100°C at a rate -10°C/min. It was held for 10 minutes at -100°C, and heat flow was measured while heating to 60°C at a rate 10°C/min. The choice of 60°C was because it is above the melting point of palm kernel oil.

A similar thermal treatment procedure as described above was followed to stabilize the sample for oxidative stability test. The sample was cooled in the furnace to -50°C at a rate -50°C/min and held for 2 minutes. It was then heated to 50°C at a rate 50°C/min and held for 4 minutes, and cooled to -50 °C at the rate of -10°C/min. The nitrogen atmosphere was replaced with oxygen and was held at -50°C for 10 minutes to expose the sample to oxygen atmosphere. The heat flow through the sample was then measured while heating the sample from -50°C to 350°C at a rate 10°C/min. 350°C was chosen as the maximum temperature because pyrolysis of alkyl ester occurs around 300°C. The thermal analysis was carried out using STARe software. All measurements were repeated three times and the averages were taken.

### **4.3.3 Pour Point Temperature**

The pour point of a sample is the lowest temperature at which the flow of the test sample is observed under standard test conditions. The test was carried out at SGS United Kingdom Ltd in accordance with IP15/ISO 3016. The sample was preliminarily heated to 48°C before the test jar was transferred to a bath maintained at  $24 \pm 1.5^\circ\text{C}$  and observation for pour point commenced. The specimen was cooled at a rate of 1.5°C and the appearance and flow characteristic of the specimen was visually examined. The test jar was tilted at temperature interval of 3°C to certain movement of the specimen in the

jar. The lowest temperature at which movement of the test specimen is visually observed was recorded as the pour point of the sample.

#### **4.3.4 Flash Point**

This test is used to assess the flammability hazard of the ester fluids. The flash point of a sample is the lowest temperature at which the vapour of a specimen from the sample will form a flammable mixture with air under atmospheric pressure. The test was carried out at SGS United Kingdom Ltd using the Cleveland Open cup in accordance with ASTM D92/IP 36.

#### **4.3.5 Acidity**

Acidity of the ester fluids is a measure of the acidic constituents that are present as impurities in the fluid. Processing of the ester involves acids. The acidic content of insulating fluid increased with ageing since acidic products are among the by-products of ageing. The test can be used as a measure of quality control of freshly prepared oil for insulation and insulating oil in use. The acidic content of the ester samples was determined using colour indicator titration and is expressed in milligrams of potassium hydroxide per gram of the sample required to neutralize the sample. The test was carried out at SGS United Kingdom Ltd in accordance with EN 62021/IEC 62021.

#### **4.3.6 Water Content**

Water content has effect on the dielectric properties of insulating fluid. Excessive water content may deteriorate the breakdown characteristic of the insulating fluid. This test assessed the quality of the synthesized esters. This test was carried out at SGS United Kingdom Ltd using automatic coulometric Karl Fischer titration in accordance with EN 60814/IEC 60814.

### **4.4 Dielectric Response**

Since the useful life time of oil-filled electric equipment is based on the insulation system, adequate knowledge of the dielectric behaviour of an intended fluid for insulation is important in terms of dielectric loss. This is to ascertain its suitability as insulating fluid in terms dielectric loss. In this section broadband dielectric spectroscopy is employed to investigate the dielectric phenomenon in the synthesized ester fluids.

#### 4.4.1 Dielectric Response Measurement Technique

Dielectric response measurements in both time and frequency domains have been in use over the years in the characterization of dielectric behaviour of materials. The complex impedance of the sample under test is measured at a specified temperature. The complex capacitance can be obtained using the frequency response analyzer in *Figure 4.3*. An alternating sinusoidal electric field is applied to the sample by the generator and the dielectric interface converts the sample current to voltage [Hinton *et al*, 1998]. The amplitude and phases of the source voltage and output voltage are measured by two phase-sensitive voltmeters. The sample's complex impedance  $Z_s^*$  is evaluated with the relation [Vassilikou-Dova *et al*, 2009]:

$$Z_s^* = \frac{V_1(\omega)}{I_s(\omega)} = -\frac{V_1(\omega)}{V_2(\omega)} \cdot R \quad 4.2$$

Where  $V_1$  is the source voltage,  $I_s$  is the sample current,  $V_2$  is the output voltage and  $R$  is the gain of the current to voltage converter of the amplifier circuit in the dielectric interface. The complex relative permittivity,  $\epsilon_r^*$  of a sample in a sample holder of capacitance  $C_0$  is related with the complex impedance with the expression:

$$\epsilon_r^* = \frac{1}{i\omega Z_s^*(\omega)C_0} \quad 4.3$$

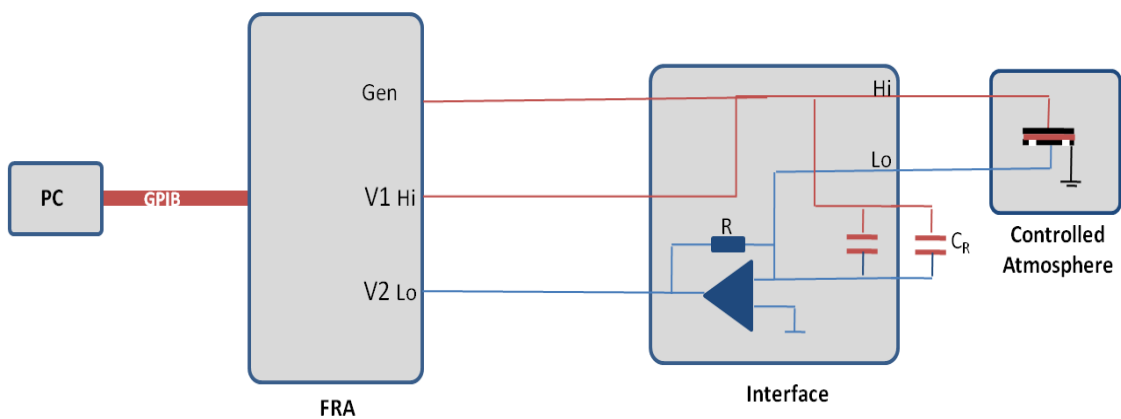


*Figure 4.3: Schematic of frequency response analyzer with dielectric interface*

Frequency response analyzers which are either based on digital lock-in amplifiers or gain-phase analyzers are available for the measurement of complex permittivity covering several decades [Vassilikou-Dova *et al*, 2009]. But such instruments cannot

distinguish between the contributions of the “pure” DC conductivity,  $\sigma_o$  and that of the dielectric loss  $\varepsilon''(\omega)$  [Zaengl, 2003]. The measured complex relative dielectric permittivity  $\varepsilon_r^*(\omega)$  can be defined from equations (4.2) and (4.3) with the expression:

$$\bar{J}^*(\omega) = i\omega\varepsilon_o\varepsilon_r^*(\omega)\bar{E}^*(\omega) \quad 4.4$$

Therefore, the measured effective complex relative permittivity by the instrument is:

$$\varepsilon_r^*(\omega) = \varepsilon_r'(\omega) - i[\varepsilon_r''(\omega) + \sigma_o / \varepsilon_o\omega] \quad 4.5$$

The real part of equation (4.5) represents the charge storage capacity of the test object, whereas the imaginary part represents the loss. Both quantities depend on frequency. They are also dependent on temperature. The dielectric loss tangent resulting from the storage capability, bulk conductivity, and polarization mechanisms of the liquid can also be expressed as [Zaengl, 2003]:

$$\tan \delta(\omega) = \frac{\varepsilon_r''(\omega) + \sigma_o / \varepsilon_o\omega}{\varepsilon_r'(\omega)} \quad 4.6$$

Where in this context,  $\varepsilon_r'(\omega)$  is the real components of the permittivity of the material as a function of angular frequency,  $\varepsilon_r''(\omega)$  is loss due to polarization as a function of angular frequency and  $\sigma_o$  is the DC conductivity. The effective AC conductivity may be defined as the ratio of the dissipated power to the square of the magnitude of the field at a given frequency arising from conduction, charge transport and dipole orientation losses; this may be expressed as [Bartnikas, 1999]:

$$\sigma_{ac}(\omega) = \omega\varepsilon''(\omega) + \sigma_o \quad 4.7$$

#### 4.4.2 Dielectric Liquid Test Cell

A three electrode liquid test cell was designed for this experiment for more accurate measurements as the arrangement prevents erroneous measurements resulting from fringing and stray capacitance effects that would have emerge from a two electrode system (*Figure 4.4*). The designed dielectric test cell consists of guarded and unguarded electrodes, and guard ring.

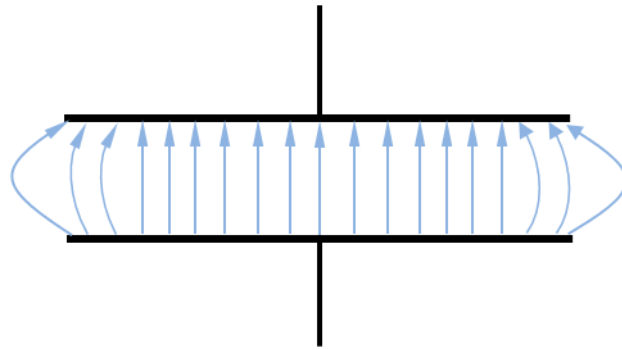


Figure 4.4: Two-electrode terminal arrangement

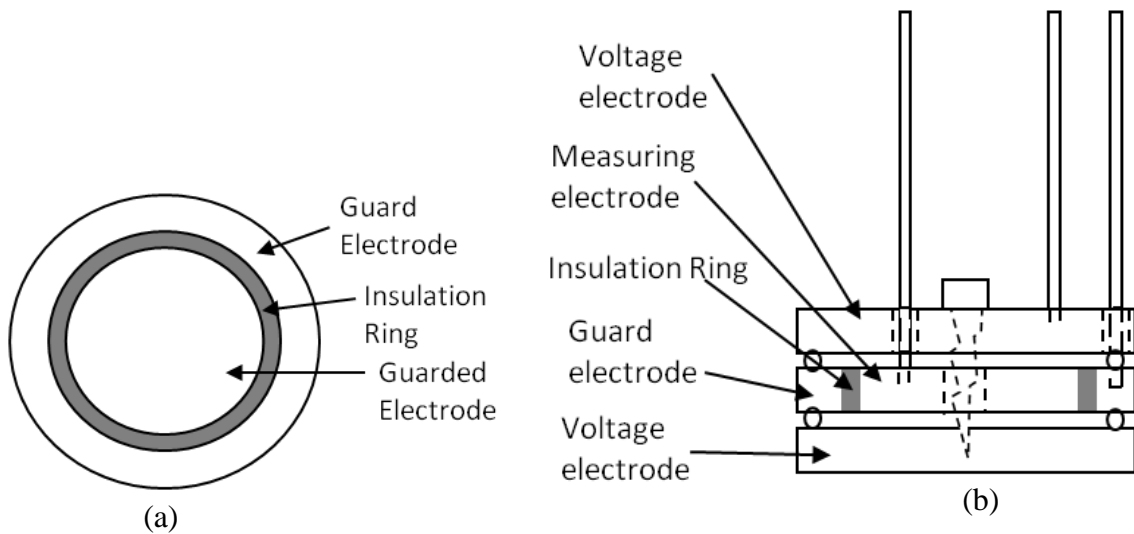
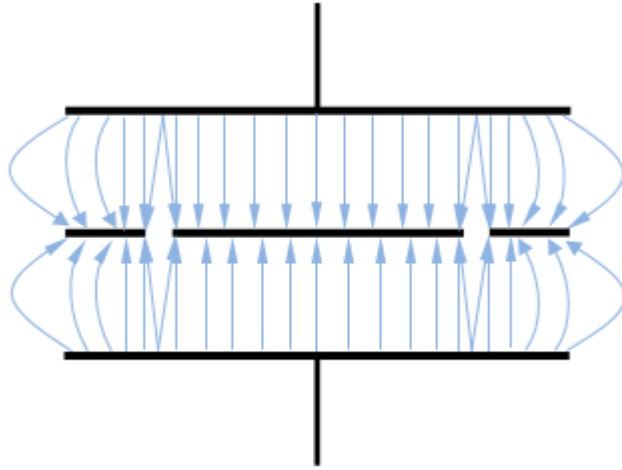


Figure 4.5: Electrodes (a) Measuring Electrode (b) Electrode Arrangement

A measurement test cell was specifically designed for dielectric spectroscopy measurement. The test cell is in two parts; A vessel with the lid, and the voltage electrodes. The voltage electrodes consist of two steel disks on either side of the measurement electrode. The measurement electrode consists of a steel disc surrounded by a guard electrode (Figure 4.5a). The guard electrode eliminates the edge capacitance created by a fringing effect of the two electrodes system (Figure 4.6) [Bartnikas, 1987]. The two voltage electrodes are connected electrically using a clamping screw and glass beads were used as spacers to maintain an electrode gap of 1 mm between the two voltage electrodes and measurement electrode. Using this arrangement doubles the effective area of the electrode system shown in Figure 4.5b. Steel rods were used to form the electrical connections to the guard, measurement and voltage electrodes. The steel rods were fixed to the lid and properly insulated. The stray capacitance between the connecting rods in the cell was eliminated by separating the two rods with aluminium strip as shown Figure 4.7b. The stray capacitance to ground will be eliminated when the cell is placed in oven due to screening by a metal enclosure. The capacitance between

the lead and electrode was minimized by making the coaxial cables as short as possible. Liquid test cells always come with complicated problems such as leakage, thermal expansion of the oil sample etc. The cell was designed such that the electrodes are suspended in the oil sample and the vessel having enough space to accommodate sample expansion. This vessel was made from Perspex cast acrylic which is highly resistant to chemical attack from alkyl esters (*Figure 4.7*). The detailed designed drawing is shown in Appendix B .



*Figure 4.6: Three-electrode terminal arrangement*

The effective area of the unguarded electrode,  $A_e$  was determined with the expression [Bartnikas, 1987]:

$$A_e = \pi \left( r + \frac{Bg}{2} \right)^2 \quad 4.8$$

where

$$B = \exp \left\{ -0.435 \frac{g}{d} \left[ \frac{\epsilon'_r}{\epsilon'_r + \left( \frac{2.182}{\alpha} - 1 \right) \epsilon'_{rg}} \right] \right\} \quad 4.9$$

$g$  = guard gap (cross sectional thickness of the Teflon ring),  $d$  = specimen thickness,  $\epsilon'_r$  = relative permittivity of the dielectric material,  $\epsilon'_{rg}$  = relative permittivity of the medium in the gap,  $a$  = thickness of electrode and  $\alpha = a/g$ ; for thick electrode  $\alpha \rightarrow 8/\pi^2$  when  $a/g \geq 1$ .

The effective area of each of the voltage electrodes is  $3.913 \times 10^{-4} \text{ m}^2$ . The capacitance calculated using  $\epsilon_0 = 8.854 \times 10^{-12} \text{ F}$  as permittivity of free space is 7.70 pF, while the average value of the measured capacitance of the cell in free space using the dielectric

spectrometer is 8.08 pF with 2.4% standard error. The test cell was calibrated using trichloroethylene. The measured value of the dielectric constant was 3.37 at 100Hz which is in agreement with the literature value of 3.347 [Wohlfarth, 2008]. It was also used to measure the dielectric constant of mineral insulating oil which was 2.19 at 100Hz and 30°C which is also comparable to the literature value of 2.1 [Pearmain *et al*, 2003].

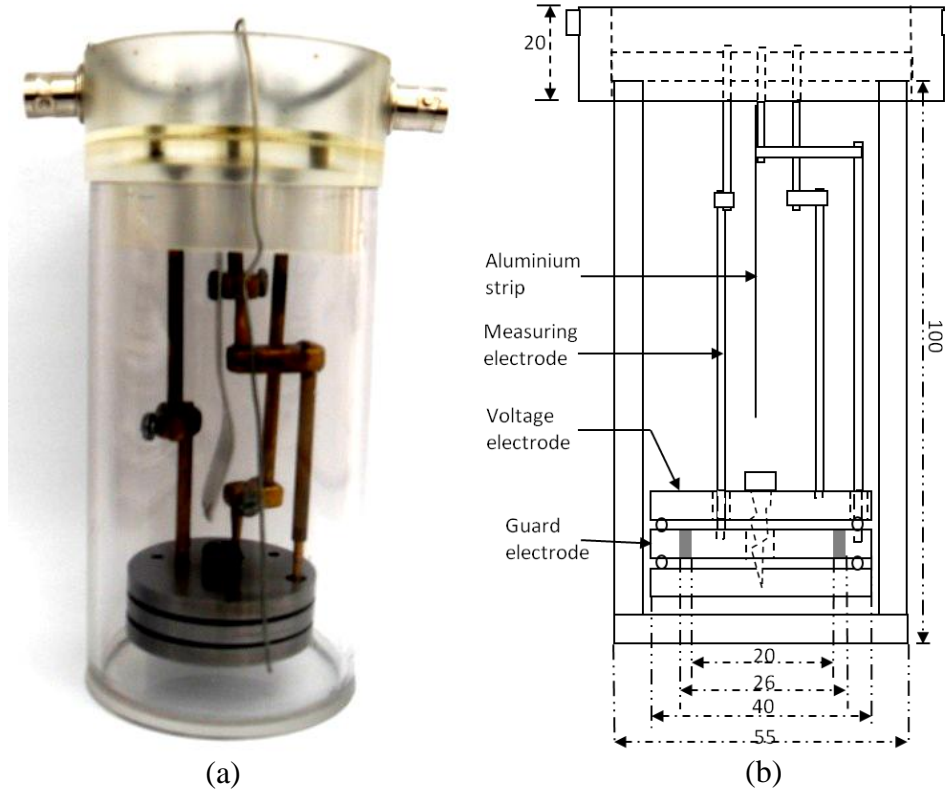
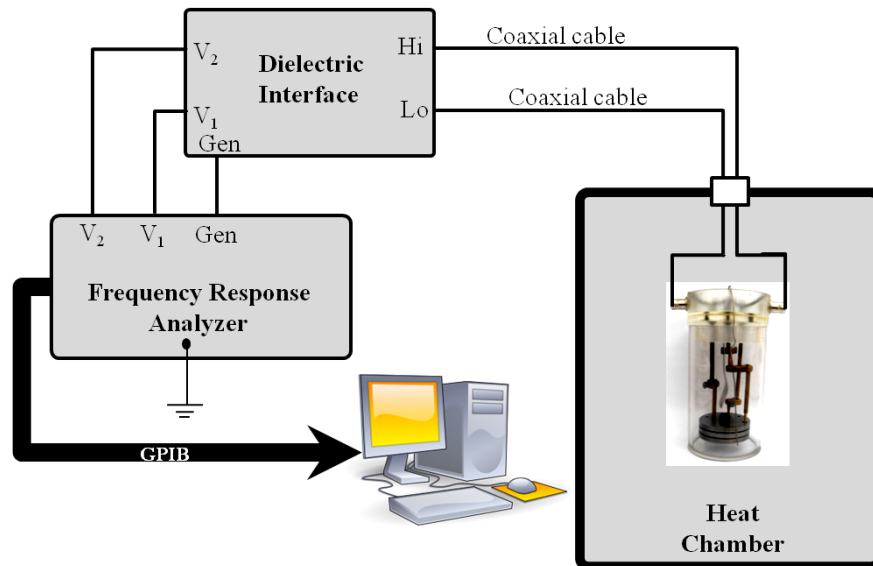


Figure 4.7: A specially designed liquid test cells, (a) three test electrode cell, (b) Schematic diagram (dimension in mm)

#### 4.4.3 Dielectric Measurement Set-up

The frequency domain dielectric response of the liquid samples was tested in the bespoke three-electrode dielectric liquid test cell. The test cell was first dismantled and each piece was cleaned with methanol, followed by acetone. They were properly dried and fixed together. A sample of about 25 ml was placed in the vessel. Filling of the test cell for each sample requires care to avoid trapping of bubbles between the electrodes. The electrode was suspended in the oil. The test cell was placed in an oven equipped with a temperature controller to control the temperature of the samples and the electrodes were connected to a Solartron 1296 Dielectric Interface. The dielectric

interface was connected to Solartron 1255 Frequency Response Analyzer and controlled by a desktop computer in order to measure the dielectric response of the sample (*Figure 4.8*). The oven also provided a noise-suppressed environment for dielectric measurements because it is a grounded metal box. Frequency domain measurements were made using a sinusoidal signal of  $2\text{ V rms}$  for excitation. The complex impedance of the sample under test was measured over the frequency range  $10^{-3} - 10^6\text{ Hz}$  and at a number of fixed temperatures. The temperature ranged from  $20$  to  $80 \pm 1^\circ\text{C}$  at an interval of  $10^\circ\text{C}$ . The impedance measurement error was about 2%. The samples were kept at each temperature for 3 hours before starting the measurement to allow the electrodes and sample to be in thermal equilibrium. The complex capacitance can be obtained from the measurement from the measured complex impedance as expressed in equation 4.3.



*Figure 4.8: FRA experimental system for Dielectric Liquid*

#### 4.4.4 DC Conductivity Measurement Set-up

The same three-electrode test cell and Keithley 6430 picoammeter was used for DC conductivity measurements. The picoammeter was connected to a PC and controlled using software running under Labview environment. The software provides features such as number of sampling per second and initial delay times. A protection circuit enclosed in a light tight shield,  $P$ , was connected between the measurement electrode of the test cell and the picoammeter input. This is to prevent damage from excessive voltage from the input. A low electric field was applied across the sample. The voltage

was varied from 5 to 500 V and no observed increase in  $V/I$ . 5 V was chosen to minimize charge carrier generation by field enhancement or injections. The software was used to acquire the current that flows through the sample. The conductivity was calculated using the acquired charging current with the geometry of the test cell.

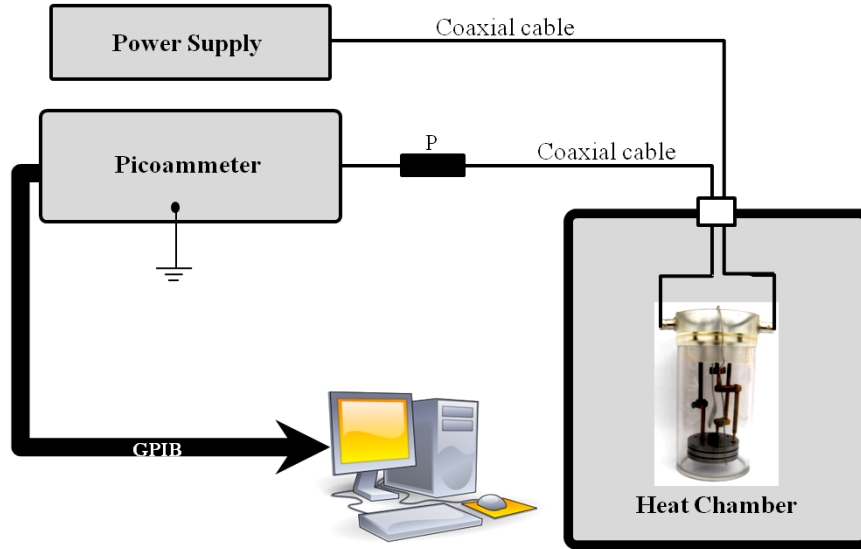


Figure 4.9: DC Conductivity Experimental System

## 4.5 Dielectric Breakdown

The breakdown field strength of a dielectric material is a very important parameter as it helps transformer designers to ensure correct distances between live and grounded conductors. This is necessary to protect the live part of transformers from the grounded part, and prevent the field in the system from increasing above the dielectric breakdown strength of the system. The insulation system often involves a combination of solid and liquid. An understanding of their breakdown behaviour under electrical stress is very important. This section describes the setup designed for the characterization of the breakdown strength of the materials.

### 4.5.1 Breakdown Test Cell

A breakdown test cell was designed especially for electrical breakdown measurement (Figure 4.10). The design took into cognisance of the limitation of sample quantity. A cylindrical cell was made from a Perspex cast acrylic block to host the oil sample and the electrodes. This material was selected as it is transparent and resistant to chemical attack by alkyl ester. A transparent material was used to ensure that there were no

trapped air bubbles in the test cell before the start of the experiment. The electrodes consist of two stainless steel spheres of a radius of 12.5 mm and in contact with brass rods to provide HV and LV electrical connection. A Perspex acrylic spacer was used between the sphere electrodes to give a gap of 1 mm. The maximum electric field strength between the spherical electrodes was evaluated using Cloete and van der Merwe's method for two conducting spheres using the method of images. The electric field enhancement was calculated to be 2.68%. This small field enhancement was due to the radius of the electrodes being much greater than the inter-electrode gap [Cloete *et al*, 1998]. The cell was designed for small sample volume ( $\approx 15$ ml) measurement as compared with the IEC 156:1995 standard designed cell with volumes of 350 ml to 600 ml. The mean breakdown voltage of Nynas 10GBN mineral oil, 26.4 kV peak-to-peak, obtained with the bespoke breakdown test cell with standard deviation of 1.8 kV is comparable with the breakdown voltage of mineral insulating oil reported in literature using the standard ASTM test cell [Dervos *et al*, 2005]. Insulating oil in electric equipment with voltage rating of 345 kV and above was reported to have a breakdown field of 26 kV/mm [Dervos *et al*, 2005]. The standard deviation of 1.8 kV/mm is approximately 7% of the breakdown strength value. The percentage of standard deviation of breakdown strength as recommended by ASTM should not exceed 10%, and the percentage standard deviation of the measurements taken with the new bespoke test cell is lower, demonstrating a good reproducibility of measurement taken using the bespoke cell. This bespoke cell is simple and useful in laboratory breakdown measurements where small volumes of liquid samples are involved and could also reduce the cost of producing large samples for laboratory analysis during processing of dielectric fluid. The test cell can be easily cleaned and the electrodes can be replaced easily in case of any damage as the parts can be easily dismantled. The sphere electrodes were separated from each other using solid insulator as spacer. Since the sphere sits on the spacer, creeping discharge may occur along the surface of the spacer and this can influence the measured breakdown values. The reported breakdown values in this work may need to be verified using standard breakdown test cell after large sample synthesis.

#### **4.5.2 Experimental Setup**

The breakdown test setup shown in *Figure 4.11* consists of a transformer control unit (TCU), a variable transformer, 50 kV step-up transformer with a low voltage secondary

tap to monitor the applied voltage using a multimeter. A current limit resistor was also connected in series with the sample cell. The test cell was cleaned up with methanol and followed by acetone. 15 ml of sample that have been dried in vacuum oven for 2 hours at 80°C was carefully introduced into the cell to avoid air bubbles. The spacer was placed between the spheres to create the 1 mm gap. The high voltage electrode was placed on top of the high voltage sphere and measurement of electrical breakdown field of an electrical insulating liquid was carried out under a progressive stress regime. The applied voltage was increased from zero at a rate of approximately  $0.5\pm 0.1$  kV/s until breakdown occurred. The TCU monitors the cell current and interrupts the supply voltage to the step-up transformer when breakdown occurs in the sample cell. The resistor provides a limitation of the current when breakdown occurs, thereby limiting the energy dissipated in the test cell and protects the TCU from damage. The voltage prior to the interruption of the voltage supply was taken as the breakdown voltage of the sample. Carbonized particles were observed in the liquid after breakdown. Since the cell is small and sample volume is small, the particles can influence subsequent breakdown. To minimize the amount of particles, fresh oil specimen was used for each breakdown and the oil was allowed 15 minutes to settle before breakdown. Electroerosion was observed on the surface of the sphere electrode after breakdown resulting from electrical discharges. New sphere electrodes were used for each breakdown since such eroded surface can lead to partial discharge.

#### **4.6 Laboratory Ageing System**

Accelerated ageing is carried out to predict the reliability of insulating material when in operation over a specified period of time. Ideal ageing test should include electrical, thermal and mechanical stresses which are actually responsible for ageing in transformers during operation. But thermal stress dominates the ageing factors and so the simulated ageing test was based on accelerated thermal ageing to induce the ageing mechanisms within a short period of time. Ageing behaviour data on ester-based oil is still very scarce and also, laboratory simulation of a replica of insulation system in transformers still poses a challenge to researchers. Since abundant data on ageing behaviour of mineral oil-based insulating fluid is available, a comparative study of accelerated aged mineral oil and natural ester insulating oil is often used to extract information on the ageing behaviour of natural ester-based insulating fluid. This section

describes the design of a pressure vessel to simulate an insulating system for accelerated ageing test and the setup for the ageing process.

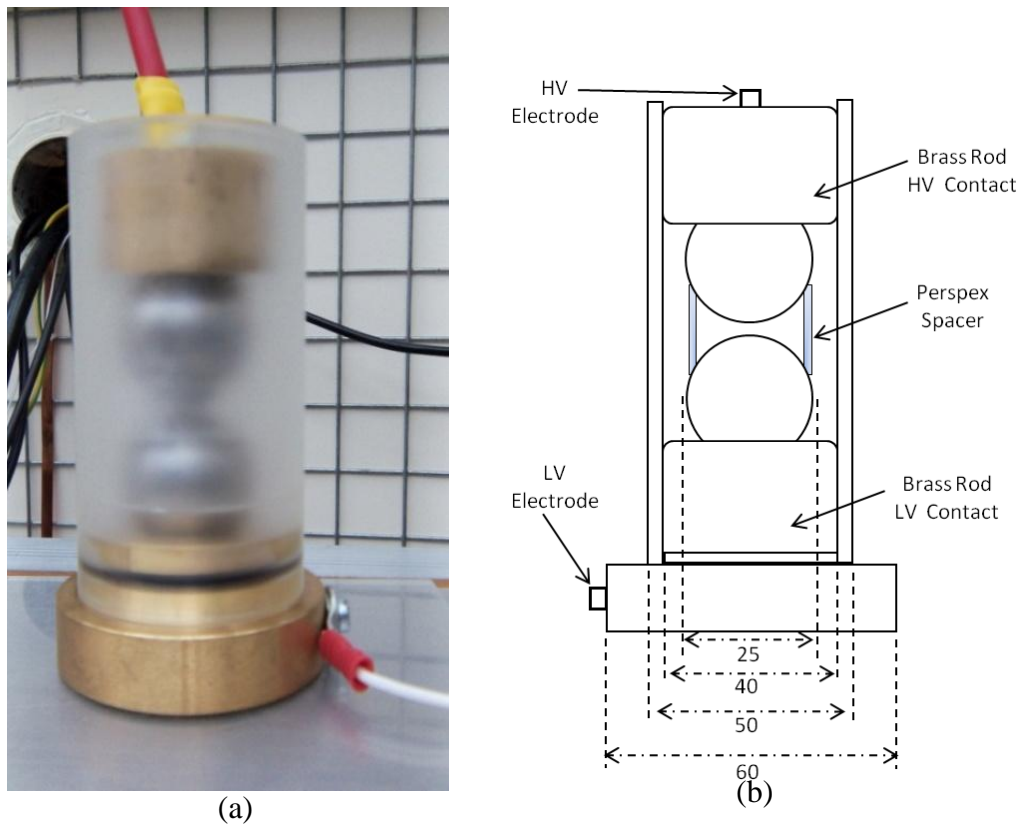


Figure 4.10: Bespoke Dielectric Breakdown Test Cell (a) sphere-sphere breakdown test cell, (b) Schematic diagram (dimensions in mm)

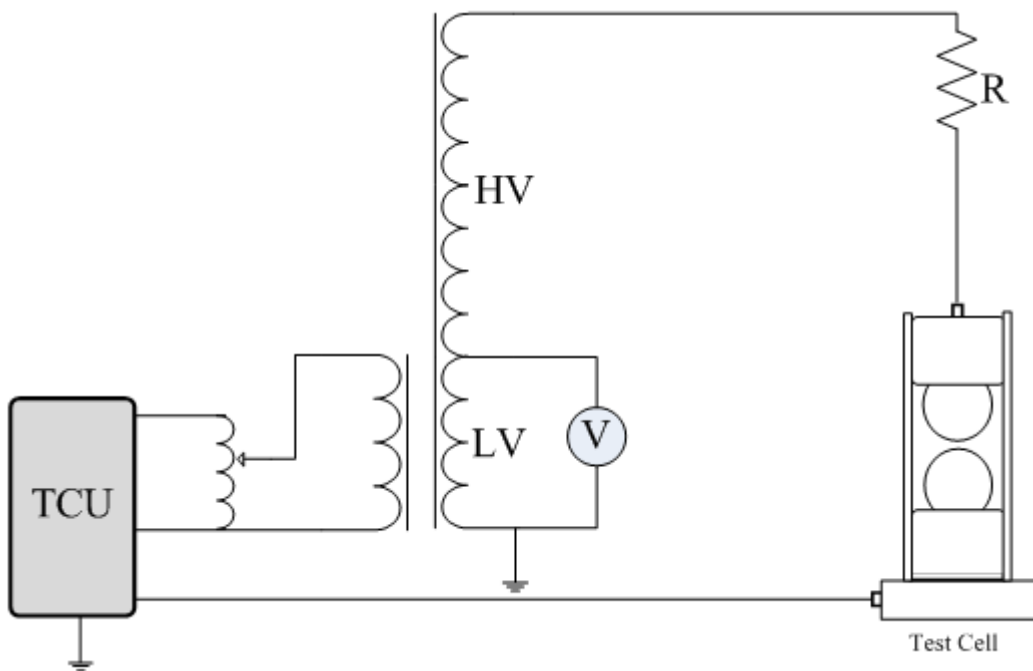


Figure 4.11: Schematic of electric breakdown test

#### 4.6.1 Ageing Vessel

A laboratory ageing system was designed to model an insulation system of a typical HV power transformer. A pressure vessel shown in Figure 4.12 was made from mild steel. The choice of mild steel is in line with the fact that the casing of transformers which hosts the transformer oil is equally made of mild steel. The vessel has been designed such that it is able to withstand the internal pressure of the vessel during the ageing experiment. The expression to determine the minimum required thickness of a cylindrical shell in ASME Boiler and Pressure Vessel Code Section III, Division 1, for a moderately thick shell pressure vessel employing thin-walled theory is [Chattopadhyay, 2005]:

$$t_m = \frac{P \cdot r}{S \cdot E - 0.6P} \quad 4.10$$

Where  $P$  = maximum operating pressure,  $r$  = radius of the vessel,  $S$  = maximum allowable stress, and  $E$  = Welding efficiency. In this design, the value of  $E = 1$  because the cylinder was machined from steel rod and the base was not welded. The wall and base thickness of the vessel was based on equation 4.10 and the full calculation is presented in Appendix D . From the theoretical calculation, the minimum thickness of the wall and base of the vessel that can withstand the expected  $600 \text{ kNm}^{-2}$  (maximum pressure) is 0.25 mm. A wall thickness of 10 mm was chosen for the designed vessel, while 5 mm was chosen for the base thickness. These values were chosen to enable the fitting of the accessories on the vessel. The vessel has internal diameter of 80 mm, external diameter of 100 mm and 135 mm deep.

The lid has a flange of diameter and thickness of 100 mm and 5 mm respectively, and a groove of diameter and thickness 15 mm and 79 mm respectively. A fluoroelastomer O-ring of cross-section diameter and inside diameter of  $2.62 \pm 0.08 \text{ mm}$  and  $74.27 \pm 0.61 \text{ mm}$  respectively seats in a groove in the lid between the lid and the cylinder. The O-ring is compressed between the lid and the cylinder creating a seal at the lid-cylinder interface. The chosen O-ring can accommodate a continuous temperature of up to  $200^\circ\text{C}$  and is resistant to vegetable oils [Walker, 2006]. The lid has an inlet and outlet connections. The outlet contained a bleeder valve serving as the outlet for the gas in the vessel. The inlet is a brass tube ( $2.5 \text{ mm OD} \times 1.8 \text{ mm ID}$ ) fitted on the lid to serve as temperature standoff to isolate the pressure transducer to monitor

the pressure of the system from the hot fluid and hot oven. The vessel was sealed with screws of diameter 4mm having tensile strength of about 81 kN, and can withstand pressure up about  $6 \text{ MNm}^{-2}$  (932 psi or 64 bar). The vessel was tested for leakage by filling it with oil and applied compressed air of about  $689.5 \text{ kNm}^{-2}$  (100 psi). The detail designed drawing is shown in Appendix C .

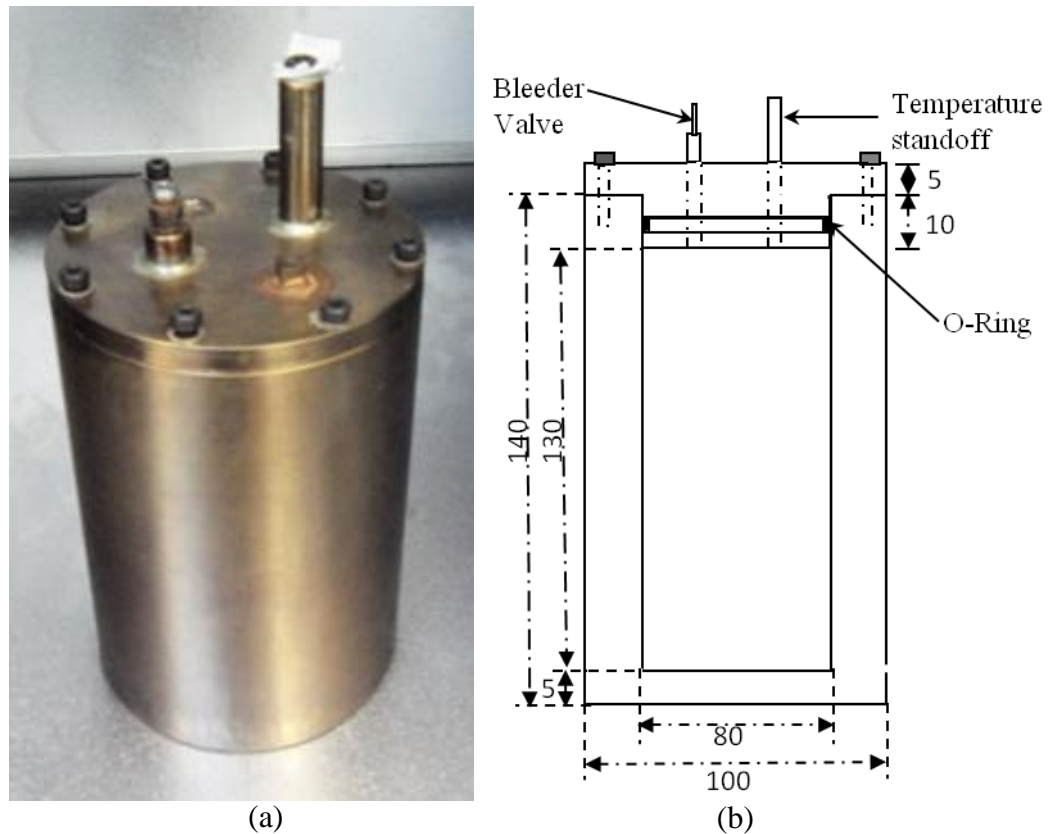
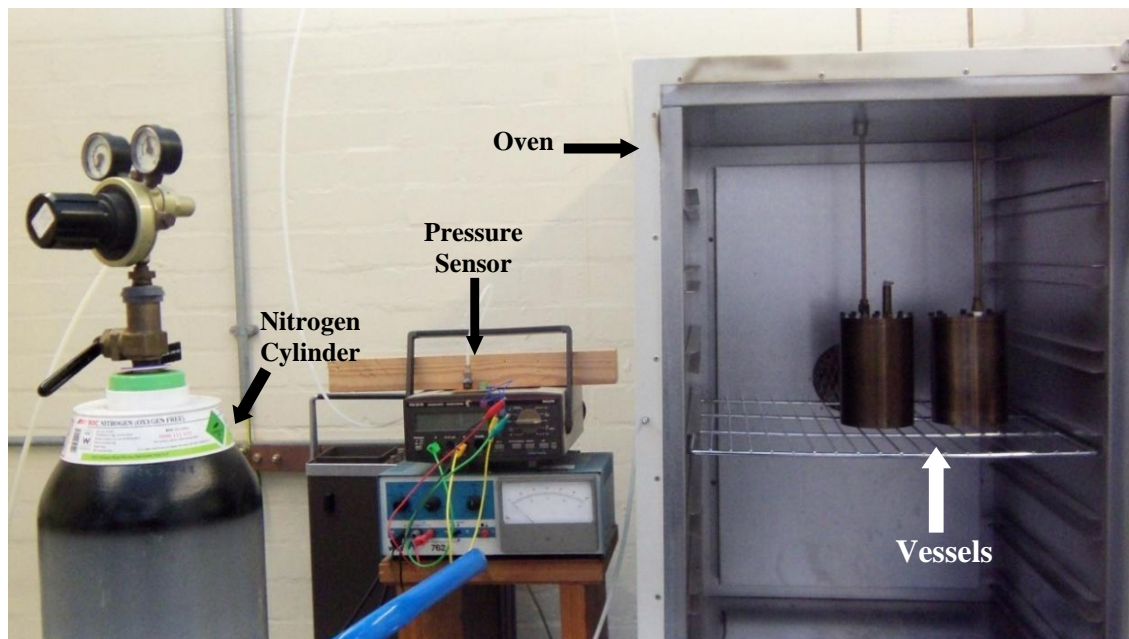


Figure 4.12: Designed Ageing Vessel (a) Pressure Vessel, (b) Schematic Diagram in mm

#### 4.6.2 Experimental Setup

400 ml each of Nynas 10GBN mineral oil and PKOAE1 was degassed and dried in an oven at  $85^{\circ}\text{C}$  for 2 hours. It was allowed to cool to ambient temperature and transferred to the ageing vessel. The thermally upgraded insulating paper was vacuum dried in oven at  $85^{\circ}\text{C}$  for 24 hours. The ageing vessel containing the oil sample, 33 g of 0.255 mm thermally upgraded paper,  $150 \text{ cm}^2$  galvanized steel strip,  $112.8 \text{ cm}^2$  copper strip, and  $150 \text{ cm}^2$  aluminium strip, was placed in vacuum oven for 30 minutes at ambient temperature following the Cooper Power System laboratory ageing setup [McShane, *et al*, 2001]. The galvanized steel represent the core of a transformer, while the copper and aluminium strip represents the conducting coils. The vessel was sealed with the lid at ambient temperature and placed in the ageing oven (Figure 4.13). A male taper straight

adaptor that can withstand pressure of  $1.5 \text{ MN}\cdot\text{m}^{-2}$  (15 bar) and temperature of  $70^\circ\text{C}$  was fixed to the tip of the brass tube. A male taper straight adaptor was also attached to a digital pressure sensor. The sensor which is fixed on a board shown in *Figure 4.14* was used for monitoring the pressure of the system. Silicone tubing was connected to the nitrogen cylinder, ageing vessel and the pressure sensor and was linked together using a female BSPP tee connector.



*Figure 4.13: Accelerated Ageing Setup*

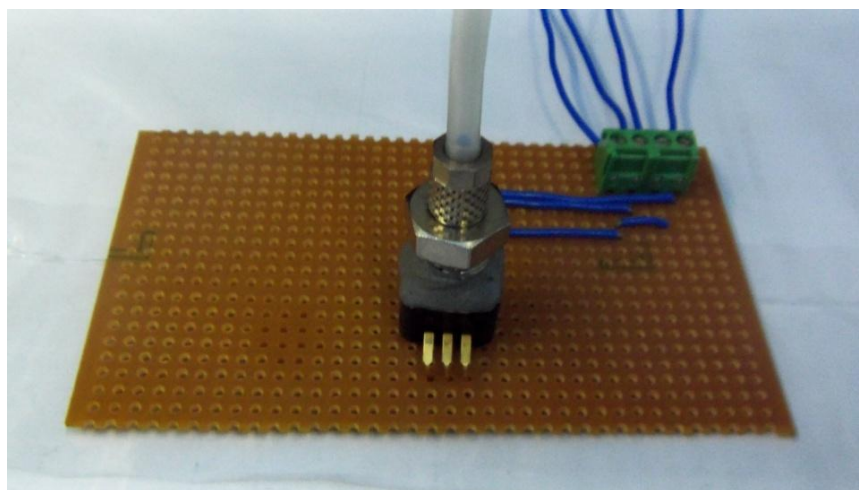


*Figure 4.14: Pressure sensor*

The air in the vessel was purged out with dry nitrogen through the bleeder valve and then locked. The pressure of nitrogen in the vessel was increased to  $400 \text{ kN}\cdot\text{m}^{-2}$ . The pressure was maintained at  $600 \text{ kN}\cdot\text{m}^{-2}$  (6 bar) throughout the ageing period. A pressure

of  $600 \text{ kN}\cdot\text{m}^{-2}$  was chosen because the saturated vapour pressure of water at  $150^\circ\text{C}$  is  $450 \text{ kN}\cdot\text{m}^{-2}$ . This was to disallow evaporation of the moisture in the oil, forming water on the lid and getting back into the oil as water droplets. The ageing was carried out at  $150^\circ\text{C}$  for 3 months. Samples of oil and paper were taken out of the vessel after 28 days, 56 days, and 84 days respectively for analysis.



*Figure 4.15: Tensile Strength Measurement*

#### **4.7 Tensile Strength Measurement**

This section describes the experimental setup for the mechanical strength of the oil impregnated insulating paper samples. The tensile strength of the impregnated paper samples was determined using an Instron 3343 Single Column Testing System (*Figure 4.15*). The instrument has force capacity of 500 N. The tensile specimens were prepared by cutting the paper samples of 0.255 mm in thickness into the appropriate “dog bone” shape. It has two shoulders and a gauge section in between. The gauge section of each specimen has length and width of 30 mm and 4 mm respectively. Five specimens were prepared from each sample. Each specimen was properly positioned in the test machine and the shoulders of the samples were firmly gripped by the upper and lower tensile grips of the test machine. Tension was applied on the specimen till deformation and

failure occurred within the gauge section. The tensile stress was analyzed using Bluehill 2 testing software.

#### **4.8 Summary**

This chapter described two spectrometric methods that are capable of identifying the fatty acids in the esters and the respective functional group of the respective fatty acids. The chapter also presented a description of the methodology used in studying the low and high temperature thermo-physical properties of the ester fluids. The melting and thermo-oxidative behaviour of the samples will be evaluated after scanning the sample with heat flow within the temperature of  $-50^{\circ}\text{C}$  and  $350^{\circ}\text{C}$ . The dynamic viscosity of the fluids which influence the heat transferability will be determined by measuring the kinematic viscosity and density of the fluids using the described technique. Bespoke test cells have been designed for measurements involving dielectric, breakdown and ageing studies. The respective test cells in combination with the described dielectric response test setup, breakdown field test setup, and accelerating ageing setup will be used to acquire data on the dielectric behaviour and electric field strength of the synthesized esters. The influence of thermal ageing on the mechanical strength of the oil-paper system will be characterized using the tensile strength measurement setup. The acquired data from these experimental methods will be analyzed in the next chapter.

## **Chapter 5. Results and Analysis of PKO and Synthesized Esters**

### **5.1 Introduction**

This chapter presents the results and interpretation of the thermo-physical and electrical measurements on as received palm kernel oil, refined palm kernel oil, and the freshly synthesized esters of the oil.

### **5.2 Spectrometry Identification of Ester Molecules**

Natural ester is known to consist of fatty acids of various chain lengths as described in Chapter 1. The synthesis involves the modification of the chemical structure through conversion of the double bonds to a more complex structure as discussed in Chapter 3. It was necessary to monitor the chemical reaction to know when the required product is obtained and identify the functional groups in the synthesized esters. GC-MS and FTIR were used for the chemical analysis and samples PKOAE1, PKOAE2, PKOAE3, and PKOAE4 were analyzed in this section.

### **5.3 Gas Chromatography-Mass Spectrometry (GC-MS) of the Synthesized Esters**

Alkyl ester of palm kernel oil is an ester containing different fatty acids. Gas chromatography (GC) is an analytical chemistry tool that can separate the ester into its respective components and the analysis of the individual fatty acids can be done using mass spectrometry. The composition of the alkyl esters was analyzed using a Perkin Elmer AutoSystem XL Gas Chromatograph and TurboMass Mass spectrometer (GC-MS). The GC separates the various chemical components of the respective samples and then the mass spectrometer (MS) identify each component in the sample based on its mass-to-charge ratio.

The samples were analysed with GC-MS to identify the components of PKOAE1 and to compare this with the chemically modified esters that were subsequently synthesized. After the injection of the sample into the oven of the Gas Chromatogram, further heating in the oven caused the vaporization of the sample. The volatile components of the oil were transferred by helium gas through the column. The column has a stationary phase which consists of beads of an inert solid supported and coated with a high-boiling liquid. The elution time of the components in the stationary phase depends on the chemical structure of the respective components. The characteristic of gas

chromatography separating two adjacent peaks can be expressed according to the equation 5.1.

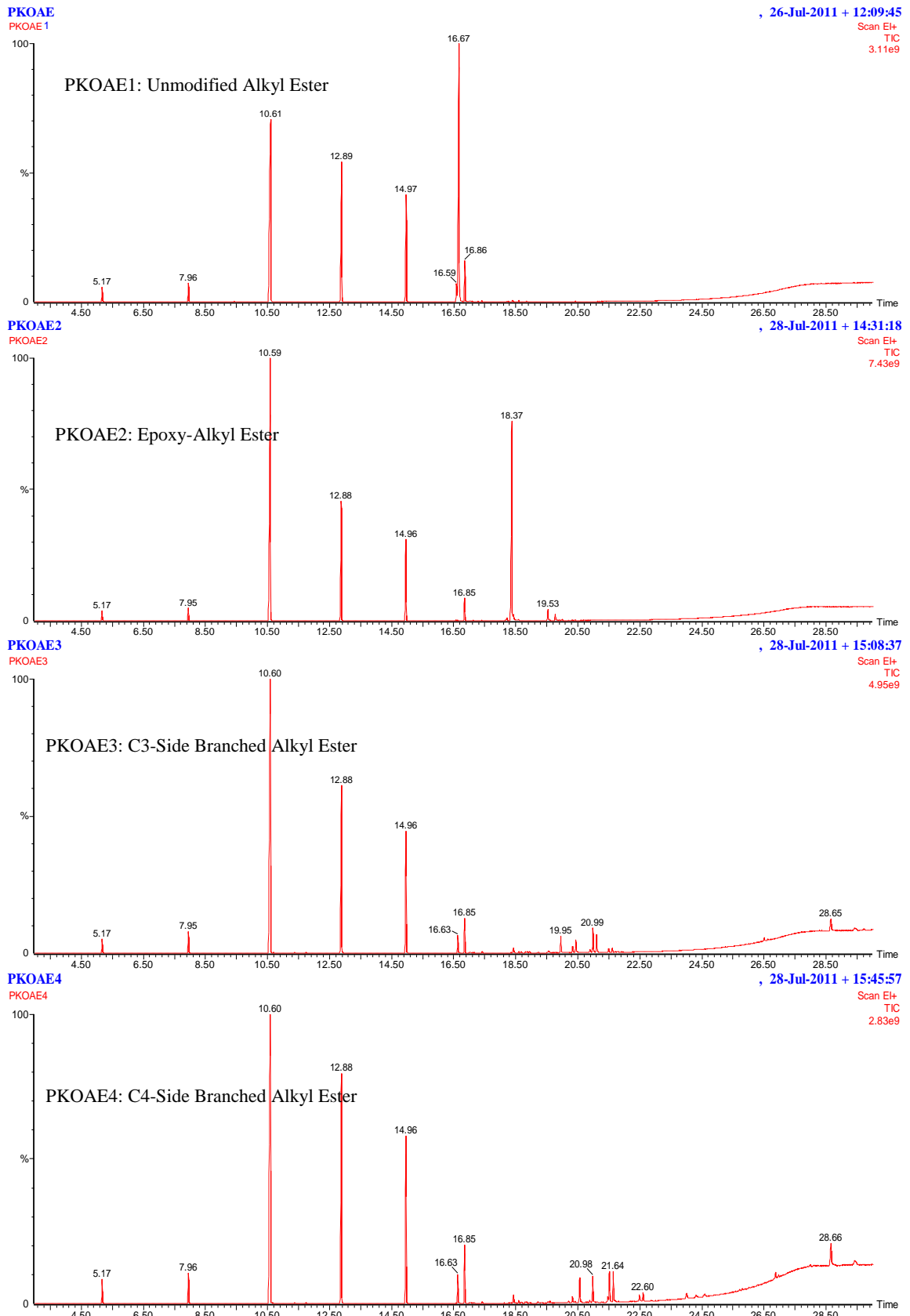


Figure 5.1: GC of Ester samples (time in minutes)

$$R_{AB} = 2 \frac{|d_R(B) - d_R(A)|}{|w(B) + w(A)|} \quad 5.1$$

where  $R_{AB}$  is the resolution,  $d_R(A)$  and  $d_R(B)$  are the retention distances (time) of each eluted component  $A$  and  $B$ , and  $w(A)$  and  $w(B)$  are the respective width each peak base [IUPAC, 2011].

The gas chromatograms of the alkyl esters are shown in *Figure 5.1*. The peaks displayed on such chromatograms represent the chemical components of the respective esters. The peaks in each chromatogram are normalized to the peak with the maximum height. The relative percentage of the components can be determined from area of the peak. From the displayed chromatograms, the samples appeared to have some common peaks. These are likely to be related to the components of the saturated fatty acid esters that did not undergo modification during synthesis. The first elution occurred after 5.17 minutes. This peak was followed by elution at 7.96 minutes, 10.61 minutes, 12.89 minutes, 14.97 minutes, and 16.86 minutes respectively. PKOAE1 had additional elution peaks at 16.59 minutes, and 16.67 minutes which disappeared during the synthesis of PKOAE2. This indicates that the components with peaks at 16.59 minutes, and 16.67 minutes were involved in the modification processes. The PKOAE2 chromatogram in turn displayed additional elution peaks at 18.37 minutes and 19.53 minutes due to the presence of epoxides. This is an indication that a complete conversion of C=C to epoxy rings had taken place. The chromatograms of PKOAE3 and PKOAE4 show the disappearance of peaks at elution time of 18.37 and 19.53 minutes, and appearance of elution peaks of 19.95 and 20.99 minutes. These are likely to have resulted from the fragmentation of the components of the grafted side branched hydrocarbon chains.

The interface responsible for the transfer of the effluents from GC to MS is such that the analytes did not condense at the interface or decompose before arriving at the mass spectrometer ion source [Kitson *et al*, 1996]. On the injection of the chemical constituents from the gas chromatogram, they were directly exposed to an ion source which breaks up the electron gas into a number of molecular fragments which were then characterized in terms of their  $m/z$  ratio. The detector detects the ions with a resolution of a single atomic mass unit. The resultant ‘fingerprints’ are then compared with a data base of known chemical structures. The mass spectra show the fingerprints of the

detected gas chromatogram peaks. The mass spectra of GC peak around 5.17 minutes as shown in *Figure 5.2* is expected to be methyl caprylate (C8:0), the fatty acid with the shortest chain length in palm kernel oil. The notation in bracket means a linear C8 carbon chain and the 0 indicates that the component is saturated. The mass spectra displayed a clear molecular ions at  $m/z = 101$  ( $[M-57]^+$ ) and  $115$  ( $[M-43]^+$ ). These ion peaks are due to fragmentations which lead to loss of carbons 1 to 4 and 1 to 3 respectively. M is the molecular mass of the eluted component. The loss of methoxyl group from the methyl caprylate is clearly seen with the ion at  $127$  ( $[M-31]^+$ ), confirming the methyl ester. The ion at  $[M-29]^+$  is worthy of note as it is common to all the mass spectra of the identified saturated ester straight chains. It may be a characteristic peak for saturated fatty acid ester. A clear but short molecular ion peak was seen at  $m/z = 158$ , confirming the elution of methyl caprylate.

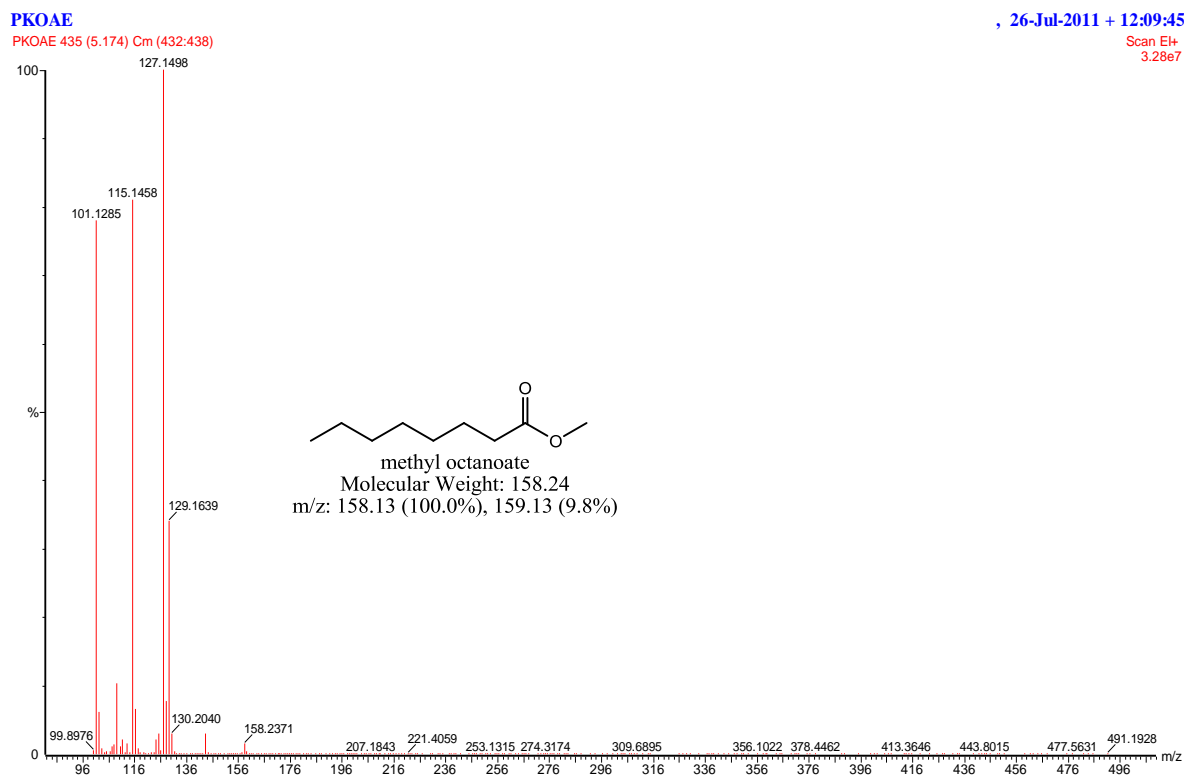


*Figure 5.2: Mass Spectra of Methyl Octanoate (Caprylate)*

The elution peaks around 7.96 minutes, 10.61 minutes, 12.89 minutes, 14.97 minutes, and 16.86 minutes were identified from mass spectra to be methyl caprate (C10:0), methyl laurate (C12:0), methyl myristate (C14:0), methyl palmitate (C16:0), and methyl

stearate respectively (C18:0) [Christie, 2011]. The mass spectra of these components are shown in (Appendix E ).

The mass spectra of the GC peaks around 16.59 minutes and 16.67 minutes are methyl linoleate (C18:2) and methyl oleate (C18:1) respectively. The notation in bracket means a linear C18 carbon chain and the 1 and 2 indicates that the components have one and two double bonds respectively. Similar to observations in methyl caprylate, ions representing loss of methoxyl group ( $m/z = [M-31]^+$ ) and methanol ( $m/z = [M-32]^+$ ) are present in the mass spectra of the other components. The ion representing  $[M-32]^+$  is slightly more abundant than that for  $[M-31]^+$ . The mass spectra for methyl linoleate and methyl oleate displayed clear molecular ion peaks at  $m/z = 294$  and  $296$  respectively, confirming the fatty acids. The mass spectra of these components are shown in (Appendix E ).

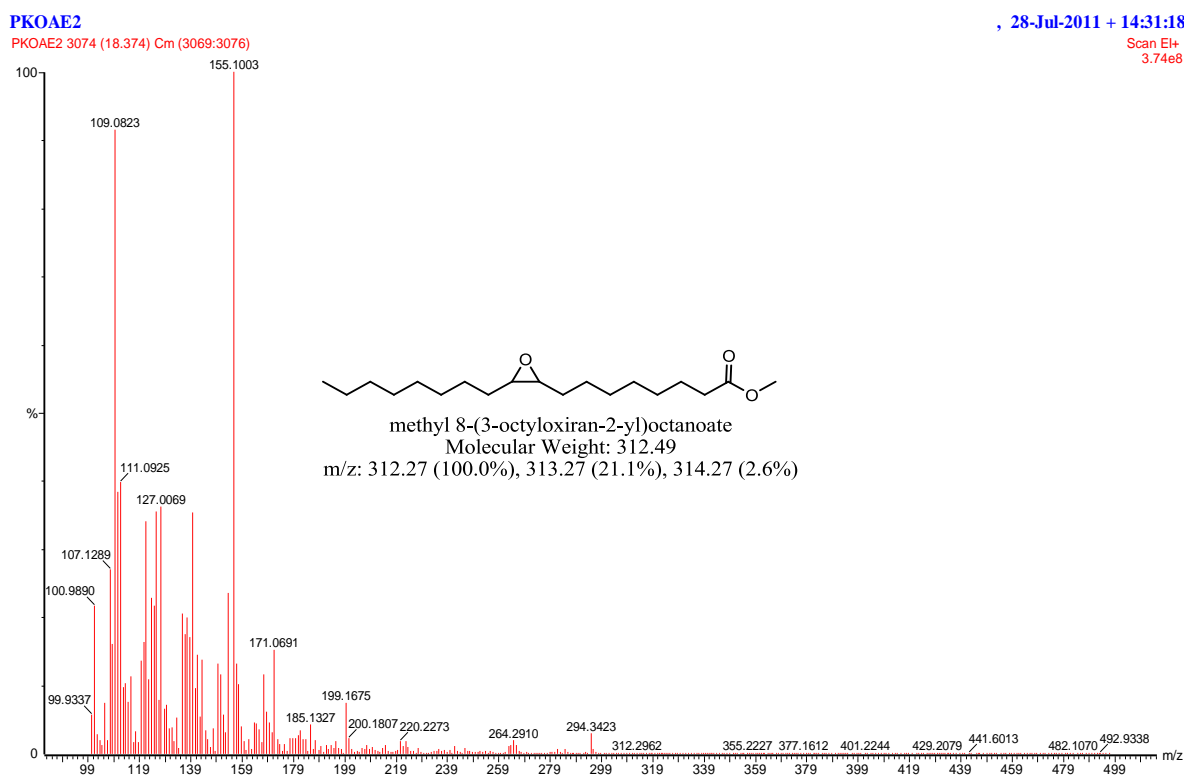


*Figure 5.3: Mass Spectra of Methyl 8-(3-octyloxirane-2-yl)Octanoate (methyl 9,10-epoxyoctadecanoate)*

The complete disappearance of peaks corresponding to methyl oleate and methyl linoleate in the PKOAE2 gas chromatogram demonstrates that the epoxidation reaction proceeds with complete conversion to corresponding epoxy esters. The mass spectra of the GC peak around 18.37 minutes as shown in *Figure 5.3* clearly displayed loss of

oxygen ion of the epoxy group ion at 294 ( $[M-18]^+$ ), confirming the epoxy methyl ester. There was also a display of a molecular ion peak at  $m/z = 312$  which correspond to the molecular mass of epoxidized methyl oleate. The mass spectra of the GC peak around 19.53 minutes displayed a molecular ion at  $m/z = 327$ , and indication of epoxidized methyl linoleate [Christie, 2011].

PKOAE3 displayed elution peaks around 20 minutes, while PKOAE4 displayed elution peaks at 21 minutes. The mass spectra of branched hydrocarbon could be dominated by fragmentation at the branched points [Kitson *et al*, 1996]. This makes the analysis of esters with multiple branches quite complex. C-3 contained ester with 2 side branched chains and 4 side chains. The molecular ions of C-3 branched esters were not clearly seen on the mass spectra possibly due to the dominance by fragments. The loss of the branched ions was identified at 294 ( $[M-148]^+$ ). Ions equivalent to  $m/z = 171$ , 199 and 243, are presumed to be due to fragmentation at the branched points of the esters with two side branched chains. The molecular ions of C-4 branched esters were also not seen on the mass spectra. The loss of ions at  $m/z = 171$  was identified. This is suspected to be due to ions of methyl nonanoate resulting from fragmentation at the branched points. Ion losses equivalent to  $m/z = 215$  are 257, are presumed to be loss of other branched fragments. The mass spectra of these components are shown in (Appendix E ).

In summary, the GC-MS analysis of the samples indicates that PKOAE1 contained unsaturated fatty acids which were converted to saturated fatty acids following epoxidation. The GC analysis of PKOAE2 sample shows complete conversion of C=C and the epoxy group formed were identified. Mass spectra analysis of PKOAE3 and PKOAE4 revealed molecular fragments that corresponds to branches of the products formed after esterification of the epoxy group to graft side branched hydrocarbon chains.

### **5.3.1 Fourier Transform Infrared (FT-IR) Spectrometry of the Synthesized Esters**

The FT-IR spectra were measured using a Perkin Elmer Spectrum One FT-IR spectrometer. A drop of the sample was placed on the spectrometer measurement cell. The sample was scanned with infrared radiation to obtain the spectra response. The amount of radiation absorbed by the sample was plotted as a function of the wave number of the absorbed radiation by a detector. Each spike (absorption band) in the IR

spectrum represents absorption of energy by vibrational modes having frequencies dependent on the chemical bond involved. The functional groups of the samples were identified from the spectra.

*Table 5.1: FTIR Spectra Assignment and mode of Operation for PKO Esters*

Freq cm <sup>-1</sup>	Assignment and mode of vibration	Relative intensity			
		PKOAE1	PKOAE2	PKOAE3	PKOAE4
3003	=C-H stretching vibration	Weak	None	None	None
2922	C-H asymmetric stretching vibration of CH <sub>2</sub>	Very strong	Very strong	Very strong	Very strong
2853	C-H symmetric stretching vibration of CH <sub>2</sub>	Strong	Strong	Strong	Strong
2473	Overtone of C=O	Weak	Weak	Weak	Weak
1741	C=O stretching vibration	Very strong	Very strong	Very strong	Very strong
1465	C-H scissoring vibration of CH <sub>2</sub> and CH <sub>3</sub>	Medium	Medium	Medium	Medium
1378	C-H symmetric bending vibration of CH <sub>3</sub>	Medium	Medium	Medium	Medium
1197	Methyl ester band	Medium	Medium	Medium	Medium
1169	Methyl ester band	Strong	Strong	Strong	Strong
1080	C-3 Side branched ester band	None	None	weak	None
930	C-4 Side branched ester band	None	None	None	weak
844	asymmetric ring stretching vibration of the C-C during the contraction of the C-O	None	Weak	None	None
827	12 micron band of the epoxy functional group	None	Weak	None	None
721	C-H rocking vibration of CH <sub>2</sub>	Medium	Medium	Medium	Medium

The FT-IR spectra of the PKOAE1, PKOAE2, PKOAE3, and PKOAE4 samples are shown in *Figure 5.4* and *Figure 5.6*. As shown in *Figure 5.4*, the spectra of PKOAE1 and PKOAE2 have some common peaks. The assignment of the peaks and the mode of vibration that resulted in the peaks are shown in *Table 5.1* for all the ester samples. The ester samples have some common peaks and the other peaks are characteristic peaks which are unique to each sample. These peaks were used served as fingerprints for the respective samples. The characteristic medium peaks around  $1250\text{ cm}^{-1}$  and  $1197\text{ cm}^{-1}$ , and strong peak around  $1170\text{ cm}^{-1}$ , are fingerprints of the methyl ester of long-chain fatty acid. This could be attributed to the twisting and wagging of the methylene group which are usually observed between  $1350\text{ cm}^{-1}$  and  $1150\text{ cm}^{-1}$  [Silverstein *et al*, 2005]. PKOAE2 has peaks around  $844$  and  $829\text{ cm}^{-1}$ . The peaks at  $844$  and  $829\text{ cm}^{-1}$  inset in *Figure 5.4* and zoomed in *Figure 5.5* are fingerprints of epoxidized ester. Although a maximum yield is obtained within a short time at high temperature, the epoxy ring is highly unstable and decomposes after a reaction time corresponding to the maximum yield. The magnitude of these epoxy peaks was found to be dependent on the reaction time. The epoxy yield increased with reaction time to a threshold yield. Beyond that time, the epoxy ring started decomposing leading to reduction in the yield. The maximum epoxy yield as monitored with FTIR was obtained after four hours.

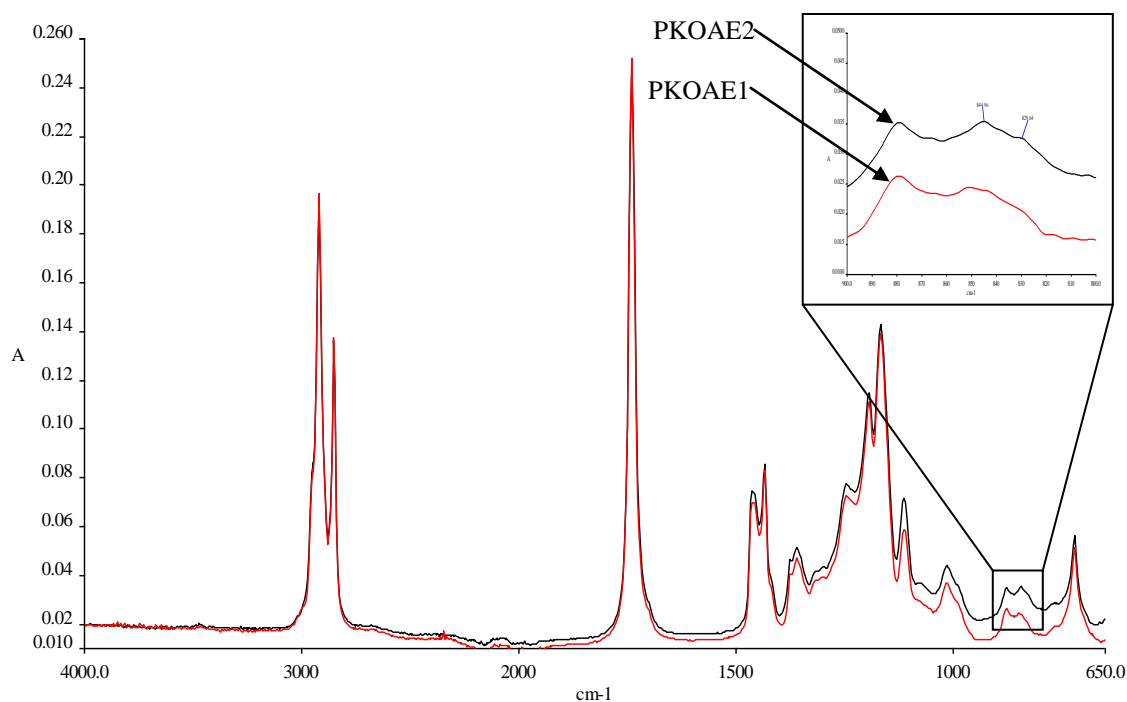


*Figure 5.4: FTIR Spectra of Palm Kernel Oil Methyl Ester and Epoxy Methyl Ester*

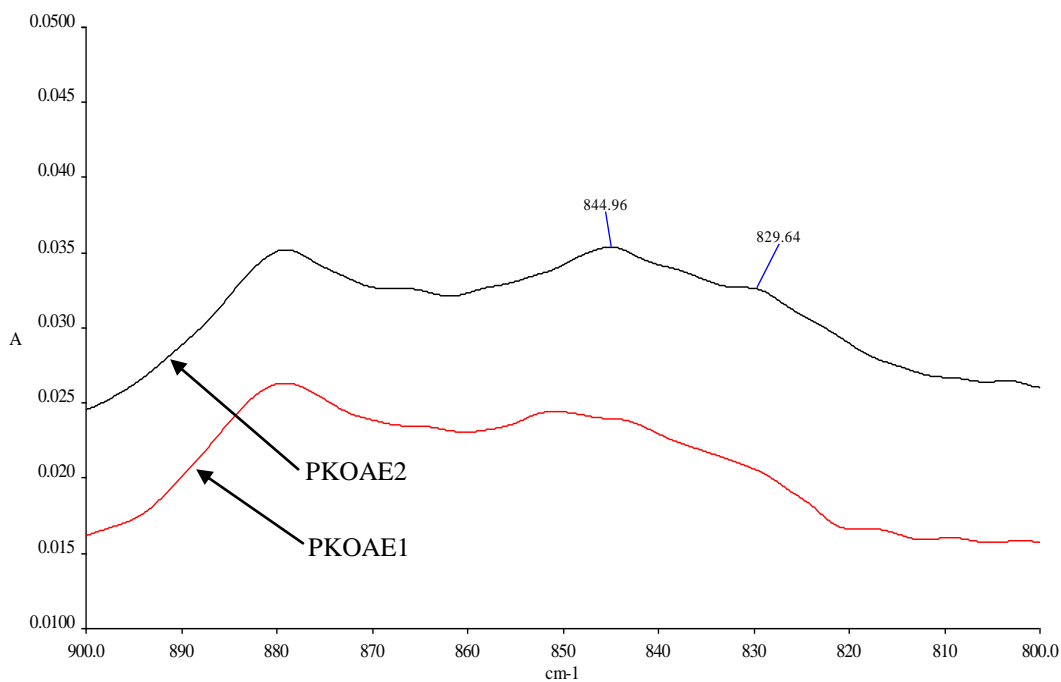


Figure 5.5: FTIR Spectra of Palm Kernel Oil Ester showing Epoxy peak

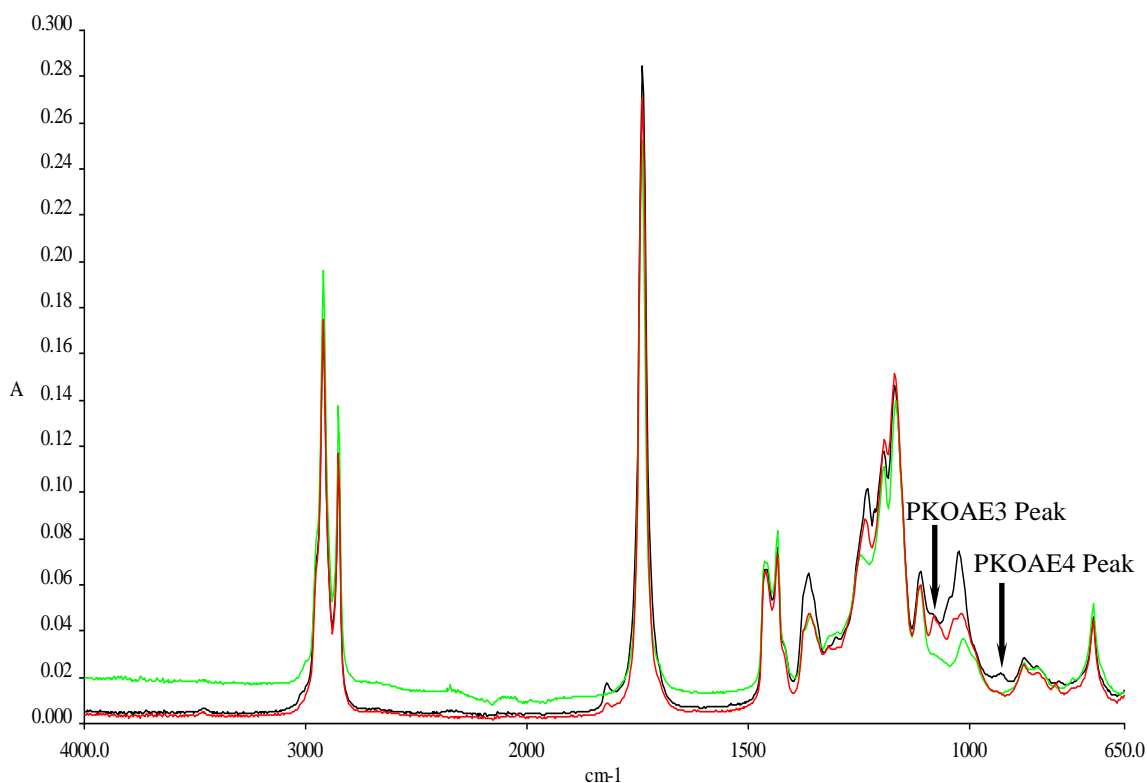


Figure 5.6: FTIR Spectra of Palm Kernel Oil Methyl Ester and Branched Methyl Ester

In Figure 5.6, PKOAE3 and PKOAE4 shared some common peaks with PKOAE1 and PKOAE2 as tabulated in Table 5.1. The ester peak which appeared around  $1740\text{ cm}^{-1}$  is slightly broader in PKOAE3 and PKOAE4 compared to PKOAE1. This could be attributed to the grafted side chains. PKOAE3 has a peak at  $1080\text{ cm}^{-1}$  while PKOAE4

has a peak at  $930\text{ cm}^{-1}$  as shown by the arrows in *Figure 5.6*. These peaks appeared at the fingerprint region and can be regarded to be the fingerprint of the respective esters. The peaks are unique to the respective esters and they differentiate the two alkyl esters.

## 5.4 Thermo-Physical Properties of Ester Fluids

This section presents the analysis of dynamic viscosity of the ester samples which was evaluated from density and kinematic viscosity measurements. The characteristic melting temperatures, heats of fusion, specific heat capacities, and oxidation onset temperatures of the samples were evaluated from the DSC thermogram. As the sample is heated from  $-100^{\circ}\text{C}$  to  $50^{\circ}\text{C}$ , a characteristic endotherm was observed in the region where phase transitions from solid to liquid state occur. At higher temperature, oxidative degradation sets in.

### 5.4.1 Dynamic Viscosity

Samples of CPKO, PPKO, PKOAE1, PKOAE2, PKOAE3, and PKOAE4 were measured and placed in to the viscometer. The initial temperature was set and from the flow time, viscosity was determined. Samples were also introduced into the density meter. The initial temperature was set and from the period of oscillation, the density of the sample was evaluated.

The density and viscosity of the palm kernel oil and the ester derivatives were observed to change with chemical structure modification as shown in *Table 5.2*. PPKO was found to have a density and kinematic viscosity of  $912.7\text{ kgm}^{-3}$  and  $44.49\text{ cSt}$  respectively at  $30^{\circ}\text{C}$ . Measurement temperature was started from  $30^{\circ}\text{C}$  for the crude and refined palm kernel oil because that is the lowest temperature to get a clear liquid as the melting point of palm kernel oil is about  $26^{\circ}\text{C}$ . Separating the fatty acids of palm kernel oil from the glycerol to produce PKOAE1 resulted in a change in viscosity and density. The density and kinematic viscosity reduced to  $874.2\text{ kgm}^{-3}$  and  $4.57\text{ cSt}$  respectively at  $20^{\circ}\text{C}$ . The glycerol initially bonds together the fatty acids in the oil. Separating the glycerol from the oil reduced the average molecular mass, thereby decreasing the dynamic viscosity of the fluids. The separation of glycerol also reduced the resistive frictional force acting between layers of the alkyl ester travelling at different speeds leading to a reduced viscosity. The incorporation of an epoxy ring at the double bond site to produce PKOAE2 increased the density and kinematic viscosity of the alkyl ester to  $878.0\text{ kgm}^{-3}$

and 6.14 cSt respectively at 20 °C. This increase is due to the epoxy group which increased the molecular weight of the ester. Addition of side chains to the alkyl ester to produce PKOAE3 lead to a further increase in both the viscosity and density. The density and kinematic viscosity of the alkyl ester increased to 892.8 kgm<sup>-3</sup> and 6.92 cSt respectively at 20°C with the grafting of C-3 side chain. Grafting of C-4 side chain produced PKOAE4 with density and kinematic viscosity similar to PKOAE3 at 20°C.

Table 5.2: Physical Properties of Some oil Samples

Sample	Density (kgm <sup>-3</sup> )	Viscosity (cSt)	E <sub>a</sub> (eV) of viscosity	Coefficient of vol. expansion (%K <sup>-1</sup> )
PPKO	912.7	44.49	0.28	0.070
PKOAE1	874.2	4.57	0.17	0.075
PKOAE2	878.0	6.14	0.19	0.075
PKOAE3	892.8	6.92	0.19	0.080
PKOAE4	893.2	6.99	0.20	0.077
Min Oil	886.6	21.4	0.32	0.070
FR3	920.0	33.0	-	0.074

Note: Values for PPKO are at 30°C, FR3 at 40°C, while the values for Min Oil, ester samples are at 20°C

The double bonds present in the alkyl oleate and alkyl linoleate exist in *cis* configuration, producing a bend (kink) in the geometry of the molecules. This creates resistance to the ability of the molecules to be closely packed. This results in an increase in fluidity (i.e. a reduction in viscosity). However, the impact of the bends at double bond sites is low due to low content of unsaturated fatty acids compared with saturated fatty acids in palm kernel oil. Grafting of side hydrocarbon chains around the double bond site changed the molecular shape thereby decreasing the fluidity. This effect increased with side-chain length. There is also a corresponding increase in the density of the ester with increase in side chain length, indicating an increased dynamic viscosity. The heat exchange property can be measured using a liquid parameter known as Reynolds number. This parameter is used to determine whether oil has a turbulent or laminar flow. Reynolds number is related to dynamic viscosity with the expression:

$$\text{Re} = \frac{w \cdot d}{\mu} \quad 5.1$$

Where  $\mu$  is the dynamic viscosity,  $w$  is the oil velocity and  $d$  is diameter of the channel. A turbulent oil flow is reported to have more effective cooling effect than laminar flow [Massey *et al*, 2006]. Turbulent flow has Reynolds number greater than 4000, while value below 2000 is regarded as laminar flow. From the expression in equation 5.1, a lower viscosity gives higher Reynolds number. With the esters having viscosities less than mineral insulating oil, it suggested that the esters will possess higher Reynolds number, making it more effective in cooling compared with mineral oil.

As earlier stated, the heat transfer coefficient of the oil has a direct link with the oil dynamic viscosity, and the viscosity is dependent on temperature change in the oil. The relationship between dynamic viscosity and temperature is considered here. The dynamic viscosity of palm kernel oil and the ester derivative exhibit similar “Arrhenius” behaviour within the temperature range studied as shown in *Figure 5.7*. The increase in temperature leads to an increase in the thermal or kinetic energy of each molecule and consequently reduces the cohesive energy of the molecules of the liquid. This also reduces the resistive force acting between layers of the alkyl ester travelling at different speeds. This increases the mobility of the molecules, resulting in the reduction in the viscosity [Massey *et al*, 2006]. *Figure 5.7* shows an unambiguous trend of a dependence of viscosity of palm kernel oil and the alkyl esters on temperature. The viscosity-temperature relationship exhibits a thermally activated behaviour. The straight lines fit on the data points with correlation coefficients ( $R^2$ ) that range from 0.997 to 0.9995. The activation energy of viscous flow of PPKO is 0.28 eV. The separation of the glycerol from the ester fatty acids reduced the activation energy by 0.11 eV. PKOAE1, PKOAE2, PKOAE3 and PKOAE4 have activation energies as shown in *Table 5.2*. The activation energies are similar, suggesting that the esters have similar viscous processes. This should be expected since the saturated fatty acids dominate the composition of the esters. The viscosity of the alkyl ester is considerably lower than Nynas 10GBN mineral insulating oil whose viscosity is 21 cSt at the same temperature. Viscosity often has an overwhelming effect on the heat transfer capability of a fluid which is a strong function of temperature. Equation 2.7 in chapter two shows an inverse relationship between heat transfer coefficient and viscosity. The constant  $C$  is dependent on thermal conductivity, density, thermal expansion coefficient, and specific heat of the oil. The density, thermal expansion and specific heat capacity of the ester samples are close to that of mineral oil sample. This implies that the low viscosity of the ester fluid

will give a higher heat transfer coefficient. Viscosity also influences the circulation flow speed of the oil while in operation. The flow speed also has an inverse relation with viscosity. The ester's low viscosity at operating temperature (60°C) of the transformers may ensures low resistance against flowing in the system. From the empirical relation in equation 2.5, the low viscous alkyl ester could be very good in heat transfer and dissipation since low viscosity enhances good heat transferability.

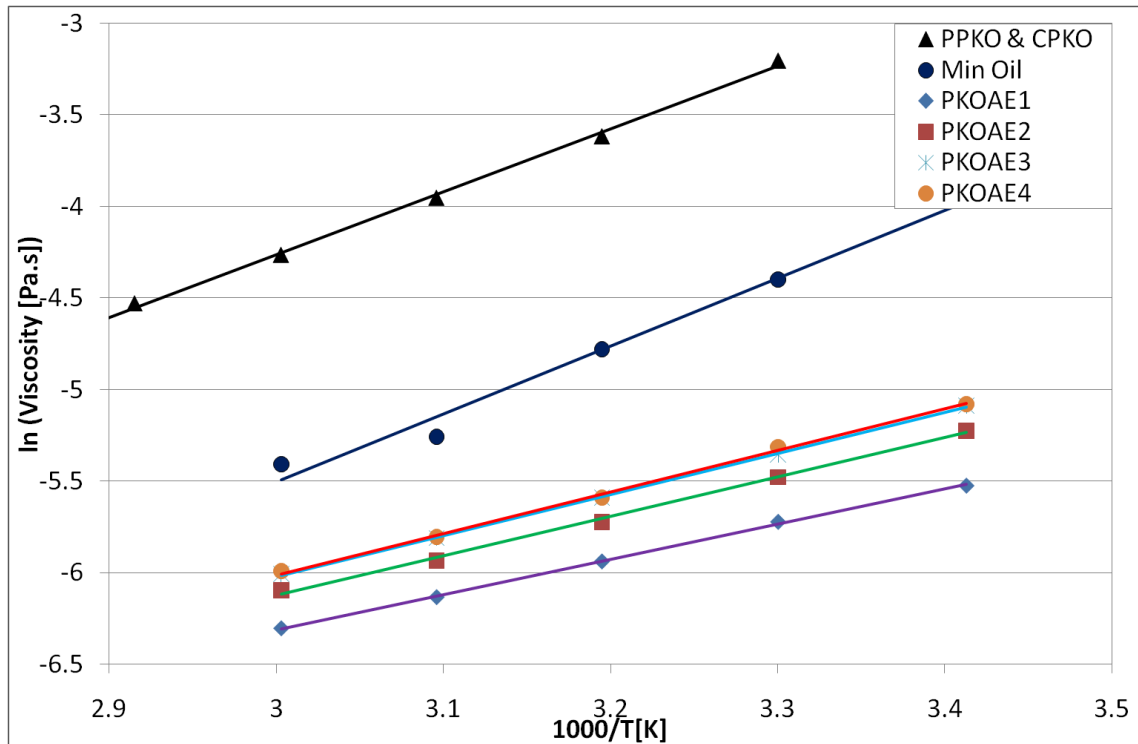


**Figure 5.7: Arrhenius Plot for Viscosity of the Oil Samples**

The coefficient of thermal expansion of the laboratory purified palm kernel oil (PPKO) and its esters was calculated from the density measurements obtained from the Paar DMA 40 digital density meter. The expression;  $\gamma = \frac{S_1 - S_2}{S_1(T_2 - T_1)}$ , where  $\gamma$  is the coefficient of volume expansion,  $S_1$  is the specific gravity at lower temperature,  $S_2$  is the specific gravity at higher temperature,  $T_1$  is the lower temperature and  $T_2$  is the higher temperature was used to evaluate the volume expansion coefficient. This determines the volume change that occurs after heat absorption. The coefficient of thermal expansion of purified palm kernel oil and Nynas 10GBN mineral oil are similar (Table 5.2).

### 5.4.2 Low Temperature Thermal Analysis

The performance of a dielectric liquid at low temperature, for example, during extreme weather conditions, cannot be taken for granted when considering such a liquid for use in oil-filled electric equipment such as oil-filled transformers. The thermal properties of the ester samples at low temperatures are analyzed in this section using differential scanning calorimetry (DSC). *Figure 5.8* shows the thermogram of the samples at low temperature while cooling and *Figure 5.9* shows the thermogram while heating the samples. Palm kernel oil contains fatty acids of different chain lengths, and each fatty acid has its melting point. The broad peaks of the thermograms during cooling and heating results from the distribution of melting points of the respective fatty acids in the esters. Vegetable oil is therefore considered to have a melting range rather than a sharp melting point, and the melting point is often defined as the temperature at which the oil is free of crystals [Dewettinck *et al*, 2007].

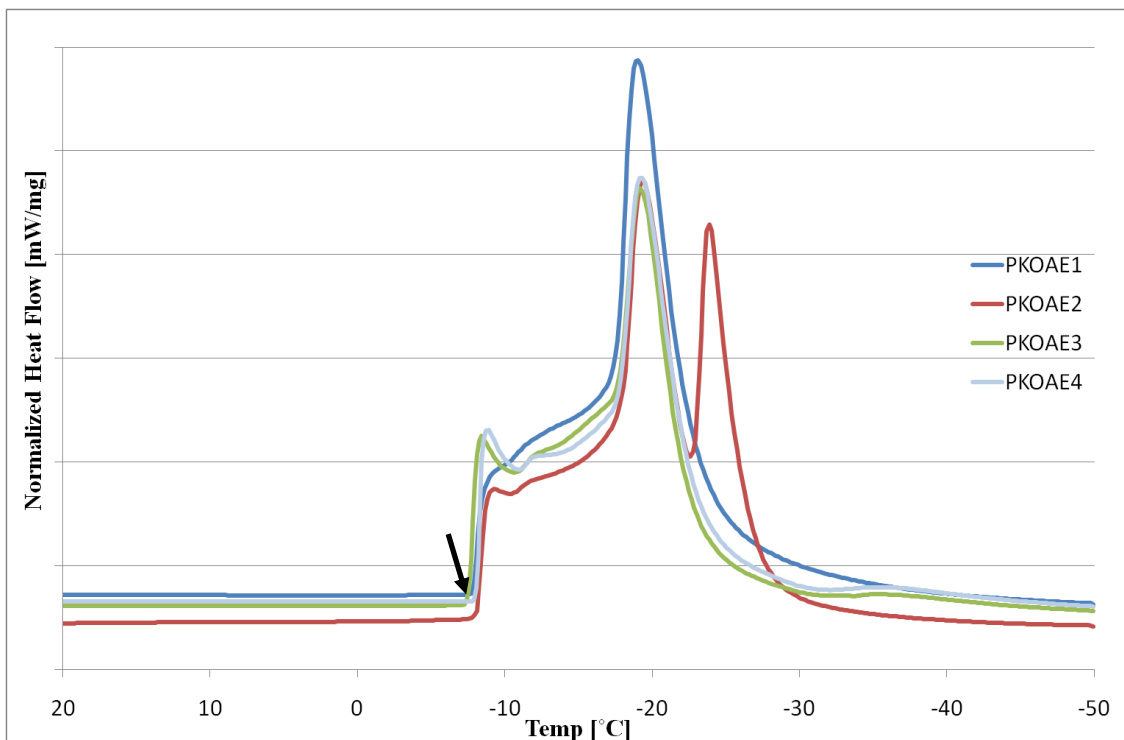


*Figure 5.8: DSC Thermogram of PKO ester sample while cooling showing onset of crystallization*

From *Figure 5.9*, it can be seen that the melting peak temperature of the alkyl ester samples which occurred  $-7 \pm 0.5^\circ\text{C}$  occurs at a significantly lower temperature than PPKO which occurred at  $26^\circ\text{C}$ . The beginning of the broad peak in *Figure 5.8* indicates

the onset of crystallization. The onset of crystallization of the esters while cooling is slightly lower compared with the melting peak temperature while heating. While the other ester samples exhibit single peak while cooling, PKOAE2 has double peaks. This may be that the epoxy group crystallized at temperature outside the range of the other saturated fatty components in the ester.

The splitting of the oil into its respective fatty acids with the removal of glycerol reduced the number of O-H hydrogen bonding. This reduced the average molecular mass of the oil and the ability of the fatty acid to entangle, thereby reducing the melting temperature of the ester. A comparison of the thermogram of PKOAE2 with that of PKOAE1 in *Figure 5.9* shows the presence of melting peak at -40 °C. This can be assigned to the melting peak of the unsaturated fatty acids in the methyl ester. The peak is absent in PKOAE2 reaffirming the complete conversion of the double bonds to epoxy rings.

**Table 5.3: Thermal properties**

Sample	Melting Temperature (°C)		Onset of Crystallization (°C)	Heat of Fusion (kJ.kg <sup>-1</sup> )	Heat Capacity (kJ.kg <sup>-1</sup> .K <sup>-1</sup> )
	Onset	Peak			
PPKO	14.56	26.19	-	90.11	2.02
PKOAE1	-14.1	-6.86	-7.53	109.48	2.03
PKOAE2	-16.52	-6.90	-7.82	132.42	1.86
PKOAE3	-13.64	-6.55	-8.21	106.46	1.78
PKOAE4	-14.53	-7.47	-9.03	95.38	1.88
Min Oil	-	-	-	-	1.67

The melting peak of PKOAE3 with C-3 side chains is close to that of PKOAE1. An increase in side-chain length was observed to slightly shift the melting peak to lower temperature as displayed by the alkyl ester (PKOAE4) with C-4 side chain. This may have resulted from the action of the side-branched alkyl esters. The longer side chain limits the ability of the fatty acids to be closely packed because the hydrocarbon is no longer a linear molecule. The longer side chains inhibit close packing of the molecules [Hwang *et al*, 2001]. Close packing is also inhibited by the bends caused by the double bonds. The pour point of the esters was determined to be -6°C. *Table 5.3* shows that

PKOAE2 has a higher heat of fusion than PPKO. This may be due to the presence of epoxy rings in the chemical structure of some of its fatty acids. The heat of fusion was observed to decrease after grafting the side chain. It also decreased with increase in chain length. This may be attributed to the action of the side chains on the melting process.

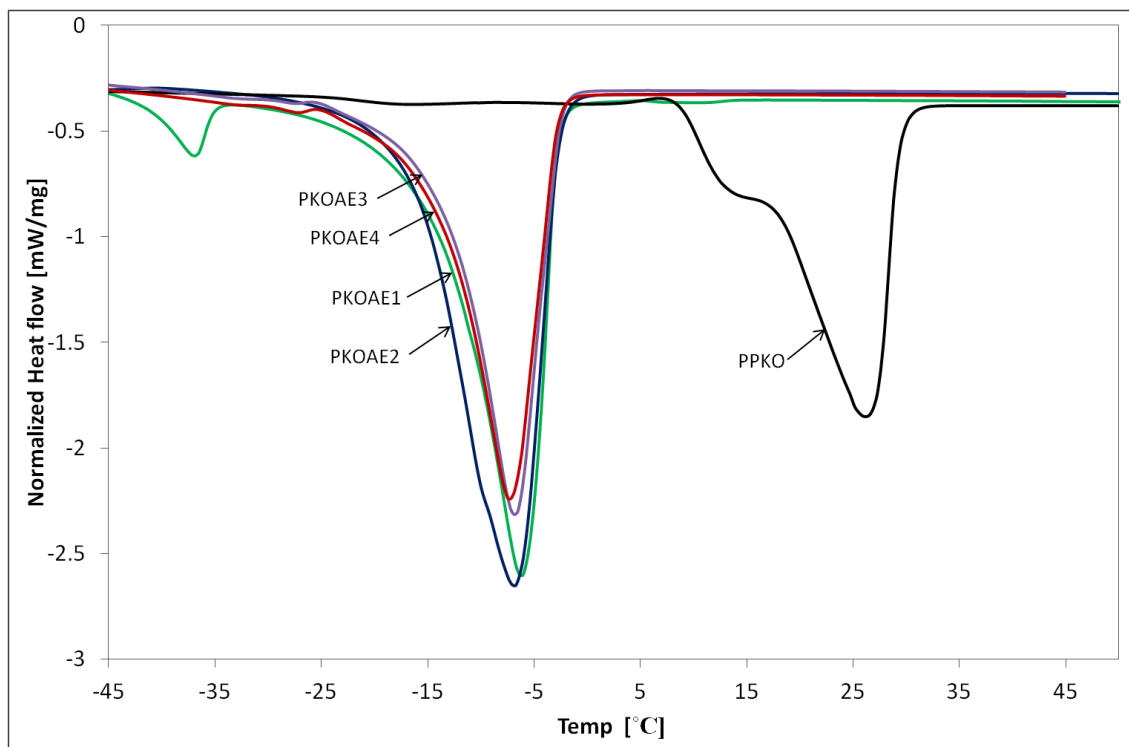


*Figure 5.9: DSC Thermogram of ester sample with melting peaks while heating*

### 5.4.3 High Temperature Thermal Analysis

Analysis of thermo-oxidative stability and flash point of the esters is considered in this subsection. The thermo-oxidative response data was obtained using differential scanning calorimetry (DSC). DSC measurements taken under oxygen atmosphere were used to determine the oxidative stability of the samples. The thermo-oxidative stability was evaluated from the onset temperature for oxidative degradation of the respective ester samples. *Figure 5.10* through *Figure 5.13* shows the thermo-oxidative behaviour at high temperature of PKOAE1, PKOAE2, PKOAE3, and PKOAE4. The curves show the behaviour of freshly prepared ester samples without additive such as anti-oxidant.

The oxidation onset temperature (OOT [°C]) of the sample, which is defined as the temperature at which a rapid increase in the rate of oxidation occurs [Moser, 2009], is determined by extrapolating a tangent line drawn on the slope of the reaction exotherm

of the thermogram as indicated in *Figure 5.10* through *Figure 5.13*. The thermograms displayed two peaks. The first peak may be attributed to thermo-oxidative decomposition, while the second peak could be due to pyrolysis of the C-H molecules. The peaks on the PKOAE1 thermogram under oxygen may have followed a sequence where the decomposition of unsaturated fatty alkyl acids first occurred, and followed by decomposition of saturated fatty acids alkyl ester and carbon residue [Moser, 2009]. The thermogram of PKOAE2, PKOAE3, and PKOAE4 have similar shape. The peaks on PKOAE2 thermogram could be due to decomposition of the saturated fatty acids and carbon residue. The decomposition of the ester samples with grafted side hydrocarbon chains (PKOAE3 and PKOAE4) may have followed a sequence where the grafted side hydrocarbon chains first decomposed, and followed by the decomposition of the saturated fatty acids and carbon residue. The evaluated OOT from the thermogram shows that PKOAE2 has higher oxidative onset temperature, and next to it is the OOT of PKOAE1. PKOAE3 and PKOAE4 has lower OOT as shown in *Table 5.4*. Grafting of side chains reduced the oxidative onset temperature.

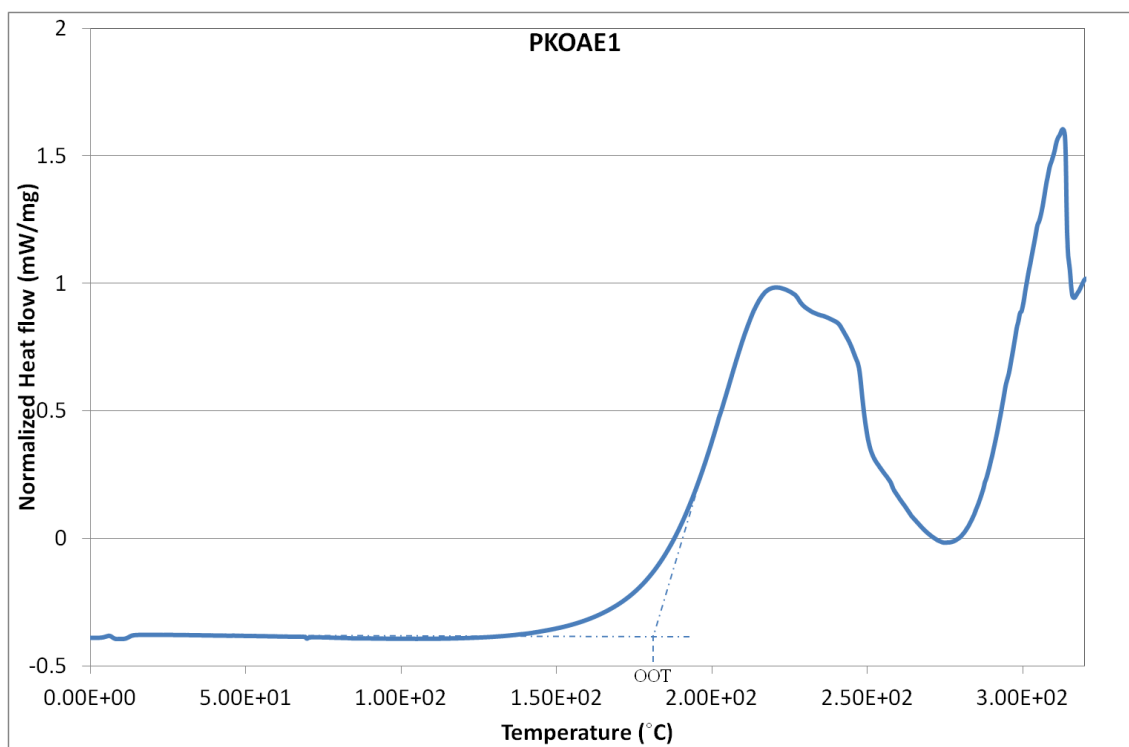


*Figure 5.10: DSC thermogram for thermo-oxidation of PKOAE1*

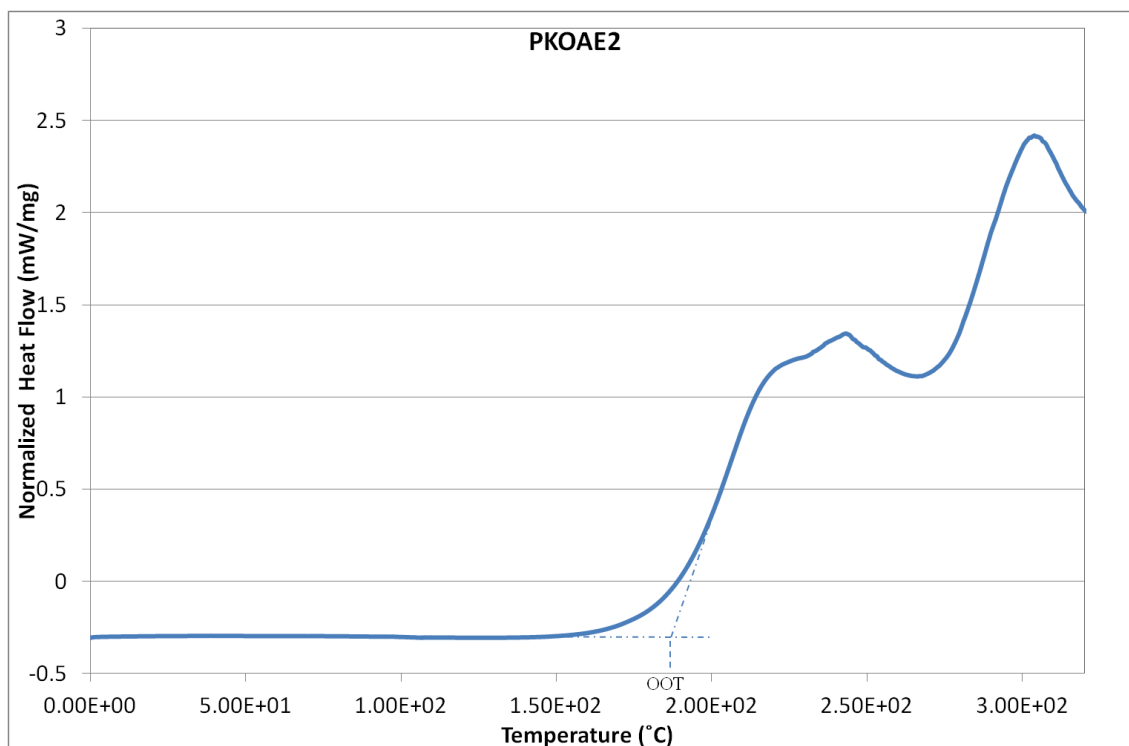


Figure 5.11: DSC thermogram for thermo-oxidation of PKOAE2

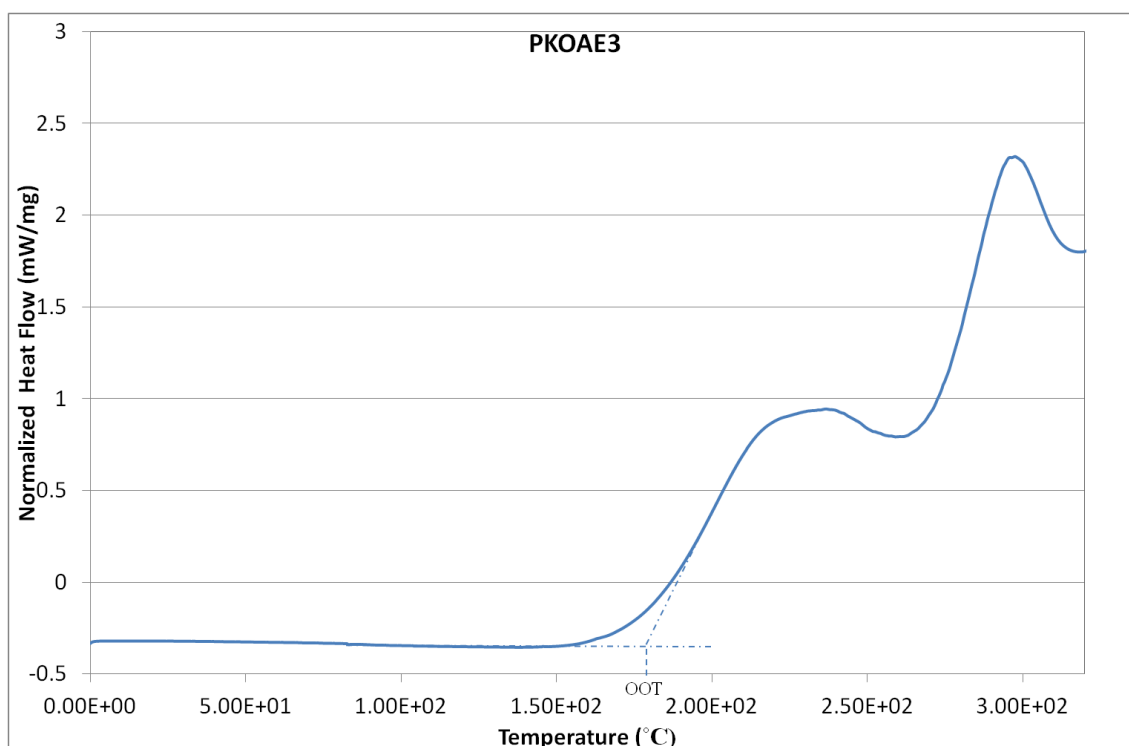


Figure 5.12: DSC thermogram for thermo-oxidation of PKOAE3

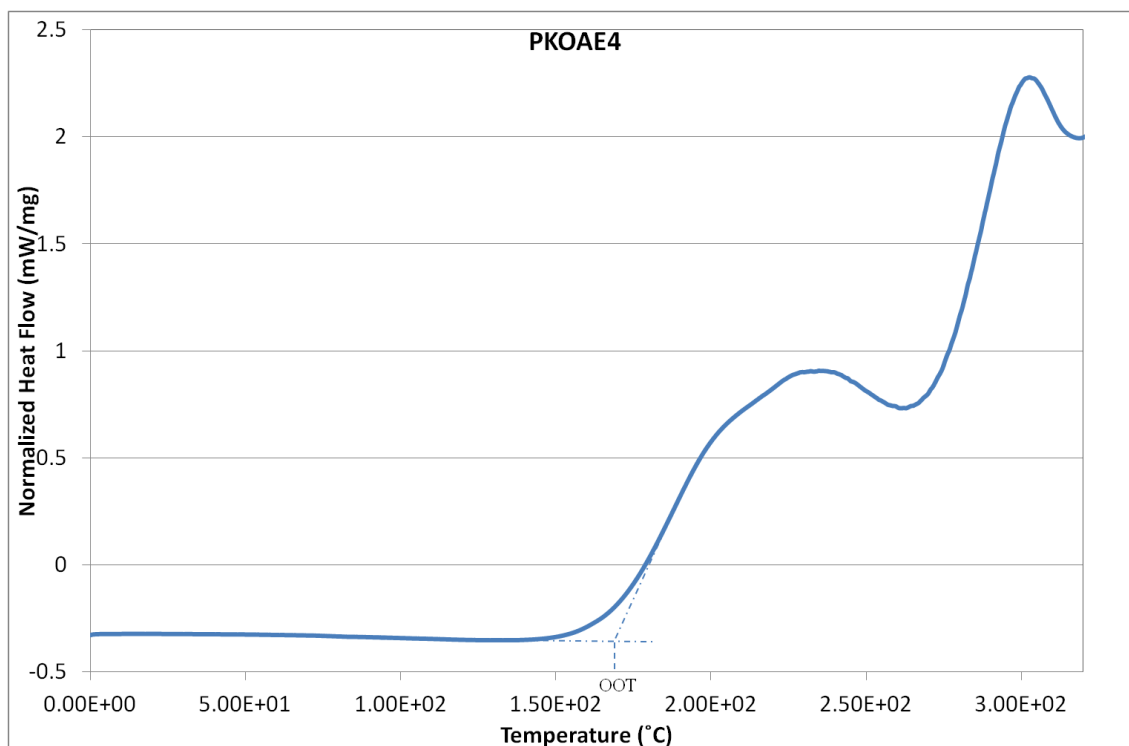


Figure 5.13: DSC thermogram for thermo-oxidation PKOAE4

Table 5.4: High temperature thermal Analysis of Samples

Sample	Oxidation Onset Temperature (OOT) in °C		Flash point °C
	Virgin	With 3% TBHQ	
PKOAE1	180	261	148
PKOAE2	187	288	146
PKOAE3	181	278	130
PKOAE4	173	286	120
Min Oil	207	-	≥140

Oxidative decomposition can be explained from the general rule that oxidation stability of C–H bonds follow an order: CH<sub>3</sub> (most stable) > CH<sub>2</sub> > CH (most reactive) [Moser, 2009]. The pathway for oxidative degradation of saturated alkyl esters is considerably slower and could occur at any point along the fatty acid backbone since the entire backbone possesses similar C-H bonds, with the exception of the terminal alkyl group [Jayadasa *et al*, 2006]. This is responsible for the high oxidative stability of alkyl esters of short chain length. The structural identification shows the absence of CH in palm kernel oil alkyl esters, while the amount of alkyl oleate and linoleate which contained CH<sub>2</sub>, is low compared with the saturated fatty acids (about 17%). This leads to its higher

oxidative stability compared with vegetable oil of higher concentration of unsaturated fatty acid such as sunflower oil and rapeseed oil [Simon *et al*, 2010]. As shown in *Table 5.4*, the OOT of PKOAE2 suggests that the epoxy rings have stronger resistance to thermo-oxidative decomposition in the presence of oxygen. The branched ester samples contained CH at the branched points which has lower stability to oxidation [Moser *et al*, 2007]. This makes the side branched hydrocarbon chains to have lower stability, this may have undergone early decomposition, leading to the decrease in the OOT of the branched alkyl ester samples. The OOT of was observed to decrease with increase in the length of side branched chains. The oxidation onset temperature of Nynas 10GBN mineral oil was 20°C higher than PKOAE2.

The flash points of PKOAE1, PKOAE2, PKOAE3, and PKOAE4 were determined to be 148°C, 146°C, 130°C and 120°C respectively; the flash point of PKOAE1 and PKOAE2 is within the minimum specification for mineral oil based insulating fluid [Nynas, 2010]. Flash and fire points are known to be dependent on volatile impurities. The lower flash point of PKOAE3 and PKAOE4 may have resulted from the remnant acid anhydrides in the samples which are more volatile with flash points lower than that of the samples.

#### **5.4.4 Effect of Additive on Thermo-Oxidative Stability**

Tertiary butyl hydroxyquinone (TBHQ) was added to the synthesized ester samples to evaluate the effect of antioxidant additive on the thermo-oxidative stability of the ester derivatives. TBHQ was selected as the preferred antioxidant because reports on effect of antioxidant on methyl ester of vegetable oil shows that ester treated with TBHQ is less susceptible to thermal oxidation compared with other antioxidants such as butylated hydroxytoluene (BHT), butylated hydroxyanisole (BHA), propyl gallate (PrG) and  $\alpha$ -tocopherol [Dunn, 2005; Ryu, 2009; Sarin *et al*, 2010]. The percentage of additive that yields optimum performance was determined by varying the quantity of the additive from 1-5% (w/w). The effect of the antioxidant was analyzed by evaluating the temperature at which the DSC thermogram displayed an onset of oxidation as shown in *Figure 5.14* and *Figure 5.17*. This was compared with the oxidation onset temperature of the respective samples without antioxidants shown in the figures.

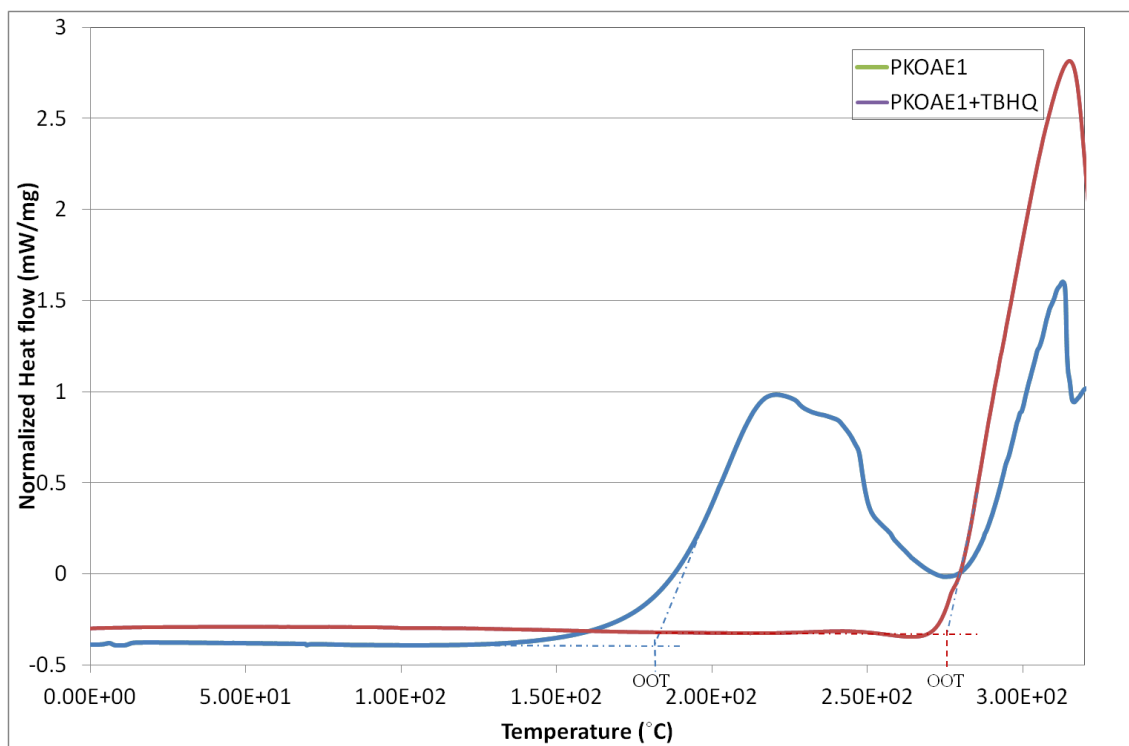


Figure 5.14: DSC thermogram for thermo-oxidation of PKOAE1

The red curve displayed in Figure 5.14 through Figure 5.17 is the thermogram of inhibited ester samples. The results obtained are shown in Table 5.4. The antioxidant was found to have great influence on the oxidative stability of the esters. It responded to the ester samples by significantly increasing their oxidation onset temperatures. 4% (w/w) tertiary butyl hydroquinone (TBHQ) in PKOAE1 was found to yield optimum performance, while 3% (w/w) yielded optimum performance in the other ester samples above which there was no significant change in OOT. However, there was a predecomposition at 241°C on the thermogram of PKOAE4. It is not certain if the decomposition is due to the remnant butyric anhydride. Although the presence of the anhydride in PKOAE4 was observed from FTIR spectra and it is more volatile than the esters. The anti-oxidant suppressed the thermal degradation of C-H bonds of the fatty acid backbone. The result demonstrates that antioxidant was able to protect the oxidative degradation of the long and branched carbon chains to much higher temperatures. This suggests that the addition of anti-oxidant has a significant improvement on the oxidative stability of the ester derivatives.

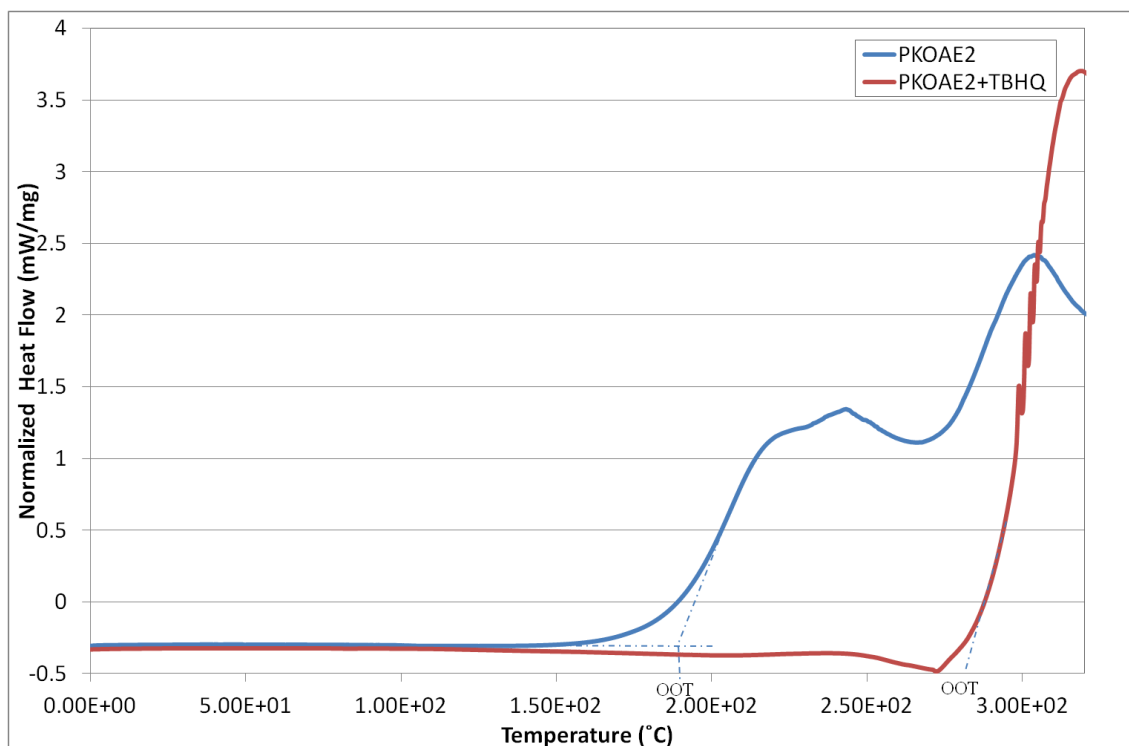


Figure 5.15: DSC thermogram for thermo-oxidation of PKOAE2

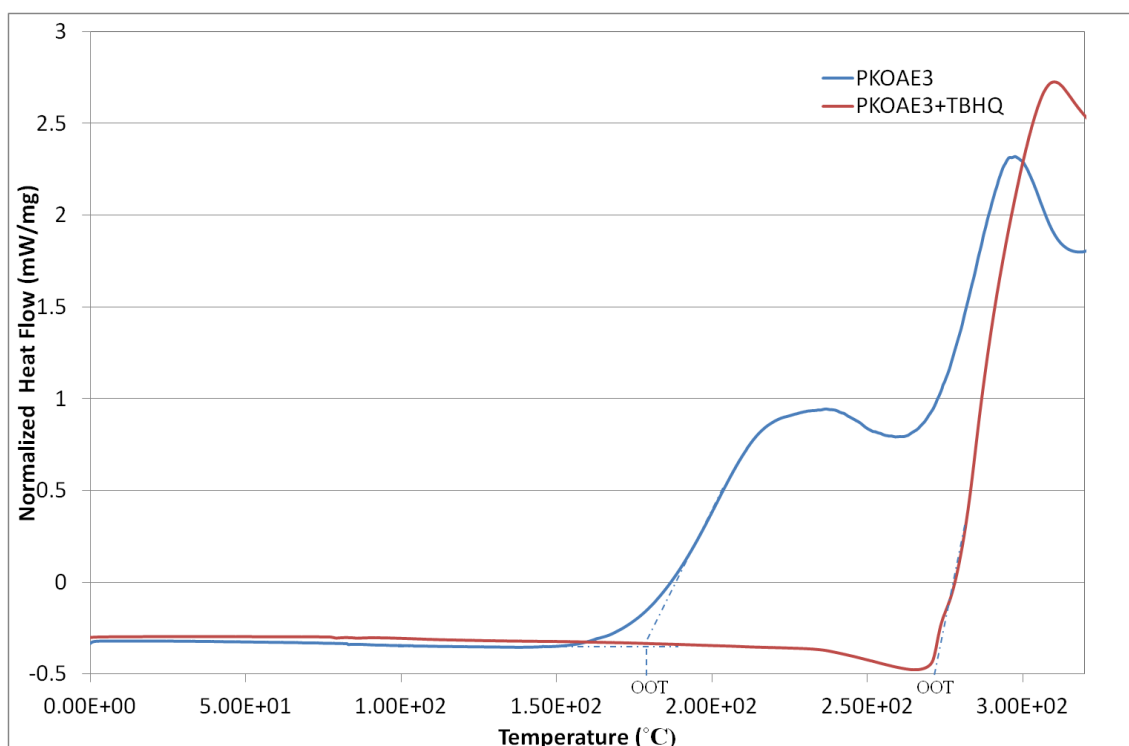


Figure 5.16: DSC thermogram for thermo-oxidation of PKOAE3

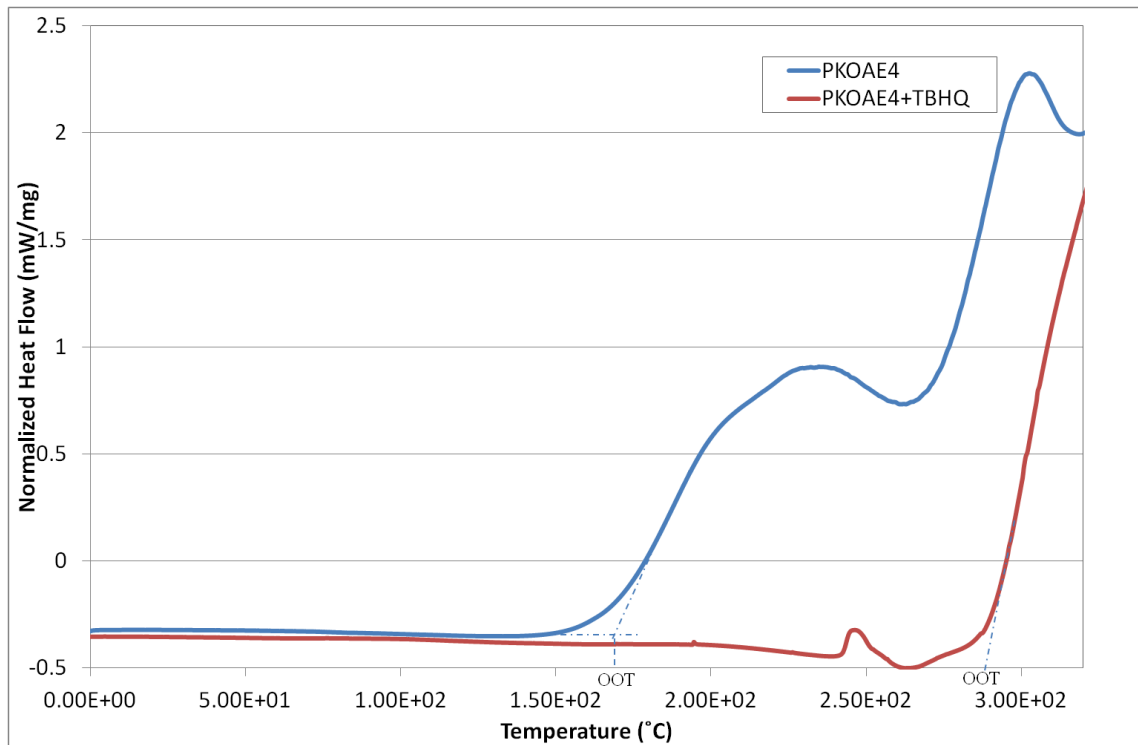


Figure 5.17: DSC thermogram for thermo-oxidation PKOAE4

## 5.5 Moisture and Acidity

The level of moisture content in transformer oil can affect the insulation properties of the oil. Knowledge of the initial water content will serve as a reference in the monitoring of the water while the oil is in service; since water is one of the by-products of ageing deterioration. An increase in the water content of used insulating oil may be a marker for deterioration. The ester samples were dried at 80°C under reduced pressure in a vacuum oven for two hours before sending the samples for analysis. It should be noted that drying the oil in a vacuum oven may not necessarily remove all moisture in the samples as the water solubility in oil increases with temperature. The water content of PKOAE1, PKOAE2, PKOAE3, and PKOAE4 were determined to be 218 mg/kg, 201 mg/kg, 115 mg/kg, and 27 mg/kg respectively.

Similarly, the acidity of insulating fluid can be increased by thermal degradation of the fluid. This is because oxidation products are often acidic in nature. Acids formed during ageing of mineral oil are classified into two; high molecular weight acids (HMWA) and low molecular weight acids (LMWA). The presence of HMWAs can lead to reaction with the bulk oil which may result in the formation of sludge and varnish deposits. The sludge in the worst case may result in blocking of oil canals in the transformer. This

may affect the efficiency of the cooling unit of the transformer, leading to overheating and eventual breakdown. High acid content in insulating oil has the consequence of increasing ionic dissociation leading to higher concentration of charge carriers and an increase in electrical conductivity. HMWAs have a deteriorating effect on the insulating properties of the oil. The acids and their peroxides intermediates can also affect the mechanical strength of the cellulose insulation. The presence of sufficient quantities of LMWAs can lower the flash point of the oil [El-Rafaie *et al*, 2009]. The fatty acids in esters have different characteristics compared with mineral oil. The acids react with the OH (hydroxyl) groups on the cellulose in transformers via transesterification [Rapp *et al*, 2005]. The esterification reaction chemically modifies and protects the Kraft paper from degradation due to ageing. The acidity of PKOAE1, PKOAE2, PKOAE3, and PKOAE4 were determined to be 0.34 mg KOH/g, 0.51 mg KOH/g, >1 mg KOH/g, and >1 mg KOH/g respectively. The acidity of PKOAE3 and PKOAE4 appeared high. This may be due to the presence of acid anhydride that remains in the samples.

## **5.6 Dielectric Response of PKO Ester Fluids**

A study of the DC conductivity of processed dielectric liquid may be used to quantify the conducting ions in the material and for quality control. An understanding of the dielectric behaviour of insulating liquid requires the study of the dielectric response over a spectrum of frequency covering several decades and temperatures. Since interfacial polarization dominates measurements at low frequencies (frequency below  $10^{-1}$  Hz); such measurement may reveal useful information about the charged particles in the liquid and their behaviour [Bartnikas, 1987]. This section presents the results and analysis of the dielectric response measurements of the synthesized ester fluids and focussing on the low frequency response of the oils.

### **5.6.1 DC Conductivity**

Samples of mineral oil (Nynas 10GBN), CPKO, PPKO, PKOAE1, PKOAE2, PKOAE3, and PKOAE4 were studied in this section. The DC electrical conductivity of the samples was evaluated from the conducting current through the respective samples after the application of a step voltage. The volume conductivity results from the presence of free ions from the dissociation of ionizable substances in the liquid samples. The application of a low electric field  $E$ , minimized both the charge-carrier generation by field-enhanced dissociation in the bulk and by electron injection at the electrodes. Also,

the thermodynamic equilibrium of the charge carriers will not undergo significant disturbance at these low fields. [Tobazeon *et al*, 1994]. The current that follows the application of a DC electric field is time dependent. The response of the step voltage, which results in the decrease in the conduction current until the current becomes stable, represents the DC conduction of the oil. The DC conductivity of the samples was evaluated from the measured conduction current after one minute. The volume conductivity is related to the current density with expression;  $\sigma_0 = J_0 / E$  following Ohm's law, where  $J_0$  is the DC current density. The DC conductivity of the samples was evaluated from the current measured with the picoammeter and the geometry of the test cell. CPKO and PPKO were measured at 30°C, and other samples at 20°C. The DC conductivities of Nynas 10GBN, CPKO, PPKO, PKOAE1, PKOAE2, PKOAE3, and PKOAE4 are shown in *Table 5.6*. The DC conductivity of palm kernel oil was found to decrease by a factor of approximately 10 after purification. The purified oil, PPKO, was found to have a conductivity of approximately 10 times greater than that of Nynas 10GBN mineral oil. The alkyl esters were found to have an increased conductivity compared with PPKO. This increment may be related to the liquid reduced viscosity and impurities introduced during processing.

**Table 5.5 : DC Conductivity**

<i>Samples</i>	$\sigma_{DC} (S/m)$
Min Oil	$2.60 \times 10^{-13}$
CPKO	$2.76 \times 10^{-11}$
PPKO	$3.40 \times 10^{-12}$
PKOAE1	$1.18 \times 10^{-10}$
PKOAE2	$1.06 \times 10^{-9}$
PKOAE3	$1.73 \times 10^{-9}$
PKOAE4	$4.46 \times 10^{-9}$

Note: Values for CPKO and PPKO are at 30 °C, while the values for Min Oil, ester samples are at 20 °C

### 5.6.2 Frequency Response Analysis

Dielectric response of samples of Nynas 10GBN, CPKO, PPKO, PKOAE1, PKOAE2, PKOAE3 and PKOAE4 were measured. From the measured dielectric loss and current density expressed in equation 2.20 and conductivity relation,  $\sigma = J_1 / E$ , the expression [Bartnikas, 1994];

$$\sigma_{ac} = \omega \varepsilon''$$

was obtained to evaluate the AC conductivity of the samples. Where  $\varepsilon''$  in this context includes both the polarization loss and DC conductivity. The effect of the amount of acidified clay used in the purification process is shown in *Figure 5.18*. The histogram shows a decrease in the conducting properties of the oil with increasing amounts of activated clay used. This results in a decrease in the low frequency dispersion and dielectric loss of the oil due to a decrease in the concentration of charged particles in the oil. The more activated clay used, the more charged impurities are stripped off the oil until optimum performance of the acidified clay is reached. The calculated AC conductivity for CPKO and PPKO (treated with 10% acidified clay) was not found to be significantly different from the evaluated DC conductivity because the DC electrical conduction mechanism dominates in samples at the measurement temperature and within the spectrum of frequencies studied. The AC conductivity of PPKO reduced by an order of magnitude compared with the conductivity of the original sample (CPKO) as shown in *Table 5.6*. The magnitude of dielectric loss as evident from the imaginary part of relative permittivity decreased after the oil had undergone purification processes. This may have resulted from the cationic exchange property of the activated clay due to

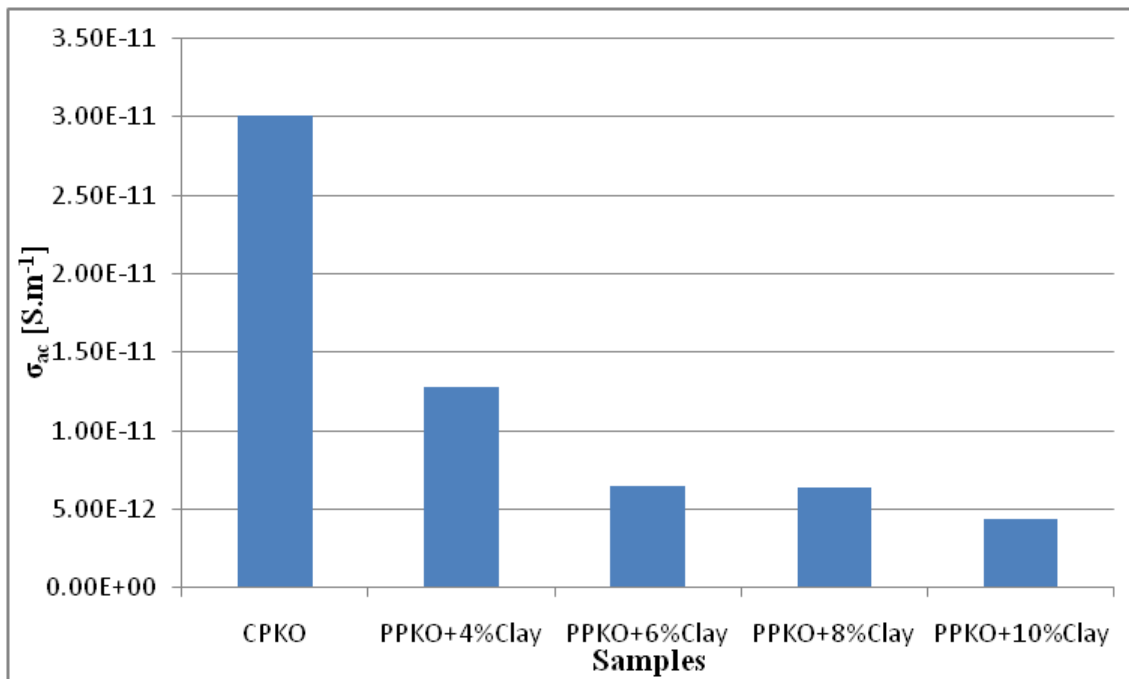


*Figure 5.18: Histogram showing effect of percentage of Acidified Clay in The purification of Palm Kernel Oil*

its highly charged surface that was covered with hydrogen ions. This action may have removed magnesium from the centre of the chlorophyll complex of the oil, rendering the phenophytin adsorbable to the clay. It may have equally removed heavy trace metal pro-oxidants such as iron, copper and nickel [Lusas, 2007] which were reported to be present in the oil sample [Obi *et al*, 2001].

**Table 5.6 : AC Conductivity and Activation Energy**

<i>Samples</i>	$\sigma_{AC}(S/m)$	<i>Activation Energy for <math>\sigma_{AC}</math> (eV)</i>
Min Oil	$4.6 \times 10^{-13}$	0.45
CPKO	$3.01 \times 10^{-11}$	0.33
PPKO	$4.35 \times 10^{-12}$	0.47
PKOAE1	$5.72 \times 10^{-10}$	0.27
PKOAE2	$1.68 \times 10^{-9}$	0.18
PKOAE3	$2.95 \times 10^{-9}$	0.13
PKOAE4	$9.89 \times 10^{-9}$	0.10

Note: Values for CPKO and PPKO are at 30 °C, while the values for Min Oil, ester samples are at 20 °C

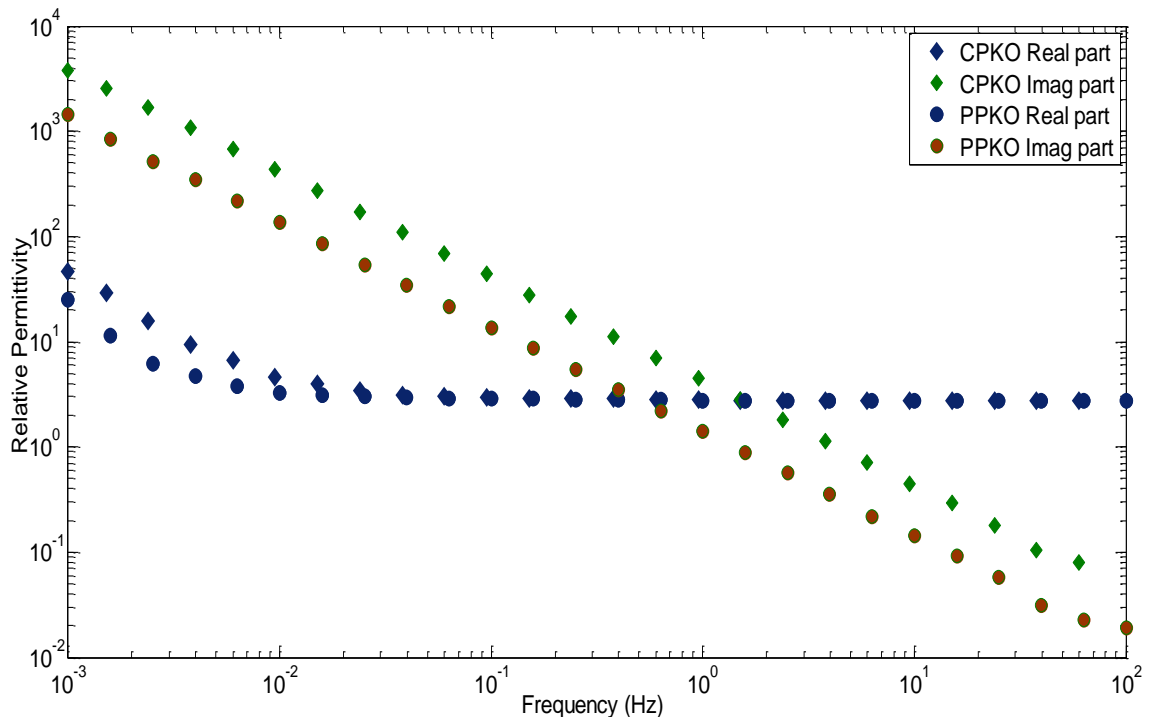


**Figure 5.19: Real and imaginary parts of the dielectric permittivity for the dielectric fluids CPKO and PPKO measured at 80 °C**

Figure 5.19 shows the real and imaginary components of permittivity as a function of frequency (i.e. a Bode plot) for CPKO and PPKO measured at 80°C using the Solatron

frequency response analyzer and dielectric interface. Above the frequency of approximately 10<sup>-2</sup> Hz the real part is constant (i.e. independent of frequency) and the imaginary part is inversely proportional to frequency. This is symptomatic of a constant capacitance in parallel with a constant conductance – that is, a constant electrical conduction mechanism dominates in this frequency range. At lower frequencies, the real part acquires a negative slope greater than 1 at 10<sup>-2</sup> Hz whilst the imaginary part still maintains a slope of -1. This is indicative of interfacial polarization [Jonscher, 1983].

Trendline was fitted on the tanδ curves and a close inspection of the experimental and the model data reveals a good fit for the experimental data of PPKO and CPKO samples. While the fit on PPKO slope of -1 and 1 at the right and left hand sides of the peak respectively, the peak of CPKO was broader with estimated slope of 0.4 at the left hand side of the peak.

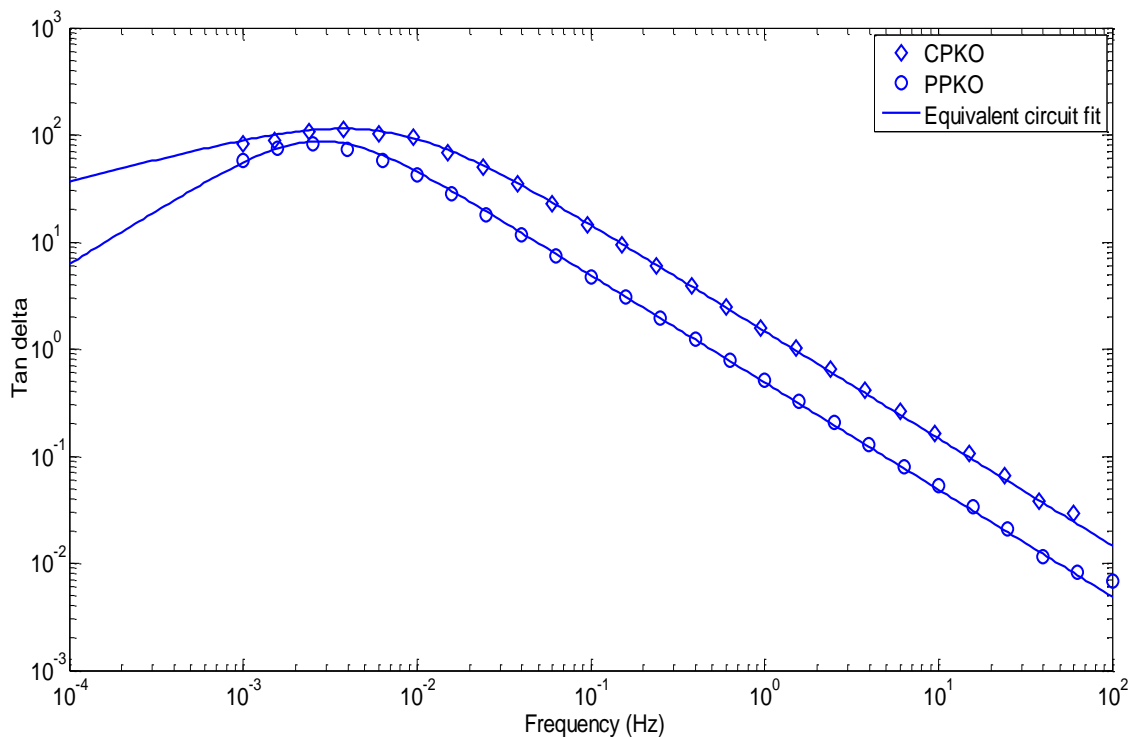


Figure 5.20: *Tanδ and fitted thread line for the dielectric fluids CPKO and PPKO measured at 80°C*

The dielectric response of the synthesised esters is similar to that of the palm kernel oil samples but with a more complex low frequency response. Temperature variations often influenced the response of dielectric material on the application of electric field. This change in temperature may lead to variation in the individual relaxation times. This will result in a shift of the respective tanδ peak along the logarithmic frequency axis. The

effect of temperature on the characteristic frequency of the materials can be studied with a single curve known as master curve. This curve is constructed by normalizing the data for different temperatures. This is done by shifting the spectra for different temperatures into coincidence. If there is more than one process, e.g. a DC conduction and an (AC) polarization processes, and if this processes have different dependencies on temperature, then it will only be possible to bring the part of spectra corresponding to one process into coincidence using this process. A logarithmic shift was performed on the response of the samples along the frequency axis by using DC conduction to bring the spectra into coincidence. The spectrum at 20°C was chosen as the reference while the spectra at other temperatures were shifted towards it. The magnitude was invariant and as a result, the logarithmic shift along the frequency axis was carried out with the relation:

$$\text{shift factor} = \log a_T = \log(\omega_i) - \log(\omega_{ref}) = \frac{E_a}{k} \left( \frac{1}{T_{ref}} - \frac{1}{T_i} \right) \quad 5.3$$

Where  $\log a_T$  is the logarithmic shift between any two frequencies,  $\omega_{ref}$  and  $\omega_i$  along the frequency axis corresponding to the same magnitude of the dielectric response function at  $T_{ref}$  and  $T_i$ .  $E_a$  is the activation energy.

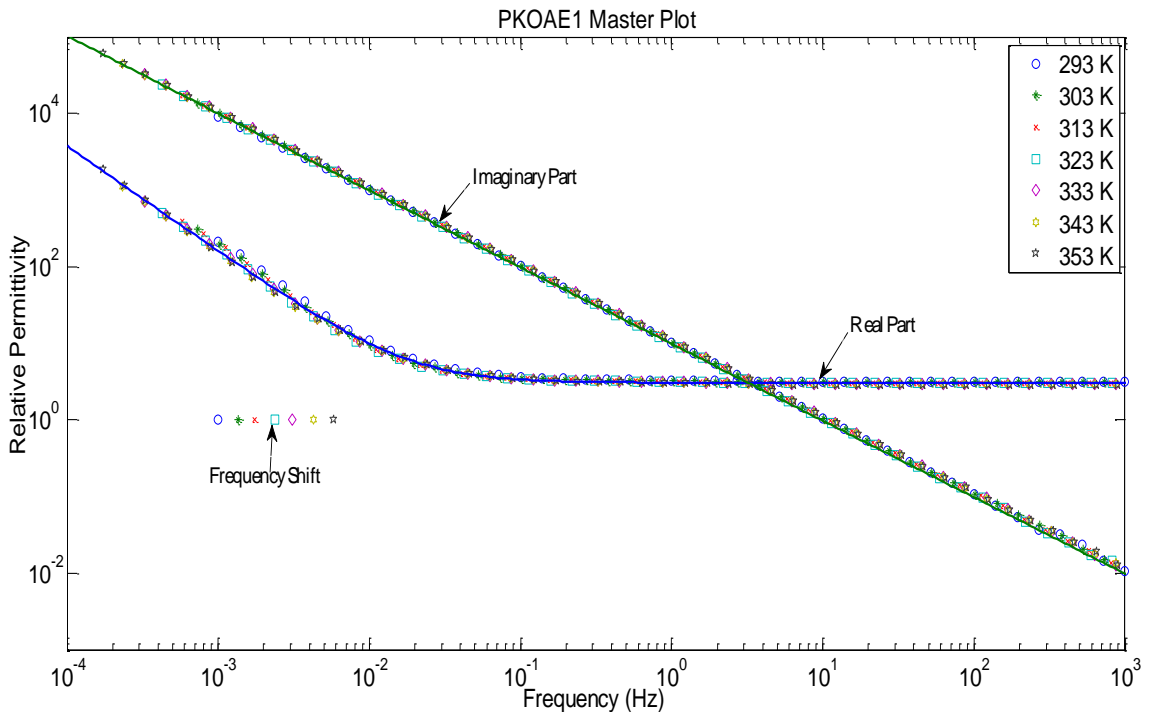


Figure 5.21: Master Curve for Dielectric Response of PKOAE1 (Solid line is the Equivalent Circuit Fit)

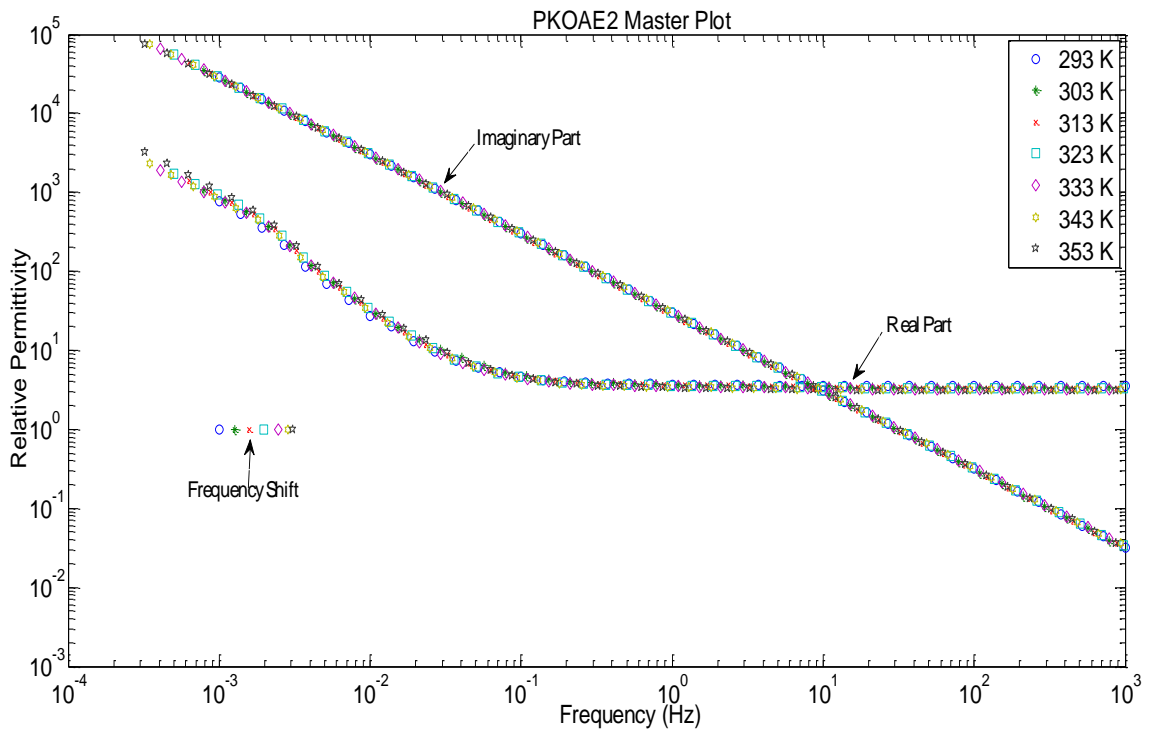


Figure 5.22: Master Curve for Dielectric Response of PKOAE2

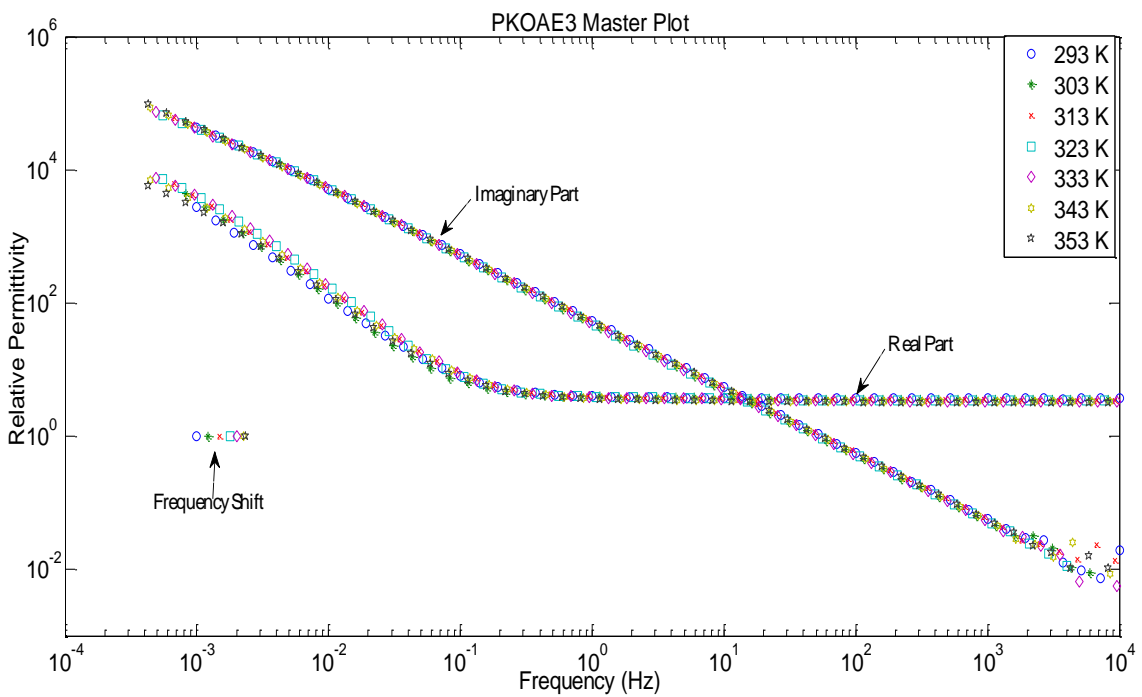


Figure 5.23: Master Curve for Dielectric Response of PKOAE3

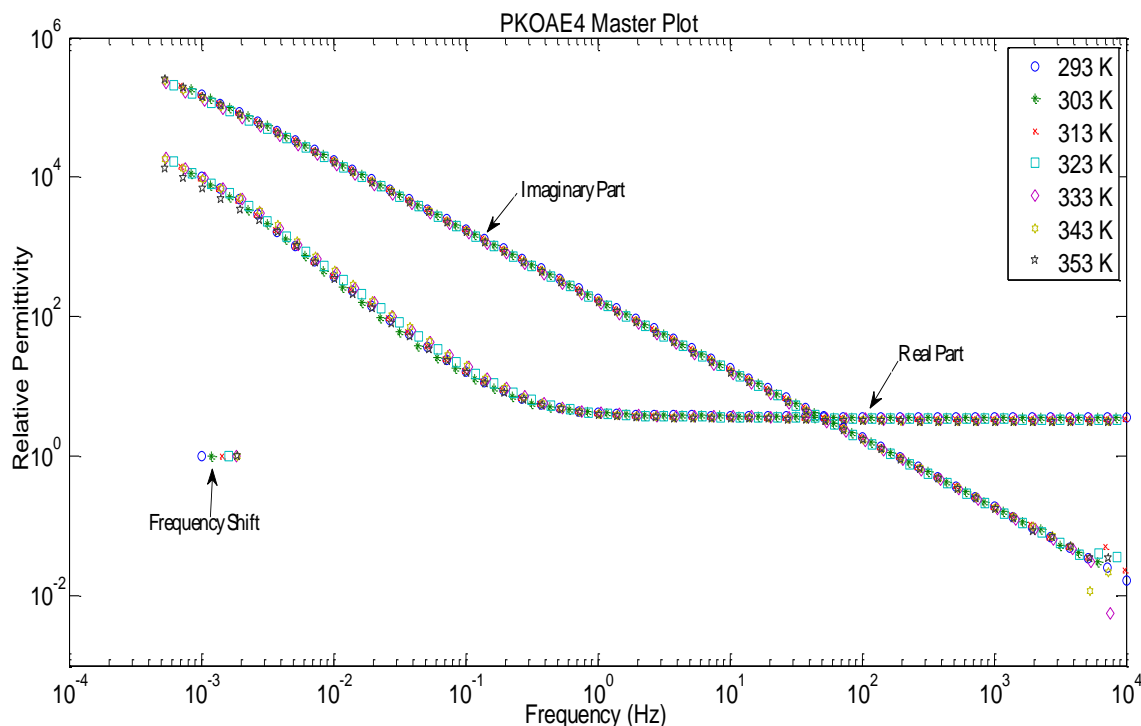


Figure 5.24: Master Curve for Dielectric Response of PKOAE4

The shift was applied to both real and imaginary parts as they are inter-dependent on Kramer Kronig relationship [Jonscher, 1983]. Figure 5.21 through Figure 5.24 displayed the master plots of the real and imaginary components of permittivity as a function of frequency (i.e. a Bode plot) of the alkyl esters of palm kernel oil. The frequency response displayed a departure from simple Debye type relaxation. The real part is constant (i.e. independent of frequency) above approximately  $10^{-1}$  Hz, while the imaginary part is inversely proportional to frequency with a slope of -1. This behaviour as explained for CPKO and PPKO is an indication of a conduction mechanism dominating in this frequency range.

The master curve of the alkyl ester samples was constructed by matching the imaginary part of the permittivity i.e. the DC conduction component. The low frequency wing of the real part was found not to match with each other, suggesting a different temperature dependent process. PKOAE1 has lower conductance compared with the other ester samples. The conductance increased with processing steps. The charges responsible for conduction in the liquid result from the dissociation of ionic and solid impurities in the liquid. Impurities introduced into the sample during processing may have contributed to the conduction current. At frequencies, below  $10^{-1}$  Hz, the imaginary part maintains a slope of -1, and the real part acquires a slope between -1 and -2. This is still an

indication of a strong dispersive behaviour (interfacial polarization), an effect arising from the capacitive layer near the electrode.

Similar to the behaviour of CPKO and PPKO samples, below the frequency of  $10^{-1}$  Hz, the ionic species drifted to the electrode-liquid interface to accumulate near the electrode surface. Reversal of the applied electric field leads to redistribution of the accumulated charges near the electrode and setting up a new equilibrium. Under constant electric field, a double layer is formed and is thought to be made up of several "layers". In a liquid with low conductivity, it is assumed that two layers exist at the electrode [Shmidt, 1994]. The closest layer to the electrode is referred to as the Stern layer. This is a compact layer of ions next to the electrode. The double layer of the ester samples may have contained the oil molecules and ionic species. Following the Stern layer is a layer of ions that are distributed in a three dimensional region called the diffuse layer. This layer is also referred to as Gouy-Chapman layer (See *Figure 5.25*). This layer extends into the bulk liquid because of the counter actions of electrostatic field and thermal agitation in the liquid. At higher frequencies, the time scale was too short for the ions to align to form the electric double layer (EDL) at the electrode liquid interface. As the frequency drops below  $10^{-1}$  Hz, the ions have much longer time to align themselves forming the EDL. The formed double layer contributed a finite value that results in increase in the real part of the capacitance.

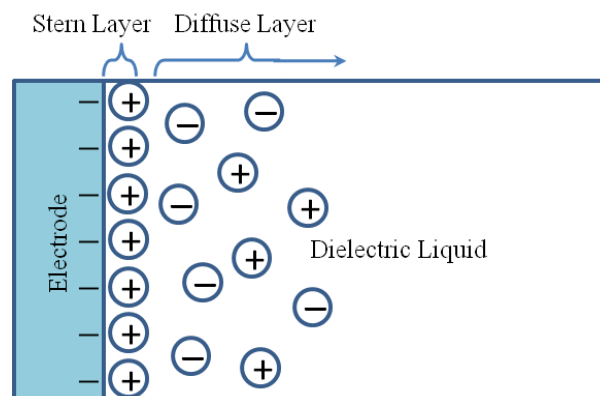


*Figure 5.25: Model of Electric Double Layer*

PKOAE2, PKOAE3 and PKOAE4 appeared to exhibit similar behaviour with PKOAE1. But a close inspection of the spectra reveals that, the real part of dielectric response of the esters undergoes a change below the frequency of  $10^{-1}$  Hz. A very slow response was observed on the real part of the permittivity with an approximate slope

of -1. The low frequency dispersion is equivalent to a dispersive barrier in series with the bulk conductance. However, the dispersive barrier appeared to have a more complex behaviour compared with the behaviour of PKOAE1 sample within the frequency range studied. At the onset of electrode polarization phenomenon, the frequency dependence of the real relative permittivity is proportional to  $\omega^{n-1}$ , where the value of  $n$  is between 0.45 and 0.65 for the three samples. This slope gradually changes to about -1 at lower frequencies. This suggests that the establishment of the EDL may be tending towards steady state. This change in the low frequency dispersion could be due to the ionic species undergoing interfacial electrochemical processes [Jonscher, 1983], or ions of lower mobility may have contributed to the EDL formation within the frequency region. Variation in the thickness of the layer at the electrode-liquid interface may also have caused the change in the slope of the real part of the dielectric response at lower frequencies.

### 5.6.3 Arrhenius Behaviour of Frequency Response

Information on the influence of thermal energy on the behaviour of the double layer can be extracted from the characteristic frequency shift. The influence of temperature on the characteristic frequency was determined with equation 5.5. The plot of the characteristic frequency shift in the dielectric response of PKOAE1, PKOAE2, PKOAE3, and PKOAE4 is shown in *Figure 5.26*.

The real and imaginary parts of relative permittivity of ester samples obey simple Arrhenius behaviour with correlation coefficients ( $R^2$ ) ranging from 0.96 to 0.99. The ester samples displayed systematic linear shift in the characteristic frequency as the temperature increased. PKOAE1, PKOAE2, PKOAE3, and PKOAE4 possessed activation energies of 0.27, 0.18, 0.13, and 0.08 eV respectively. The single activation energy is an indication that the double layer formation is a thermally activated process. The relaxation time of electrode polarization expressed as [Raju, 2003];

$$\tau_{EP} \propto \frac{1}{T} \exp \frac{c}{kT} \quad 5.4$$

decreases with increasing temperature; where  $c$  is a constant for a given liquid. The systematic shift in the characteristic frequency along logarithmic frequency axis may be due to changes in the relaxation time of electrode polarization.

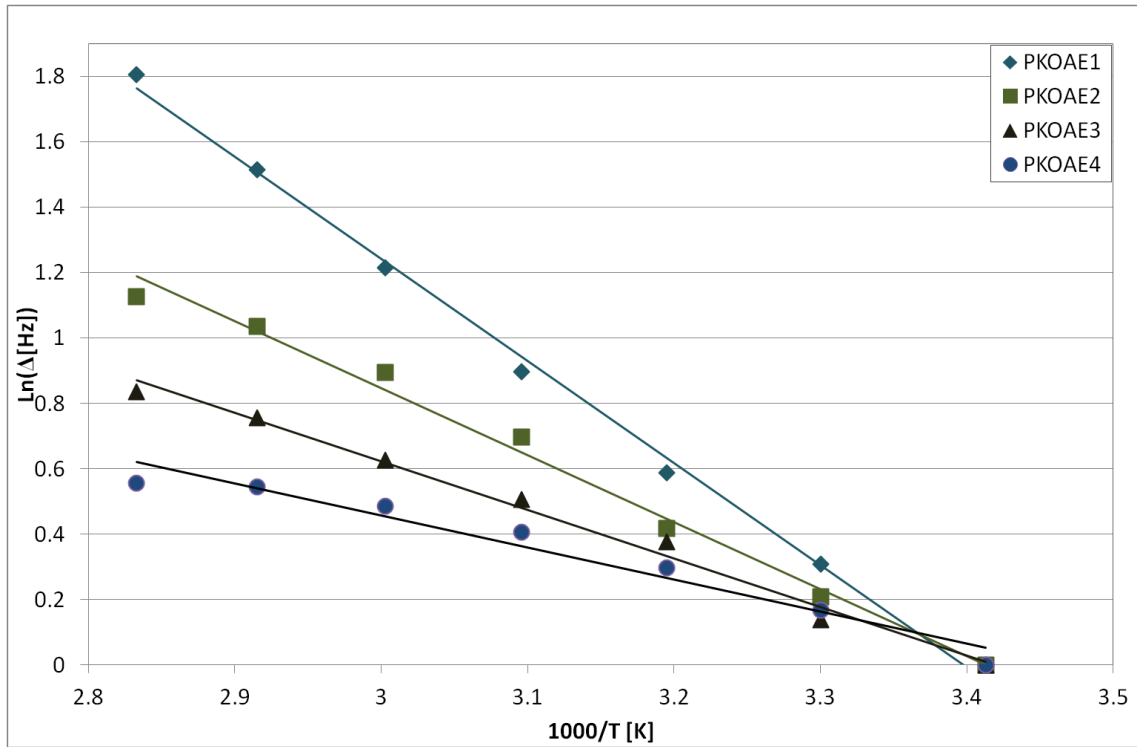


Figure 5.26: Characteristic Frequency Shift of Ester Dielectric Response on Arrhenius Axes

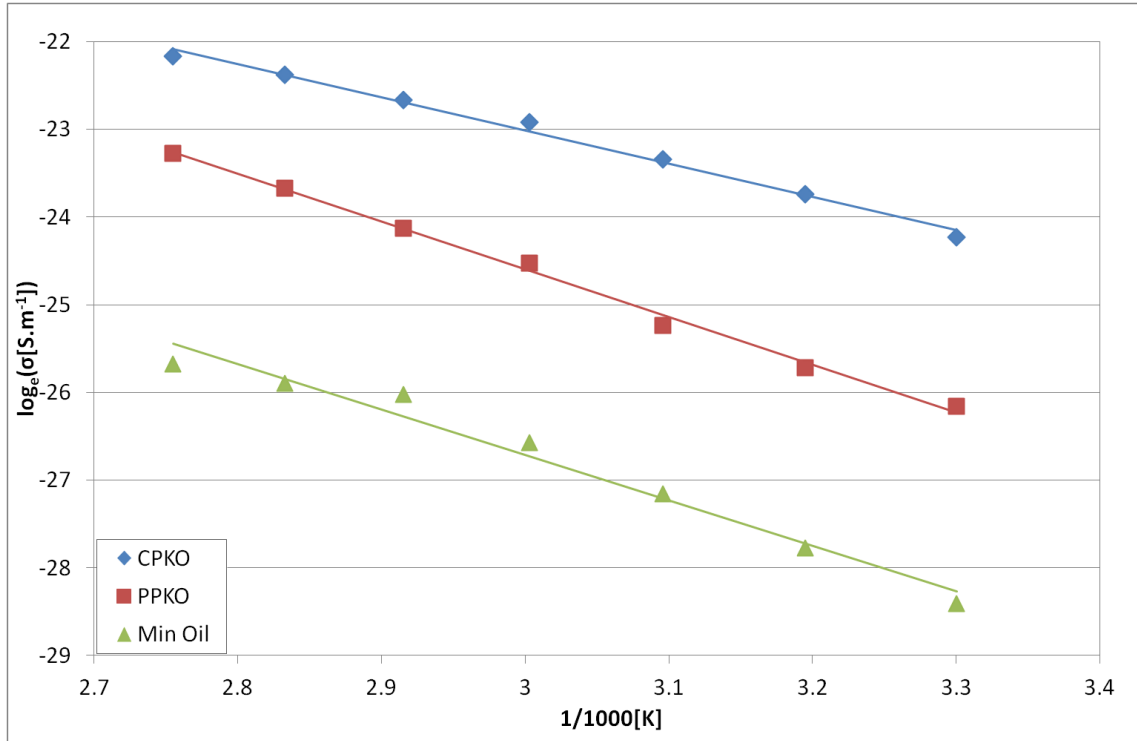


Figure 5.27: Plot of Electrical Conductivity of Oil samples on Arrhenius

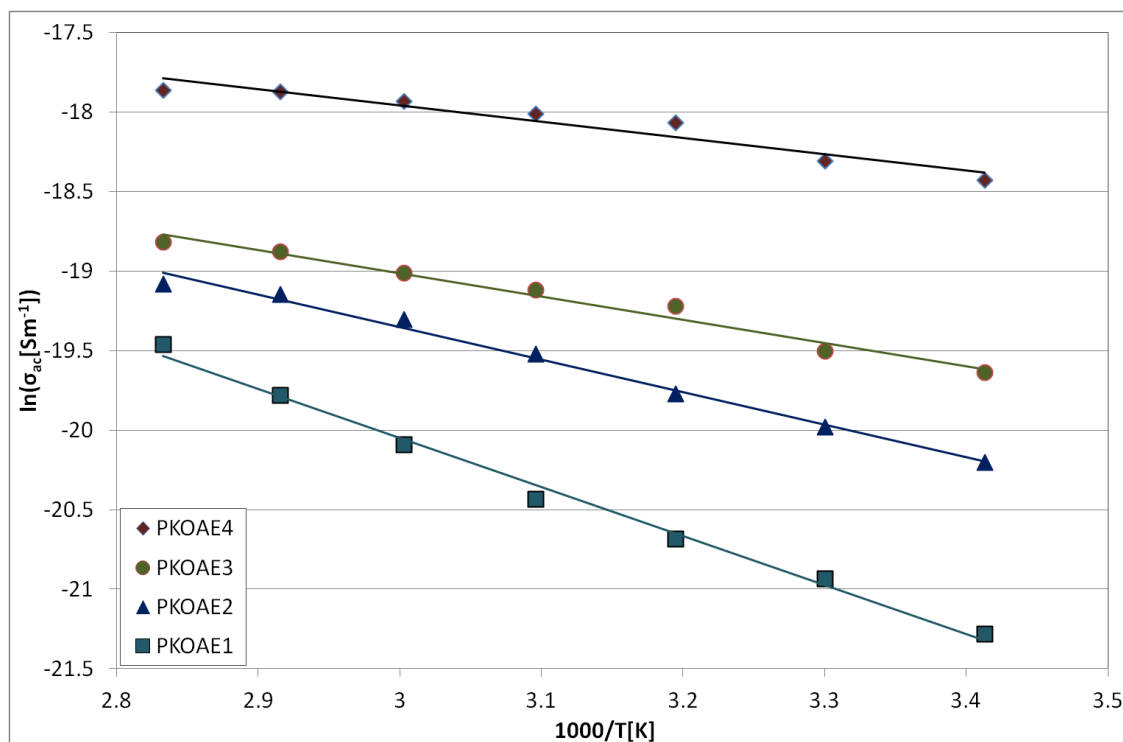


Figure 5.28: Plot of Electrical Conductivity of Ester samples on Arrhenius Axes

The AC conductivity of CPKO, PPKO, PKOAE1, PKOAE2, PKOAE3 and PKOAE4 is plotted on Arrhenius axes in Figure 5.27 and Figure 5.28. The electrical conductivity was evaluated from the imaginary part of the frequency response data of the samples within the temperature range of 20°C to 80°C. The straight lines obtained indicate thermally activated transport mechanisms. The activation energies of CPKO, PPKO, PKOAE1, PKOAE2, PKOAE3 and PKOAE4 derived from this Arrhenius plot are shown in Table 5.6. Over the temperature range of 20 to 80°C, the electrical conductivity of the palm kernel oil was found to decrease by a factor of approximately 10 after purification. The plot of conductivity of the samples calculated from the imaginary part of the dielectric response data shows single activation energies. This suggests that the ionic conduction loss may have resulted from ion transport that is thermally activated. The calculated conductivity for the ester samples is higher than the purified oil sample (PPKO) which increased from PKOAE1 through PKOAE4. The low viscosity of the esters and concentration of conducting particles may have influenced their increased conductivity. However, the activation energy decreased from PKOAE1 through PKOAE4. The electrical conductivity is therefore a thermally activated process with higher activation energy found in the samples with lower concentration of mobile impurities. Although the activation energy of Nynas 10GBN is about the same with PPKO, the Arrhenius plot of Nynas 10GBN is not quite a straight line. The off point may be due to experimental

error. The conductivity is relatively constant with frequency as was reported by Bartnikas for most insulating liquids [Bartnikas, 1994].

## 5.7 Dielectric Breakdown Characteristics of Ester Fluids

The characterization of breakdown field strength of materials requires several measurements on ‘identical’ samples. The variation in the values of each breakdown for the same sample is due to random distribution of the weakest paths. Probability density functions which include the Gaussian, the Weibull, and the Gumbel probability distribution functions can be used as analytical tool for the breakdown behaviour. The Weibull statistics is based on extreme-value statistics and is most commonly used. It was reported to have wide applicability and is based on an extreme value distribution in which the system fails when the weakest link fails [Dissado *et al*, 1992]. It also allows the analysis of small data set. The cumulative probability of failure for the two-parameter Weibull distribution is given by equation 5.5;

$$f(v) = 1 - \exp\left\{-\frac{v}{\alpha}\right\}^{\beta} \quad 5.5$$

Where  $f(v)$  is the cumulative probability of breakdown at voltage,  $v$ ,  $\alpha$ , the characteristic breakdown voltage is the value of  $v$ , at which the cumulative probability of failure is  $(1 - \exp\{-1\}) = 0.632$ , and  $\beta$ , is the shape parameter, which is a measure of the range of failure voltages within the distribution. The breakdown field data was fitted into the Weibull distribution function and the Characteristic breakdown field of the samples, the shape parameter, and the confidence bounds of the distribution describing the samples were estimated.

*Figure 5.29* through *Figure 5.33* display the Weibull plot of AC breakdown field data of palm kernel oil samples and the ester derivatives. The Weibull parameters of the oil samples are given in *Table 5.7*. The characteristic breakdown strength of the samples denoted as  $\alpha$ , and the shape parameter,  $\beta$ , are tabulated with their respective 95% confidence intervals. The correlation coefficients of the breakdown data when fitted to the Weibull function, equation 5.5, are much greater than the critical correlation coefficient of  $R^2=0.918$  for 10 breakdowns [IEEE Std 930-2004, 2005]. This demonstrates a strong linear relationship between the two variables. There is a

significant difference in the characteristic breakdown strength of CPKO when compared to the purified oil samples. The statistical data shows a slight improvement in the characteristic breakdown strength of the alkyl ester samples when compared with PPKO. This shows that the derivatives of purified palm kernel oil have improved breakdown field strength. The characteristic electric field strength of the palm kernel oil ester derivatives under 1 mm gap is about 59% higher than Nynas 10GBN mineral insulating oil.

The high values for the fitted shape parameter,  $\beta$ , of palm kernel oil ester derivatives demonstrates that the ester derivative have a narrow distribution of breakdown field. In *Figure 5.29*, the crude (CPKO) oil is compared with the purified oil (PPKO). Although the two distributions have different slopes, the characteristic breakdown strength (63.2% cumulative probability) of the purified oil is significantly higher. This could be due to reduced concentration of impurities observed as a reduction in the DC conductivity. This low breakdown strength of CPKO suggests that the impurities in the liquid may have aligned to at least partially form a bridge across the gap due to its attraction towards higher field region. This may have increased the field in the liquid within the gap, leading to breakdown after it reached critical value.

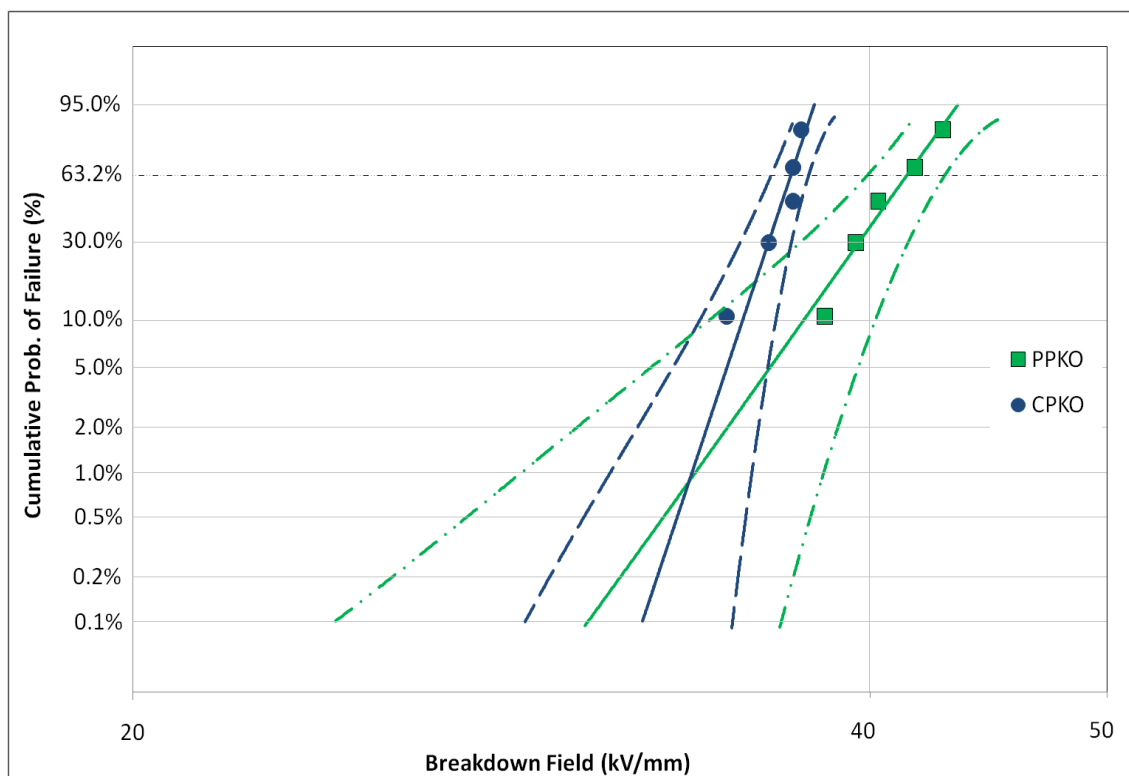


*Figure 5.29: Weibull Plot of CPKO and PPKO*

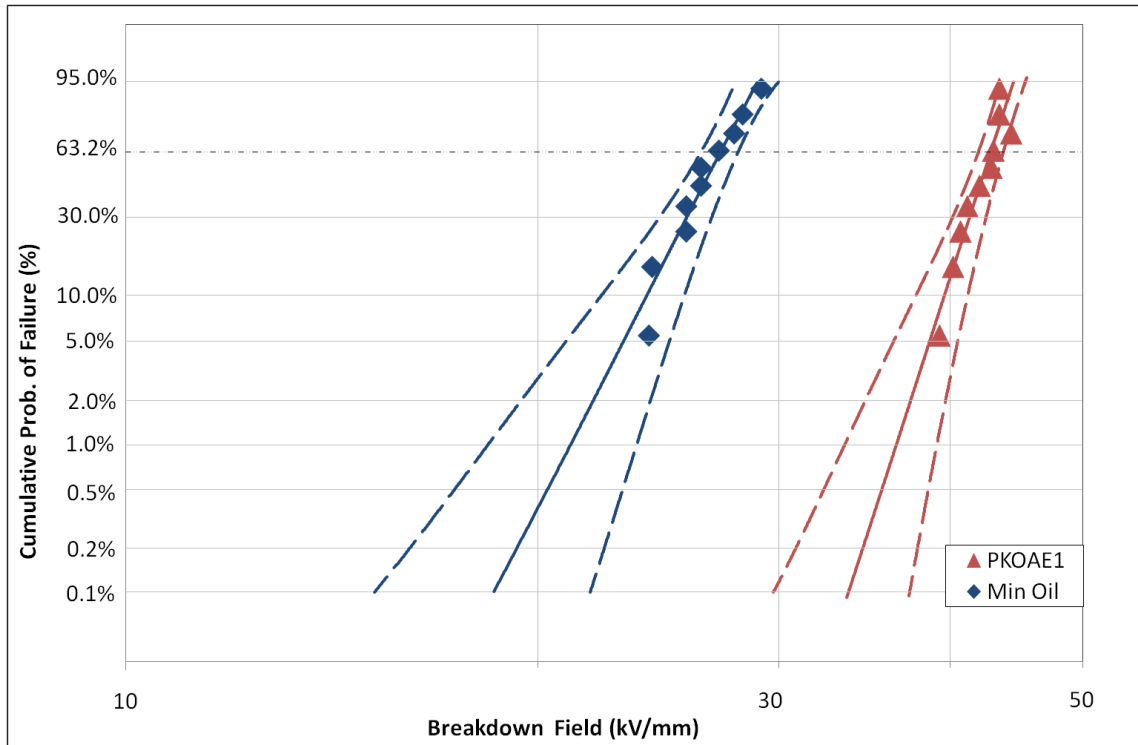


Figure 5.30: Weibull Plot for Synthesized Esters

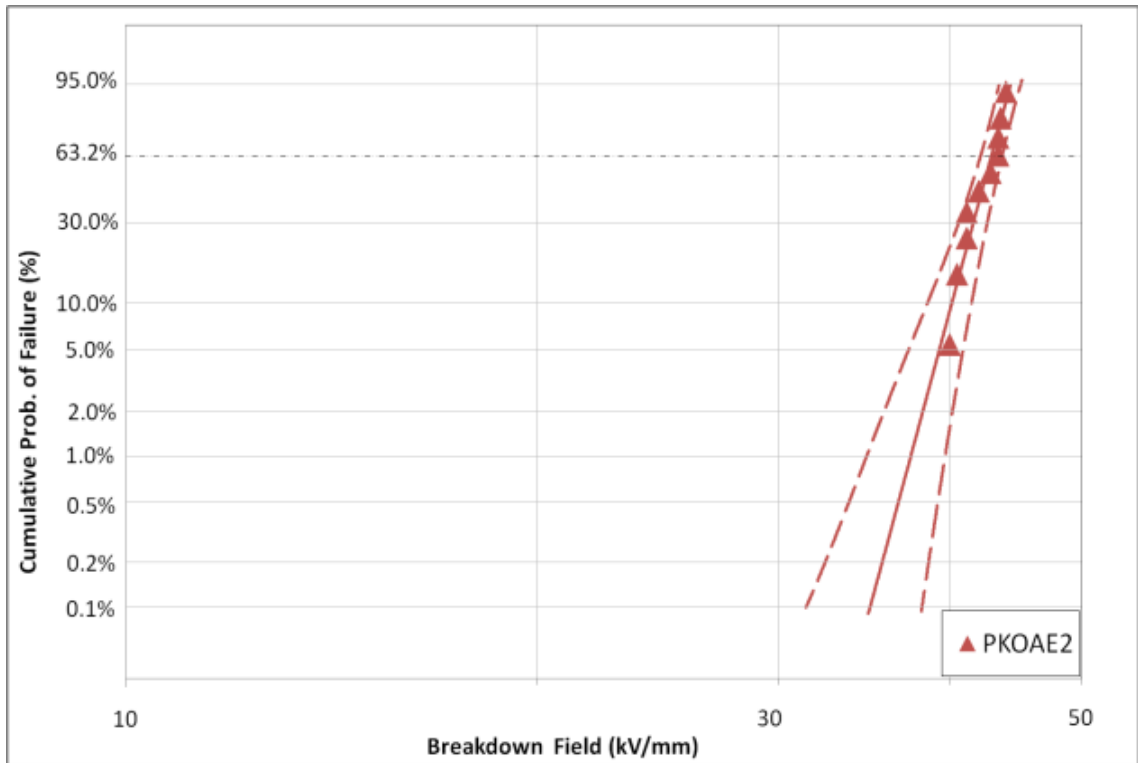


Figure 5.31: Weibull Plot for Synthesized Esters

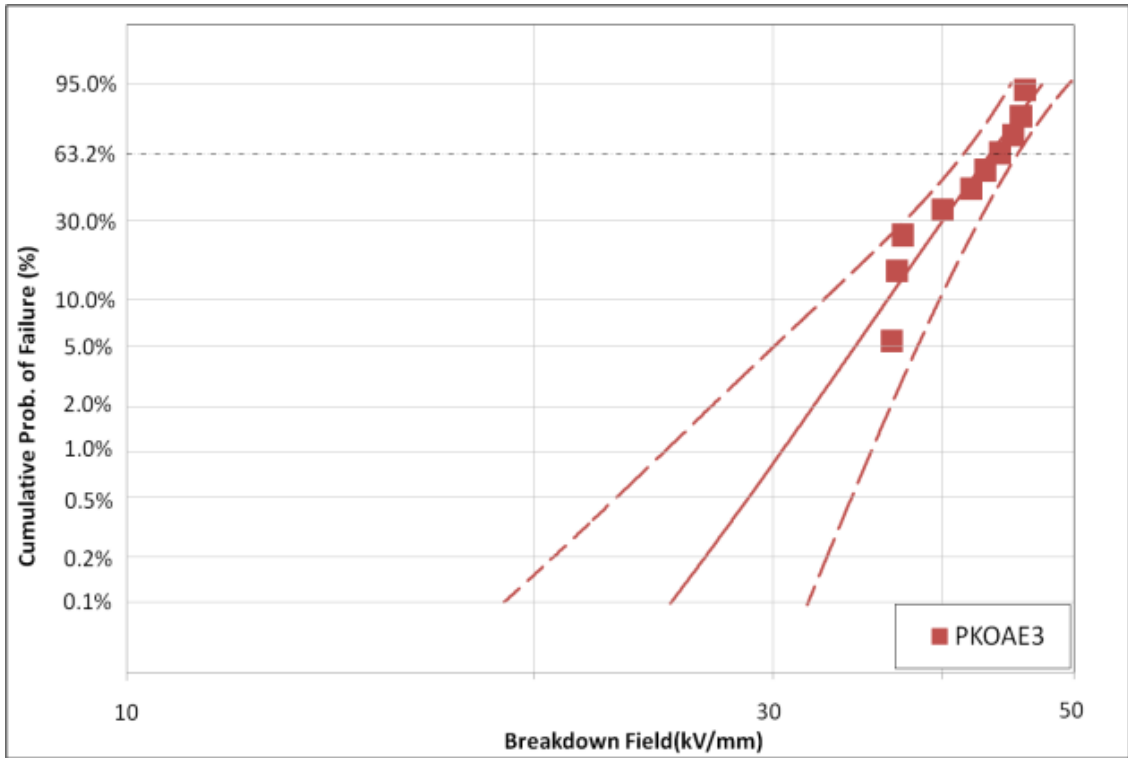


Figure 5.32: Weibull Plot for Synthesized Esters

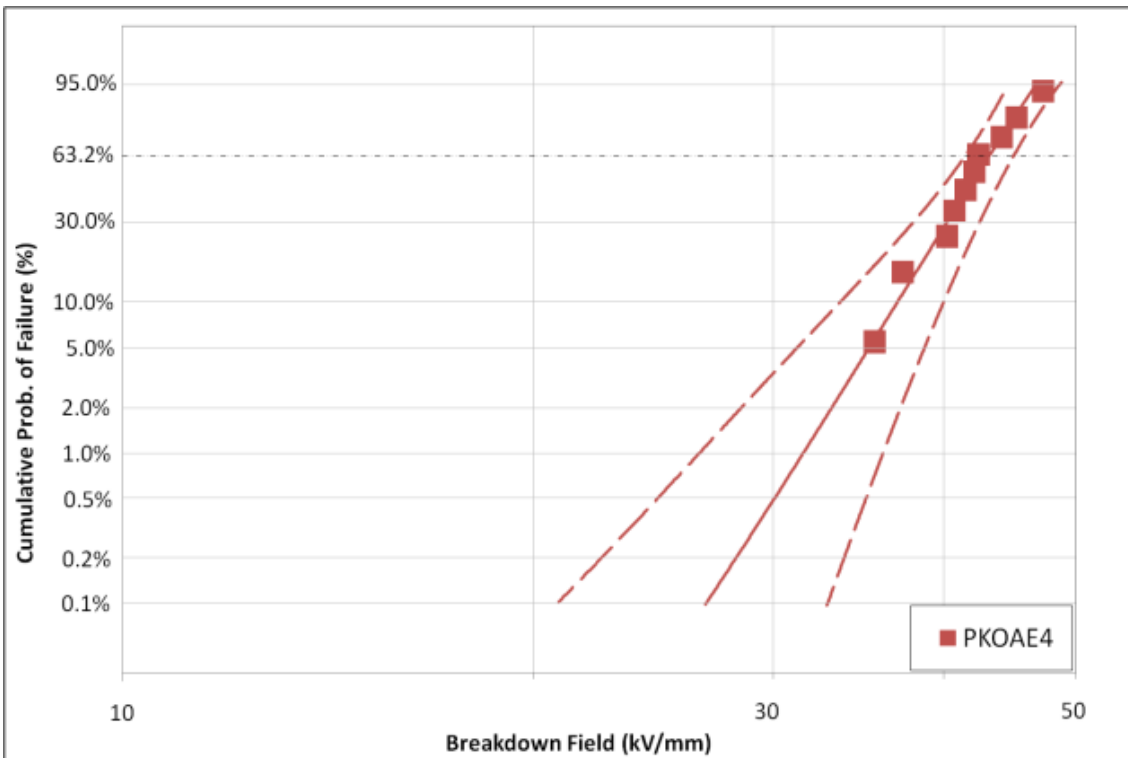


Figure 5.33: Weibull Plot for Synthesized Esters

Over the full range of failure probability, the characteristic breakdown strength of the esters is significantly greater than the mineral oil. The ester samples contain particles as impurities which are dispersed in the liquid. Application of a high electric field may

have caused the particles to drift towards the region of strongest field. The strongest field is around the region of shortest distance for the sphere-sphere electrode gap. The particles in the field region may have resulted in flux concentration at the surface of the high voltage electrode. Other particles may also have been attracted towards the higher flux concentration and may have aligned to form a partial bridge across the gap. This may have possibly led to an increase in the field in the liquid. The number of particles may not be sufficient to bridge the gap to cause early breakdown. The partial bridge particles caused local field enhancement which may have resulted in local breakdown near the particles when the field exceeds the dielectric strength of the liquid. This could result to formation of gas bubbles. Discharges may then occur when the electric field in the spherical gas bubbles becomes equal to the gaseous ionization field. The end result is the decomposition of the liquid and the eventual breakdown of the samples. The Weibull distribution of the synthesized esters was compared to that of mineral oil (Nynas 10GBN).

*Table 5.7: Weibull Parameters of the Breakdown Test*

Samples	$N$	Characteristic Value, $\alpha$ (kV/mm)	95% Conf. Bound for $\alpha$ (kV/mm)	Shape Parameter, $\beta$	95% Conf. Bound for $\beta$	Correlation Coefficient
CPKO	5	37	36.50 – 37.65	49.69	21.29 – 119.2	0.958
PPKO	5	41	39.92 – 42.73	23.05	13.13 – 55.31	0.981
PKOAE1	10	43	41.96 – 43.60	28.85	19.25 – 48.32	0.983
PKOAE2	10	43	42.18 – 43.59	33.84	22.58 – 56.68	0.947
PKOAE3	10	43	41.48 – 45.25	12.76	8.51 – 21.37	0.937
PKOAE4	10	43	41.51 – 44.82	14.49	9.67 – 24.27	0.948
Min Oil	10	27	26.33 – 28.00	18.10	12.08 – 30.32	0.931

The results demonstrate that there is no significant difference in the Weibull distribution following epoxidation and esterification. However, the shape parameter of PKOAE1 and PKOAE2 demonstrates that the breakdown values tend to cluster around a modal value with low variability, while that of the branched alkyl esters are more dispersed. High  $\beta$  values for PKOAE1 and PKOAE2 suggest low dispersion in the breakdown data of the samples. The dispersion of the breakdown data of PKOAE3 and PKOAE4 as seen from the  $\beta$  values is higher than that of PKOAE1 and PKOAE2, but close to that of Nynas 10GBN mineral oil. The presented results are comparative studies within the experimental limit of the bespoke breakdown test cell. Large quantity of oil sample is

required for a repeat measurement using standard breakdown test cell to be confident of the values.

## 5.8 Summary

The GC-MS of the samples revealed the changes that occur in the samples during the chemical synthesis. The GC-MS of PKOAE2 displayed the presence of epoxy-alkyl oleate and linolate. The Gas Chromatogram of PKOAE3 and PKOAE4 show the disappearance of the epoxy peaks and appearance of peaks related to the fragments of side branched esters. The FTIR spectra affirmed the structure of the synthesized ester with the appearance of peaks for epoxy functional group in PKOAE2, and appearance of peaks at the fingerprint region of the spectra that is unique to PKOAE3 and PKOAE4 respectively. The separation of glycerol resulted in reduced dynamic viscosity of the synthesized ester. Synthesis of epoxy rings led to slight increase of the dynamic viscosity of PKOAE2. Grafting side branched hydrocarbon chains further increased the dynamic viscosity. Although, the change in the viscosity is not very pronounced, this may be due to the content of unsaturated fatty acid in palm kernel oil. The viscosity of the samples was low compare to mineral insulating oil. The viscosity temperature dependence like most oil follows Arrhenius behaviour. The low temperature thermal analysis revealed a melting point of  $-7\pm 0.5^{\circ}\text{C}$  and pour point of  $-6^{\circ}\text{C}$ . The esters have heat capacity and coefficient of thermal expansion that is comparable to mineral oil. The high temperature thermal analysis shows that the PKOAE1 and PKOAE2 possessed flash point that is above the specified minimum while PKOAE3 and PKOAE4 possessed flash points below the specified minimum. This reduction in flash point may have a link with the presence of anhydride in the sample since flash point is known to be very sensitive to impurities. The oxidative stability is higher than conventional vegetable oil and the addition of anti-oxidant greatly improved the stability of the esters to oxidation.

This chapter also discussed the dielectric behaviour of the ester samples. Purification of the oil sample before synthesis decreased the conductivity by a factor of approximately 10. The synthesized esters have increased conductivity which is possibly related to the reduced viscosity that led to easy transport of charge. Ion transport was identified to be the dominant polarization mechanism in the ester samples. The interfacial barrier that builds up at the electrode sample interface was observed to possess fractional power law

behaviour. Careful inspection of PKOAE2, PKOAE3 and PKOAE4 shows that at lower frequencies, distribution of interfacial effects at the electrode-liquid interface may have caused the non-steady slope of the real part of the dielectric response. The characteristic breakdown field of the esters at small gap is higher than that of mineral oil and the specified minimum for natural ester-based insulating fluid. Statistical analysis of the breakdown field data using Weibull distribution function shows that the characteristic breakdown field of the esters is higher than mineral insulating fluid with comparable shape parameters.

## Chapter 6. Effect of Ageing on the Alkyl Ester-Paper System

Generally, a combination of oil and paper system serves as insulators in transformers. Insulation papers are sheet of materials made from cellulose fibres with voids within the structure when in a dried state. The strength of a dried sheet of insulation paper is dependent on the condition and strength of the fibres of which it is made and the hydrogen bonding between the cellulose molecules [Shroff, 1985]. Voids are present within the structure of the cellulose insulation when it is dried due to space between the fibres. Impregnation of the insulating paper with oil fills the voids. This increases the electrical strength of the composite material as the oil and paper shares the applied electrical stress [Martin *et al*, 2007] and prevents partial discharge in the voids. Ageing leads to deterioration of the composite insulation system. This may in turn lead to decrease in the electrical and mechanical strength of the system. McShane *et al* at Cooper Power System reports that thermally upgraded paper in natural ester possesses slower ageing rate compared with when immersed in mineral oil [McShane *et al*, 2001].

In this chapter, an attempt is made to identify the chemical changes that occurred in the ester fluid after thermally accelerated ageing of alkyl ester-paper system. Aged ester samples were compared with the unaged sample. The effect of ageing on the dynamic viscosity of the oil,  $\tan\delta$  of the oil, and breakdown field of the oil is presented. The chapter also presents the result of the dielectric response of aged alkyl ester impregnated paper. The electrical and tensile strength of the aged alkyl ester-paper system is compared with the mineral oil impregnated paper. Accelerated ageing test could not be performed on the ester samples because to time limitation. The PKAOE1 sample was used for the accelerated ageing experiment since it is the base ester oil. The ageing procedure as shown with a flowchart in *Figure 6.1* involves samples of Nynas 10GBN mineral oil and PKOAE1. These samples were degassed and dried in oven at 85°C for 12 hours. It was allowed to cool to ambient temperature and transferred to the ageing vessel. The thermally upgraded insulating paper that has been vacuum dried at 85°C for 24 hours was placed with the oil in the vessel for vacuum impregnation. Galvanized steel strip, copper strip, and aluminium strip were placed in the vessel. The vessel was sealed with nitrogen at ambient temperature and pressure of 400 kPa. The vessel was thermally aged at 150°C and pressure of 600 kPa for 3 months. Samples taking out of the vessel for analysis are shown in *Table 6.1*. PKOAE00D, EIP00D and MIP00D are samples of unaged ester, ester-paper and mineral oil-paper respectively. PKOAE28D,

PKOAE56D, and PKOAE84D are samples of ester after 28 days, 56 days, and 84 days of ageing respectively, EIP28D, EIP56D, and EIP84D are samples of ester-paper after 28 days, 56 days, and 84 days of ageing respectively, and MIP28D, MIP56D, and MIP84D are samples of mineral oil-paper after 28 days, 56 days, and 84 days of ageing respectively.

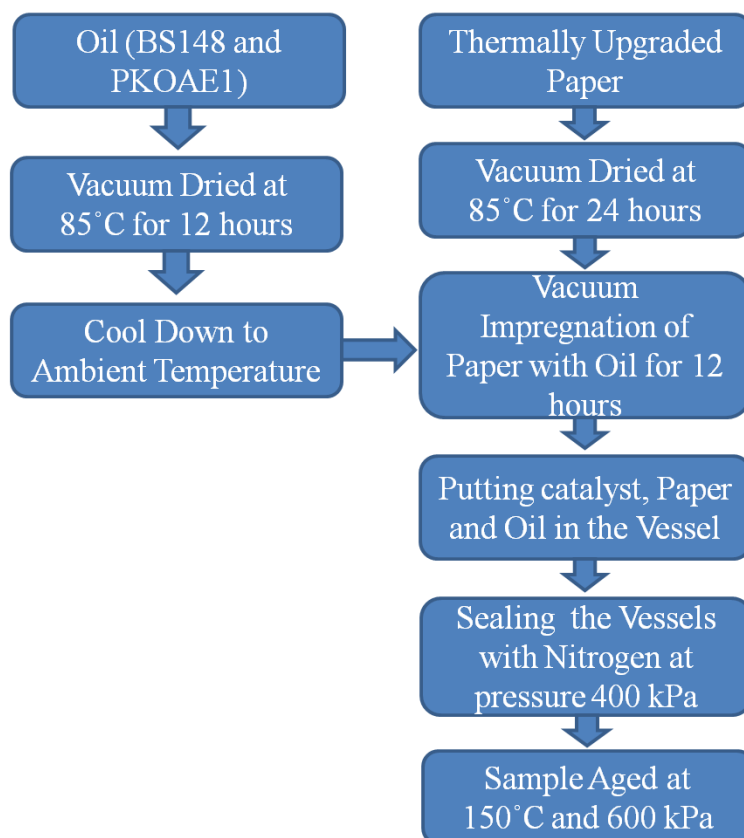


Figure 6.1: Flowchart of Ageing Procedure

## 6.1 Physical Appearance of the Aged Oil Samples

The alkyl ester of palm kernel oil contained about 17% unsaturated fatty acids and 83% saturated fatty acids as mentioned in section 1.2 of Chapter 1. A change was observed as the ester aged with time. There was an appearance of a brownish, gummy substance in the aged samples. This may be due to polymerization of some of the fatty acids forming triglyceride. Solidification deposition was observed on the papers aged in mineral oil. This deposition may have resulted from copper sulphide which was reported to form during mineral oil ageing in the presence of copper due to redox reaction [Hao *et al*, 2011]. The product formed a coat on the copper plates and papers in the mineral oil.

Table 6.1: Aged samples

<i>Sample</i>	<i>Description</i>
<b>PKOAE00D</b>	Unaged Inhibited Alkyl Ester for 0 day
<b>PKOAE28D</b>	Aged Inhibited Alkyl Ester after 28 days
<b>PKOAE56D</b>	Aged Inhibited Alkyl Ester after 56 days
<b>PKOAE84D</b>	Aged Inhibited Alkyl Ester after 84 days
<b>EIP00D</b>	Ester impregnated Kraft paper
<b>EIP28D</b>	Aged Ester impregnated Kraft paper after 28 days
<b>EIP56D</b>	Aged Ester impregnated Kraft paper after 56 days
<b>EIP84D</b>	Aged Ester impregnated Kraft paper after 84 days
<b>MIP00D</b>	Nynas 10GBN Mineral oil impregnated Kraft paper
<b>MIP28D</b>	Nynas 10GBN Mineral oil impregnated Kraft paper after 28 days
<b>MIP56D</b>	Nynas 10GBN Mineral oil impregnated Kraft paper after 56 days
<b>MIP84D</b>	Nynas 10GBN Mineral oil impregnated Kraft paper after 84 days

## 6.2 Identification of the Aged Ester Molecules

The gas chromatogram of the aged ester samples is shown in *Figure 6.2*. There was no additional elution at lower times except at 10.92 minutes in PKOAE28D aged for 28 days. This elution was identified to be tertiary butyl hydroquinone (TBHQ) which was the anti-oxidant that was added to the natural ester-based fluid. After the elution that corresponds to methyl stearate which is the last peak for the unaged alkyl ester in *Figure 6.2a*, the aged sample produced elution at 21.10 minutes, 21.24 minutes, 22.57 minutes, 22.73 minutes, 23.95 minutes and 25.31 minutes as shown in *Figure 6.2b-d*. The longer elution time of these components suggests that they are products with higher molecular weight. This may have resulted from thermal polymerization of the fatty acids. The area under the peaks of the degradation products increased with ageing time, an indication that the formation of the degraded products increased with ageing time.

The FTIR scan of the freshly prepared ester samples displayed spectra with a weak peak around  $3464\text{ cm}^{-1}$  as shown see *Figure 6.3*. This peak is associated with the overtone of the ester of the carbonyl absorption which is about twice the frequency of the glyceride ester carbonyl absorption band. The absorption band around  $3464\text{ cm}^{-1}$  was found to increase after the addition of antioxidant (see Appendix F ). TBHQ exhibit peaks around  $3600 - 3430\text{ cm}^{-1}$  [Ammawath *et al*, 2004]. The band around  $3464\text{ cm}^{-1}$  was

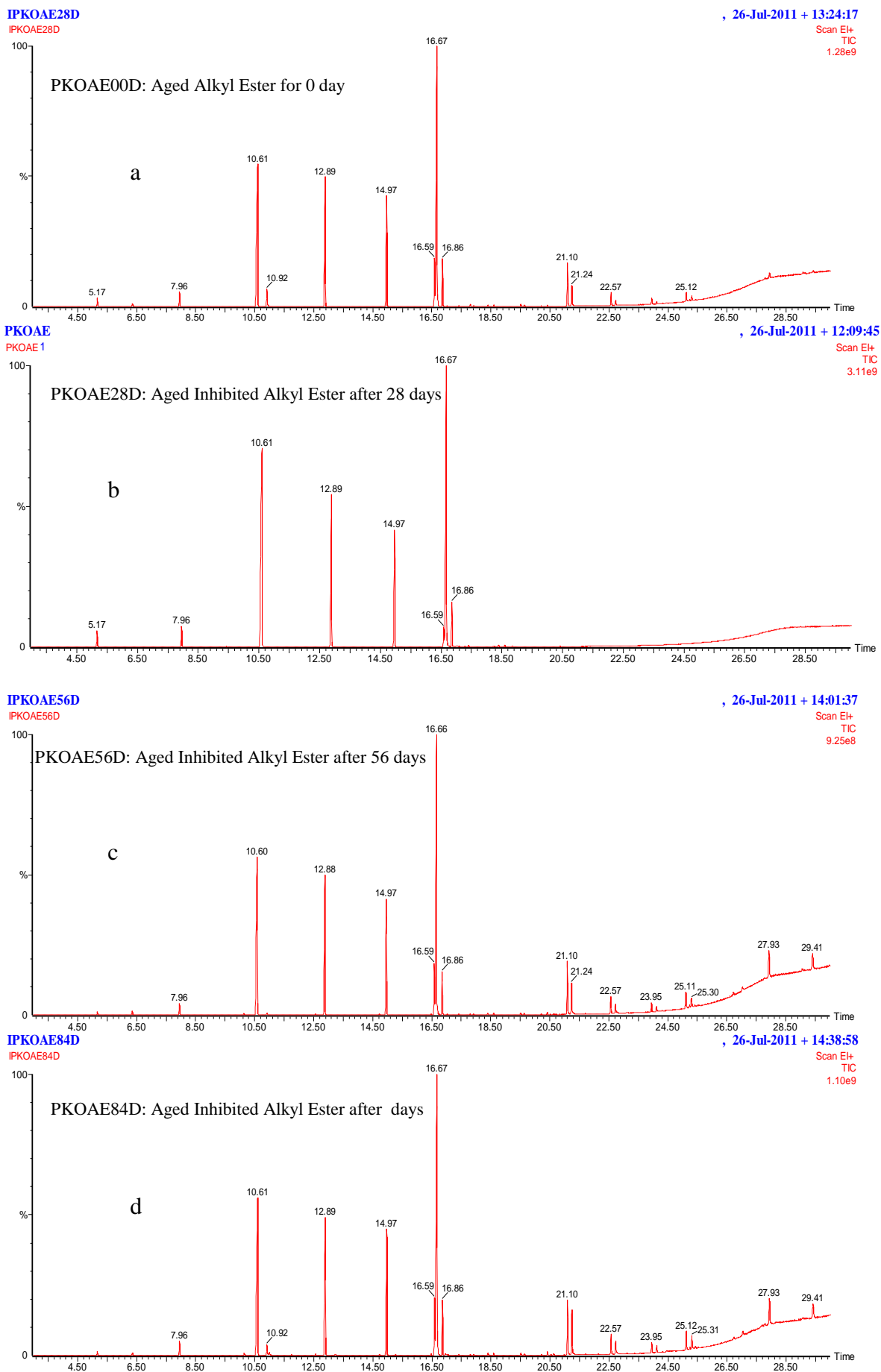


Figure 6.2: GC of Aged PKO Esters

observed to be similar in all samples after thermal ageing. This may indicate that the antioxidant was not consumed during the ageing process. The hydroperoxy functional group peak often appeared around  $3319\text{ cm}^{-1}$  [Hameed *et al*, 2006]. The presence of hydroperoxy functional group peak may be embedded within the TBHQ band.

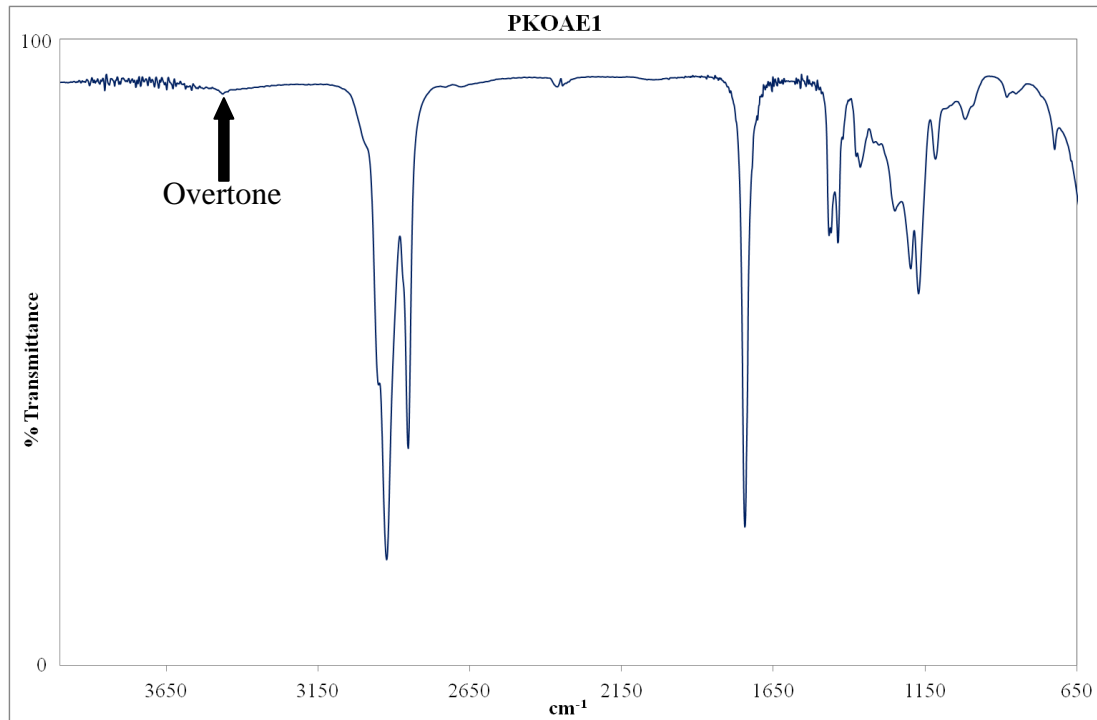


Figure 6.3: Mass FTIR Spectra of Alkyl Ester

### 6.3 Thermo-Chemical Properties of Aged Ester Fluids

Ageing most often leads to an increase in viscosity, and this in turn decreases the cooling efficacy. The viscosity of the ester increased with thermal ageing and exhibited temperature dependent behaviour. The viscosity of the aged ester after 84 days (7.1cSt at  $20^{\circ}\text{C}$ ) was still lower than the viscosity of unaged Nynas 10GBN mineral oil (21.5 cSt at  $20^{\circ}\text{C}$ ). This is an indication that the aged sample can still serve as an effective coolant. The temperature dependence of the aged alkyl ester (PKOAE1) plotted on Arrhenius axis in Figure 6.4 shows a thermally activated process with single activation energy. The viscosity of a polymeric material has been established to be related to its average molecular weight,  $\bar{M}$ , with the expression [Topallar *et al*, 1997]:

$$[\mu] = K\bar{M}^{\alpha} \quad 7.1$$

Where  $[\mu]$  is the viscosity of the polymeric material,  $K$  and  $\alpha$  are constants which depend on solvents and temperature.

There appeared an increase in the viscosity of the aged samples as shown in *Table 6.2*. The high molecular ageing products in the sample as identified from Gas Chromatogram after the thermal stress may have been responsible for the increasing viscosity. The activation energy for viscous flow evaluated from *Figure 6.4* is about the same for all the aged samples, but slightly higher than the unaged sample.

The water content of the sample aged for 80 days increased to 452 mg/kg compared with the initial value of 218 mg/kg. The acidity of the aged ester increased from 0.34 mg KOH/g to 1.68 mg KOH/g.

*Table 6.2: Chemical Analysis of Aged Alkyl Ester*

Sample	Kinematic Viscosity (cSt)	Activation Energy (eV)	Water Content (mg/kg)	Acidity (KOH/g)
<b>PKOAE00D</b>	4.57017	0.17	218	0.34
<b>PKOAE28D</b>	6.09356	0.19	-	-
<b>PKOAE56D</b>	6.77342	0.19	-	-
<b>PKOAE84D</b>	7.15112	0.19	452	1.68

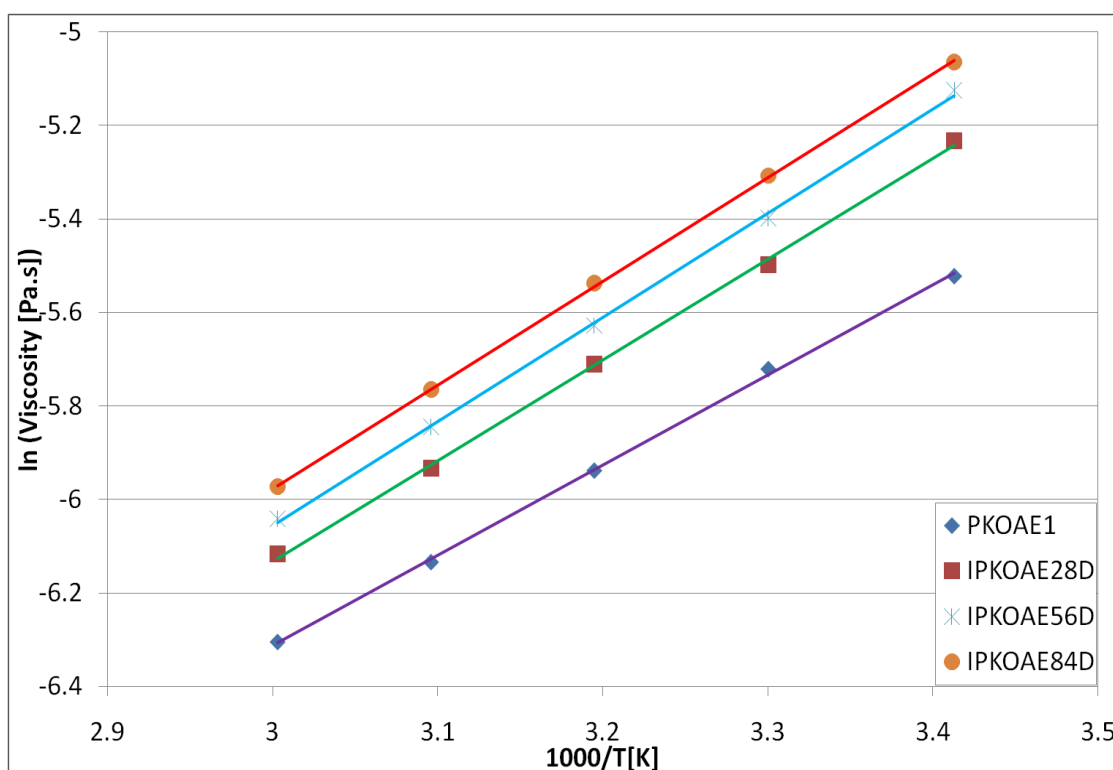


*Figure 6.4: Dynamic Viscosity of Aged Samples on Arrhenius Plot*

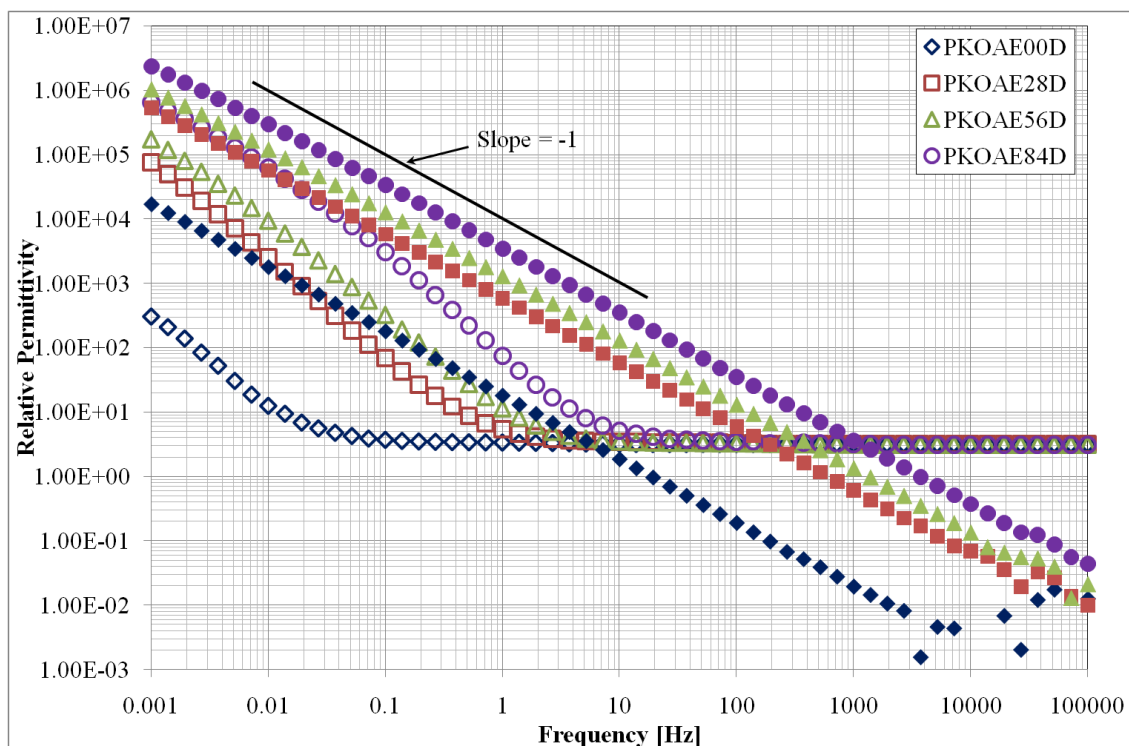


Figure 6.5: Real and Imaginary Permittivity of Aged Samples at 20°C. (Open data point- Real part, and Filled data points-Imaginary part)

#### 6.4 Dielectric Response of Aged PKO Ester Fluid

The dielectric response of aged ester samples shows an interfacial polarization at low frequency and imaginary part of -1 slope, an indication of a DC conduction dominated the loss process shown in Figure 6.5. The AC conductivity evaluated using equation 5.2 is presented in Table 6.3. The result shows an increase in dielectric loss with ageing. Figure 6.6 shows the  $\tan\delta$  spectra of freshly prepared ester and the aged samples. The  $\tan\delta$  of the aged samples at 50Hz is greater than 1, which could lead to significant dielectric heating. The spectra shape of the dielectric response of the freshly synthesized alkyl ester is similar to that of the aged ester sample, but the frequency of the absorption peak was found to be influenced with ageing. Contrary to the usual decrease in dielectric loss of liquid with increase in its viscosity, the viscosity of the ester was found to increase with ageing, while the  $\tan\delta$  peak shifts towards higher frequencies with ageing. There is a slight decrease in the  $\tan\delta$  maxima of the aged esters. Thermal ageing led to polymerization of the ester liquid as observed from the brown gum that was formed. This led to an increase in average molecular mass of the fluid and the observed higher viscosity. This higher viscosity reduced ionic mobility. This polymerization process may have produced more ionic charge carriers, resulting in increased losses due to ionic conduction, and hence the observed shift in the  $\tan\delta$  peak towards higher

frequency as the ageing time increased. The mobile charges responsible for the increase in the dielectric loss may have been generated from the dissociation of the molecules of the liquid due to thermal ageing, ageing of the paper samples and the impurities introduced by the metal catalysts in the liquid. The 84 days aged oil was reported in the previous chapter to have increased acidity and moisture content. The formation of organic acids and water during ageing sample may have also contributed to the increase in ionic conduction loss in the aged sample which results in the observed increase in the relative permittivity.

Table 6.3: Dielectric Parameters of Aged Alkyl Ester at 20°C and 50 Hz

Sample	$\sigma_{AC}$ (S/m)	$\tan\delta$
<b>PKOAE00D</b>	$1.04 \times 10^{-9}$	0.1
<b>PKOAE28D</b>	$3.29 \times 10^{-8}$	>1
<b>PKOAE56D</b>	$7.17 \times 10^{-8}$	>1
<b>PKOAE84D</b>	$1.96 \times 10^{-7}$	>1

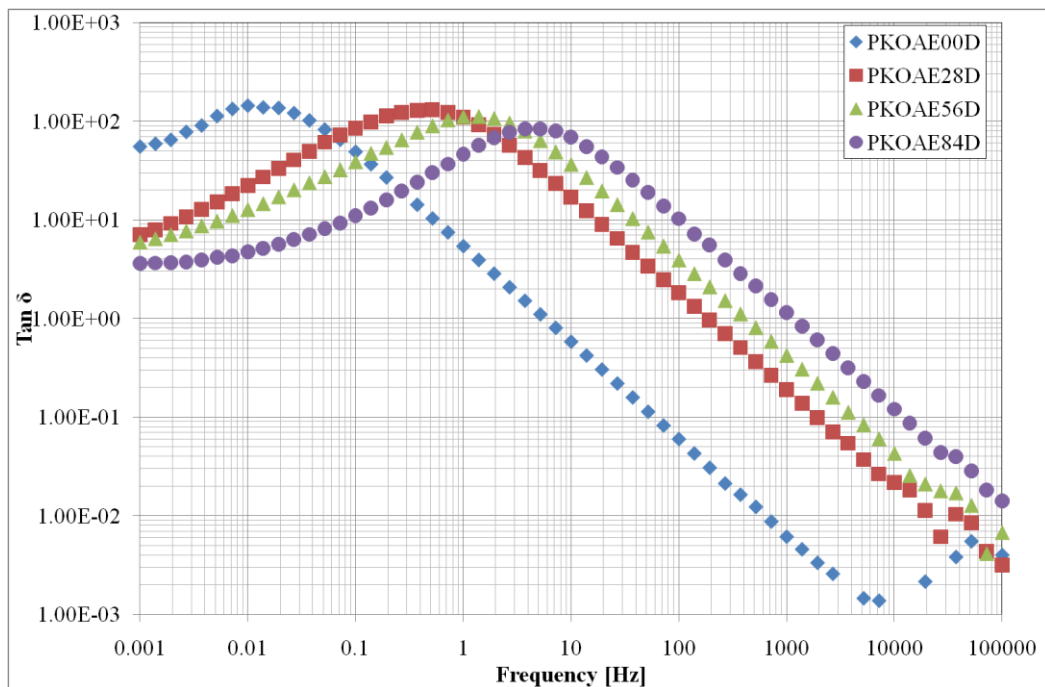


Figure 6.6:  $\tan\delta$  of aged samples at 20°C

## 6.5 Dielectric Breakdown Characteristics

*Figure 6.7* shows the Weibull plot of AC breakdown field data of unaged palm kernel oil alkyl ester samples while *Figure 6.8* through *Figure 6.10* shows the Weibull plot for the aged samples. The characteristic breakdown strength and the shape parameters are tabulated with their respective 95% confidence intervals in *Table 6.4*. The correlation coefficient of the breakdown data when fitted to the Weibull function in equation 5.12 shows a good fit. The breakdown fields of the aged palm kernel oil ester samples have narrow distributions as indicated by the high values for the fitted shape parameter,  $\beta$  in *Table 6.4*. The characteristic breakdown strength (63.2% cumulative probability) of PKOAE28D is higher than the unaged sample (PKOAE00D). Thermal ageing led to chemical change in the liquid sample. This change may have made the liquid between the electrodes more resistive to breakdown, leading to higher breakdown field. The  $\tan\delta$  values of the aged samples greater than 1 suggest that thermal runaway may have contributed to breakdown mechanisms in the samples. Further ageing led to decrease in the characteristic breakdown strength of the ester. As more charge carriers become available for conduction, there will be an exponential increase in conductivity when the heat gained by the liquid cannot be balanced by the heat loss. This caused accelerated breakdown mechanism. The aged samples appeared to exhibit a threshold for electrical breakdown as shown with arrows in *Figure 6.8* through *Figure 6.10*. The threshold value decreased with ageing as shown in *Table 6.4*. This is an indication that ageing products which increases with ageing period may have led to breakdown mechanisms that caused the decreasing breakdown strength. The decreasing shape parameter with ageing perhaps indicates that the material is not quite so homogeneous after ageing.

*Table 6.4: Weibull Parameters for Aged Samples*

Samples	$N$	Characteristic value, $\alpha$ (kV/mm)	95% Conf. Bound for $\alpha$ (kV/mm)	Shape parameter, $\beta$	95% Conf. Bound for $\beta$	Threshold BD Field (kV/mm)
PKOAE00D	10	43	41.96 – 43.60	28.85	19.25 – 48.32	-
PKOAE28D	10	51	49.75 – 52.36	21.78	14.53 – 36.49	42.76
PKOAE56D	10	49	47.26 – 49.99	19.85	13.24 – 33.25	39.40
PKOAE84D	10	44	42.13 – 44.76	18.35	12.25 – 30.74	36.41

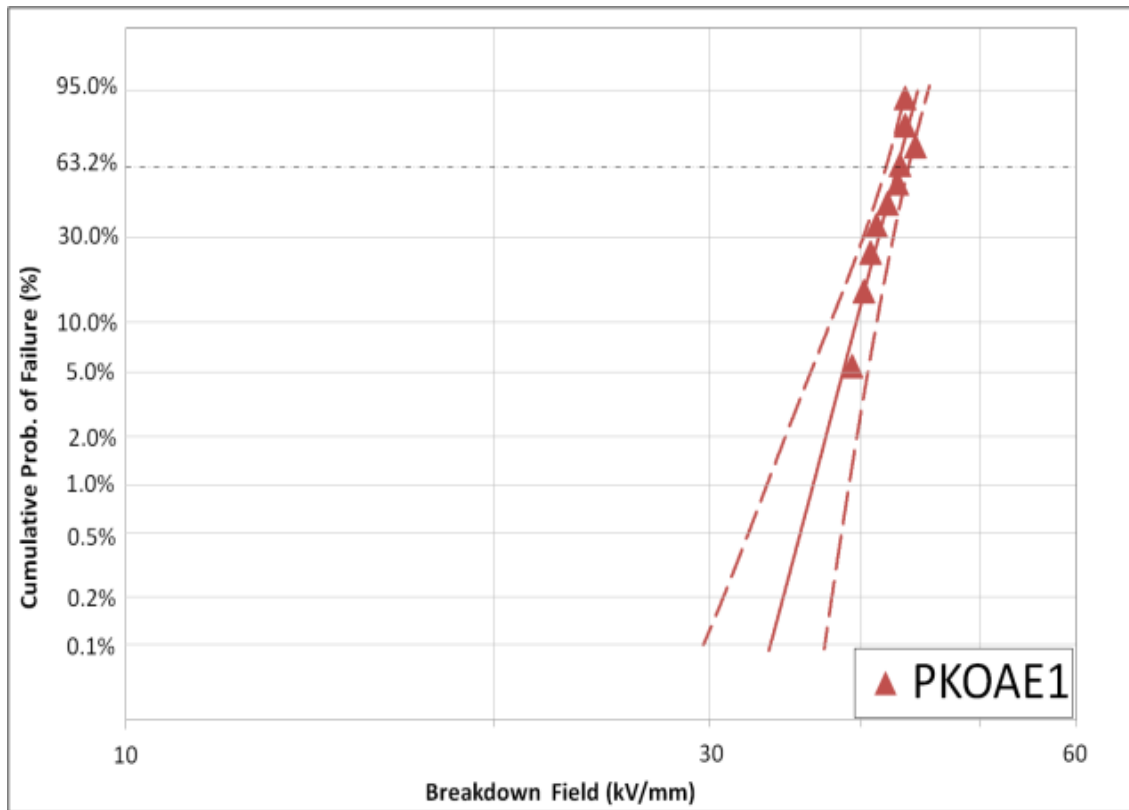


Figure 6.7: Weibull Plot for Unaged Ester Sample

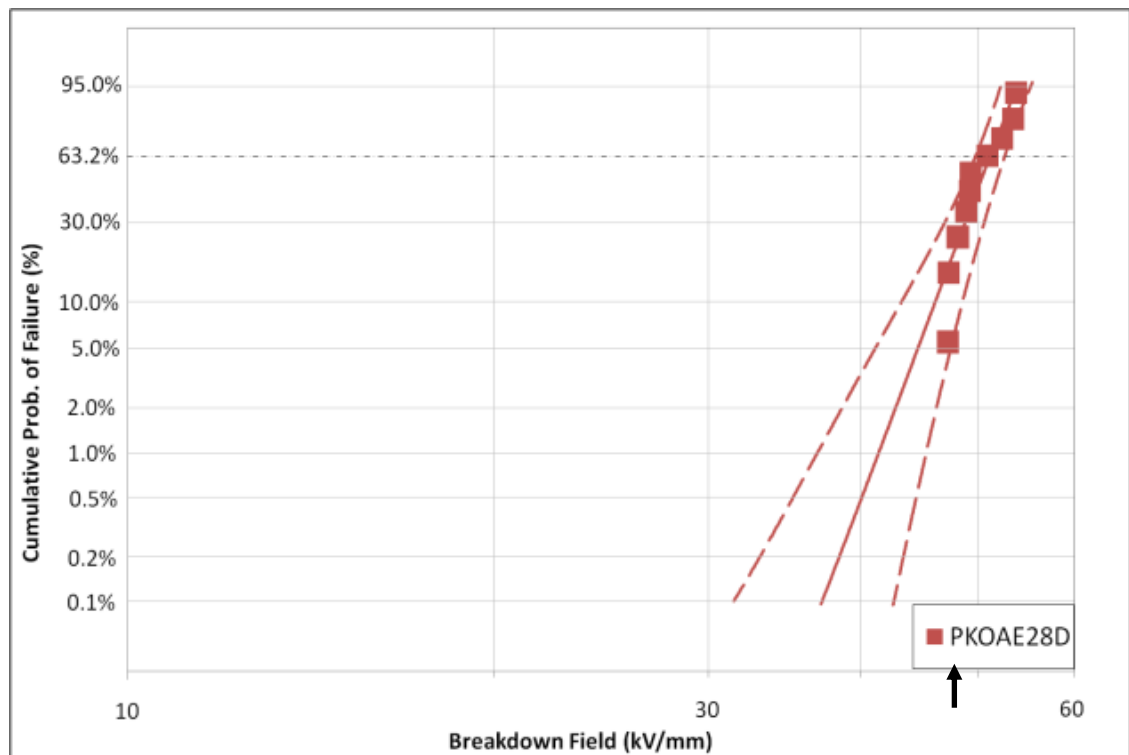


Figure 6.8: Weibull Plot for Aged Ester Sample for 28 Days

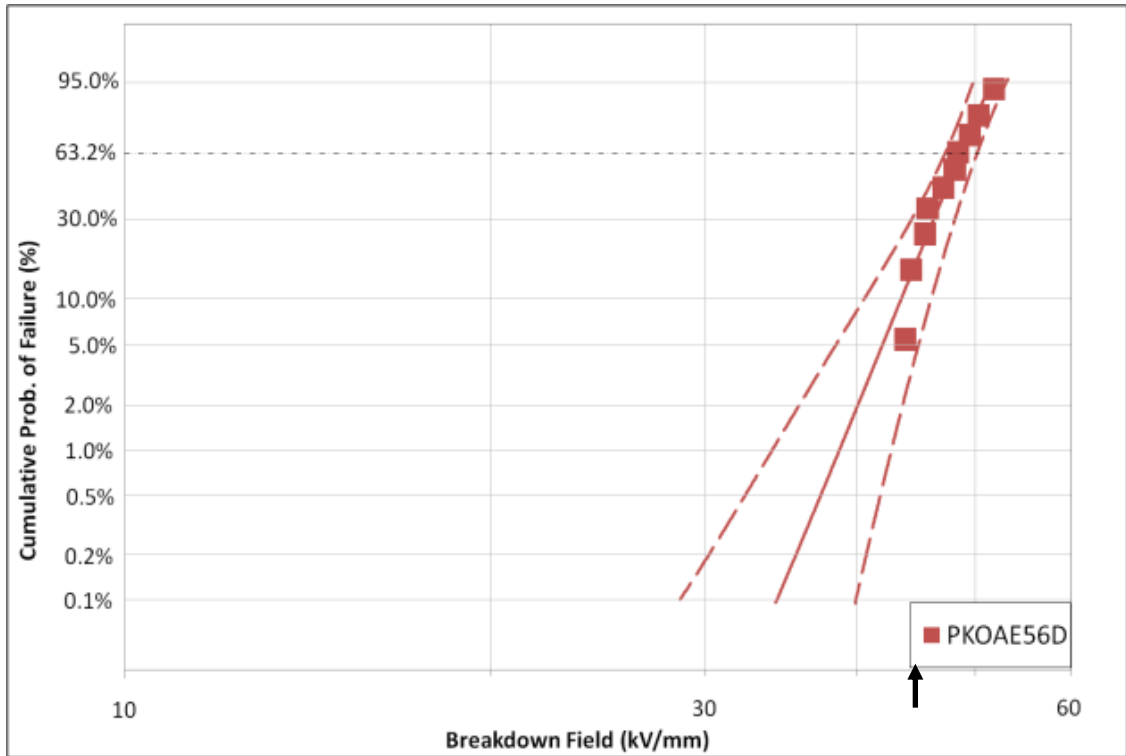


Figure 6.9: Weibull Plot for Aged Ester Sample for 56 Days

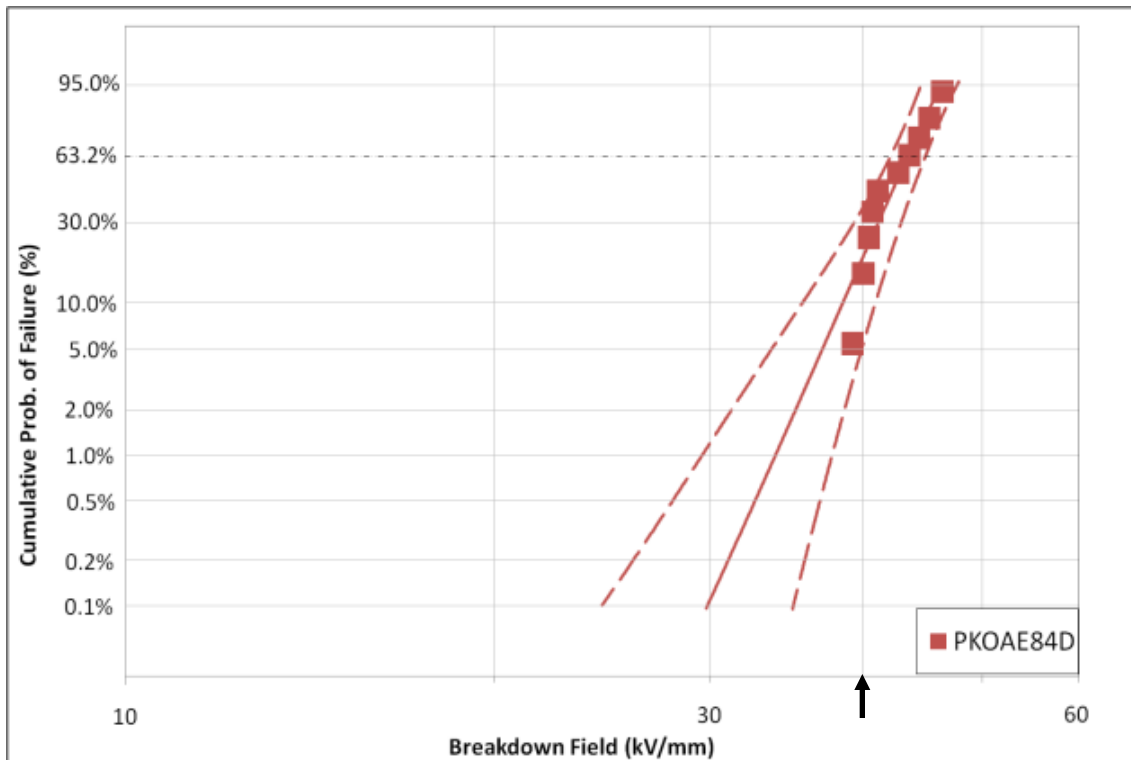
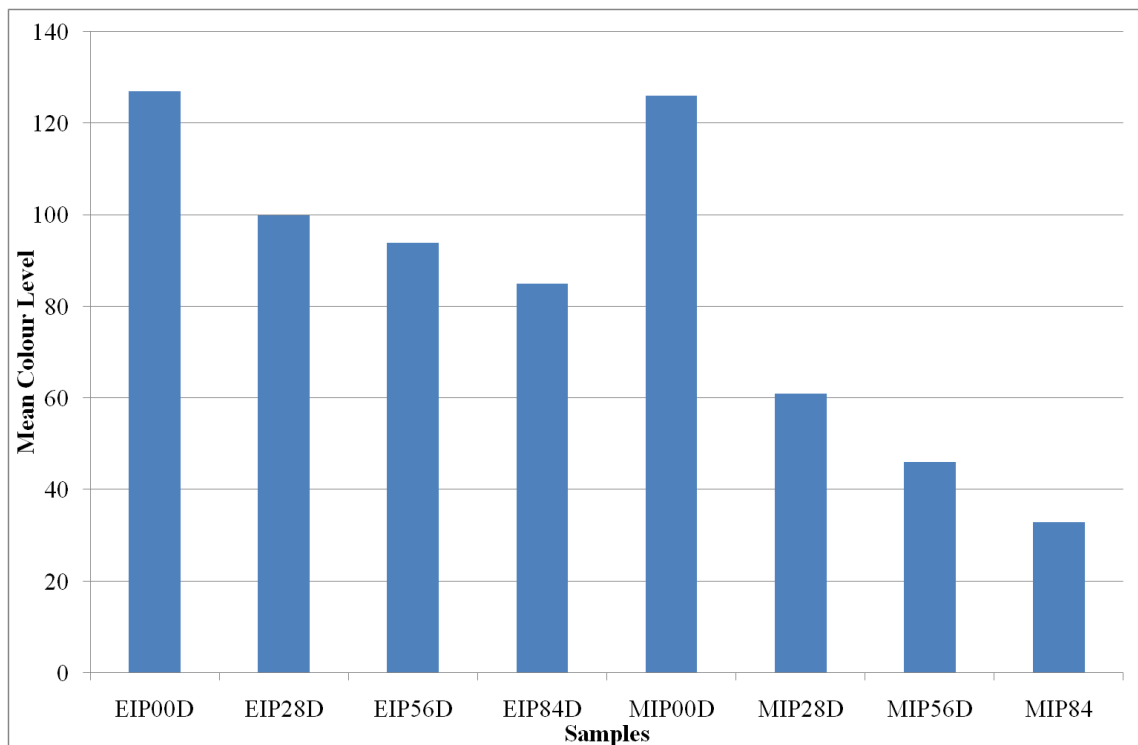


Figure 6.10: Weibull Plot for Aged Ester Sample for 84 Days

## 6.6 Characteristics of Ester Impregnated Paper

This section presents the ageing effect on the dielectric and mechanical strength of the thermally upgraded paper. The colour of the oil impregnated paper samples were observed to change with ageing time. The picture of the aged samples was taken under the same illumination. The change in the mean colour level of the aged oil impregnated paper samples is shown in *Figure 6.11*. The figure compared the change in the colour level of ester-paper and mineral-oil paper samples. The chart shows that the colour level of the paper samples decreased as the ageing time increases. The rate of decrease in the colour level of aged paper sample impregnated with mineral oil appeared more than that of ageing alkyl ester impregnated paper sample. After 88 days of ageing, the mean colour level of mineral oil impregnated paper sample decreased by 73% compared with the unaged sample. With same ageing time, the mean colour level of aged ester impregnated paper decreased by 33% in comparison with the unaged sample. This suggests that the rate of paper degradation leads to decrease in colour level of the samples and paper in mineral oil possessed faster ageing rate than paper in the alkyl ester fluid.



*Figure 6.11: Change in Colour Level of Aged Paper Samples*

### 6.6.1 Tensile Strength

Ageing of paper insulation involves chemical reactions that include pyrolysis, oxidation and hydrolysis. These mechanisms are accelerated at elevated temperatures. One of the degradation products of oil-paper composite material as it ages is water. The water content in the system increases over time. This attacks the oxygen bridge between the glucose rings leading to shortening and weakening of the cellulose fibre. The attack on the linkage bond reduces the mechanical strength of the paper. The mechanical strength of an insulating paper can be determined by evaluating the maximum mechanical stress it can withstand when stretched before deformation occurs. This is referred to as the tensile strength of the paper.

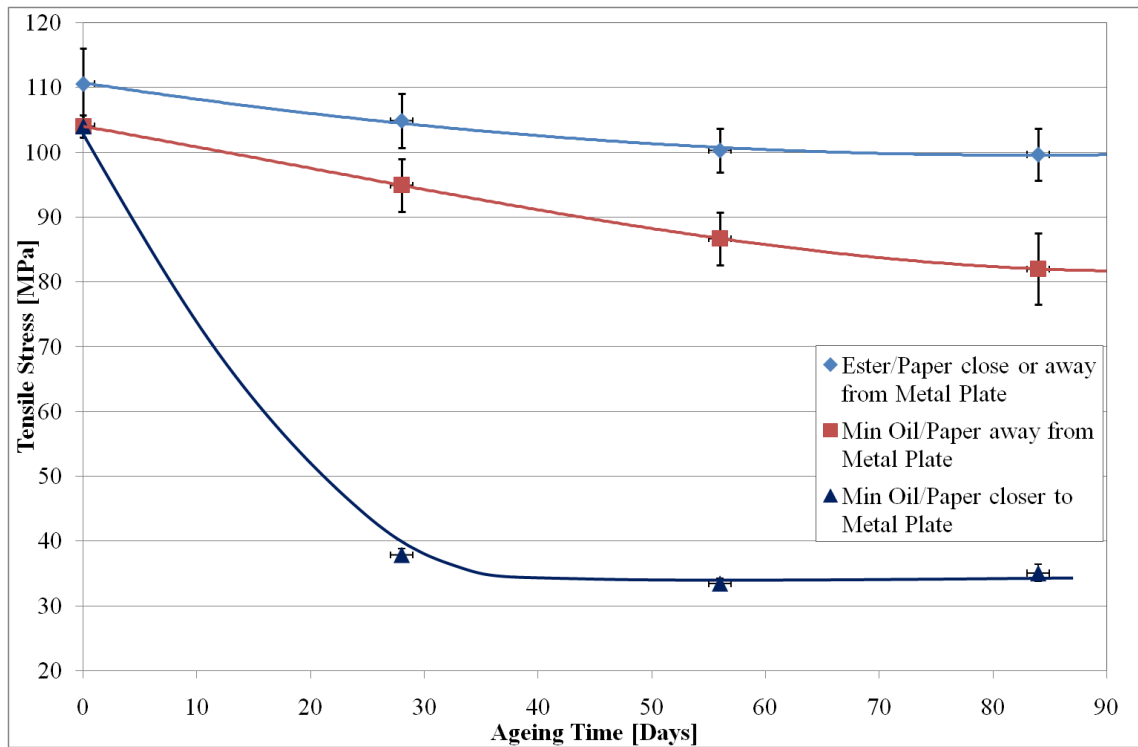


Figure 6.12: Tensile Strength of Thermally Upgraded Paper Aged in Oil Samples

During the ageing experiment, six sheets of the insulation paper samples were packed together and placed in between the metals in the vessel for vacuum impregnation and ageing. The vessel was sealed with nitrogen and thermally aged at 150°C and pressure of 600 kPa. Figure 6.12 shows the variation in tensile strength of the thermally upgraded paper samples immersed in mineral oil and alkyl ester after undergoing thermal accelerated ageing. Under nitrogen and 150°C, oxidation of furan degradation products (2-furfuraldehyde) of the cellulose by oxygen should not occur [Hill *et al*, 1996]. The most probable ageing mechanism is charring of the paper fibre due to thermal stress to

produce solid residue, water, CO<sub>2</sub>, CO and H<sub>2</sub>. However, the available water in the system may attack the oxygen that bridged the monomers to form two hydroxyl ions attached to each monomer. This causes scission of the inter-monomer bonds and eventual degradation of the material. The number-average degree of polymerisation (DP) is the ratio between the number of monomers and the number of chains of all lengths. Degradation led to decrease in the DP and the mechanical strength of the paper and hence a reduction in its tensile strength [Oommen et al, 2006].

For PKOAE1, the presence of the copper did not affect the ageing process significantly. All paper layers exhibited approximately 5% reduction in tensile strength during the 28 days of ageing. Two sets of response were obtained for paper samples aged in Nynas 10GBN mineral oil. The paper samples closer to the metal plates were found to have a significantly faster degradation rate. The tensile strength of samples closer to the copper plates after ageing for 28 days dropped to about 35% of the tensile strength of the unaged sample, while the tensile strength of the paper layers farther away from the copper plates decreased by about 10%. The presence of metals such as copper in the oil acts as degradation catalyst in the oil. This led to thermo-oxidative decomposition of the hydrocarbon compound, producing acidic residues as by-product. This residue can accelerate the ageing of cellulose [Hill *et al*, 1996]. The effect of the oil degradation products on the cellulose paper may have been more within the vicinity of the copper plate due to the formation of copper sulphide. This may have caused the faster degradation of paper samples closer to the copper plates than the inner paper samples as observed from the tensile strength values in *Figure 6.12*.

Paper samples aged in alkyl ester have higher tensile strength in line with previous reports on ageing behaviour of thermally upgraded papers in natural ester. The improved thermal stability of the paper immersed in natural ester accounts for the significant difference in its tensile strength after ageing, compared with the paper immersed in mineral oil. Earlier works reported that water scavenging and steric hindrance of the cellulosic hydrolytic reaction by natural esters provides ageing protection to the paper [McShnae *et al*, 2001; Rapp *et al*, 2005; Frimpong *et al*, 2011]. Natural ester as a weak polar liquid has stronger affinity for water than mineral oil. This causes the water generated during pyrolysis process to be absorbed by the ester. The liberation of water produced in the cellulose reduces the action of thermo-hydrolytic

action on the oxygen linkage between the monomers, leading to reduced rate of degradation. This slows down the deterioration rate of the cellulose insulation. The paper samples became brittle with increase in ageing time. When a material becomes brittle, the amount of energy it absorbs before mechanical rupture decline. The plot of the energy of the material at maximum tensile stress versus ageing time as shown in *Figure 6.13* is a straight line. The material that becomes more brittle with ageing acquired higher slope. The higher slope of mineral oil-paper supports the assertion that darkening of the colour of the paper is accompanied with brittleness. The ester-paper with slower ageing rate has slope with lower value and is less brittle.

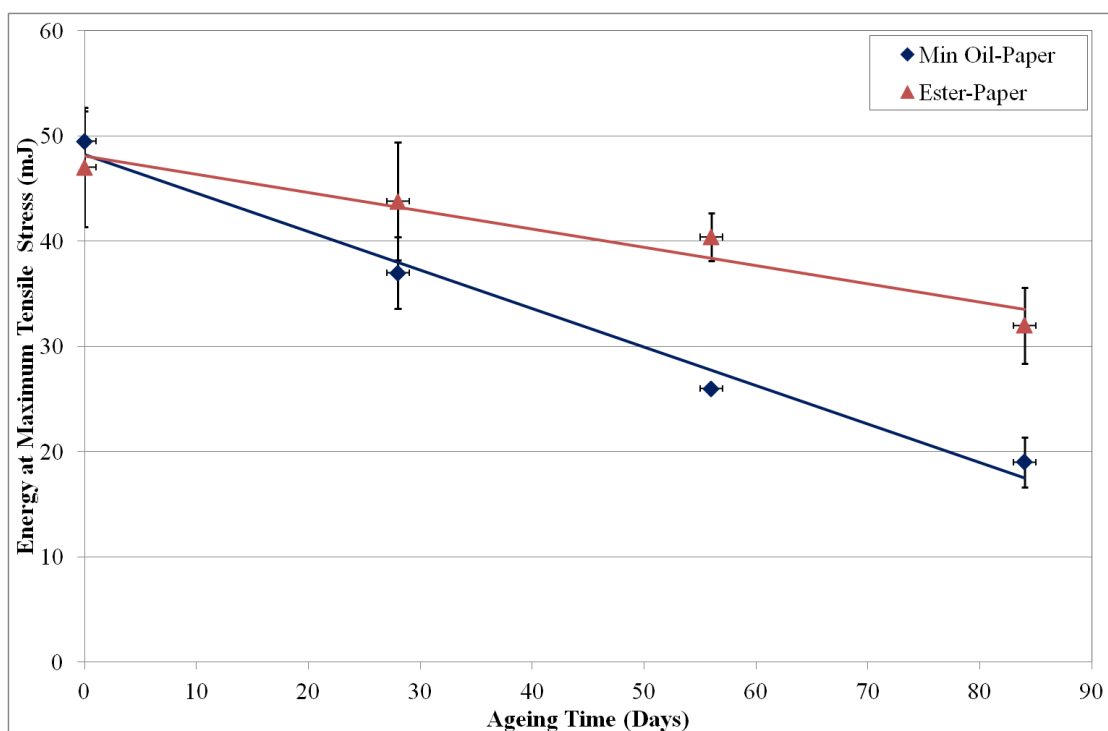


*Figure 6.13: Plot of Energy at Maximum Tensile Stress versus Ageing Time*

### 6.6.2 Dielectric Response of Aged Oil-Impregnated Paper

The frequency response of the insulating paper samples was measured using the three electrode solid test cell (Keithley model 6105). The dielectric response of dried and degassed insulating paper and unaged ester-impregnated paper samples over frequency range of  $10^{-3}$  -  $10^6$  Hz are shown in *Figure 6.14*. Three different responses can be identified from the response of the dried paper sample; the high frequency response which involved constant real part. This was followed by a clear loss peak with an associated capacitance increment in  $C'(\omega)$ . The low frequency response involves an increasing  $C''(\omega)$  with a nearly constant  $C'$ . The loss process around the frequency of

0.1 Hz may be due to dipolar relaxation possibly associated with bound water or interfacial polarization. Impregnating the insulating paper with ester fluid influenced the response of the material. The impregnated paper displayed a shift in the magnitude of the real part of the capacitance to higher values across the frequency range. This is an indication of effective conductance of the insulating paper. The visible loss peak on the spectra of dried paper sample was nearly screened by a DC-like process in the unaged ester-paper sample. The imaginary part of the capacitance of the unaged ester-paper sample acquired a slope of approximately -1 around frequency of 0.01 Hz and the real part has almost flat response (see section 2.2.2). This is an indication of conduction possibly due to the movement of ions in the oil occupying the voids in the paper sample (see section 5.6).

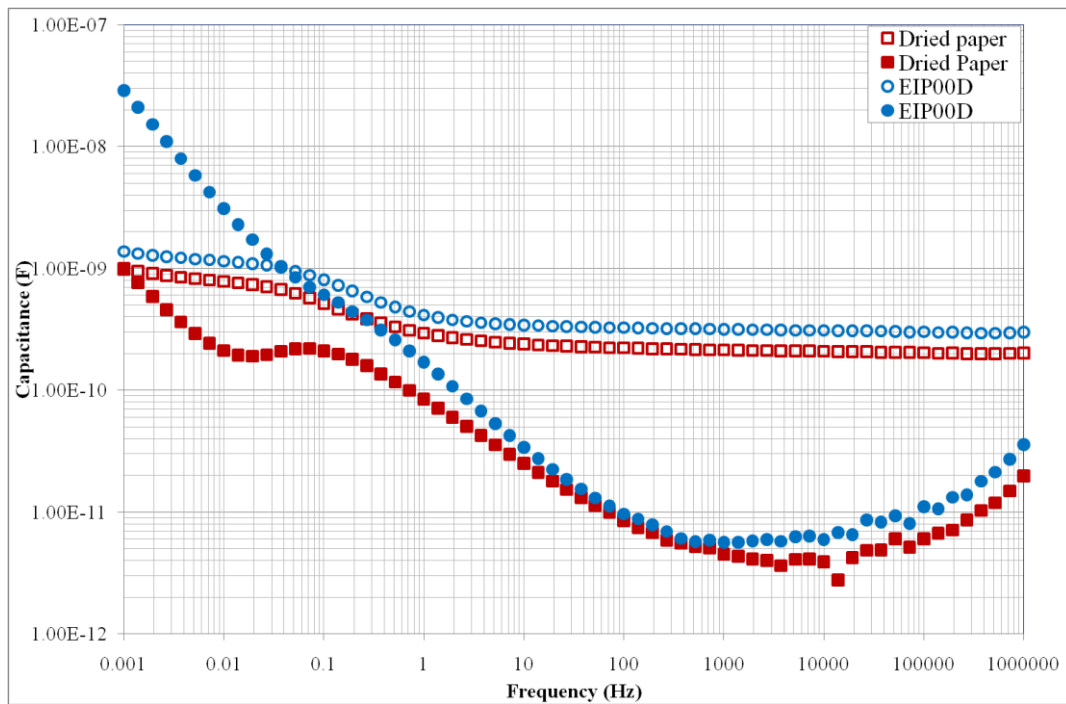


Figure 6.14: Real and Imaginary Capacitance of Unaged Dried and Ester Impregnated paper (Open data points-real part; Filled data points-Imaginary part)

The oil in the impregnated paper fills up the pores between the fibres leading to larger  $C_{\infty}$ . While the low frequency response of the dried sample may be due to hopping charges, the viscous liquid in the ester-paper sample serves as pathways for easier charge transport in the paper on the application of electric field. The pathway for charge transport is dependent on the morphology of the fibres of the paper. Some of the charges may get trapped on the way while moving through the medium. Some may move between available sites, while some may succeed in drifting from one electrode to

the other and contributing to DC conduction. A loss process was observed around the frequency of 0.1 Hz in ester-paper. At higher frequencies, induced dipolar relaxation may have dominated the dielectric response. As the frequency decreases, the probability of charge moving from one site to any available site increases. This leads to low frequency dispersion with an imaginary part acquiring a near -1 slope. The low frequency dispersion of the oil-paper system may have dominated the loss process, thereby obscuring the loss process around 0.1 Hz.

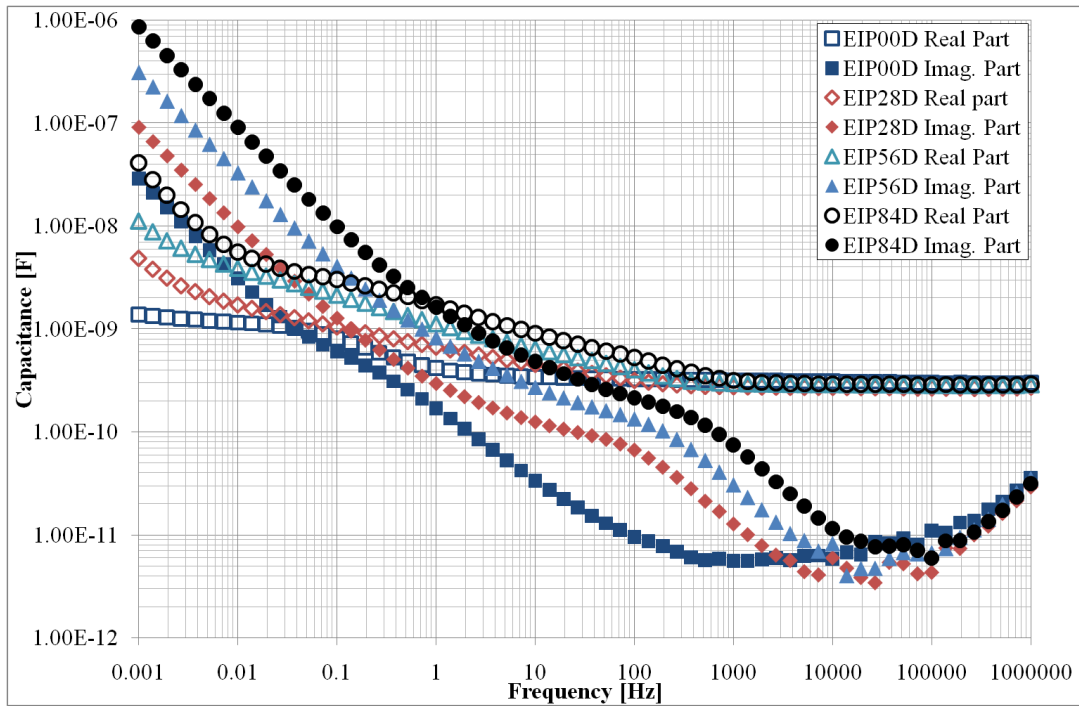


Figure 6.15: Real and Imaginary Capacitance of Aged Ester Impregnated Papers at 20°C

The dielectric response of ester-impregnated paper samples at 20°C for various ageing time is shown in Figure 6.15. A close observation of the plots shows a logarithmic shift in both the frequency and amplitude of the response with ageing. These shifts can be observed from the loss peak of the respective aged sample. Three loss processes can be identified from the dielectric response of ester-paper system; a high frequency loss process in the aged samples that produces the peak around 100-200 Hz, a low frequency loss process that produced peak around 0.1 Hz, and a low frequency dispersion (power law behaviour) at the lowest frequencies.

A master curve of unaged and the aged ester-paper samples (20°C - 50°C) was constructed by normalizing the data for different temperatures as shown in Figure 6.16 through Figure 6.19. This was done by performing a logarithmic shift of the characteristic frequency of the processes for the different temperatures to bring the

responses into coincidence along the frequency axis. The dielectric response at 20°C was made the reference spectra while the spectra at other temperatures were shifted towards it.

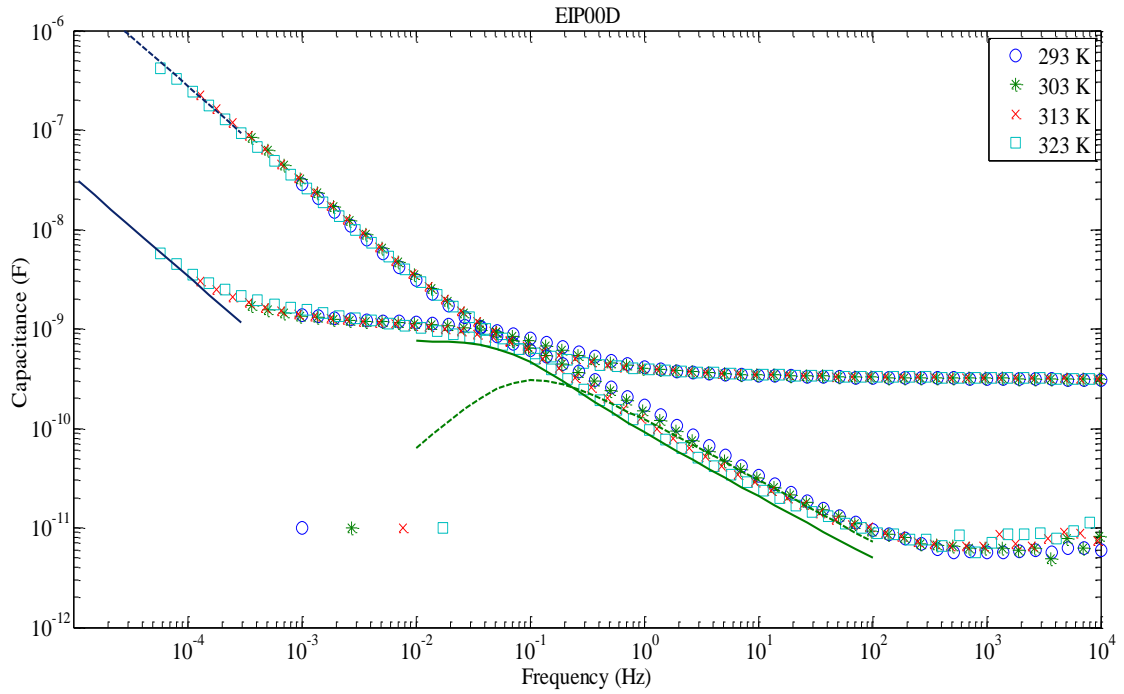


Figure 6.16: Master Curve of Real and Imaginary Capacitance of Unaged Ester-paper with the fit of the Dispersion loss and Low Frequency Power Law

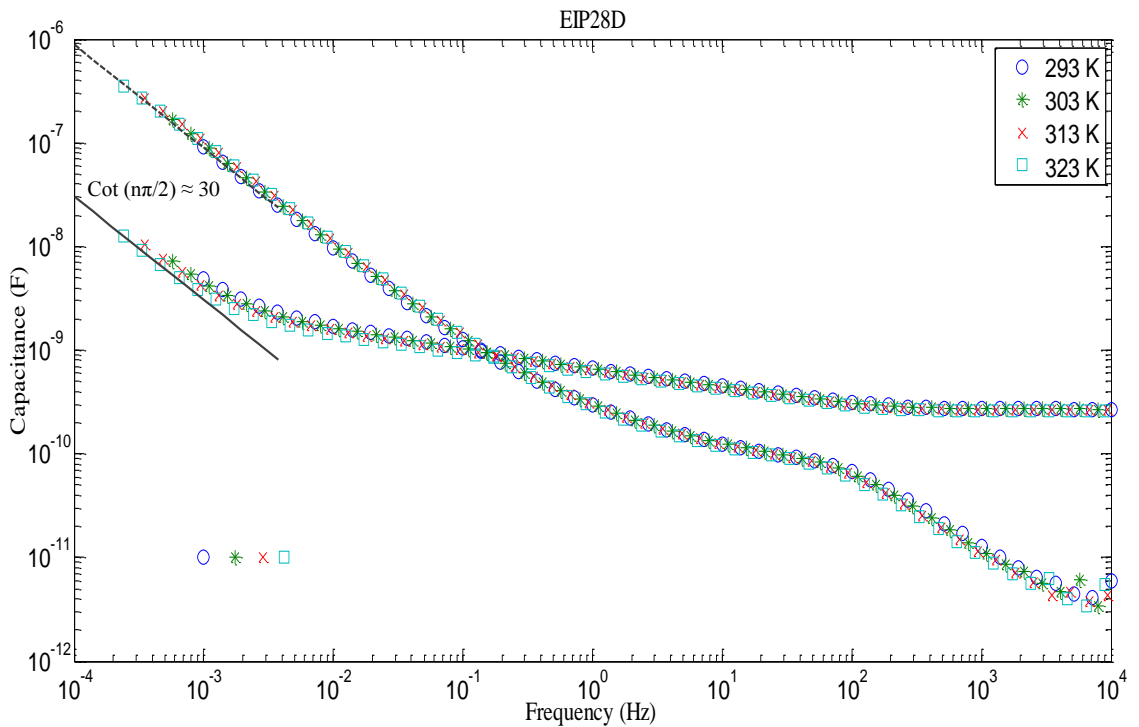


Figure 6.17: Master Curve of Real and Imaginary Capacitance of Ester-paper after 28 days with the fit of Low Frequency Power Law

The master curve of all the samples displayed a low-frequency dispersion process as explained in section 2.2.2. The real and imaginary parts of the response acquired slopes close to -1 at the lower frequency side of the low frequency loss process. Equation 7.1 was used to determine the nature of the low frequency dispersion in the ester-paper system. If the process responsible for the dispersion in the samples is the phenomenon referred to as QDC (Quasi-Direct Current) due inter-cluster interaction which involves movement of charges from one cluster to any available cluster, then the value of  $n$  in equation 7.2 should be a constant and equal to  $1 + slope$  (i.e.  $n = 1 + slope$ ) [Jonscher, 1983]. The real part of the low frequency response of unaged sample (EIP00D) appeared to be tending towards power law, but the low frequency data is not enough to make a conclusion. However, the low frequency response of aged ester-paper samples followed low frequency power law with the slope of the real parts nearly parallel to the imaginary parts. This suggests that cluster model can be used to describe charge transport in aged oil-paper system.

$$\frac{C''(\omega)}{C'(\omega) - C_\infty} = \cot\left(\frac{n\pi}{2}\right) \quad 7.2$$

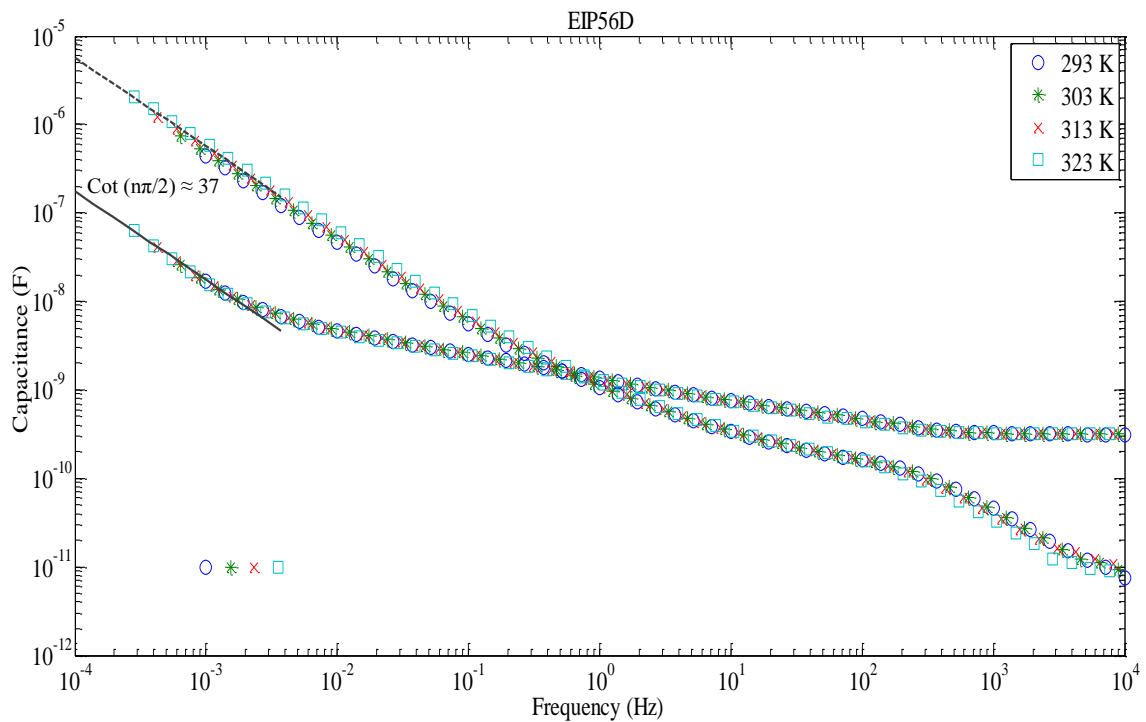


Figure 6.18: Master Curve of Real and Imaginary Capacitance of Ester-paper after 56 days with the fit of Low Frequency Power Law

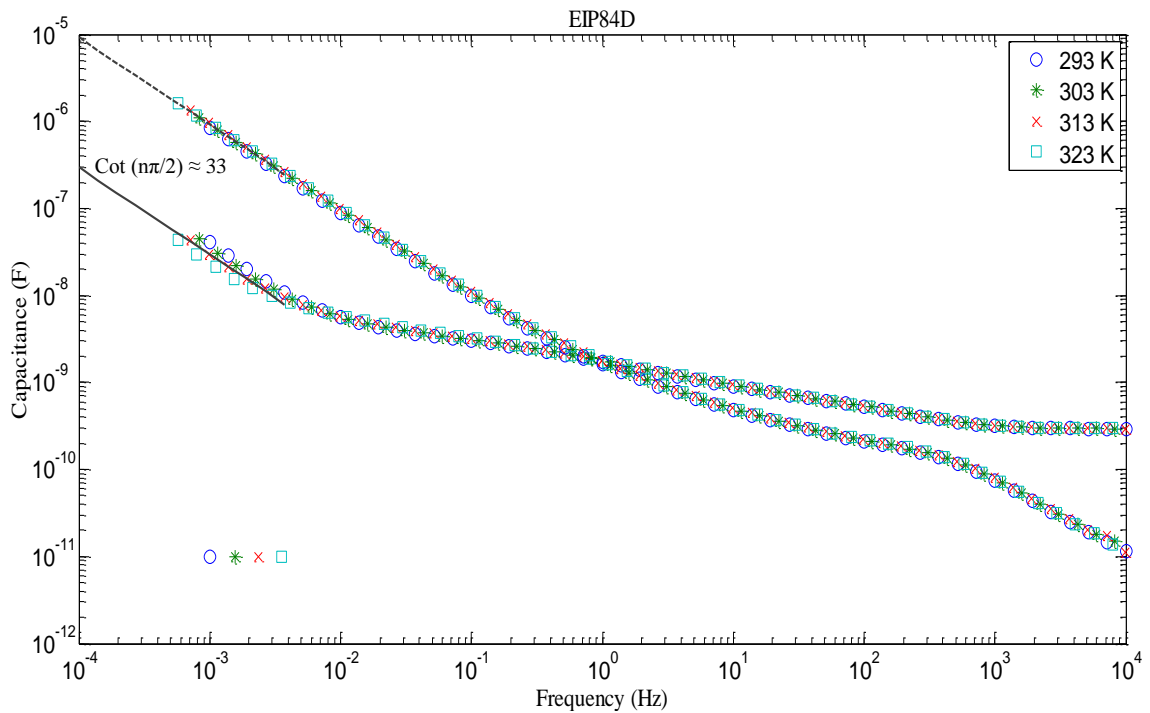


Figure 6.19: Dielectric Master Curve of Real and Imaginary Capacitance of Ester-paper after 84 days with the fit of Low Frequency Power Law

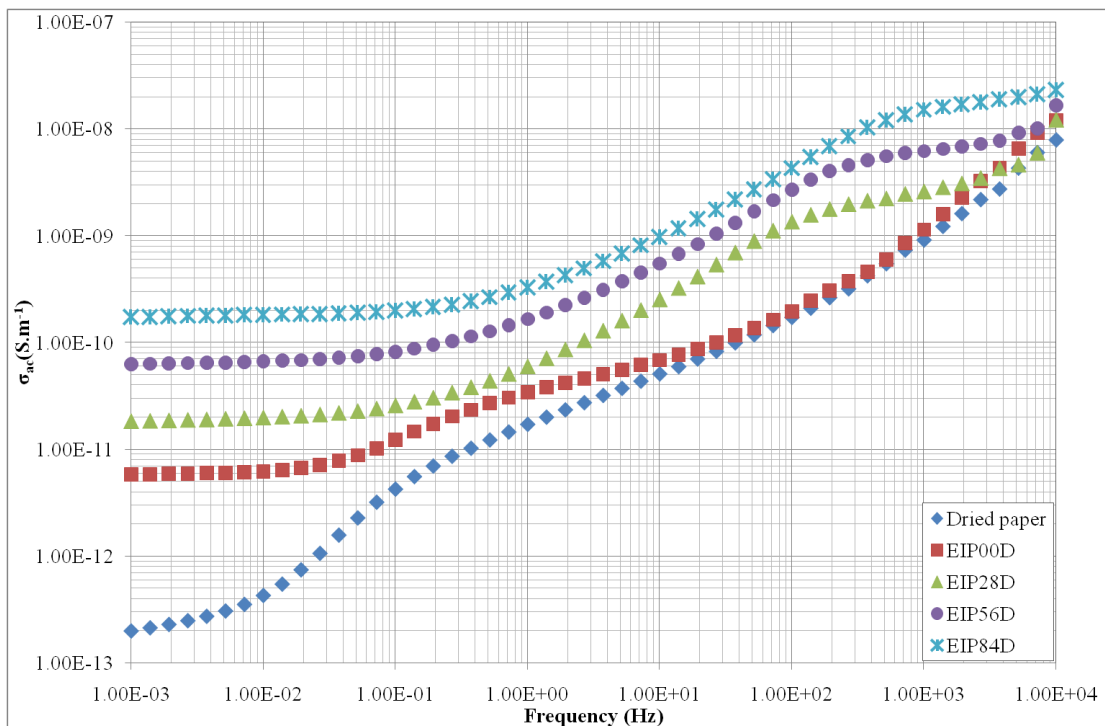


Figure 6.20: Frequency Dependence of AC Conductivity of Paper Samples at 20°C

The master curve shows that temperature has no effect on the shape of the spectra, but on the relaxation times of the polarization mechanisms i.e. just a common frequency shift in all relaxations. Figure 6.20 shows the plot of frequency dependent conductivity

versus frequency in logarithmic axis for the paper samples. The AC conductivities of the samples were calculated from the respective imaginary part of the capacitance. The oil impregnated samples shows a flattening response at low frequencies. A closer inspection of the response of unaged ester-paper revealed a slope close to zero (i.e. close to DC conduction) at less than  $10^{-2}$  Hz, while the response of aged ester-paper samples revealed near DC conduction below  $10^{-1}$  Hz. The rise in the real parts of the response of the samples is an indication of not quite a DC conduction, but a very slowly rising low frequency LFD. The electrical conductivity of the thermally upgraded paper increased with ageing.

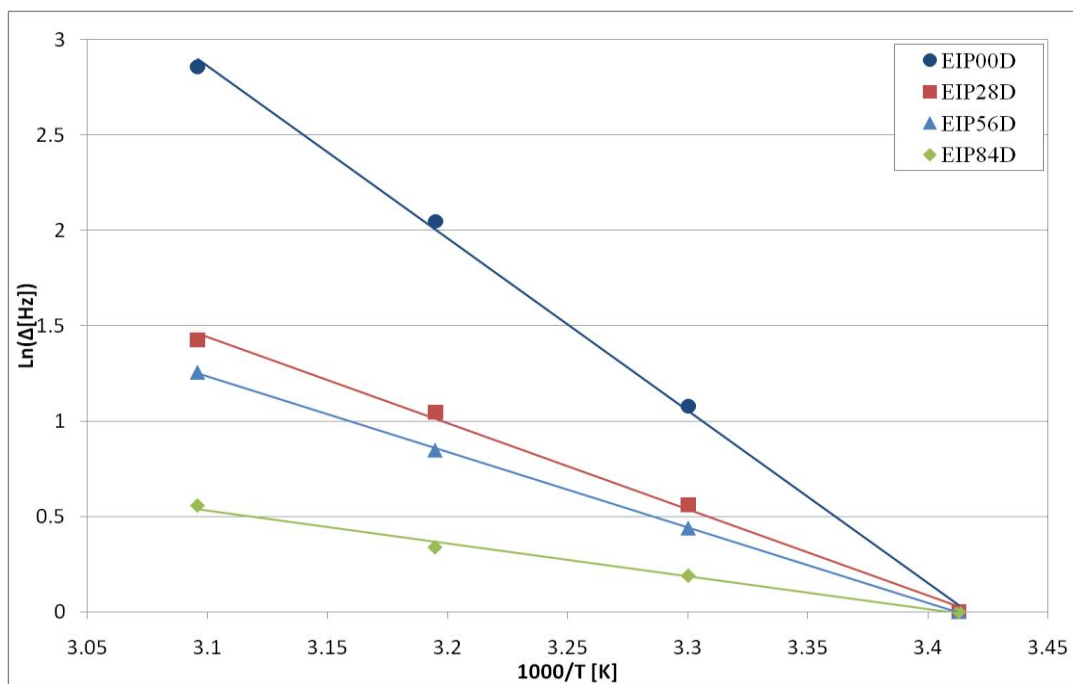


Figure 6.21: Characteristic Frequency Shift of Aged Ester/Papers on Arrhenius Plot

The Arrhenius behaviour for conduction mechanism in the samples was evaluated by plotting the log of frequency shift obtained from Figure 6.16 through Figure 6.19 with the inverse of temperature following equation 5.6 in Chapter 5. The characteristic frequency of polarization phenomenon in the material is related to the logarithmic shift in frequency. Figure 6.21 shows the Arrhenius plot of the conduction process in EIP00D, EIP28D, EIP56D, and EIP84D. The straight lines fit on the data points with correlation coefficients ( $R^2$ ) of 0.99. The activation energies decreased with ageing. EIP00D, EIP28D, EIP56D, and EIP84D have activation energies of 0.78 eV, 0.39 eV, 0.34 eV, and 0.15 eV respectively. The activation energy is related to charge transport between clusters in the respective samples. The decreasing activation energy with ageing

suggests that the potential barrier decreased with ageing thereby increasing the probability of inter-cluster interaction of the quasi-mobile ions. There is no change in amplitude, suggesting that the number of quasi-mobile ions in the relaxation process did not change with temperature.

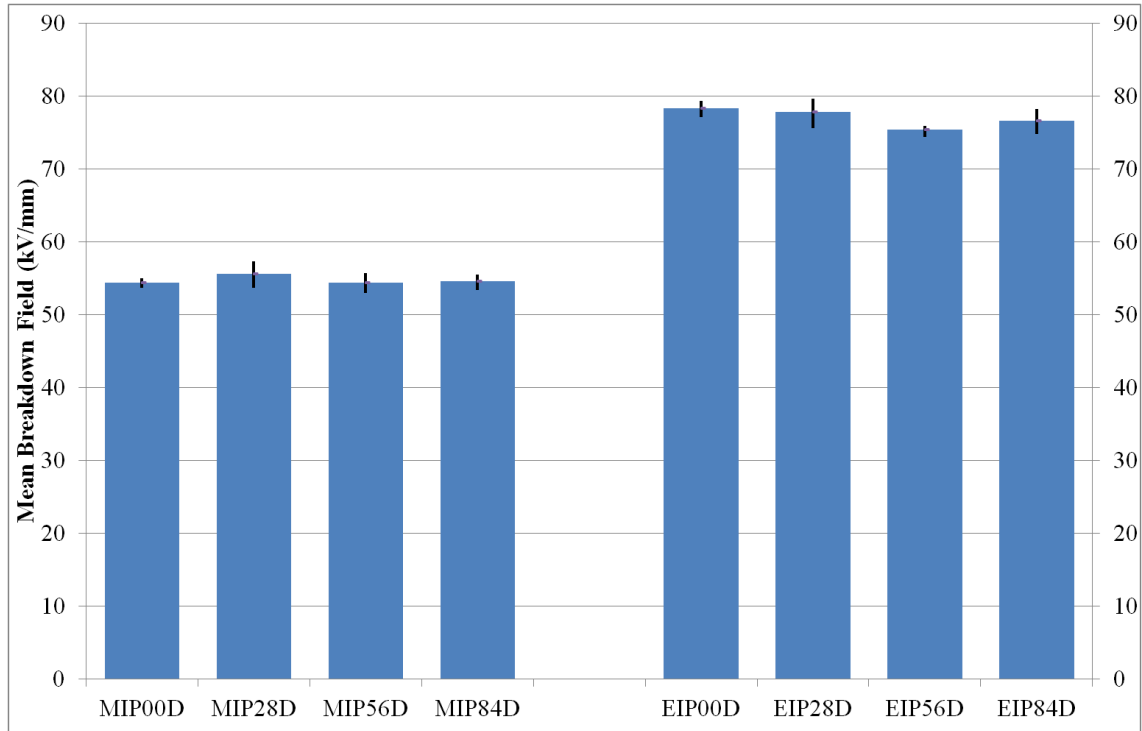


Figure 6.22: Histogram of Characteristic Breakdown Strength of Papers Samples

### 6.6.3 Breakdown Field Strength

The breakdown strength of the paper samples was performed using stainless steel ball of diameter 25 mm as electrodes. The paper samples of diameter 25 mm were sandwiched between the sphere electrodes in a test cell containing oil. Breakdown was performed on 6 specimens of each sample. The breakdown data was analysed using Weibull distribution function. Impregnation of the paper with either mineral oil or the synthesized ester shows a significant increase in the breakdown field strength because of lack of air-filled voids in the composite system which may have caused early breakdown. Figure 6.22 shows a bar chart comparing the characteristic breakdown field of synthesized ester and mineral oil impregnated paper sample at various ageing times with error bars. From that chart, the performance of the ester impregnated paper is better than mineral oil impregnated paper. The performance of ester-paper system is on the average, 42% better than mineral oil-paper system.

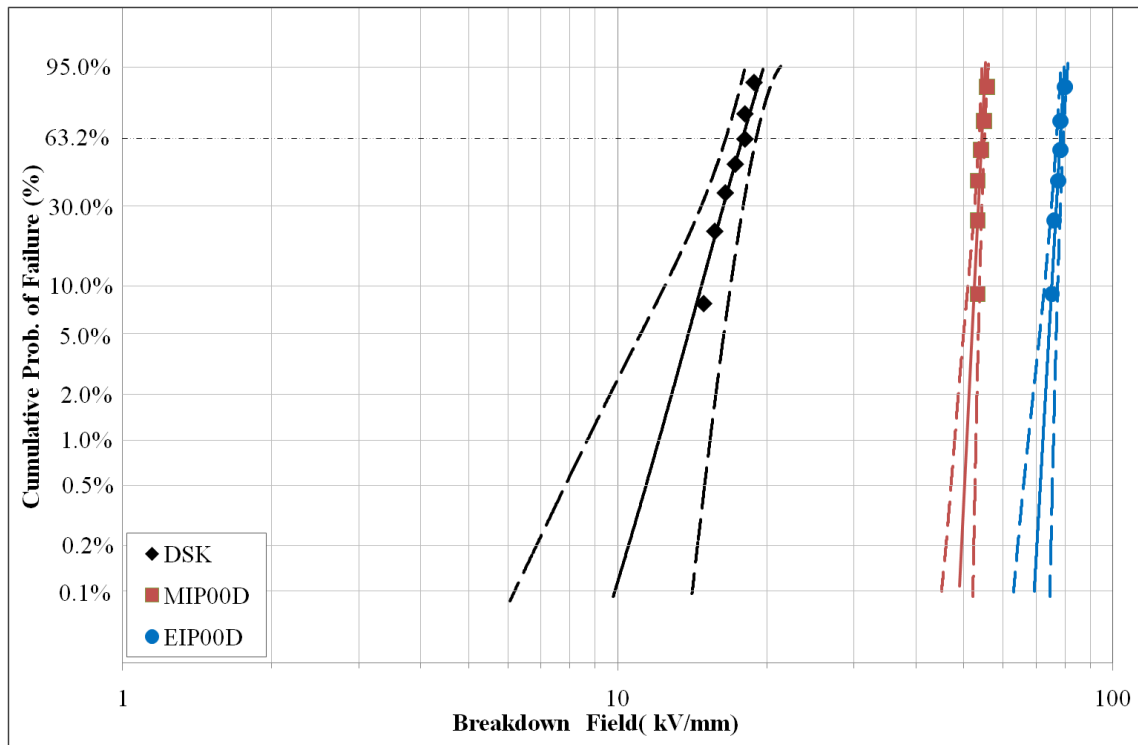


Figure 6.23: Weibull Plot of AC Breakdown Filed Data for Paper Samples

Table 6.5: Weibull Parameters of AC Breakdown Filed Data for Paper Samples

Samples	$N$	Characteristic value, $a$ (kV/mm)	95% Conf. Bound for $a$ (kV/mm)	Shape parameter, $\beta$	95% Conf. Bound for $\beta$
DKP	7	43	41.96 – 43.60	28.85	19.25 – 48.32
MIP00D	6	54	53.68 – 54.97	65.94	37.54 – 158.18
MIP28D	6	55	53.65 – 57.26	24.07	13.71 – 57.76
MIP56D	6	54	52.91 – 55.65	31.08	17.70 – 74.56
MIP84D	6	54	53.51 – 55.59	43.08	24.53 – 45.02
EIP00D	6	78	77.14 – 79.29	57.09	32.51 – 136.96
EIP28D	6	78	75.62 – 79.64	30.24	17.22 – 72.53
EIP56D	6	75	74.33 – 75.89	75.39	42.93 – 180.86
EIP84D	6	76	74.74 – 78.17	34.86	19.43 – 83.64

Figure 6.23 shows the Weibull plot of AC breakdown field data of dried and degassed paper, unaged impregnated mineral oil-paper, and unaged impregnated ester-paper samples. The characteristic breakdown strength and the shape parameters of the paper improved with impregnation as tabulated in Table 6.5. The breakdown field of the impregnated paper samples has narrow distribution as indicated by the high values for

the fitted shape parameter,  $\beta$ . The variation in the dispersion of the breakdown data of the samples may be linked to inhomogeneous ageing of the samples.

## 6.7 Summary

The GC-MS of the aged alkyl ester samples displayed the presence of higher molecular weight product that resulted from ageing process in the ester. This may have been due to thermal polymerization of the fatty acids. Polymerization was also found to have led to increase in viscosity of the aged ester. Increase in the ionic radicals due to thermal decomposition of the aged esters may have contributed to conduction processes. This resulted in increased dielectric losses due to ionic conduction and hence a shift in frequency of  $\tan\delta$  peak towards higher frequencies. Ageing decreased the characteristic breakdown strength of the ester. However, after 84 days of ageing under nitrogen at 150°C, the characteristic breakdown strength was still above the acceptable limit set for natural ester based insulating fluid.

Samples of aged ester impregnated paper shows improved ageing performance compared with the ageing behaviour of mineral oil impregnated paper. The rate of decrease in the tensile strength of paper samples impregnated with the alkyl ester within the ageing condition is significantly lower than paper samples impregnated with mineral oil. The plot of the energy of the material at maximum tensile stress versus ageing period shows that ageing rate of paper samples can be evaluated from the slope of the curve. Mineral oil-paper sample with higher ageing rate acquired higher slope. Impregnation increases the charge storage ability of the insulating papers. However, the oil also increases the DC conductivity of the paper. Cluster model was used to analyse the ageing behaviour of ester-paper system. The aged alkyl ester impregnated paper samples are suspected to possessed relaxation process that is Quasi-DC conduction. The activation energy for the quasi-DC process decreased with ageing. This is an indication that potential barrier for the dielectric loss mechanism decreased with ageing. There was no significant change in the value of the characteristic breakdown strength of the aged paper samples compared with unaged samples.

In all respects except melting point, the synthesized oil has comparable properties with standard mineral oil for HV equipment insulation. A general discussion of the results presented in this chapter and earlier chapters will be presented in the next chapter.

## Chapter 7. Discussion

Alkyl ester of palm kernel oil has been synthesized as a possible alternative insulating fluid for oil-filled electric equipment. A wide range of experiments were performed for the freshly prepared samples as well as some samples that have undergone thermal ageing. Experimental data on the physical, thermal, chemical and electrical properties of the synthesized ester fluid have been made available with this work. In this chapter, an attempt will be made to discuss the obtained results and their contribution towards understanding of the role of the molecular structure on the behaviour of the synthesized esters as alternative insulating fluid. Some of the properties of the synthesized ester samples will be compared with the mineral insulating oil sample. The behaviour of the cellulose paper when impregnated with oil will also be discussed and also a model will be derived to explain the dielectric behaviour of the ester impregnated paper. The acquired information should lead to valid deductions on the applicability of the newly developed fluid as an alternative insulating fluid.

### 7.1 Alkyl Ester Fluid

#### 7.1.1 Thermo-physical Behaviour of Alkyl Esters

Chemical modification was used to change the saturation of some of the fatty acids in the ester. The alkenes present in the ester were converted to alkanes. This implies that the modification did not affect the ester backbone and the sustainability of the ester is not impaired. The thermo-physical properties of the synthesized ester samples include fluidity, melting point temperature, heat capacity, and thermo-oxidative stability. *Figure 7.1* shows the chemical structure of the unsaturated ester molecule and the modified molecules. This was found to influence the properties of the ester samples, as reported in Chapter 5. Separation of the glycerol from the fatty acids in palm kernel oil leads to a significant decrease in viscosity. This was due to lower average weight of the ester after the removal of the glycerol. As stated in equation 2.5, viscosity has an inverse relationship with heat transfer coefficient of the fluids and velocity of flow of a fluid in a pipe is expressed as;

$$oil\ flow\ speed \propto \left( \frac{\Delta T_{oil}}{\nu} \right) \quad 7.1$$

Where  $T_{oil}$  the operating temperature of the oil and  $\nu$  is the kinematic viscosity at operating temperature. The high fluidity of the esters at a transformer's typical operating temperature (60°C) enables low resistance against flow. An increase in fluidity leads to a significantly higher circulation flow speed because of the viscosity term as the denominator in the two expressions in equation 7.1. The overall effect is a much faster heat transfer rate. This could make the esters very effective as dielectric coolants. There is a 0.07% change in volume when the temperature of the oil changes by 1°C. The volume change of the palm kernel oil ester is slightly higher. While the volume change of the straight chain alkyl ester and the corresponding epoxy alkyl ester has 0.075% C<sup>-1</sup>. The two side branched esters has volume change of 0.08% and 0.077% respectively with increase in temperature. The higher heat capacity of the alkyl ester may also be an advantage since it implies that the ester will require more heat to change its unit mass by one degree in temperature. Comparing the ester fluid with mineral oil, in terms of viscosity and heat capacity, the ester may serve better in heat transfer and dissipation. Whilst thermal ageing of the ester resulted in increased viscosity, this was still less than the mineral oil.

The epoxidation of the alkyl ester, which was aimed at improving the thermo-oxidative stability, did not appear to have a significant effect on the other measured thermo-chemical properties. The epoxidation was found to increase the temperature of onset of oxidative degradation (OOT) of the alkyl ester without anti-oxidant from 180°C to 187°C. The absence of the weak  $\pi$ -bond, which easily undergoes thermo-oxidative decomposition, may be responsible for the increase in the OOT. It was therefore shown that removing the  $\pi$ -bond in the ester chain leads to an improved stability to thermal oxidation of the ester. The addition of anti-oxidant produced an epoxidized ester with an oxidation onset temperature of 288°C. The antioxidant was able to suppress the oxidation process until the ester got to a temperature where thermal decomposition occurred and complete destruction of the structure occurred.

Grafting of side hydrocarbon chains on the fatty acids created a more complex structure. The grafting of C-4 side chains was found to inhibit the melting process of the ester. The bends on the structures shown in *Figure 7.1* were possibly responsible for inhibiting the melting. The limitation on the influence of the side chains on the melting process may be linked to the low concentration of unsaturated fatty acids. With a higher

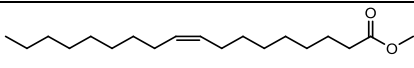
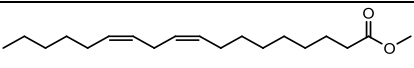
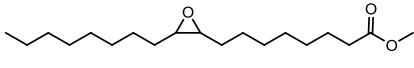
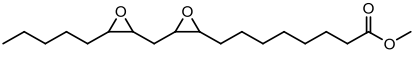
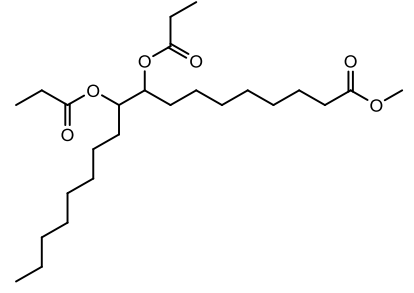
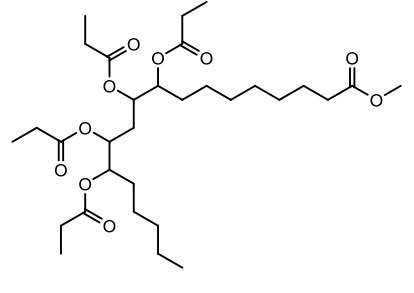
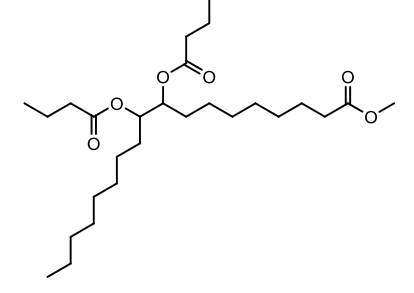
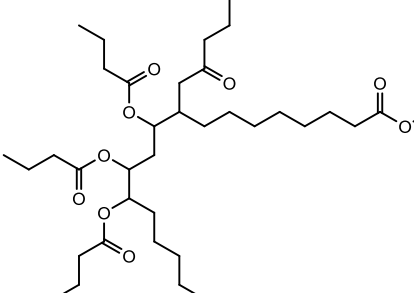
Classification	Mono-	Di-
Unsaturated Fatty Acid (PKOAE1)		
Epoxy Fatty Acid (PKOAE)		
C-3 Side Chains Fatty Acid (PKOAE3)		
C-4 Side Chains Fatty Acid (PKOAE4)		

Figure 7.1: Nature of Typical Ester Molecules showing the unsaturated state and three modifications for both mono- and di-unsaturated chains.

concentration of unsaturated acids and/or longer chain length, the influence of branching may be greater. Although side chains appeared to have a positive effect on the melting process, the oxidative stability of the side branched esters was lowered. As stated earlier, CH is most reactive to oxidation. Branching of the fatty acids created a CH at the branching point. This led to early decomposition around the branched point, resulting in the decrease in the OOT of the branched esters. Inclusion of antioxidants in the ester protected the CH, leading to increased OOT. In summary, while side branch hydrocarbons improve the low temperature properties by reducing the melting point temperature of the ester, they slightly reduce the oxidative stability of the ester. Although grafting of side branched chains was found to inhibit the melting temperature, the pour point of the samples appeared the same. This suggests that side branching may not be an effective option in a quest to further reduce the pour point of esters of palm kernel oil. *Biotemp*, a bio-based dielectric fluid developed by ABB was energized after

being frozen in a lab cooling chamber and there were no failures [Oommen, 2002]. From the report, failure did not occur because vegetable oil does not have a single melting temperature; and since it is a mixture of esters that freeze at different temperatures, it has a melting temperature range. This gradual freezing process prevents the formation of cracks and voids that could trigger partial discharges. The synthesized esters contained fatty acids that had different melting points. Although it has not been demonstrated, the gradual freezing process of the ester may also result in no void formation.

The synthesized ester, being a mixture of esters with different properties influenced the flash point of the material. The flash point is dependent on the most volatile components of the material. The content of the ester is a mixture of esters of different chain length. The short chain lengths are more volatile because of their low boiling point. There is no significant change in the flash point of the ester after epoxidation because vaporization of methyl caprilate and caprate may have been responsible for the formation of the ignitable mixture at flash point.

Insulation paper impregnation rate is highly dependent on the viscosity of the oil. Impregnation of cellulose insulation structure of laminated blocks that has significant thickness and large size with oil having high viscosity posed a technical or undesirable economic challenge [Dai *et al*, 2008]. Impregnation of such cellulose insulation structure with the synthesized ester having a viscosity less than that of mineral oil will pose less of a challenge. The viscosity of the synthesized esters is more than three times lower than mineral oil at 20°C. This makes paper impregnation easy and the methods used for impregnation of mineral oil-paper can effectively be used for the synthesized ester-paper impregnation without modification.

### **7.1.2 Dielectric Response of Palm kernel Oil and Alkyl Esters**

A three electrode dielectric test cell that can accommodate small sample volume was designed for the measurement of permittivity and conductivity. The measurements, taken with the designed cell were comparable to standard measurements using standard liquids. To fit the experimental data from dielectric response of crude and refined palm kernel oil (CPKO and PPKO), the equivalent circuit shown in *Figure 7.3* was used. The equivalent circuit gives physical representation of the dielectric response. The dielectric

behaviour corresponds to an equivalent circuit having a layer (Electrode Polarization) in series with a parallel combination of a capacitance and bulk conductance  $G$  ( $1/R$ ). This barrier is a non-conducting electric double layer at the electrode-liquid interface resulting from electrode polarization. The equivalent circuit parameters were estimated to give a good fit to the data of *Figure 5.19*. The fitted response is shown as the solid lines in *Figure 7.2*. The fitted bulk conductance and capacitance correspond to the calculated bulk conductance and capacitance of the samples respectively.

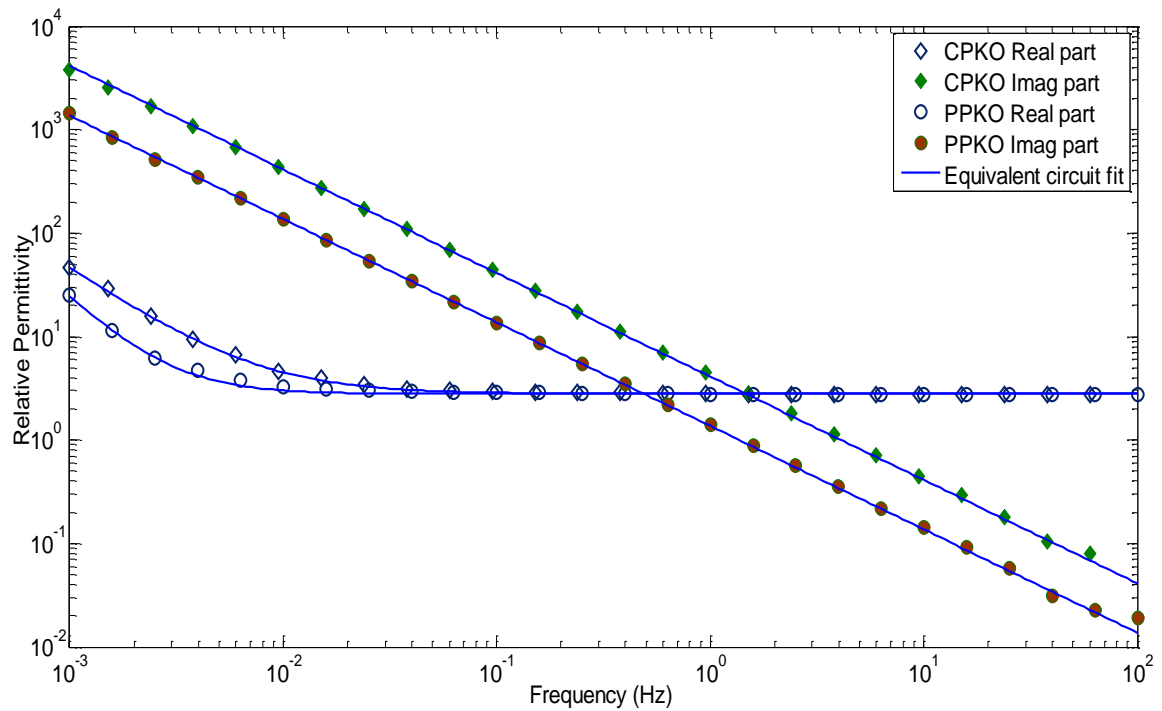


*Figure 7.2: Real and imaginary parts of the dielectric permittivity and fitted equivalent circuit model for the dielectric fluids CPKO and PPKO measured at 80°C*

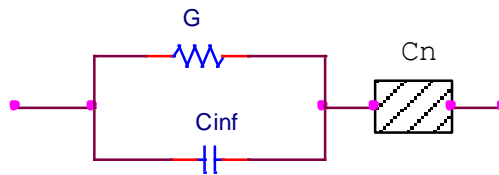


*Figure 7.3: Equivalent circuit model*

The equivalent circuit model indicates that the dielectric response of PPKO is similar to a simple Debye type relaxation with the real part of the relative permittivity acquiring a slope of approximately -2 at low frequencies. The dielectric spectra for CPKO deviated from the simple Debye process. The real part of the relative permittivity acquired a negative slope that is between 1 and 2. The interfacial barrier that builds up at the electrode liquid interface has a fractional power law behaviour represented as  $C_n$ . It can

be described as a low-loss capacitor that is expressed as [Jonscher, 1996]:

$$C_n = A(i\omega)^{n-1} \quad 7.2$$

Where  $A$  is a pre-exponential factor and  $n$  is a fractional exponent with values of 0.4 and 1 for CPKO and PPKO respectively. The value of  $n = 1$  for PPKO, is an indication that Maxwell-Wagner interfacial polarization may be responsible for the double layer formed in PPKO. The  $\tan\delta$  spectra of the crude palm kernel oil in comparison with the purified sample shows a broader spectrum. The broadness indicates a distribution of relaxation times in the sample due to the presence of impurities of various mobilities. Relaxation time for the polarization is defined to be proportional to the square of the radius of the charged particles and inversely proportional to the diffusion coefficient ( $D=\mu kT$ ), where  $\mu$  is the ion mobility,  $k$  is the Boltzmann constant and  $T$  is temperature [Arulanandan *et al*, 1968]. The ionic impurities have different mobilities which lead to a distribution of relaxation times for the formation of the double layer at the electrode interface, resulting in dispersion over a wider frequency range. The particles may also have different sizes with different values of radius. This may also contribute to the spread in the distribution of relaxation times resulting in the broader  $\tan\delta$  peak as obtained in *Figure 5.20*, and a greater overall conductivity. From the equivalent circuit model, the formed electric double layer in the sample was found to obey Jonscher's fractional power law with  $n$  having a value of about 0.4. Purification of the oil eliminates some of the impurity charged particles in the oil leading to a less broad  $\tan\delta$  spectra. This results from the reduction in the distribution of relaxation times of charged impurity particles in the palm kernel oil. An equivalent circuit fit shows that the dispersion in the purified oil is very close to a simple Debye type of relaxation with  $n$  in the fractional power law having a value of 1. Palm kernel oil is a weak polar liquid and can be described as liquid with low concentration of dispersed polar molecules. The spectra of the dielectric response are therefore assumed to be due to the effects of ion transport. The impurities present in the oil sample may also have permanent dipoles. The relaxation time of the ions in the purified palm kernel oil sample was estimated from the equivalent circuit parameters to be  $10^4$  s. It should be noted that a low loss does not imply low concentration of charge particles in the oil. It may be that only few charged particles were mobile due to the viscosity of the oil, and only the mobile charges contribute to the conduction loss. Ionic conduction loss in liquid is dependent

on ion mobility and concentration as expressed in equation 2.23. The ion concentration is dependent on purification, while the transport of ions and hence their mobility is influenced by the dynamic viscosity of the liquid [Umemura *et al*, 1982]. Purification reduces the concentration of impurities in the sample, leading to a decrease in loss and it also narrows the width of the loss spectra.

The calculated AC conductivities from the imaginary part on Arrhenius plot are higher than the corresponding DC conductivity that was measured. This maybe because the AC conductivity is a combination of DC conductivity and polarization in the liquid as equation 2.63 expressed. The activation energy of the characteristic frequency shift on Arrhenius plot corresponds with the activation energy of the AC conductivity. This is expected since the increase in conductivity as temperature change is due to increase in the dielectric loss due to polarization. Applying Fröhlich model, the ions in the liquid have two equilibrium positions separated by a distance. Application of electric field displaced the ions from their equilibrium positions. They acquired sufficient thermal energy from their surroundings to overcome the potential barrier separating the two equilibrium positions. The probability of the ions oscillating over the barrier is related to the relaxation time of the ions. Under alternating voltage, the potential barriers that the ions overcome are separated from one another by relatively short distances whereas, under direct voltage, the contributing conduction ions are those that were able to overcome all the barriers over the relatively large distance between the electrodes leading to less ions contributing to DC conduction process [Bartnikas, 1994]. The number of ions that contribute to AC conduction is more than DC conduction. The activation energies from *Figure 5.27* and *Figure 5.28* indicate the potential barriers that were overcome by the conducting ions which contributed to conduction current. The relaxation time for the reversal of the polarization under the applied AC field is related to the ionic drift velocity. The relaxation time of the conducting ions decreases with temperature as indicated by the shift in  $\tan\delta$  peaks towards high frequency.

The dielectric response of the synthesised esters has a strong deviation from Debye response with LFD-type interfacial behaviour. The viscosity of the samples increased with processing. The conductivity also increases with processing. Since mobility decreased with increasing viscosity, it follows from the conductivity expressed in equation 7.2 that an increased concentration of ions may be responsible for the increase

in conductivity. This increased concentration may have resulted from impurities formed or introduced during the processing stages.

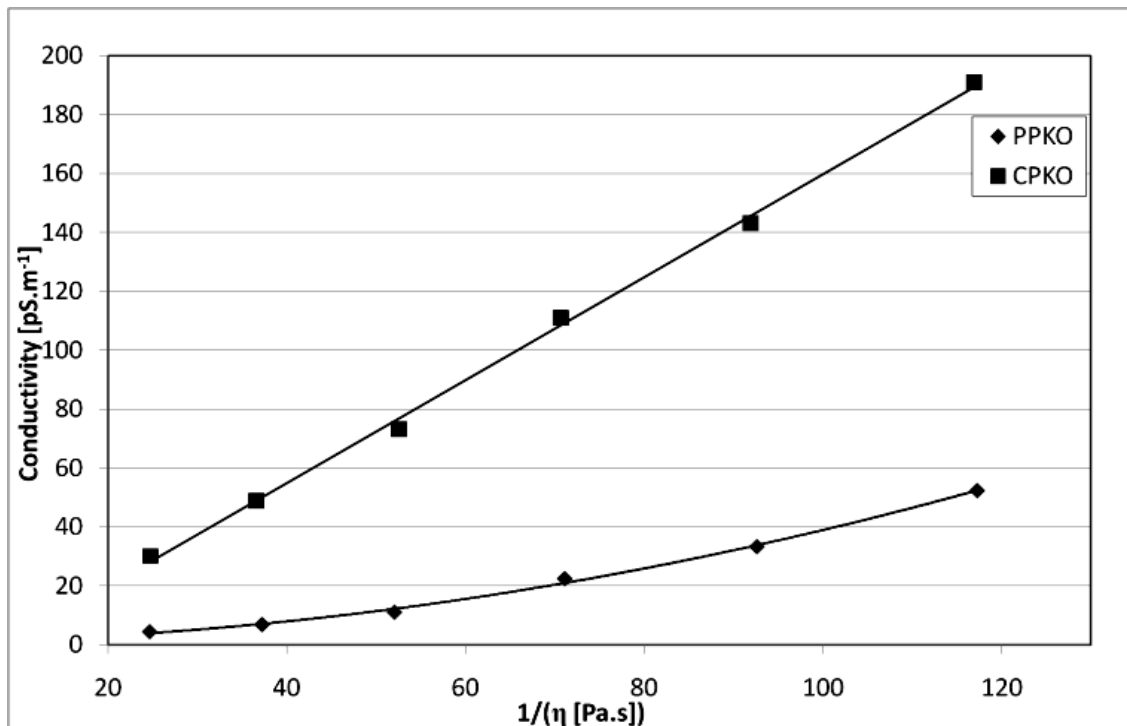


Figure 7.4: Plot of Conductivity-Viscosity Relationship

Information on the electrical conduction of the oil samples can be extracted from the activation energy of the dielectric loss. The activation energy for conduction reflects the difficulty experienced by the charged particles in contributing to conduction in the viscous liquid. The crude palm kernel oil sample has an activation energy of 0.33 eV. Purification of the oil increased the activation energy to 0.47 eV. The activation energy of the purified oil corresponds to the activation energy of Nynas 10GBN mineral insulating oil (0.45 eV). This may either be a mere coincidence or a value of 0.45 - 0.47 eV is typical for liquid with fewer mobile impurity charges. Removing glycerol from the oil, which significantly reduced the viscosity of the oil, resulted in decreased activation energy. This is an indication that activation energy for conduction may at times depend on viscosity of fluids. The alkyl ester (PKOAE1) acquired activation energy of 0.27 eV. The other ester samples; PKOAE2, PKOAE3 and PKOAE4, which were obtained through epoxidation and esterification of PKOAE1 have lower activation energies which are 0.18, 0.13, and 0.10 eV respectively. However, the modification of ester was observed to result in slight increase in viscosity. The decreasing activation

energy suggests that the impurities give rise to conduction of ions through low potential barrier.

The dielectric dispersion of the oil increased with temperature due to change in viscosity that accompanied the temperature variation. The decreasing viscosity enhanced the mobility of the charged particles due to the viscosity dependence of mobility of charge carriers in liquids [Bartnikas, 1999]. This ease in the mobility of more charge carriers results in more mobile charge carriers contributing to the loss phenomena at higher temperatures. The effect leads to a gradual increase in the conductivity of the oil as viscosity decreases.

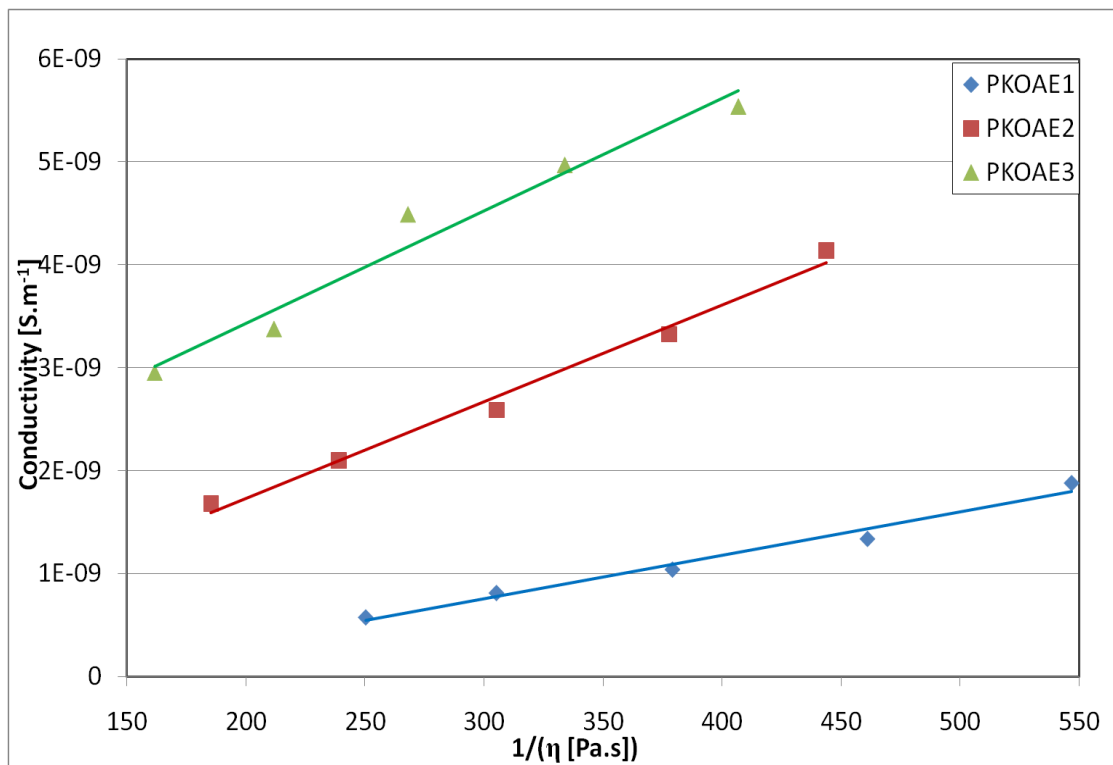


Figure 7.5: Plot of Conductivity-Viscosity Relationship

The relationship between the calculated electrical conductivity and inverse of dynamic viscosity of the fluids is plotted in Figure 7.4. and Figure 7.5 There is a straight line fit on the inverse relationship between the electrical conductivity of CPKO and its dynamic viscosity. The activation energy for conductivity and viscous flow of CPKO are 0.33 eV and 0.29 eV respectively. The inverse relationship and the close values of the activation energies suggest that electrical conductivity of CPKO is highly dependent on its viscosity. Increase in the fluidity of the impurity rich sample leads to an increase in the mobility of the charge carriers and hence the electrical conductivity. The purified PPKO

sample slightly deviates from the linear relationship indicating that conductivity in the sample is not simply controlled by oil viscosity. *Figure 7.5* shows a straight line fits between conductivity and reciprocal of viscosity for PKOAE1, PKOAE2 and PKOAE3. But comparison of the activation energies of conductivity and viscosity in *Table 5.2* and *Table 5.6* of Chapter 5 indicates that only in the PKOAE2 sample does the viscosity change has a dominant effect in its conductivity. For the other ester samples, there may be other mechanisms involved in the increase in conductivity with temperature. This may include increased dissociation leading to increasing ionic concentration.

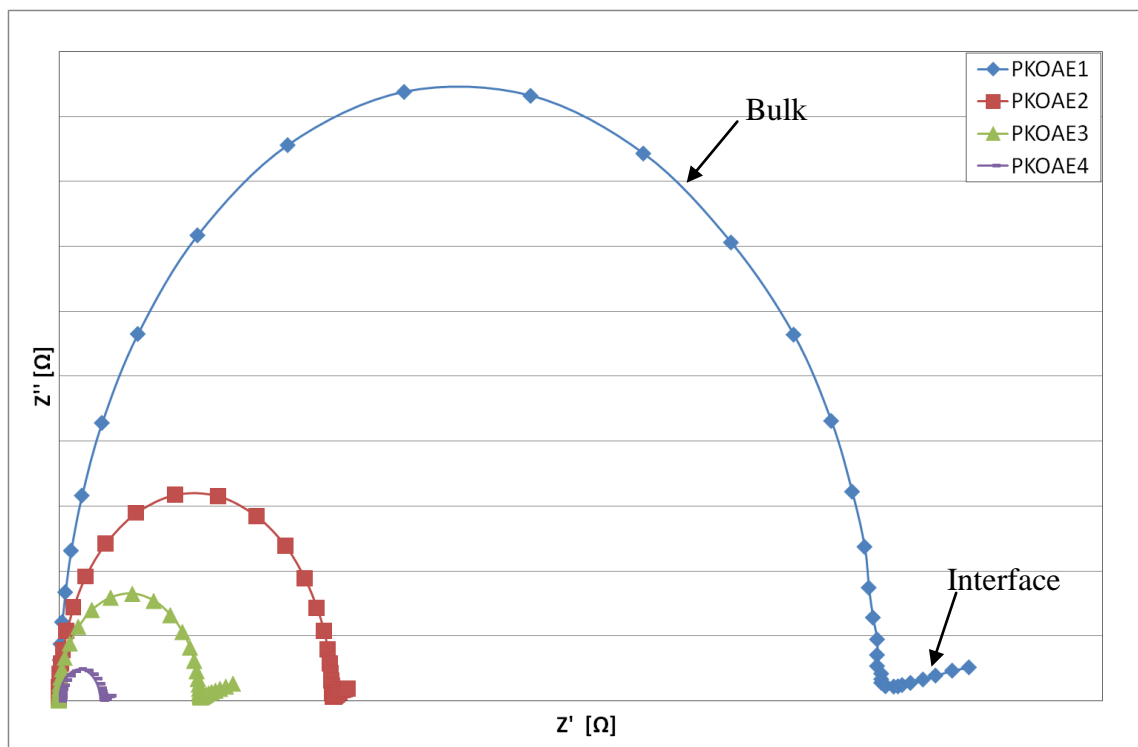
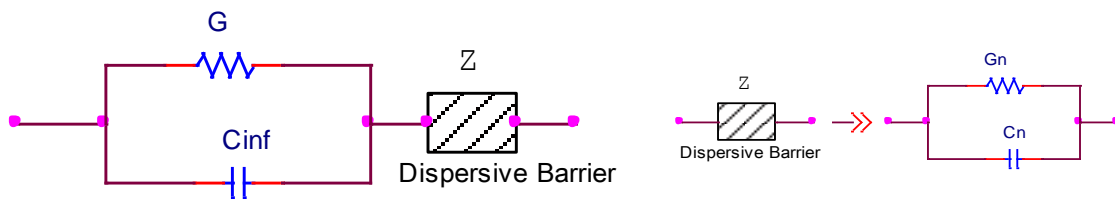


Figure 7.6: *Complex plane ( $Z''$  vs  $Z'$  plot)*

The dispersive barrier formed in the ester samples appeared to have a more complex behaviour compared with the behaviour of the original palm kernel oil samples within the frequency range studied. The plot of the response of the ester samples in complex impedance plot is shown in Figure 7.6. It clearly displayed a separation of the bulk mechanism from the interfacial phenomenon. The semicircular-like arc which occurs at high frequency region indicates that conductance is the dominant process in the bulk material, while the spurs resulted from the interfacial phenomenon which includes interfacial polarization and a suspected electrochemical or low ionic mobility processes. This means that charge-transfer kinetics alone dictate the conduction process at high frequency region. The area under the semicircular arc reduced as the conductivity of the

samples increases. To understand the physical interpretation of the arc, let us consider parallel R-C for the bulk liquid, and the double layer to involve two parallel processes that consists of the double layer capacitance,  $C_n$  and polarization resistance,  $R_n$ . At very high frequency, the contribution of the double layer to the imaginary part of the impedance ( $Z'' = -1/\omega C_n$ ) is zero. As the frequency decreases, the contribution of  $C_n$  becomes finite.  $C_n$  then gives a high reactance and the current passes predominantly through the bulk conductance and polarization resistance. This overall effect is an increasing  $Z'$  and diminishing  $Z''$ . There exists a transition between the semicircular arc and the inclined spur for the respective ester samples. The lowest value for the imaginary part of the impedance corresponds to frequency of  $\tan\delta$  peak. This is the relaxation frequency for electrode polarization ionic species and the corresponding relaxation time can be evaluated from it. The frequency dependence of this region is only from interfacial polarization. At lower frequencies when  $\omega \rightarrow 0$ , the electric double layer becomes dominant and low frequency dispersion as indicated by a low frequency power law, played a significant role in the dielectric response of the material. Interfacial dispersion may be responsible the nature response obtained for the alkyl esters. This response can be represented as a dispersive barrier in series with parallel bulk R-C as shown in *Figure 7.7*. The frequency dependent dispersive barrier may be a set of series combination of polarization resistance,  $R_n$  ( $1/G_n$ ) and capacitance,  $C_n$  connected in parallel as shown in *Figure 7.7* [Brett *et al*, 1993; Bard *et al*, 2001].



*Figure 7.7: Equivalent Circuit for Electrode Polarization in Alkyl Ester*

The accelerated ageing test was found to increase the viscosity of the ester, while the  $\tan\delta$  peak shifts towards higher frequencies with ageing as stated in Chapter 6. This shows an increased dielectric loss with ageing. Equation 7.2 suggests that contributions due to charge carrier concentration dominate the conduction processes. The oil samples were aged with insulating papers and metal foils. Impurities from these materials may have contributed to the increased dielectric loss. Thermal degradation results in polymerization of the oil. The resulting ionic radicals in the aged esters may have also

contributed to conduction ions. This results in increase losses due to ionic conduction and hence the observed shift in the  $\tan\delta$  peak towards higher frequencies.

### 7.1.3 Ester Breakdown Strength

The electric field strength of the oil samples was assessed using dynamic tests in which progressive electrical stresses were applied to samples until breakdown occurs. The test was performed using a bespoke breakdown test cell. The test cell was designed to accommodate a sample volume of 15 ml because of the limited sample volume. The magnitude of the electrical field at breakdown of each sample was recorded. The characteristic breakdown strength of crude palm kernel oil as reported in *Table 5.7* was found to be 37 kV/mm. The purification of the oil significantly improved the breakdown strength by 4 kV/mm. The presence of significant impurities may have influence on the breakdown strength of insulating oils as discussed in section 5.5. The synthesized ester samples from the purified oil sample have breakdown strength not significantly different from the purified oil. The shape parameter, which is related to the statistical consistency of the data, was high for breakdown data for PKOAE1 and PKOAE2. However, it was found to decrease for PKOAE3 and PKOAE4 samples. This is an indication of lower predicted breakdown field value for low probabilities (for example, 1% probability). Although the alkyl ester samples have similar characteristic breakdown fields, the predicted 1% breakdown probability of PKOAE3 and PKOAE4 are below the values for PKOAE2 as shown in *Table 7.1*. This suggests that the breakdown strength for PKOAE1 and PKOAE2 has lower probability of failure at lower applied fields compared with that of PKOAE3 and PKOAE4 samples. Increase in the conductivity of a dielectric material leads to generation of heat in the material. The measured characteristic breakdown strength of the aged ester samples was still within the acceptable limit. The alkyl ester still possessed good breakdown strength after ageing at 150°C for 84 days.

The AC conductivity of the alkyl ester was found to increase with processing steps due to increasing impurity level. Ageing also contributed to a conductivity increase and the  $\tan\delta$  for aged esters samples is greater than 1. This may cause thermal breakdown in the samples. Application of high fields may result in continuous generation of heat within the dielectric due to conduction currents and dielectric loss [Kuffel *et al*, 2000]. When the rate of heating exceeds the rate of cooling, instability conditions are reached and

thermal breakdown of the liquid may occur. While there is an indication for possible thermal breakdown in aged ester samples, it is not certain if the conductivity of the unaged ester fluid can initiate thermal breakdown that may result in significant decrease in breakdown strength with increasing temperature. There will be the need to examine the influence of varying temperature on the breakdown strength of unaged ester sample. Breakdown strength reduced with electrode gap and investigations by Wang and her research group at Manchester revealed that the breakdown field of commercially available natural ester dielectric fluid at wide gaps is lower than mineral oil due to the relatively low tolerance of the esters to fast streamers [Liu *et al*, 2011]. It is not certain if the synthesized low viscous liquid possessed similar behaviour with the rest of the natural fluids.

*Table 7.1: Breakdown Probabilities from Weibull Distribution*

<i>Samples</i>	$U_{1\%}$ (kV/mm)	$U_{50\%}$ (kV/mm)	$\alpha$ (kV/mm)	$\beta$
PKOAE1	36.63	42.28	43	28.85
PKOAE2	37.47	42.46	43	33.84
PKOAE3	30.30	42.22	43	12.76
PKOAE4	31.48	42.16	43	14.49
Min Oil	21.10	26.66	27	18.10

#### **7.1.4 Dielectric Response of Ester-Paper System**

Insulating paper possesses randomly distributed voids between its fibres. These voids are filled up when the paper is immersed in oil. “Clusters” of charged particles may accumulate in the oil-filled voids. The distribution and connectivity of the clusters in the paper dominates the effective properties of the composite material. The properties of the oil and the paper play a vital role in the ageing of the composite material. An ageing factor could be defined as the decrease in the tensile strength of the material after ageing, expressed as a percentage of that before ageing. The ageing factor of the ester impregnated paper samples as shown in *Table 7.2* was significantly lower than that of mineral oil impregnated paper samples. This is a clear indication that insulating papers in palm kernel oil alkyl ester have a much slower degradation rate than those in mineral oil. This result is in agreement with McShane report [McShane *et al*, 2002] on ageing behaviour of Kraft paper in FR3 ester insulating fluid. The results show that the greater affinity of natural ester fluid for water, combined with hydrolysis, caused water to move from the Kraft paper insulation into the natural ester fluid in larger quantities than in

conventional transformer oil. This cumulative equilibrium shift of water effectively dries the paper and reduces ageing due to thermo-hydrolytic degradation. Water is consumed by hydrolysis of the natural ester, producing free fatty acids. During accelerated ageing at elevated temperatures, this may react with the cellulose backbone via transesterification protecting the cellulose from hydrolysis [Rapp *et al*, 2005].

Table 7.2: Ageing Factor of Paper Samples

Materials	State	Tensile stress [MPa]	Ageing factor
Mineral oil/paper closer to metal plate	New	99	0%
	Aged for 28days	38	61.6%
	Aged for 56 days	34	65.7%
	Aged for 84 days	35	64.6%
Ester/paper closer to metal plate	New	111	0%
	Aged for 28days	105	5.4%
	Aged for 56 days	100	9.9%
	Aged for 84 days	99	10.8%
FR3/paper <sup>1</sup>	New	121	0%
	Aged for 20 days	80.8	33%
	Aged for 42 days	74.9	38%
	Aged for 83 days	63.6	47%

<sup>1</sup>[McShane *et al*, 2002]

The oil-paper system is a composite system that possessed randomly distributed oil-filled voids between the fibres with clusters of charges. Interpretation of dielectric spectroscopy results of oil-paper system is reported to be a difficult task [Fofana *et al*, 2010]. This is possibly because there are various factors that influence the response which include the system ageing condition, moisture content and the environmental conditions. The application of electric field results in interaction between charges and the field within the voids at higher frequencies. This is a form of displacement of the charges within the cluster. The displacement of an effective charge over the cluster size and ion movement over a distance less than the cluster size contributes to the cluster polarization at high frequencies. These induced dipoles are distributed over the whole cluster and the relaxation gave rise to a loss process with slopes of about  $-0.7 \pm 0.05$  at the higher frequency side of the loss peak. At crossover frequency ( $\omega_c$ ), the effective charge displacement attains the maximum range with corresponding amplitude that

defines that dipole moment of the displacement. At frequencies lower than  $\omega_c$ , there is sufficient time for charge transfer between neighbouring clusters. That resulted to the observed low frequency dispersion in the dielectric response of the ester-paper samples. The presence of oil may have created regions of high concentration of quasi-mobile charge carriers in the cellulose paper. The response was denominated by a near DC type of conduction due to movement of charges between the nearest neighbour clusters in the paper [Dissado *et al*, 1983; Shablakh, 1984; Raju, 2003].

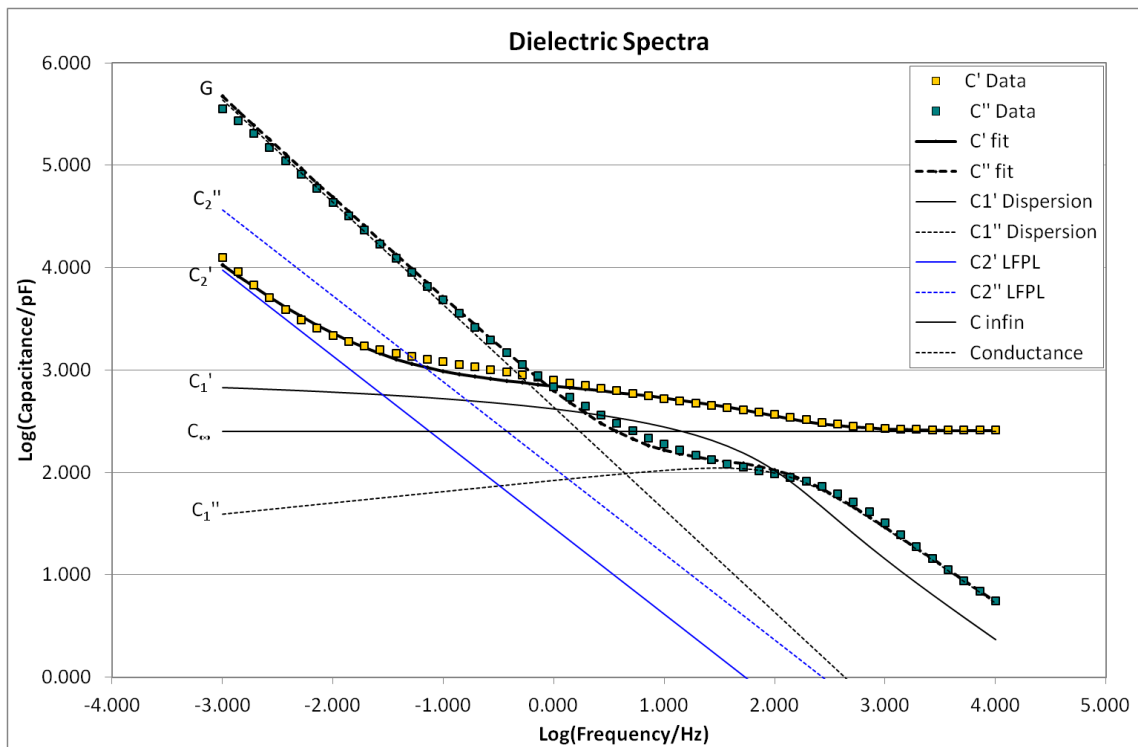


Figure 7.8: Equivalent Circuit Fit of 28 Days Aged Ester-paper Dielectric Response

Ageing caused degradation of the samples which included charring of the fibres. Some of the by-products may include ionic radicals and water. The charring leads to weakening of the cellulose fibres and this may have modified the surface of the voids. The relaxation of ageing by-products may have caused the high frequency loss process at about 1 kHz. There is an increase in the magnitude of the peak maxima with ageing. This may have resulted from an increase in the amount of dipole relaxation in the degraded oil. The slopes of the response at the LFD region for the ester-paper samples were estimated to be  $-0.96 \pm 0.01$ . The slopes of approximately -1 were acquired around the frequency of  $10^{-3}$  Hz. The LFD was observed to be more pronounced in the aged samples. The value of  $n$  for EIP28D, EIP56D, and EIP84D were evaluated to be 0.02

for the respectively aged samples. Similar to EIP00D, these LFD correspond to the real and imaginary parts falling with frequency approximately as  $1/\omega$ .

The equivalent circuit fit shows that parallel processes are involved in the dielectric response [Dissado *et al*, 1983]. The model separates three contributions to the dielectric loss of ester-paper samples as displayed in *Figure 7.8*. The first process is dominated by a constant real capacitance,  $C_\infty$ , resulting from higher frequency dipolar relaxation in the oil-paper at frequencies  $> 10^3$  Hz, and frequency independent conductance,  $G$ , due to charge movement through the system. This process was followed by contribution from a capacitive dispersion,  $C'_1$ , that results in a broad loss peak ( $C''_1$ ) around 100 Hz. Ageing of paper as discussed above caused a cumulative equilibrium shift of water from the paper insulation into the ester fluid. This was observed from the increase in the moisture content of the ester fluid after ageing. This and the other ageing products may have caused an increase in concentration of ions or dipoles involved in cluster interactions. The broad loss peak may have resulted from dipolar orientations, charge displacements, and displacement of free water molecules along the surface of the fibres connecting the voids that is filled with the oil. The capacitive dispersion process was followed by a low-frequency dispersion around frequencies  $< 0.01$  Hz. The LFD process is characterized in two frequency ranges which crossed over at  $\approx 0.1$  Hz. Above this frequency, the response is principally “intra-cluster” – i.e. polarization within the voids in the paper. This may be due to charge separation within the oil in the voids. Below the crossover frequency, these charges move between voids (i.e. inter-cluster movement) leading to a more lossy process with a greater polarization. This relaxation process obscures the DC contribution. This QDC process is referred to as a near DC conduction process. Effective charge transport formally takes place in this system over any arbitrary range, but DC conduction does not. This conductivity was observed as a very slowly falling response at low frequencies. The characteristic difference between pure DC and near-DC is that the near-DC involved a massive charge storage process together with the ability to deliver discharge current, a situation that is impossible in true DC [Jonscher, 1996]. The fit for other ester-paper samples is in Appendix H .

A number of equivalent circuits have been proposed for modelling the transformer oil-paper insulation system to enhance the understanding of the dielectric response of the system without reference to possible charge transport between oil-filled voids in the

system [Fofana *et al*, 2010]. Figure 7.9 shows the proposed equivalent circuit for the ester-paper response. The conduction current in the insulation is due to the insulation resistance with DC conductance value,  $G$ , while  $C_{inf}$  represents the geometric capacitance of the insulation system and high frequency polarization. The dispersive capacitance,  $D$ , is sometimes represented as a set of series R-C networks connected in parallel representing the relaxation processes taking place in the material. However, this does not consider the interaction between the dipoles and so the dispersion,  $D$ , here is represented by a Dissado-Hill function [Dissado *et al*, 1984]. Quasi-DC results from the interaction of the quasi-mobile charges within the voids of the paper with the applied field. This resulted in the strong low frequency dispersion that followed the broad loss peak.

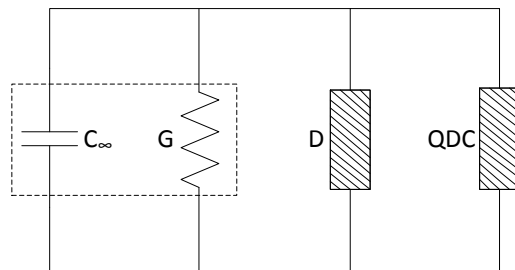


Figure 7.9: Equivalent Circuit Model of Dielectric Response of Ester-paper system

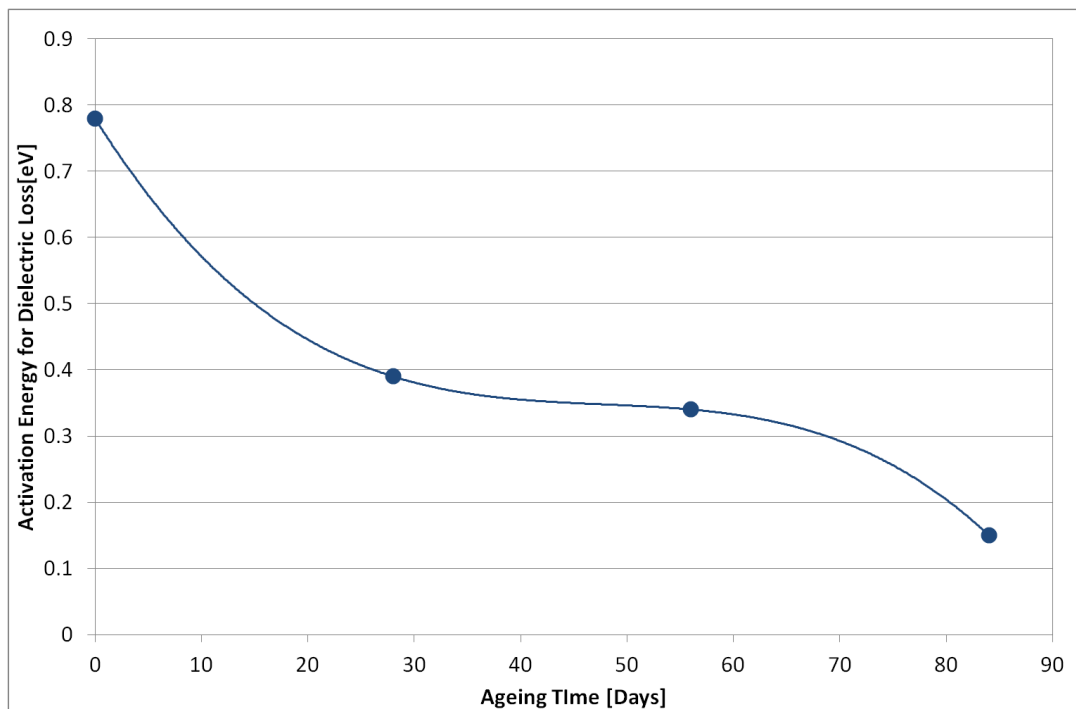


Figure 7.10: Relationship between Dielectric Loss Activation Energy and Ageing Period

A plot of the activation energy versus ageing time (*Figure 7.10*) shows that the activation energy of the obtained data did not follow a simple relation. Dielectric response of aged ester-paper is dependent on various factors which includes the ageing characteristic of both the oil and the paper. This makes the analysis of dielectric response of ester-paper system complex. Looking at the relationship between ageing time and the activation energy, it suggests that ageing behaviour of ester-paper system may be difficult to predict from the activation energy of the loss process.

Ageing may have resulted in small modification of the morphology of the fibres of the paper leading to frequency shift of the dielectric response. An increase in the magnitude of the observed loss processes in the ester-paper system may be an indication of an increase in the amount of ionic species contributing to the loss processes as the material aged with time. This ionic species may have taken their source from the ageing products such as hydrocarbon acids and moisture in the paper which increase with ageing. The activation energy for dielectric loss in the paper decreased with ageing. This suggests in decrease in the potential barrier required for the quasi-mobile ions to overcome.

Impregnation of the paper with oil was seen to cause a significant increase in the breakdown field strength as presented in section 6.6 of Chapter 6. The oil-paper combination shared the applied electrical stress. Insulating paper impregnated with the synthesized palm kernel oil ester shows significantly higher characteristic breakdown field. This may be related to the higher breakdown strength of the ester compared with the mineral oil. Although thermal ageing reduced the breakdown strength of the ester impregnated paper, the decrease in the characteristic breakdown strength of the paper samples after 84 days of ageing under nitrogen at 150°C is not very significant. Comparing the breakdown strength of the ester and mineral oil impregnated paper, the performance of the ester impregnated paper is better than that of mineral oil impregnated paper. The performance of insulating paper impregnated with the synthesized ester of palm kernel oil is about 42% better compared to impregnation with mineral oil.

## **Chapter 8. Conclusions and Further Research Work**

The work presented in this thesis has been an attempt to develop and characterize a bio-based insulating fluid to test the hypothesis that “A natural ester-based dielectric fluid can be developed by synthesis and chemical modification of esters of palm kernel oil (PKO)”. The overall goal is to utilize the abundantly available but less utilized Nigerian palm kernel oil as the base oil for an insulating fluid. This was achieved by chemical modification of the refined oil, focussing on utilization of the C=C bond which is reactive, to achieve improved thermo-chemical properties that are comparable to the characteristics of mineral oil. The electrical response of the synthesized ester samples, and ester-paper system were investigated to acquire information on the behaviour of the fluid as insulating oil. These were also aged in a laboratory system to mimic a power transformer.

The next section of this chapter summarises major findings of the thesis. The second section explores the contributions and limitations of the research. The last section proposes potential areas for further research.

### **8.1 Summary of Major Findings**

The development of a new natural-ester insulating fluid was achieved through the modification of the molecular structure of the fatty acids containing double bonds in the ester. The chemical process produced a more complex structure in the ester molecule which altered the original behaviour of the material. Pour point and flash point, and viscosity and conductivity, are interrelated and an attempt to improve one of the parameters affected the other. The synthesis of four different ester samples enabled the determination of the ester with the optimum combination of the desired properties.

The transesterification process produced palm kernel oil-based ester fluid (PKOAE1) of low viscosity, while the epoxidation process enhanced the thermo-oxidative stability of the fluid. Grafting side-branched hydrocarbon chains on the ester was observed to initiate the depression of melting temperature. The percentage composition of unsaturated fatty acids in ester and the length of the grafted side chain have roles to play in the extent of the impact of modification on the properties of the ester. Alkyl ester of palm kernel oil possessed thermo-physical properties that may make it more efficient in heat transfer and dissipation in transformers. The flash points of the unmodified alkyl

ester and epoxy-alkyl ester samples were about the same and satisfied the specified minimum for mineral oil, while the flash points of the branched ester were below the specified minimum.

The dielectric characterization of the synthesized samples was performed over the frequency range  $10^{-3}$  -  $10^6$  Hz and at a number of fixed temperatures. The temperature ranges from 20°C to 80°C at an interval of 10°C. The measurements results presented on master plots enabled the observation of the dielectric responses of the samples down to a frequency of  $10^{-4}$  Hz at 20°C. Ion transport in the ester samples is a thermally activated process with obtained activation energies that varied between 0.08 - 0.27 eV. The activation energy decreased with processing steps. The esters displayed strong low frequency dispersion (LFD). The impurity charge carriers in the fluids influenced the real part of the permittivity,  $\epsilon'$  at very low frequencies ( $< 10^{-1}$  Hz). Although the synthesized esters possessed low viscosity, they had higher conductivity compared with the existing insulating fluids. This may have resulted from an increase in concentration of impurity charges and/or high mobility due to low viscosity. A bespoke breakdown test cell, designed to accommodate small sample volumes, was used for breakdown field measurement. The characteristic breakdown field of the esters for small electrode gaps was higher than that of mineral oil and the specified minimum for natural ester-based insulating fluid. The Weibull distribution analysis of the electrical breakdown data showed that the characteristic breakdown field of PKOAE2 had a higher predicted breakdown field for low probability of breakdown failure.

All the four synthesized ester samples have comparable viscosity and melting temperatures, and characteristic breakdown strengths. The obtained results show that the unmodified ester (PKOAE1) has lower thermo-oxidative stability, and epoxidation increased the thermo-oxidative stability. Branching of side hydrocarbon chain that was aimed at further reducing the pour point and melting temperature caused reduced thermo-oxidative stability and did not have much influence on the depression of the melting process. This suggests that side branching is not an effective option in further depressing the pour point of esters of palm kernel oil. Reduced viscosity caused faster ion mobility. The manifestation of this was the ester having higher conductivity compared with refined palm kernel oil. Processing also appeared to introduce more impurities. The overall effect is increased conductivity with processing.

Ageing does not seem to have a very significant negative impact on the properties of ester-paper system. However, the aged alkyl ester was observed to produce brownish gummy substance on ageing. This was suspected to be due to polymerization of the ester as the Gas Chromatogram of the waxy substance was similar to that of the aged ester. It is not certain if the chosen ageing temperature was too high for the ester that resulted in the polymerization process.

Samples of aged ester impregnated paper exhibited an improved ageing performance compared with the ageing behaviour of mineral oil-paper. The rate of decrease in the tensile strength of alkyl ester-paper within the ageing condition was significantly lower than mineral oil-paper. The dielectric characterization of alkyl ester-paper was performed over the frequency range  $10^{-3}$  -  $10^6$  Hz at four fixed temperatures. Impregnation increased the charge storage capacity of the insulating paper as observed from the proportionate increase in the magnitude of the real part of the capacitance,  $C'$ , across the frequency range studied. The measurements results on master plots enable the observation of the dielectric responses of the ester-paper samples down as a consequence of ion transport domination to a frequency of about  $10^{-4}$  Hz at 20°C. Characteristic frequency shift of ester-paper response is a thermally activated process with obtained activation energies that varied between 0.15 - 0.78 eV. There was a display of strong low frequency dispersion (LFD). This became more pronounced with ageing. An attempt was made to apply cluster model to explain the dielectric response at low frequency. Quasi-DC conduction was deduced to have dominated the low frequency response of alkyl ester-paper. The near-DC conduction process involved a massive charge storage process together with the ability to deliver discharge current. The activation energy for ion transport decreased with ageing. This, is an indication that potential barrier for dielectric loss mechanism decreased with ageing. There was no significant change in the value of the characteristic breakdown strength of the aged paper samples compared with the unaged sample.

In summary, the synthesized epoxy-alkyl ester of palm kernel oil (PKOAE2) possessed better properties in comparison with the other synthesized ester samples. It has a simple chemistry and the flash point satisfied the specified minimum flash point for mineral oil. It possessed less impurities, higher thermo-oxidative stability and more reliable breakdown strength from the distribution of breakdown data. The statistical analysis of

the electrical breakdown data shows that the characteristic breakdown field of the epoxy-ester is more consistent with a higher predicted breakdown field for low probability of breakdown failure.

## **8.2 Contributions and Limitations**

### **8.2.1 Contributions**

A technique has been identified in this research work to develop improved natural ester insulating fluid from vegetable oil. This technique can be used to develop natural ester-based fluid that may serve as “all purpose” alternative to mineral insulating fluid. Comparing the properties of Epoxy-alkyl ester of palm kernel oil (PKOAE2) developed using the said technique with Nynas 10GBN mineral oil; it possessed comparative thermo-oxidative stability, comparable flash point, lower viscosity, superior breakdown strength (43 kV/mm). The conductivity is higher which can be reduced by further purification if further test shows that the conductivity affects the breakdown strength that may lead to dielectric heating in transformer applications. It has higher melting and pour point which may be reduced using appropriate pour point depressant. The outcome of the study indicates that subject to further tests, the characteristics of epoxy-alkyl ester of palm kernel oil is at least as good as mineral oil in many ways and therefore might be useful as a potential alternative fluid for cooling and insulating power transformers.

### **8.2.2 Limitations**

Laboratory synthesis was designed around small sample volume to minimize the cost of the research. In view of this, the synthesis and characterization of the ester fluids was designed around small sample volume. Measurement test cells were designed that can accommodate the small sample volume. Accelerated ageing test setup was also designed to study the ageing characteristics. The analysis of the measurement results indicate that epoxy-alkyl ester of palm kernel oil have the potential of serving as alternative to mineral oil. However, the research is not without some limitations.

The processing set-up could only process small sample volume: this makes it difficult to quantify the cost of the proposed alternative fluid. The Kugelrohr distillation unit that was used in this research work could not effectively separate the remnant chemical impurity from the synthesized ester samples with branched hydrocarbon chain. The presence of the impurities was suspected to affect flash point and thermo-oxidative

stability of the side branched esters. The breakdown test setup have maximum limit of 50 kV rms as a result, breakdown down test of wide gap could not be performed. This limits the electrode gap used for the investigation of the proposed alternative fluid. Accelerated ageing test of only one of the ester samples was carried out at high temperature because of time frame for the research. A single temperature accelerated ageing test was performed because of time frame for the research. Ageing test for the suitability of the oil in free-breathing system was not performed due to time limit.

### **8.3 Areas for Further Research Work**

The research work presented in this thesis focused on developing an insulating fluid from palm kernel oil; which will be comparable to mineral insulating oil in performance. This was accomplished through chemical modification of alkyl esters of palm kernel oil to improve some of the properties. Perfection cannot be assumed to have been reached and there is still need for further work to firmly establish its applicability; but the outcome so far appears promising. Epoxy-alkyl ester of palm kernel oil (PKOAE2) has, however, been established to possess superior properties among the synthesized esters. The areas that needed to be looked into are given below;

- Investigation of the impact of pour point depressant on the melting temperature of the ester on the fluid is necessary in an attempt for further reduction of the pour point. Flash point depends on the most volatile component of a fluid. The ester contained fatty acids of different chain lengths. Removing the short chain esters such methyl caprylate and methyl capriate which is just about 7% of the total content of the ester and the most volatile, may improve the flash point.
- Although the characteristic breakdown field of the synthesized ester is very high compare to mineral oil, the high DC conductivity can possibly cause thermal breakdown due to dielectric heating. In view of this, further investigation of the ester may be necessary to ascertain if further purification of the ester to reduce the conductivity is required to avoid the possibility of dielectric heating. Investigation of the breakdown strength and mechanisms of the alkyl ester at varying gap will offer information on the breakdown behaviour of the low viscous fluid at wide gaps.

- Natural ester as a weak polar liquid has stronger affinity to water than mineral oil. Studying the effect of increase in relative humidity on the dielectric breakdown of the sample will reveal the effect of increased moisture in the liquid while in use.
- Accelerated ageing was performed on the ester sample containing a certain percentage of saturated fatty acids. Ageing behaviour of epoxy-alkyl ester sample needs to be studied and compared with the obtained ageing results. This may enable understanding of the effect of replacing the C=C with epoxy ring on ageing of alkyl ester. The chosen ageing temperature of 150°C was found to produce polymerization (*Figure 8.1*). The ageing test may need to be performed at temperatures ranging from 100 - 130°C and for a longer ageing period to obtain more information on the ageing behaviour. Ageing test under a system exposed to air is needed to be carried out for the suitability of the oil in free-breathing system.



*Figure 8.1: Photograph of the Polymerized Ageing Product after 84 Days at 150°C*

- Application of the branching technique discussed in this thesis on esters of other vegetable oils with higher concentration of unsaturated fatty acids may produce an interesting outcome. Meanwhile, analysis of the synthesized side branched chain alkyl ester samples indicate that the samples still contained remnants of the respective acid anhydride used to create the side branched hydrocarbon chains. Purification of the samples was performed using Kugelrohr distillation unit to separate the remnant impurity from the samples. This impurity was observed to have affected the properties of the ester samples. Better instrumentation needs to be implemented that can properly separate the remnant impurity from the samples.

In conclusion, the set objective for this project was not fully achieved as the test for the suitability of the fluid in free-breathing system could not be performed due to time

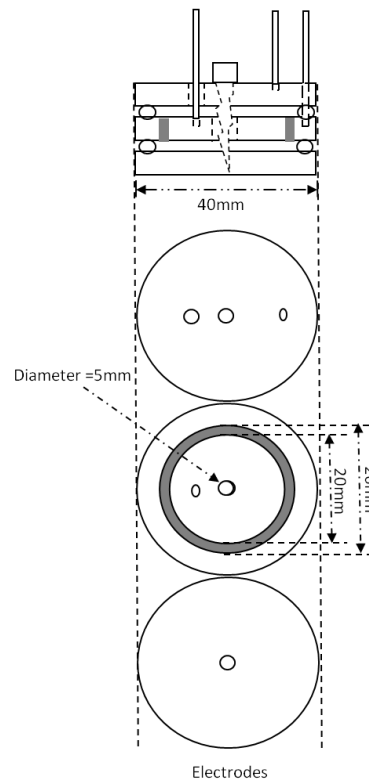
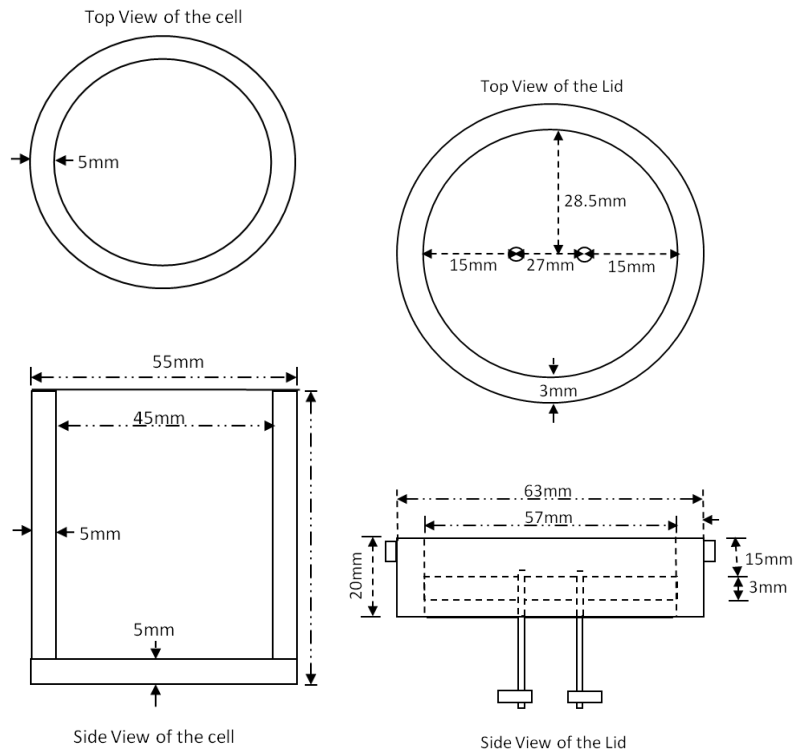
limitation. But the characteristics of the fluid developed in this work, suggest that, even without the further work suggested above, the fluid should now be tested in a full-size transformer under normal load conditions. Following the research presented here, the palm kernel oil epoxy alkyl ester (PKOAE2) may now require a development stage for testing and adoption by electrical distribution companies.

## Appendix A Properties of Typical Insulating Fluids

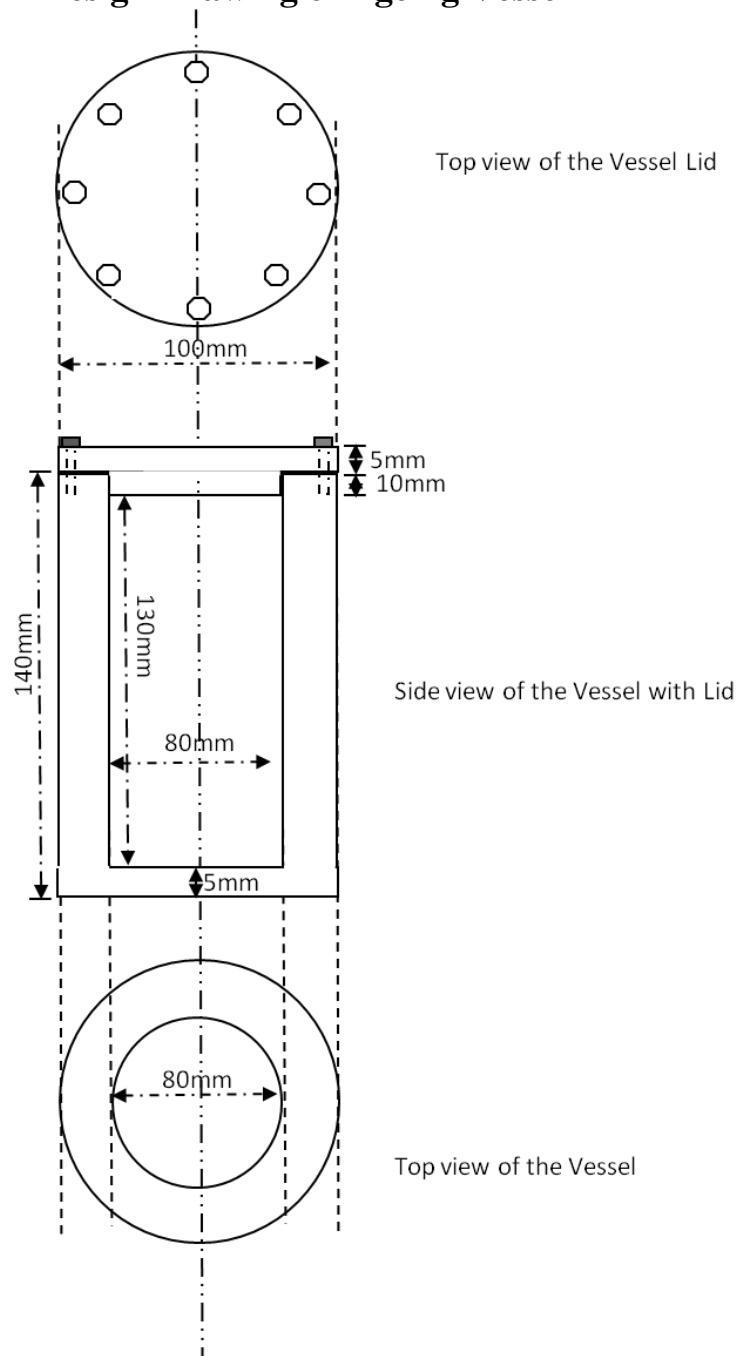
Properties	Unit	Mineral Oil <sup>1</sup>	FR3 Fluid <sup>2</sup>
Density	Kg.m <sup>-3</sup>	886	920
Viscosity at 40°C	cSt	11	34
Water content	mg/kg	30	30
Flash point (closed cup)	°C	140	316
Pour point	°C	-45	-21
Sludge	%	0.8	-
Acidity	KOH.kg <sup>-1</sup>	0.03	0.04
Breakdown voltage	kV	30	56
		(2.5 mm gap)	(2 mm gap)
Relative Permittivity at 50 Hz	-	2.1 at 20°C	3.2 at 25°C
Loss tangent at 50 Hz	-	0.005 at 90°C	0.08 at 25°C
Coefficient of thermal expansion	Per °C	0.0008	0.00074

[<sup>1</sup>Nynas, 2010 *et al*, 2003; <sup>2</sup>Bulletin-B900-00092]

## Appendix B Design Drawing of Dielectric Test Cell



## Appendix C Design Drawing of Ageing Vessel



## Appendix D Pressure Vessel Calculation

The vessel will have a diameter of 80 mm and a height of 124 mm.

$$\text{Volume of vessel} = \pi r^2 h = \pi \times 4 \text{ cm} \times 4 \text{ cm} \times 12.4 \text{ cm} = 623.292 \text{ cm}^3$$

Volume of oil,  $V_1$ , at  $22^\circ\text{C} = 400 \text{ ml}$

The coefficient of volume expansivity is expressed as:

$$\beta = \frac{V_2 - V_1}{V_1(t_2 - t_1)}$$

If the coefficient of volume expansivity is  $7.733 \times 10^{-4}$  per deg Celsius, then

Volume of oil,  $V_2$  at  $150^\circ\text{C}$  will be:

$$V_2 = V_1 [1 + \beta(t_2 - t_1)] = 500 [1 + (7.733 \times 10^{-4} (150 - 20))] = 550.2645 \text{ cm}^3$$

$$\Delta V = V_2 - V_1 = 550.2645 \text{ cm}^3 - 500 \text{ cm}^3 = 50.2645 \text{ cm}^3.$$

$$\text{Volume of free space, } V_i, \text{ at } 20^\circ\text{C} = 623.292 \text{ cm}^3 - 500 \text{ cm}^3 = 123.292 \text{ cm}^3$$

$$\text{Volume of free space, } V_f, \text{ at } 150^\circ\text{C} = 623.292 \text{ cm}^3 - 550.2645 \text{ cm}^3 = 73.0275 \text{ cm}^3$$

The pressure of the vessel at  $150^\circ\text{C}$  should not be less than the saturated vapour pressure of water at that temperature. The saturated vapour pressure of water is 5 atm (74 psi) at  $150^\circ\text{C}$ . The final pressure of the vessel is therefore set at 6 atm (87 psi).

Using ideal gas equation;

$$P_i = \frac{P_f V_f T_i}{T_f V_i} = \frac{607\,950.06 \text{ Nm}^{-2} \times 65.294 \text{ cm}^3 \times 293 \text{ K}}{443 \text{ K} \times 123.292 \text{ cm}^3}$$

$$P_i = 212946.34 \text{ Nm}^{-2} \approx 2 \text{ atm} \approx 31 \text{ psi}$$

The initial pressure of the vessel will be 2 atm.

The expression to determine the minimum required thickness of a cylindrical shell thin-walled pressure vessel is:

$$t_m = \frac{P \cdot r}{S \cdot E - 0.6P}$$

Where P=maximum operating pressure, r=radius of the vessel, S=maximum allowable stress, and E=Welding efficiency.

For example, SA-515 Gr. 60 carbon steel has an allowable stress of 14,400 psi for temperature limit of 700°F (370°C), the minimum required thickness for cylindrical shell will be:

$$t_m = \frac{87 \text{ psi} \times 1.6 \text{ in}}{(14400 \text{ psi} \times 1) - (0.6 \times 87 \text{ psi})}$$

$$t_m = 9.7 \times 10^{-3} \text{ in} \approx 0.25 \text{ mm}$$

Stress on the vessel

Circumferential or hoop stress,  $S_h$  will be;

$$S_h = \frac{P \cdot r}{t} = \frac{87 \text{ psi} \times 1.6 \text{ in}}{0.4 \text{ in}}$$

$$S_h = 348 \text{ psi}$$

Axial or longitudinal stress  $S_a$  will be;

$$S_a = \frac{P \cdot r}{2t} = \frac{117.6 \text{ psi} \times 1.6 \text{ in}}{2 \times 0.2 \text{ in}}$$

$$S_a = 348 \text{ psi}$$

Force on the bolts will be;

$$F = P\pi R^2 = 600 \text{ 000 Nm}^{-2} \times \pi \times (4 \times 10^{-2})^2 \text{ m} = 3017 \text{ N}$$

For 8 bolts, the force on each bolt will be;

$$F_b \approx 377 \text{ N.}$$

Remark: The wall, lid and top thickness of 5 mm can withstand the pressure produced at the temperature of 170°C. Bolts that can withstand a minimum force of 1.3 kN will be used.

# Appendix E Appendix A: Mass Spectra of Oil Samples

PKOAE

, 26-Jul-2011 + 12:09:45

PKOAE 991 (7.955) Cm (988:994)

Scan E1+  
3.79e7

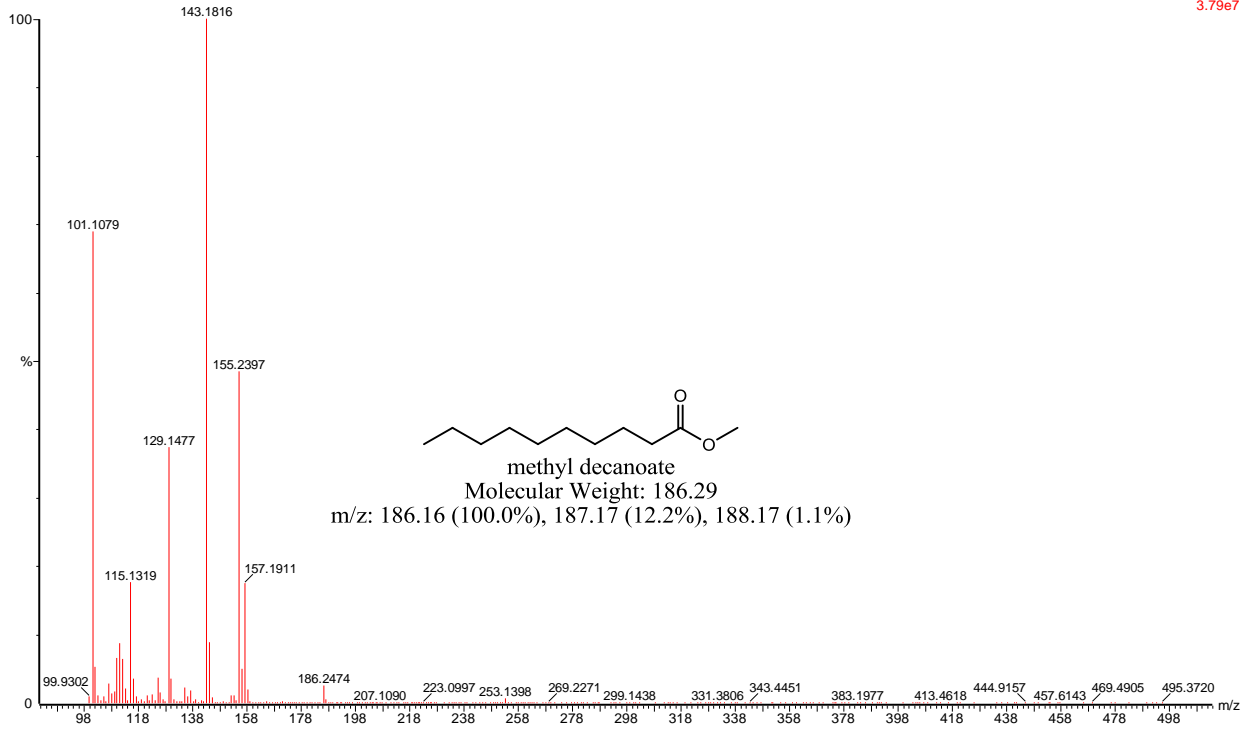


Fig E1: Mass Spectra of Methyl Decanoate (Caprate)

PKOAE

, 26-Jul-2011 + 12:09:45

PKOAE 1521 (10.606) Cm (1511:1522)

Scan E1+  
3.01e8

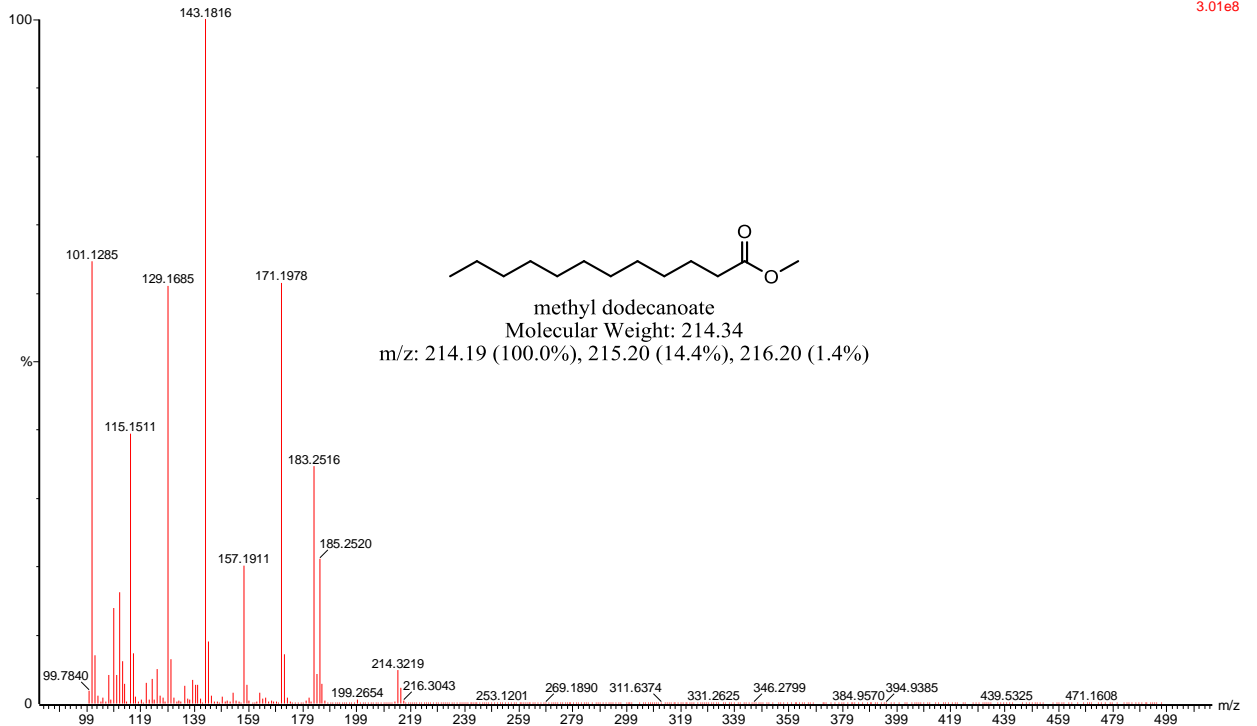


Fig E2: Mass Spectra of Methyl Dodecanoate (Myristate)

PKOAE

PKOAE 1978 (12.892) Cm (1972:1980)

, 26-Jul-2011 + 12:09:45

Scan E+  
2.40e8

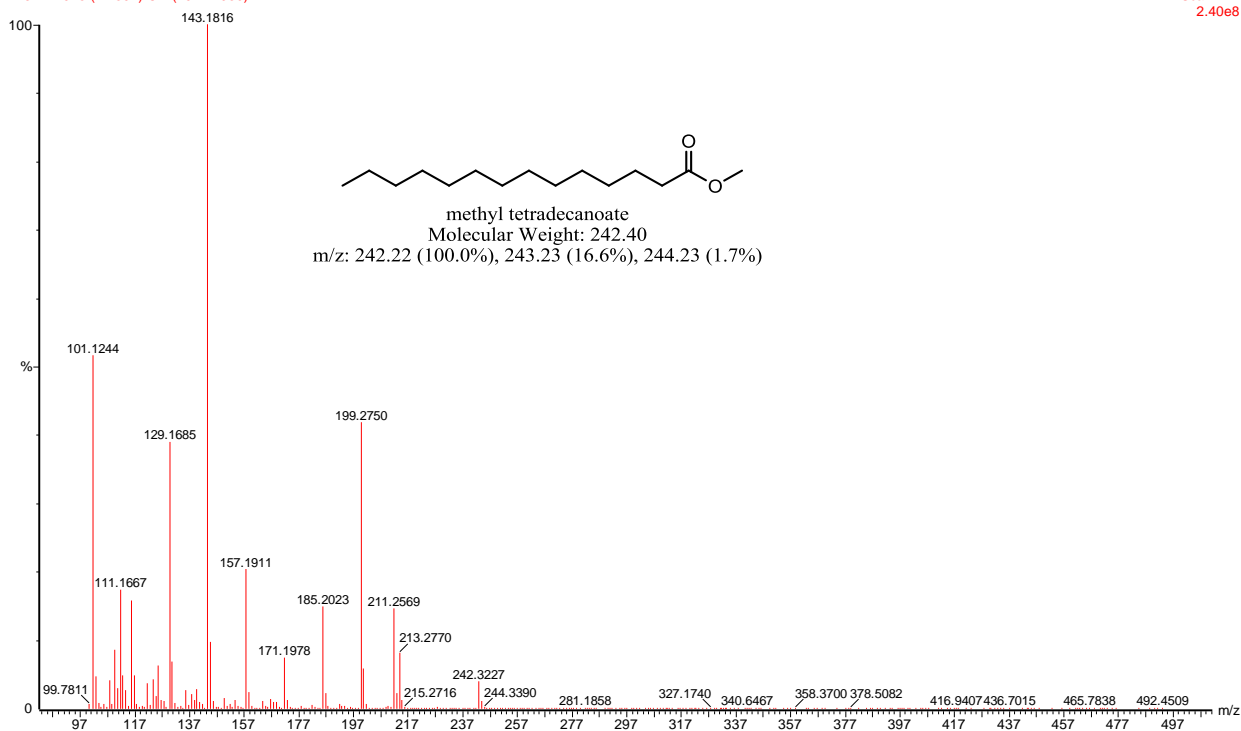


Fig E3: Mass Spectra of Methyl Tetradecanoate

PKOAE

PKOAE 2394 (14.973) Cm (2388:2396)

, 26-Jul-2011 + 12:09:45

Scan E+  
1.49e8

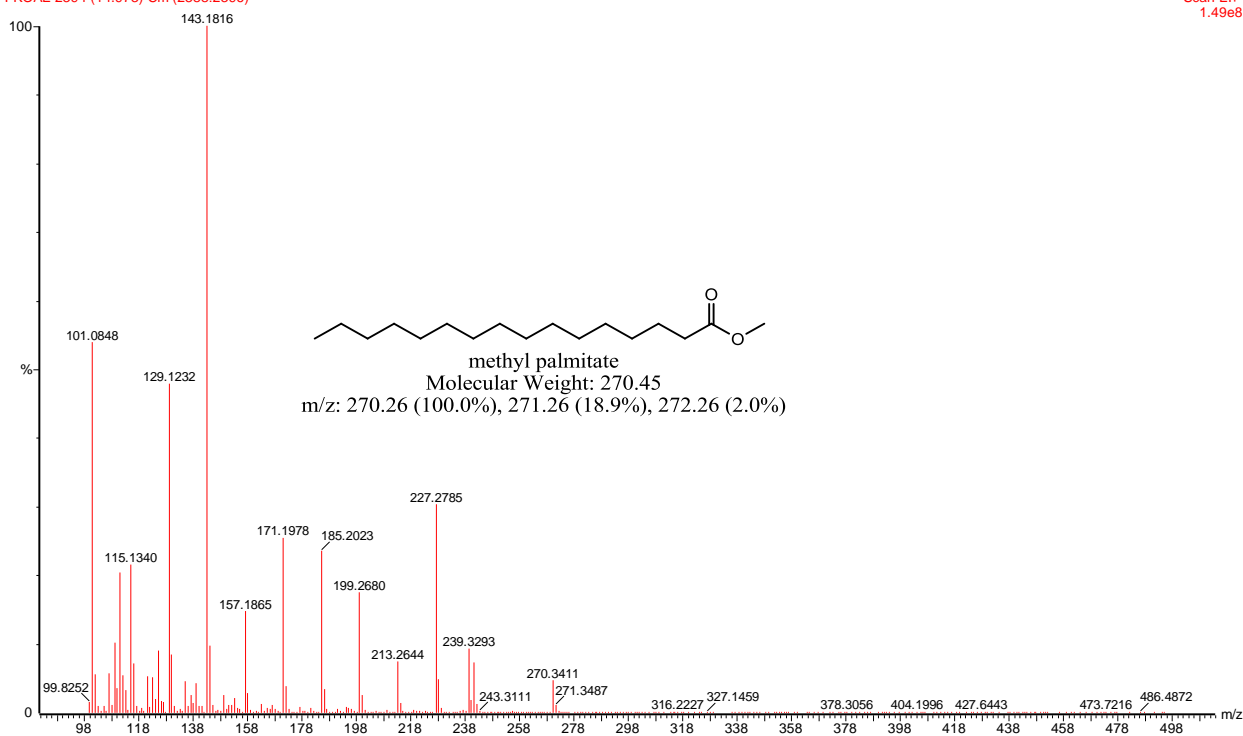


Fig E4: Mass Spectra of Methyl Palmitate

PKOAE

PKOAE 2717 (16.589) Cm (2715:2720)

, 26-Jul-2011 + 12:09:45

Scan E1+  
1.90e7

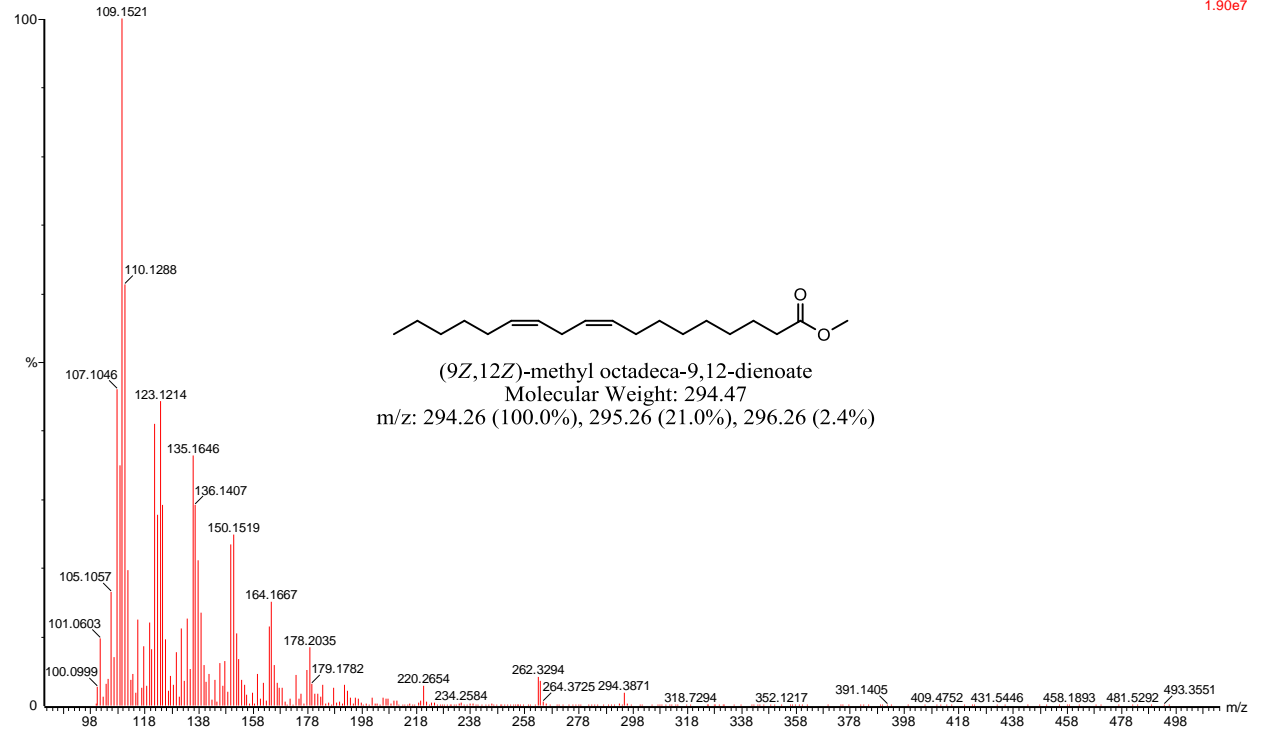


Fig E5: Mass Spectra of Methyl Linoleate

PKOAE

PKOAE 2734 (16.674) Cm (2727:2735)

, 26-Jul-2011 + 12:09:45

Scan E1+  
1.64e8

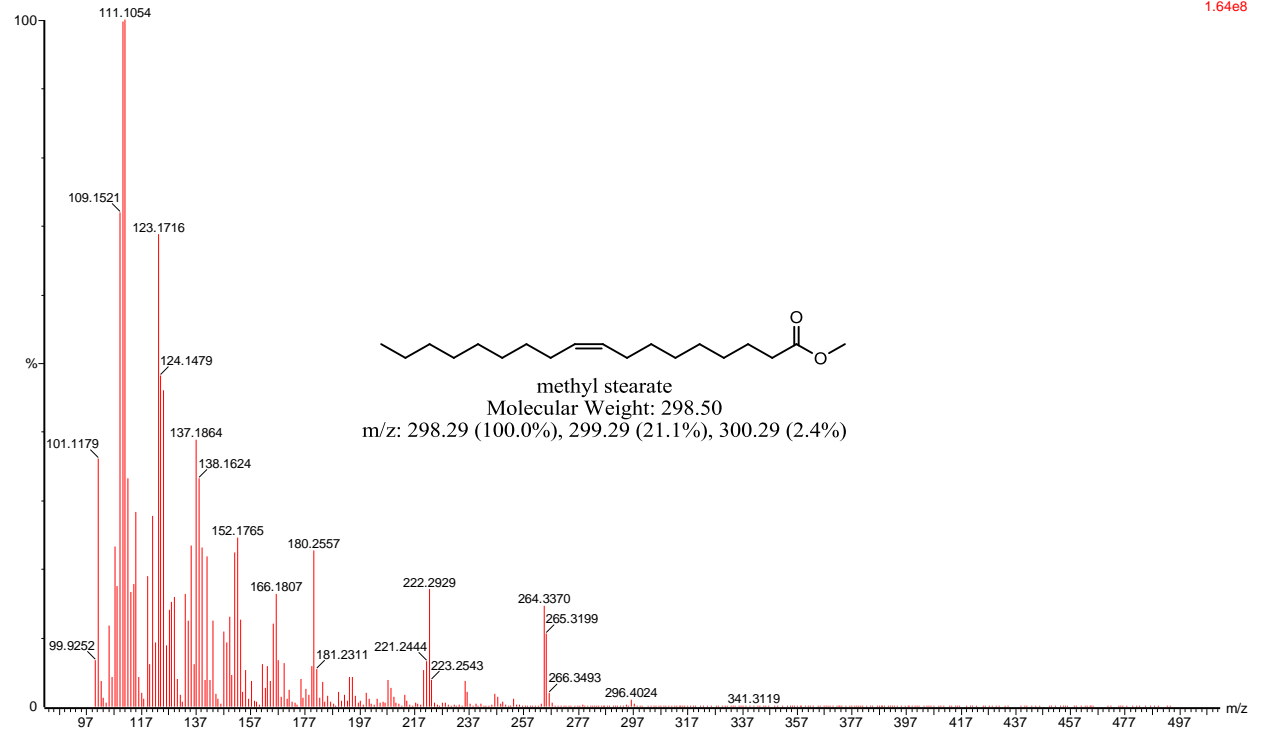


Fig E6: Mass Spectra of Methyl Oleate

PKOAE

PKOAE 2771 (16.859) Cm (2769:2773)

, 26-Jul-2011 + 12:09:45

Scan E1+  
7.63e7

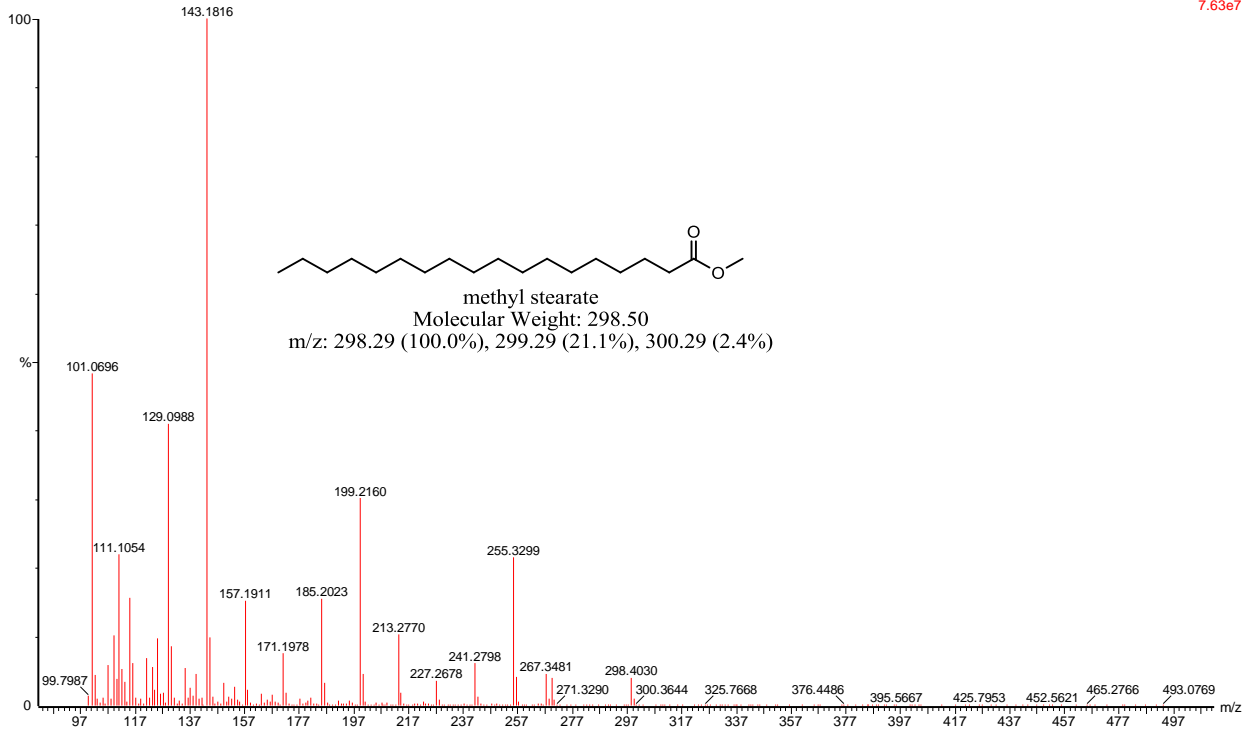


Fig E7: Mass Spectra of Methyl Stearate

PKOAE2

PKOAE2 3306 (19.535) Cm (3303:3310)

, 28-Jul-2011 + 14:31:18

Scan E1+  
2.19e7

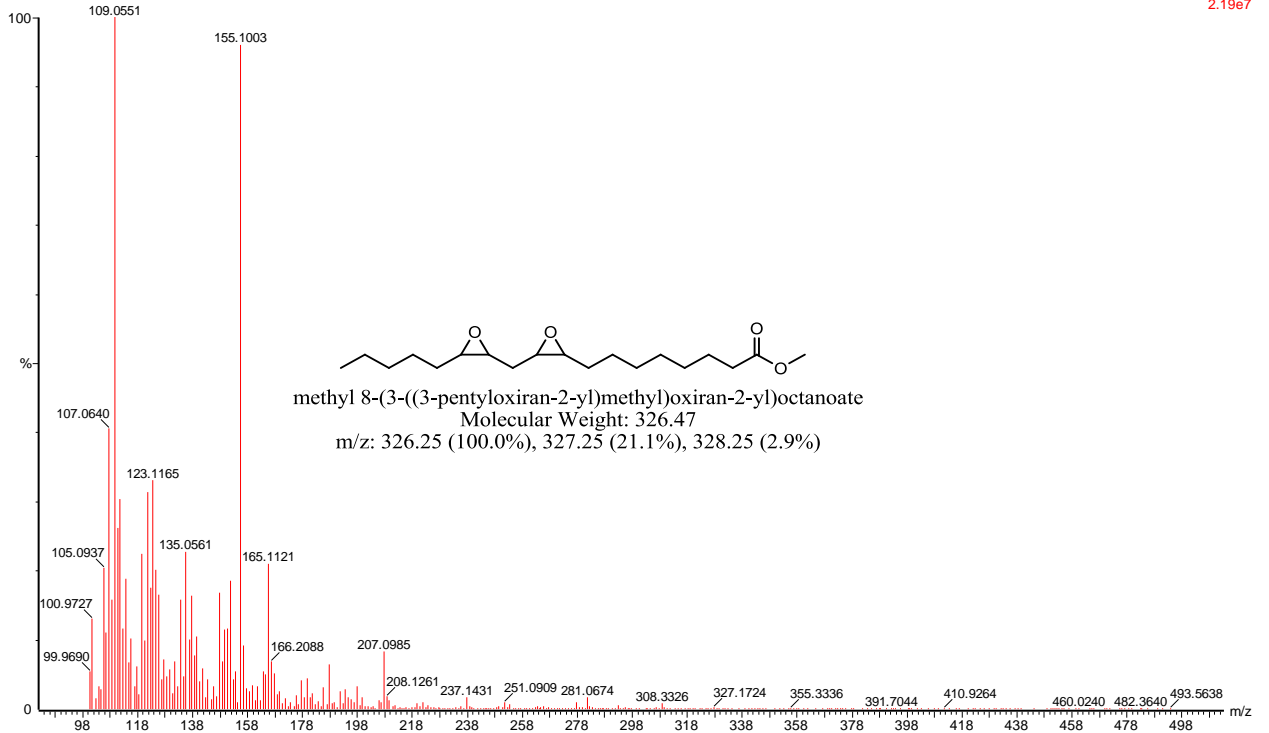


Fig E8: Mass Spectra of Methyl 8-(3-((3-pentylloxiran-2-yl)methyl)oxiran-2-yl)octylloxirane-2-yl)Octanoate

PKOAE3

PKOAE3 3390 (19.955) Cm (3387:3393)

, 28-Jul-2011 + 15:08:37

Scan E1+  
1.63e7

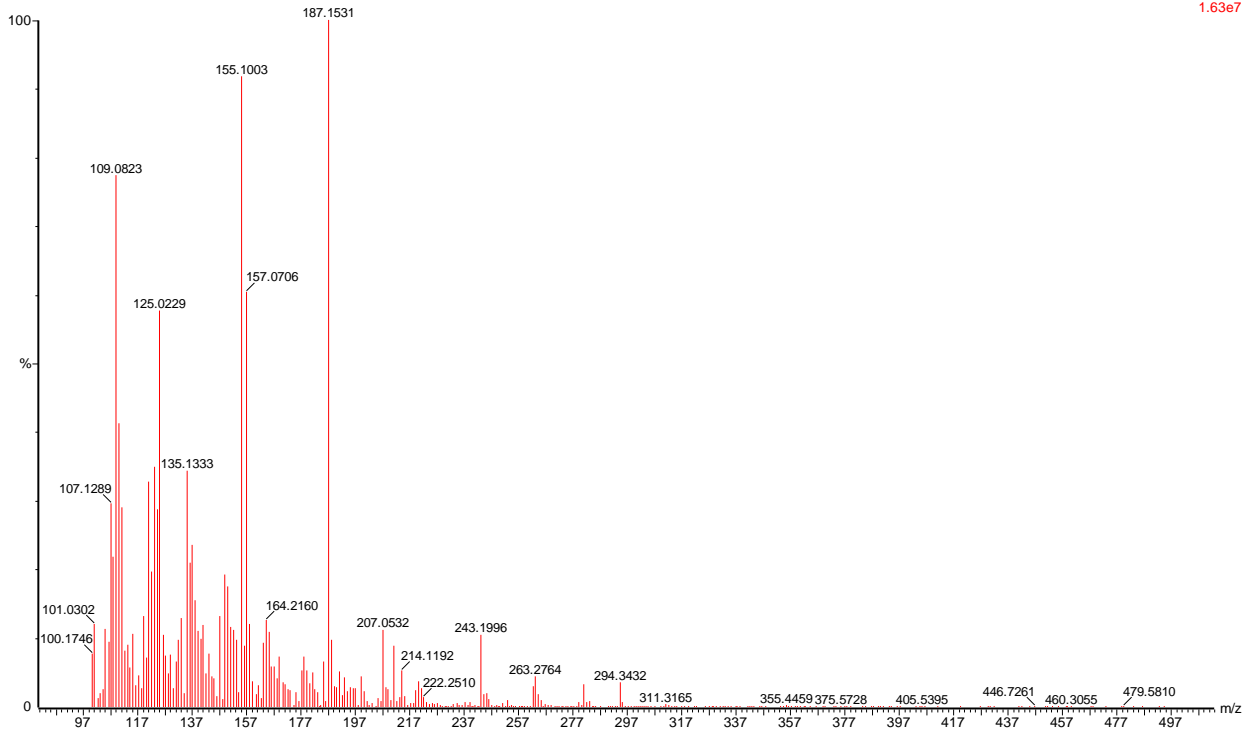


Fig E9a: Mass Spectra of C-3 Side Branched Ester

PKOAE3

PKOAE3 3487 (20.440) Cm (3485:3490)

, 28-Jul-2011 + 15:08:37

Scan E1+  
3.03e7

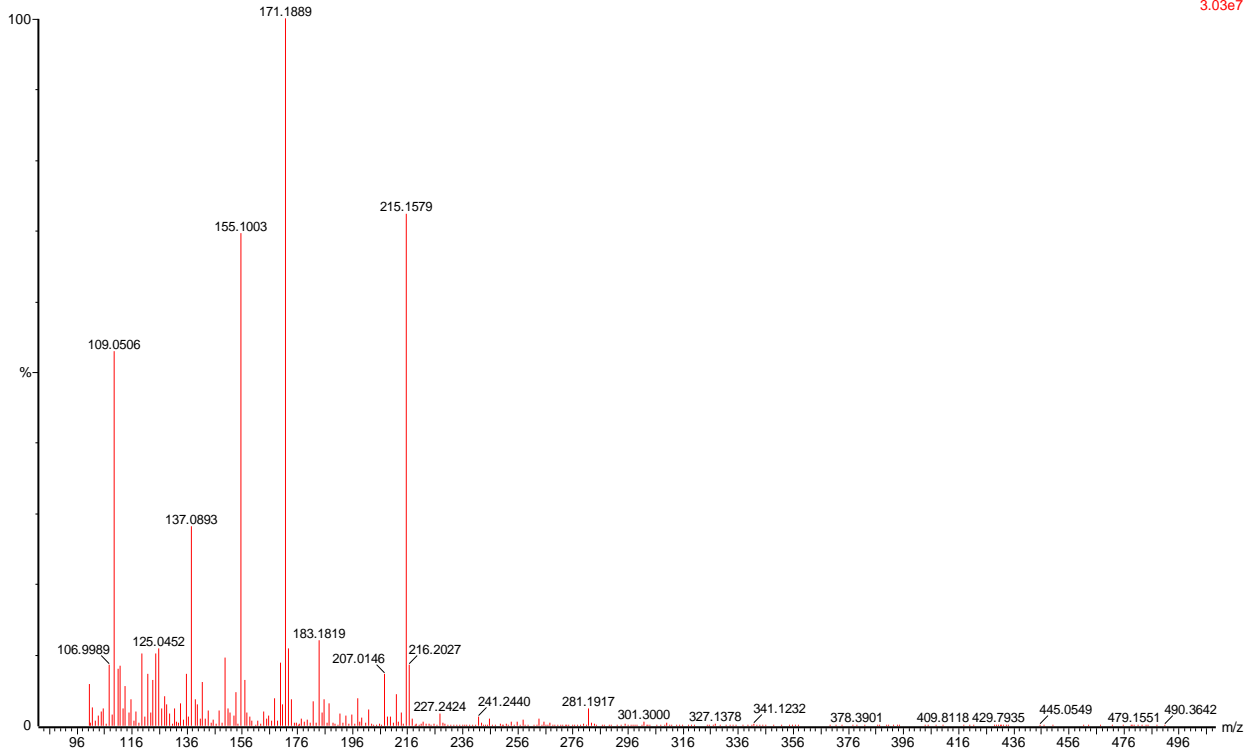


Fig E9b: Mass Spectra of C-3 Side Branched Ester

PKOAE4

PKOAE4 3727 (21.641) Cm (3725:3730)

, 28-Jul-2011 + 15:45:57

Scan E1+  
3.90e7

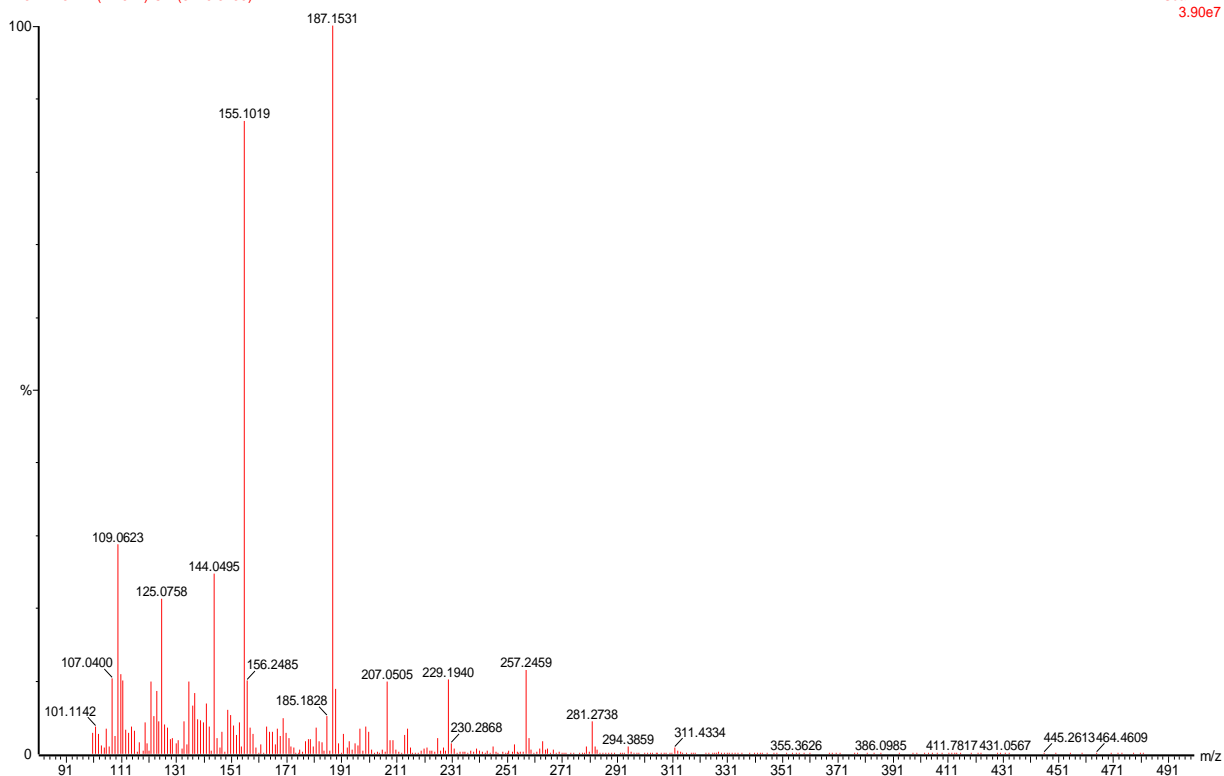


Fig E10a: Mass Spectra of C-4 Side Branched Ester

PKOAE4

PKOAE4 3595 (20.980) Cm (3593:3598)

, 28-Jul-2011 + 15:45:57

Scan E1+  
3.23e7

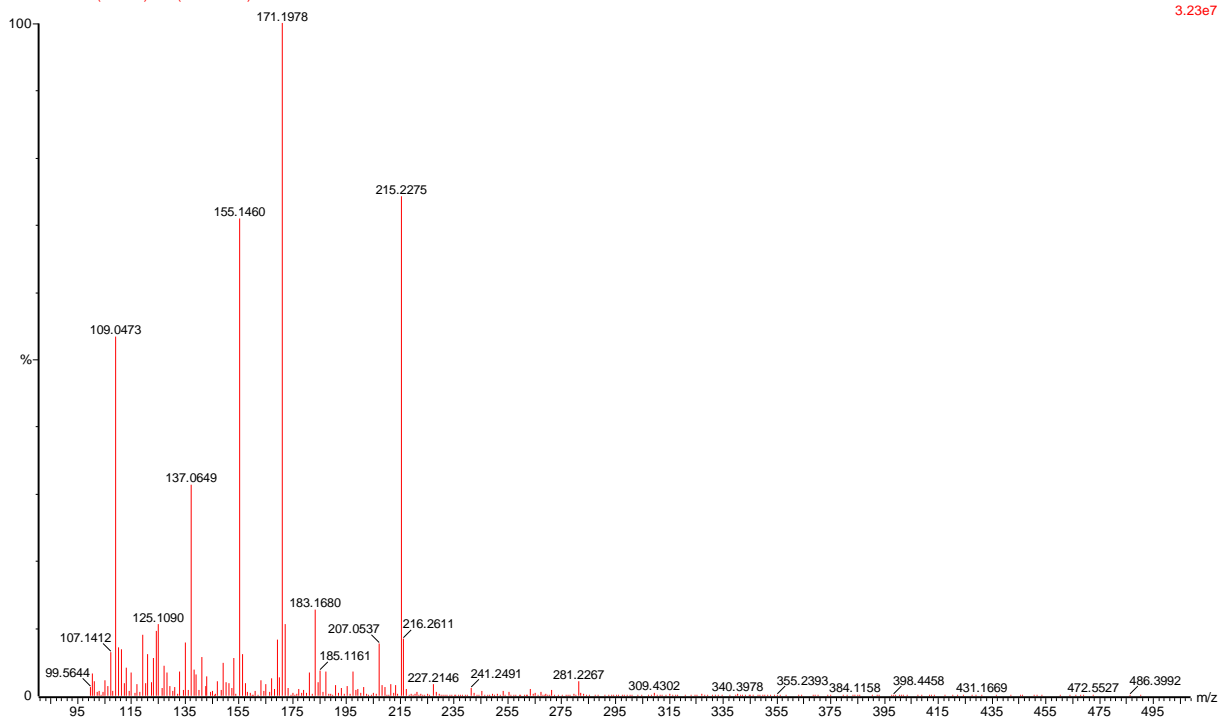


Fig E10b: Mass Spectra of C-4 Side Branched Ester

## Appendix F FTIR Spectra of Oil Sample

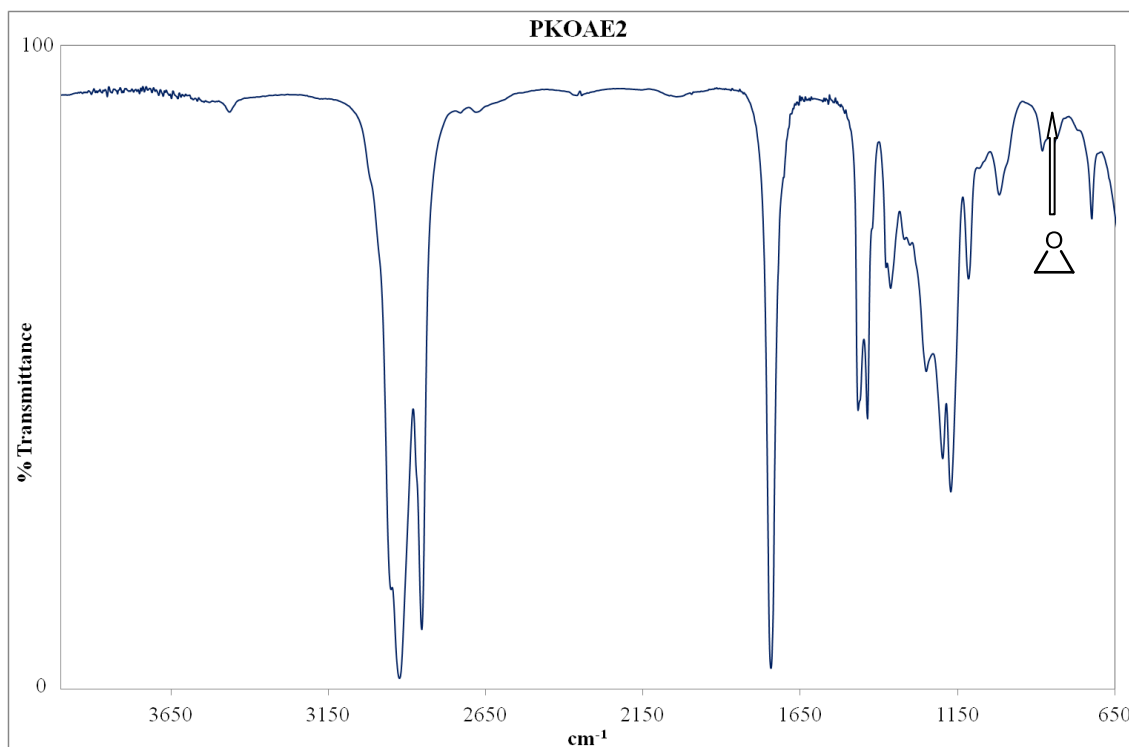


Fig F1: Mass FTIR Spectra of Epoxy-Alkyl Ester

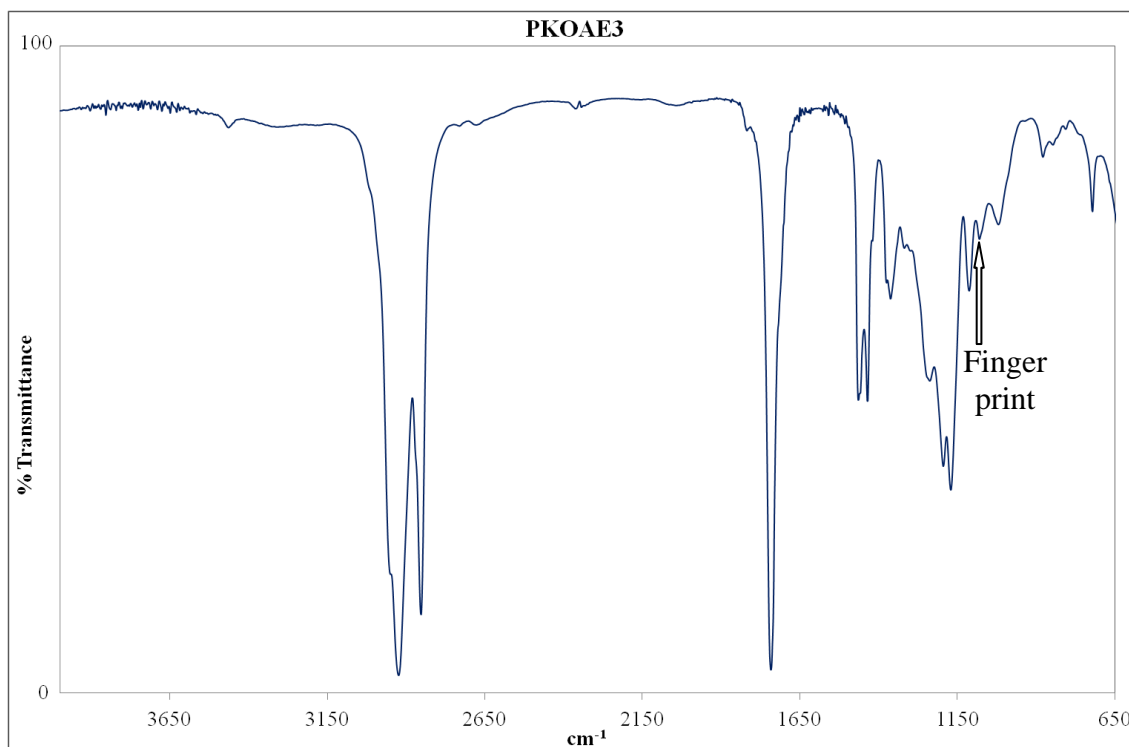


Fig F2: Mass FTIR Spectra of C3-Side Branched Alkyl Ester

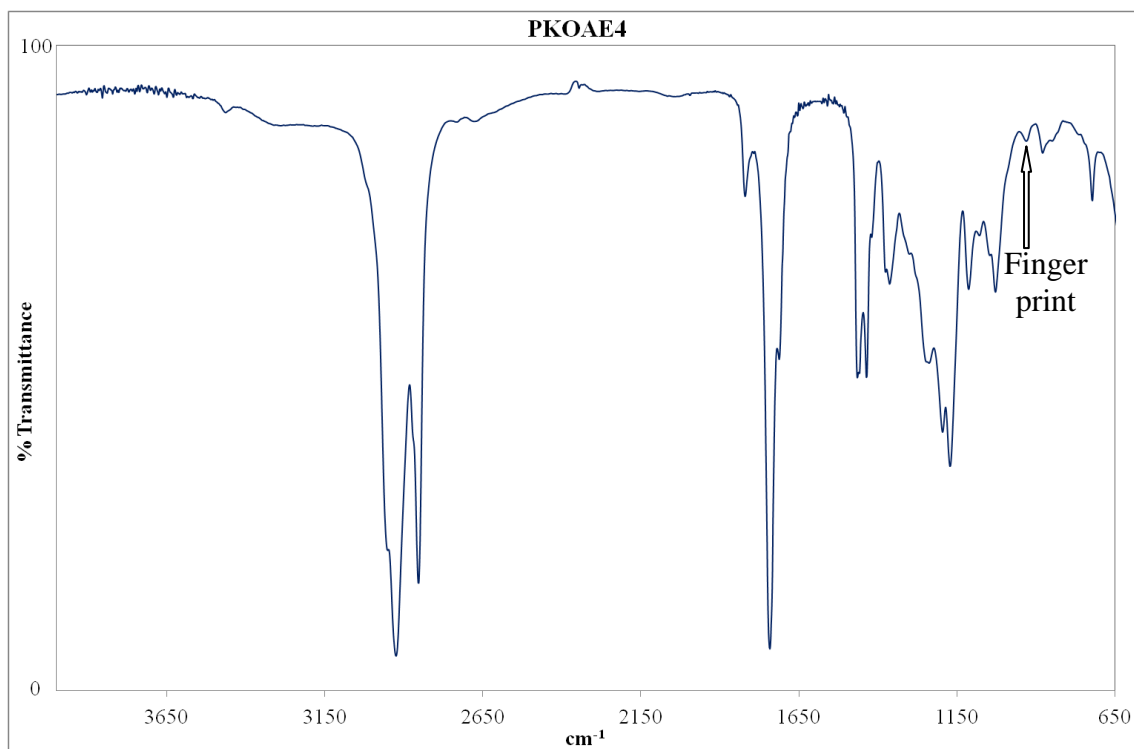


Fig F3: Mass FTIR Spectra of C4-Side Branched Alkyl Ester

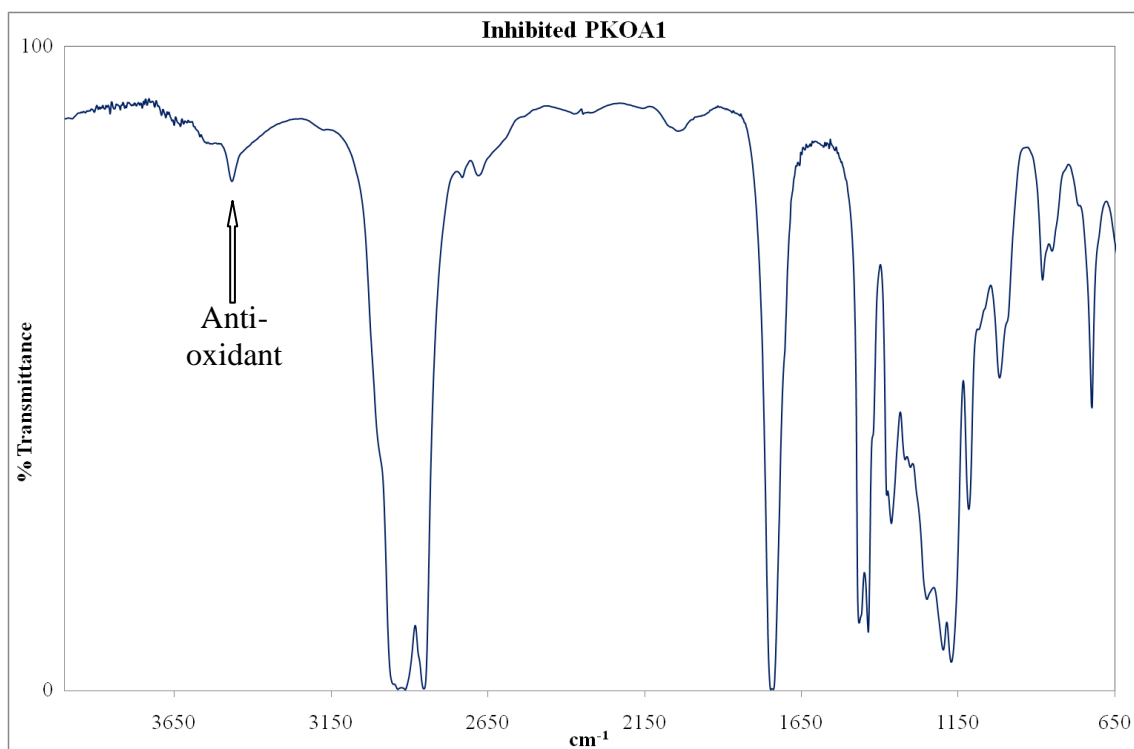


Fig F4: Mass FTIR Spectra of Inhibited Alkyl Ester

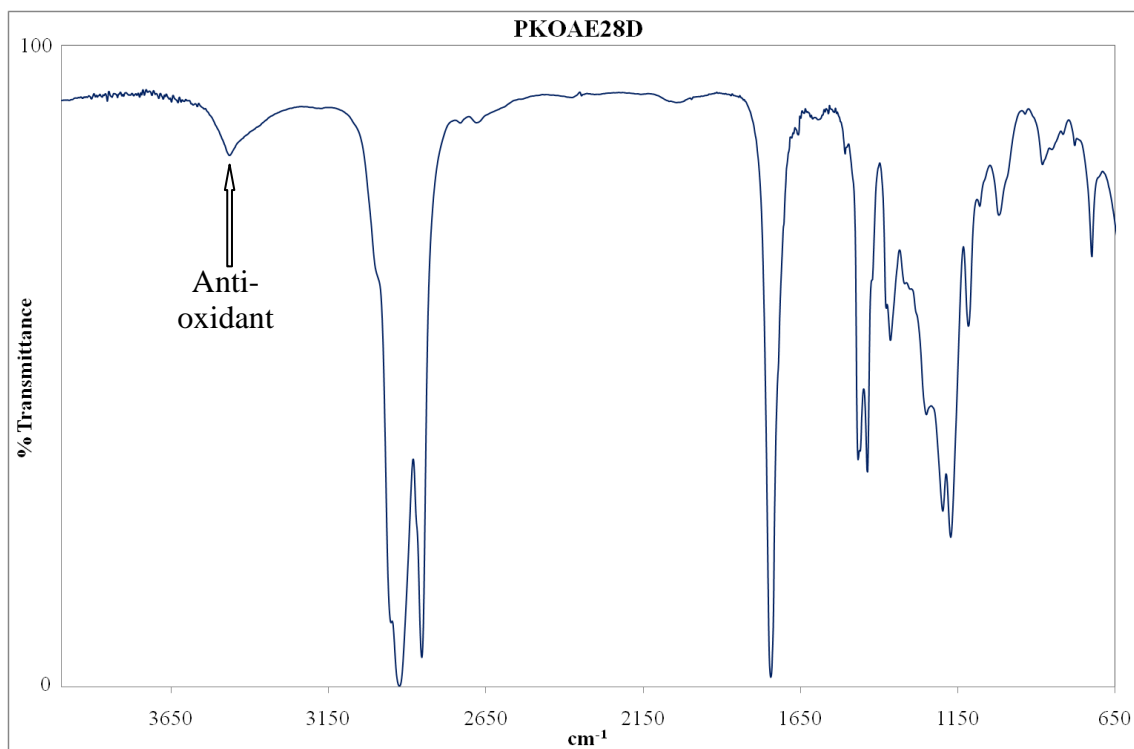


Fig F5: Mass FTIR Spectra of 28 days Aged Alkyl Ester

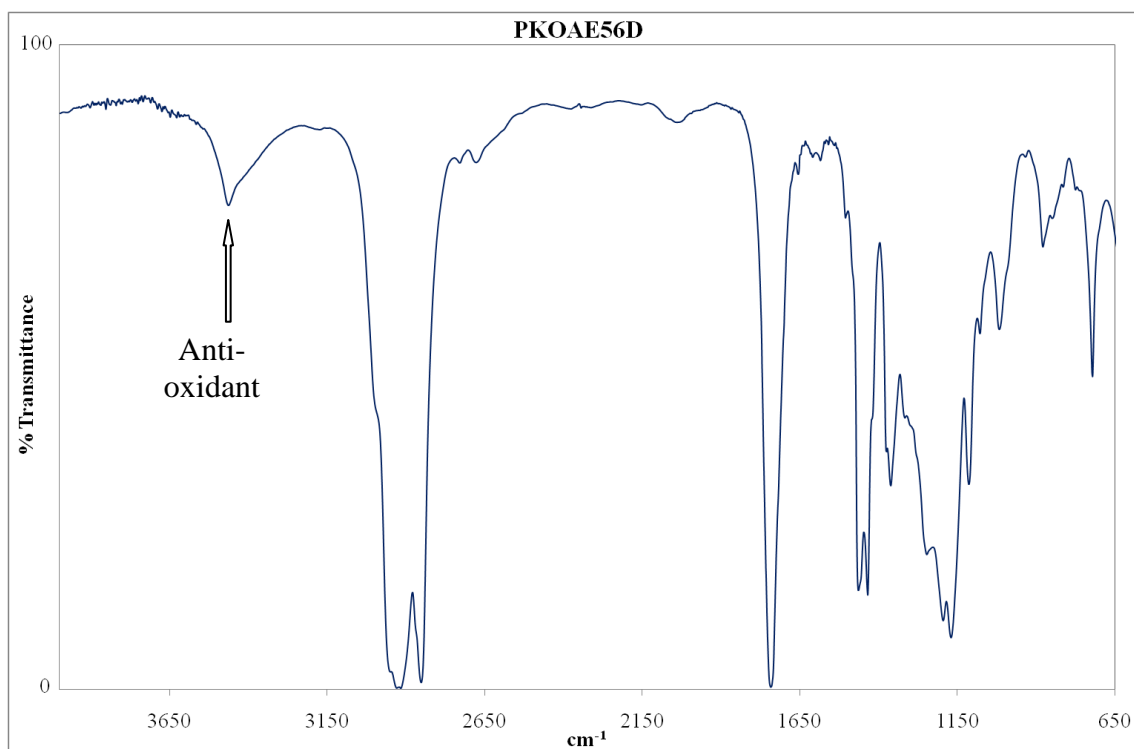


Fig F6: Mass FTIR Spectra of 56 days Aged Alkyl Ester

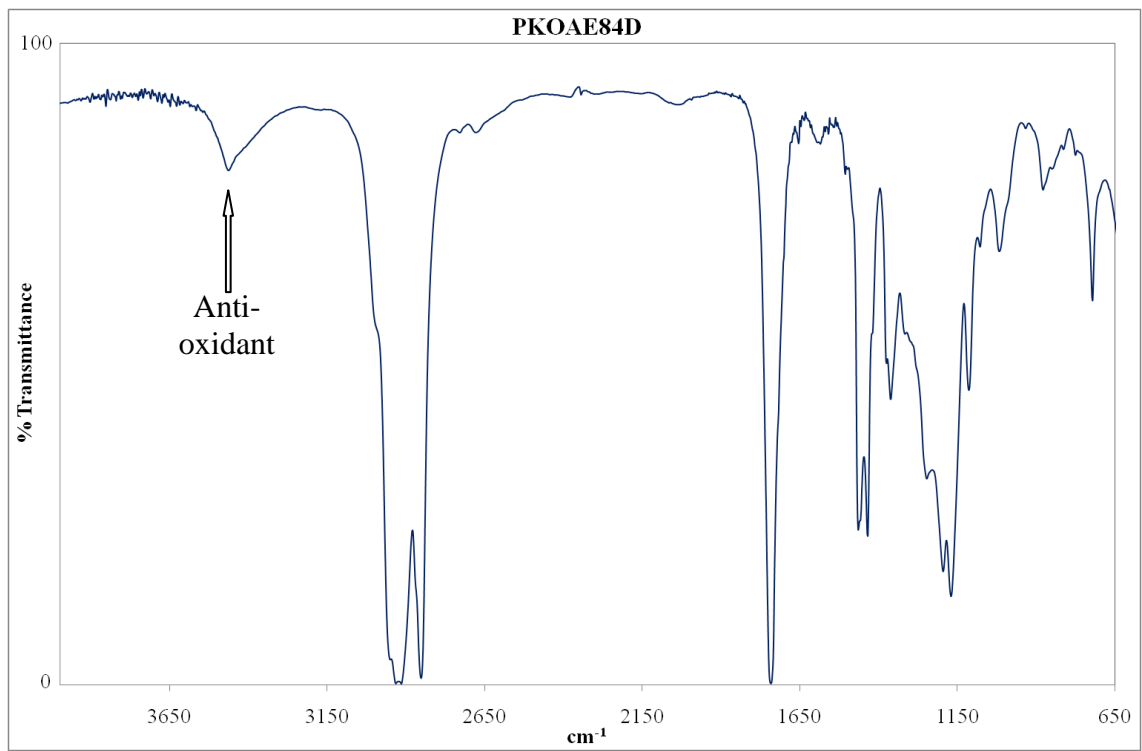


Fig F7: Mass FTIR Spectra of 84 days Aged Alkyl Ester

## Appendix G Dielectric Spectra of Paper Samples

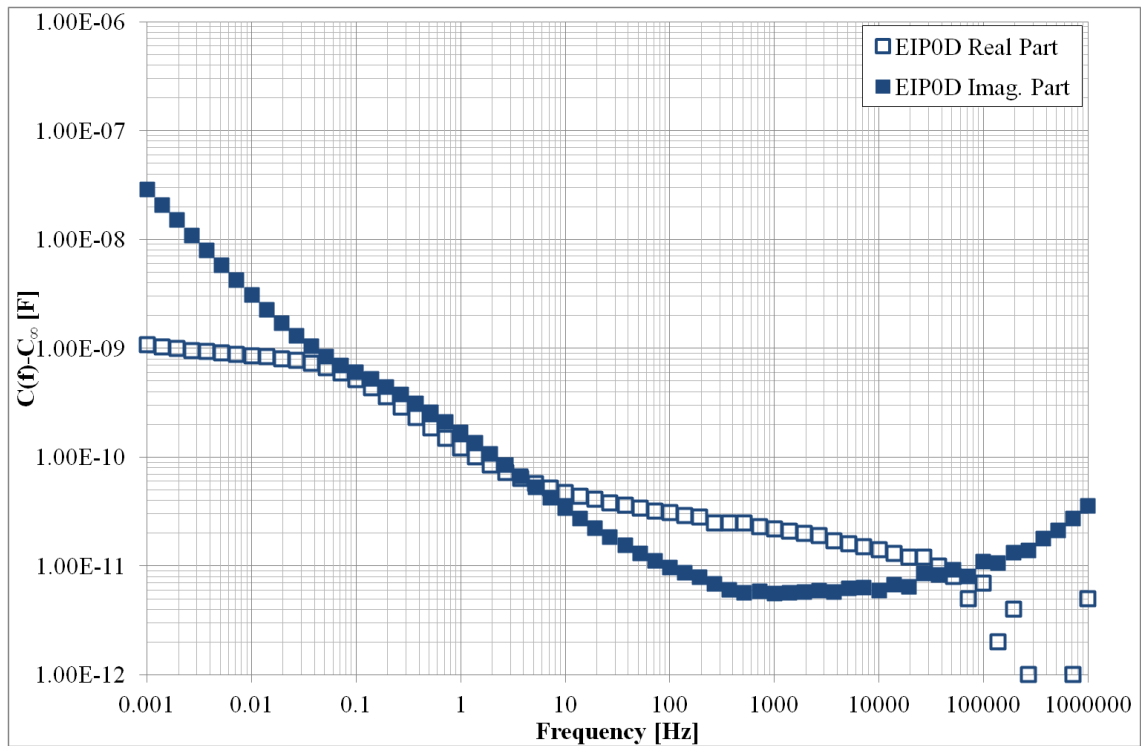


Fig G1: Plot of  $\{C(f) - C_{\infty}\}$  versus Frequency for Unaged Ester-Paper at  $20^{\circ}\text{C}$

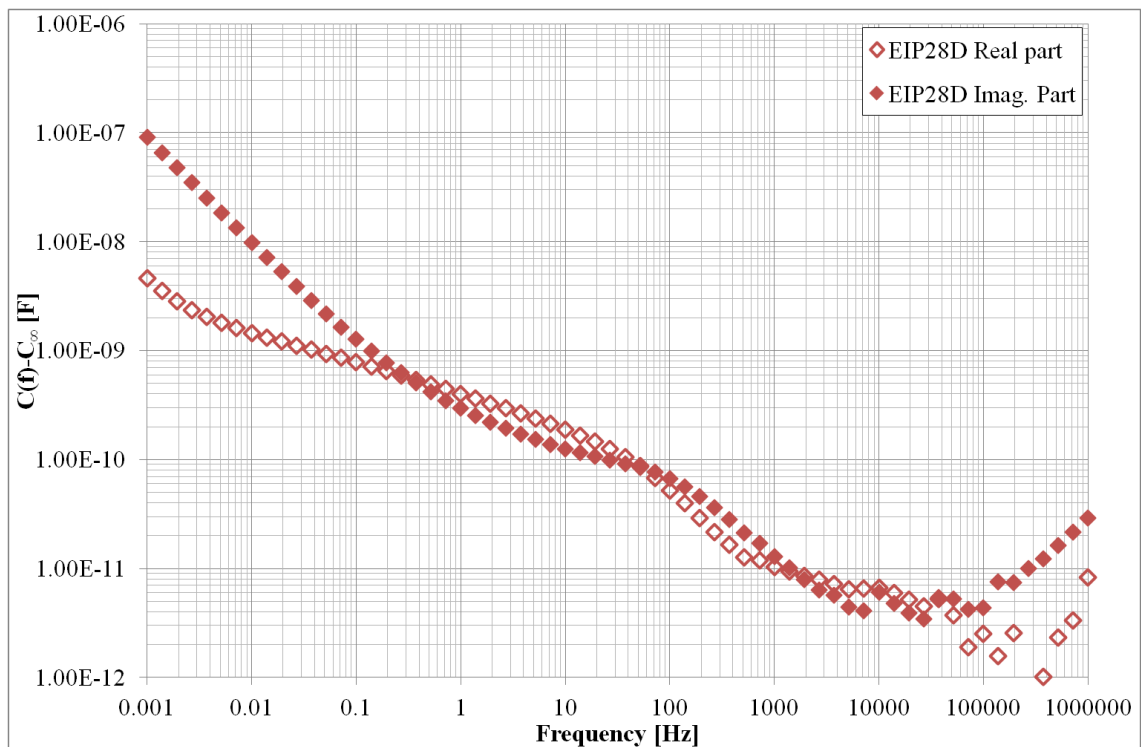


Fig G2: Plot of  $\{C(f) - C_{\infty}\}$  versus Frequency for 28 days Aged Ester-Paper at  $20^{\circ}\text{C}$

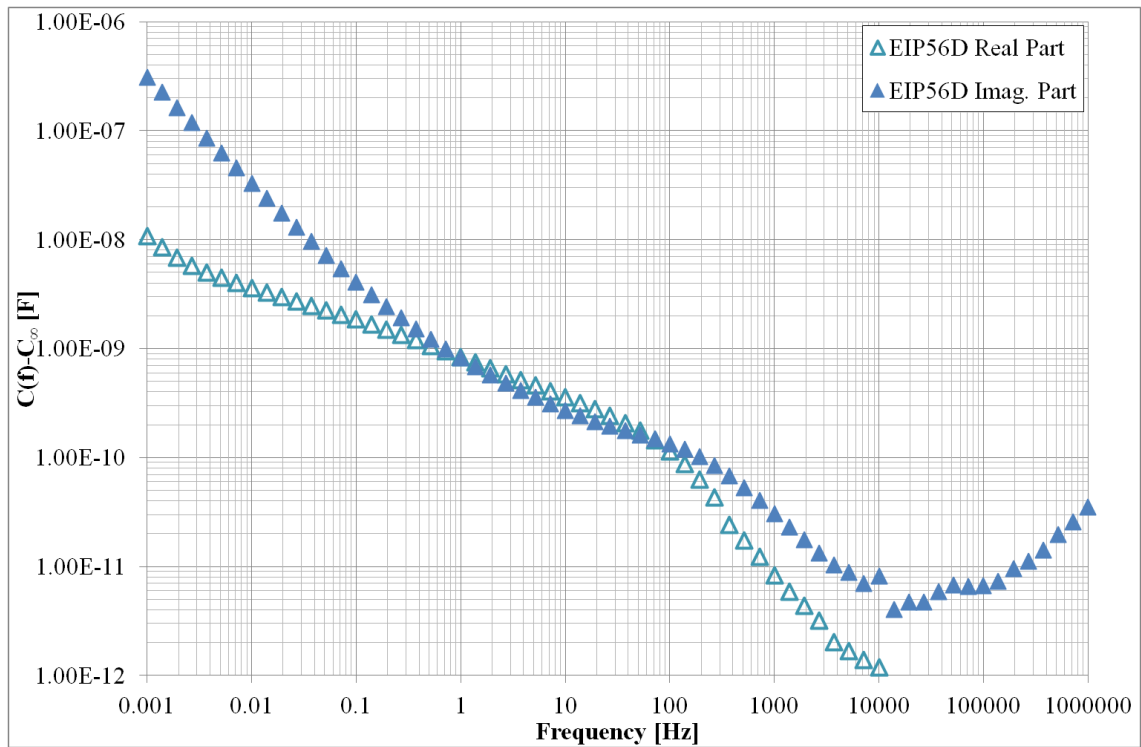


Fig G3: Plot of  $\{C(f)-C_\infty\}$  versus Frequency for 56 days Aged Ester-Paper at 20°C

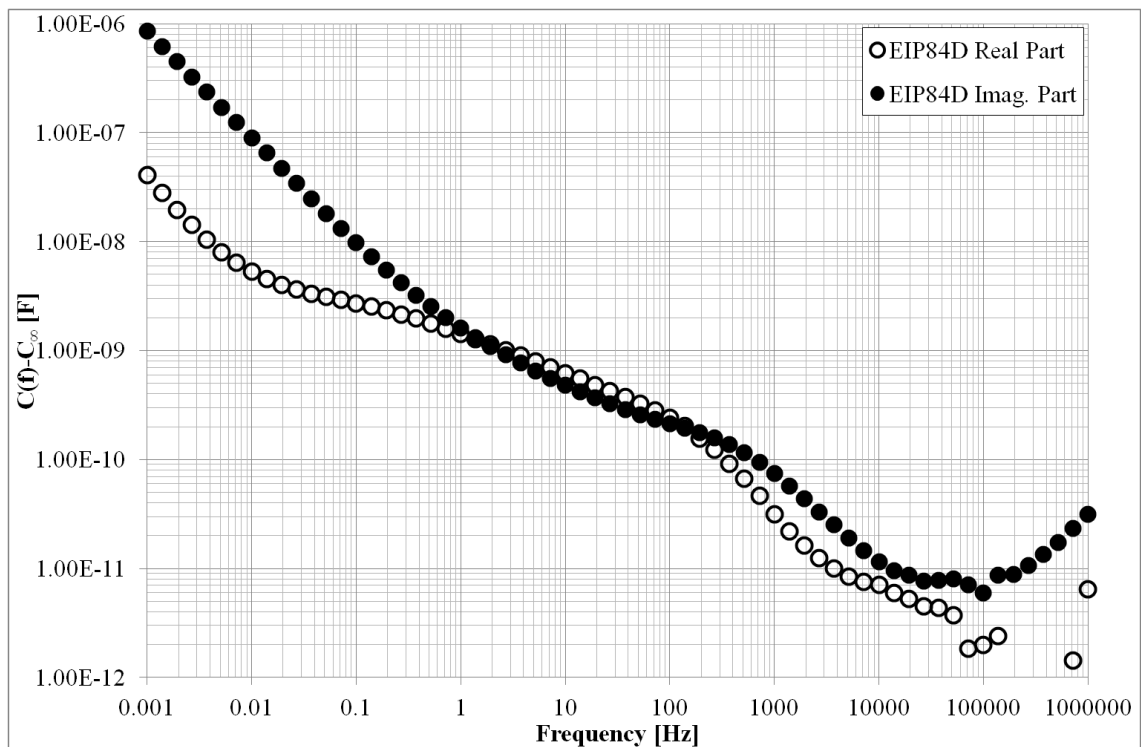
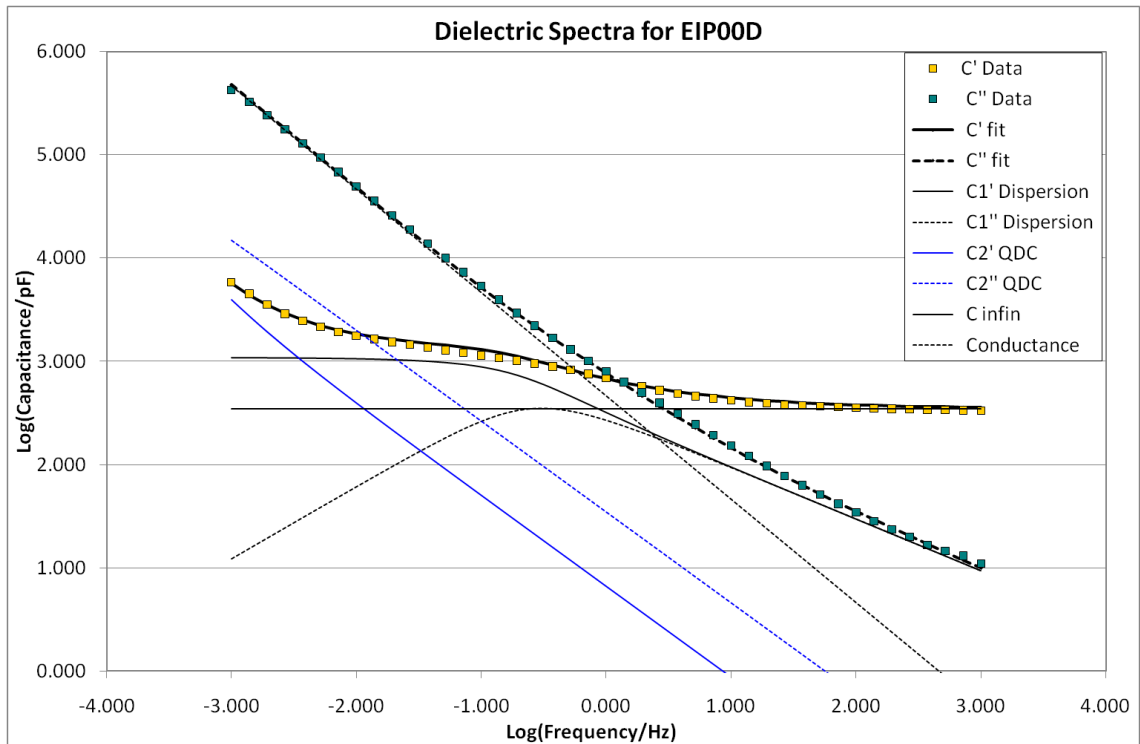
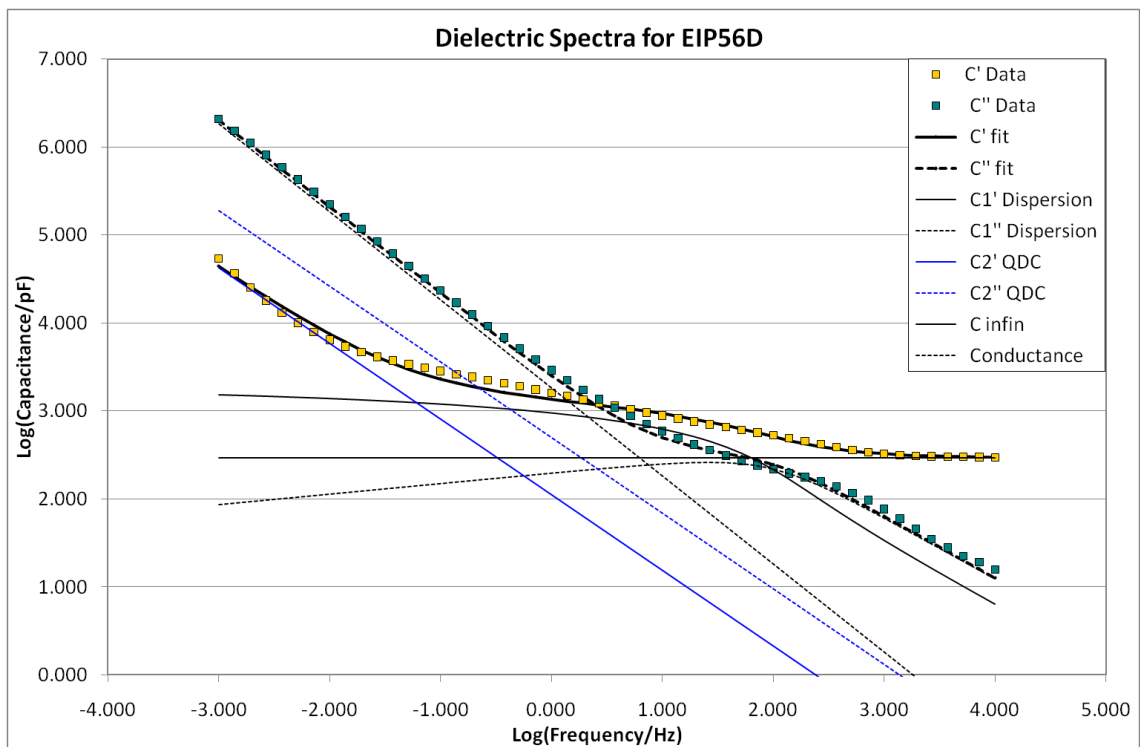


Fig G4: Plot of  $\{C(f)-C_\infty\}$  versus Frequency for 84 days Aged Ester-Paper at 20°C

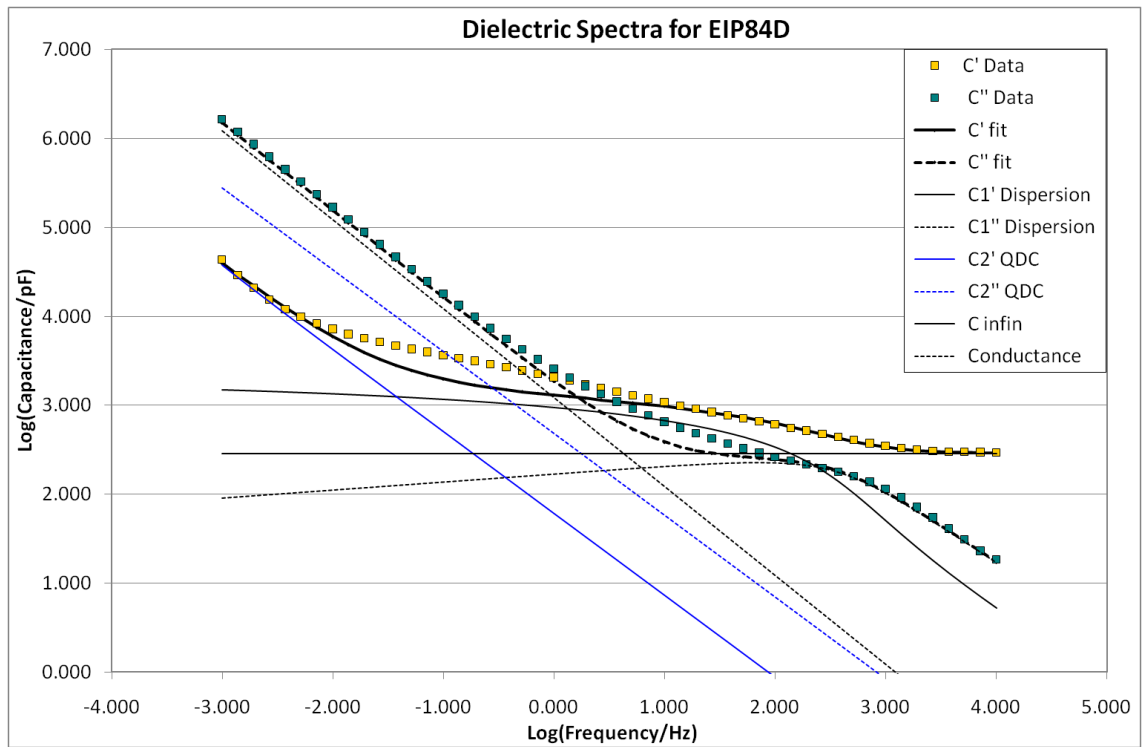
## Appendix H Equivalent Circuit fit for Ester-Paper



Appendix H1: Unaged Ester-paper



Appendix H2: 56 Days Aged Ester-paper



Appendix H3: 84 Days Aged Ester-paper

## Appendix I Publications

- 1: A.A. Abdelmalik, A.P. Abbott, J.C. Fothergill, S. Dodd & R.C. Harris, “Synthesis of a Base-Stock for Electrical Insulating Fluid based on Palm Kernel Oil”, *Industrial Crops and Products* 33 (2011) 532–536
- 2: A.A. Abdelmalik, J.C. Fothergill, S.J. Dodd, A.P. Abbott & R.C. Harris, Effect of Side Chains on the Dielectric Properties of Alkyl Esters Derived from Palm Kernel Oil, (2011) *Proceedings- IEEE International Conference on Dielectric Liquids*, Trondheim, Norway. 10.1109/ICDL.2011.6015413.
- 3: A.A. Abdelmalik, J.C. Fothergill, & S.J. Dodd, Electrical Breakdown Strength Characteristics of Palm kernel oil Ester-based Dielectric Fluids, (2011) Annual Report IEEE Conference on Electrical Insulation and Dielectric Phenomena, **1**, 183-186.
- 4: A.A. Abdelmalik, J.C. Fothergill, & S.J. Dodd, Electrical Properties of Ester Dielectric fluids from Palm kernel Oil, (2011) Annual Report IEEE Conference on Electrical Insulation and Dielectric Phenomena, **2**, 415-418.
- 5: A.A. Abdelmalik, J.C. Fothergill, & S.J. Dodd, Electrical Conduction and Dielectric Breakdown Characteristics of Alkyl Ester Dielectric Fluids obtained from Palm Kernel Oil, *IEEE Transactions on Dielectrics and Electrical Insulation* (under review)

## References

- [1] Abdullah U.U., S.M. Bashi, R.Y. Mohibullah, Hj. A. Nurdin, 2004. The Potential of Palm Oil as a Dielectric Fluid, *National Power & Energy Conference (PECon) 2004 Proceedings*, Kuala Lumpur, Malaysia.
- [2] Abeysundra D.C., C. Weerakoon, J.R. Lucas, K.A.I. Gunatunga and K.C. Obadage, 2001. Coconut Oil as an Alternative to Transformer Oil, *ERU Symposium*.
- [3] Amanullah M.D., S.M. Islam, S. Chami, G. Ienco, 2005. Analyses of Physical Characteristics of Vegetable Oils as an Alternative Source to Mineral Oil-based Dielectric Fluid, Proceedings of the 2005 *IEEE International Conference on Dielectric Liquids (ICDL 2005)*, 397-400.
- [4] Amanullah M.D., S. M. Islam, S. Chami, G. Ienco, 2005. Analyses of Electro-Chemical Characteristics of Vegetable Oils as an Alternative Source to Mineral Oil-based Dielectric Fluid, *Proceedings of the 2005 IEEE International Conference on Dielectric Liquids (ICDL 2005)* 365-368.
- [5] Ammawath W., Y.B. Che Man, B.S. Baharin and R.B. Abdul Rahman, 2004. A New Method for Determination of Tert Butylhydroquinone (TBHQ) in RBD Palm Olein with FTIR Spectroscopy, *Journal of Food Lipids* Vol. 11, 266-277.
- [6] Arora R., 1995. *High Voltage Insulation Engineering*, New Age International (P) Limited, Publishers, New Delhi.
- [7] Arulanandan K, J.K. Mitchell, 1968. Low Frequency Dielectric Dispersion of Clay-Water-Electrolyte Systems, *Clays and Clay Minerals*, Vol. 16, 337-351.
- [8] Bard A.J., L.R. Faulkner, 2001. *Electrochemical methods: fundamentals and applications*, 2nd ed., John Wiley & Sons, Inc.
- [9] Bartnikas, R., 1987. Alternating-Current Loss and Permittivity Measurements in *Engineering Dielectric*, Vol. IIB, Electrical Properties of Solid Materials: Measurement techniques, Bartnikas R. (Ed.), ASTM Publication, 52-123.
- [10] Bartnikas R., 1999. "Permittivity and Loss of Insulating Liquid" in *Engineering Dielectrics*, Vol. III, Electrical Insulating Liquids, Bartnikas R. (Ed.), ASTM Publication, 3-146.
- [11] Berberich L. J., 1954. "Dielectrics in Power and Distribution Equipments" in *Dielectric Materials and Applications*, Von Hippel A.R. (Ed.), The MIT Press, Massachusetts.
- [12] Bertrand Y., and L. C. Hoang, 2003. Vegetable Oils as Substitute for Mineral Oils, Proceedings of the 7<sup>th</sup> *International Conference on Properties and Applications of Dielectric Materials*, Nagoya, 491-494.
- [13] Binns D.F., K.T. Yoon, 1982. Comparison between Insulating Properties of transformer Oil and Low-flammability Ester Midel 1713, *IEE Proc.*, 129, Pt. A, **3**, 182-185.

- [14] Biochem & Science Notes. <http://biochem.co/2008/08/hybridisation-mixing-up-orbitals/> [04 March 2012].
- [15] Brett C.M.A. and A.M.O. Brett, 1993. *Electrochemistry: principles, methods, and applications*, Oxford University Press.
- [16] Bruice P.Y., 2003. *Organic Chemistry*, Fourth Edition, Prentice Hall.
- [17] Bulletin-B900-00092,  
<http://www.electricalmanuals.net/files/TRANSFORMERS/COOPER/OIL/Bullet-Bu-B900-00092.pdf> [12 March 2012]
- [18] Butcher M., A.A. Neuber, M.D. Cevallos, J.C. Dickens & H. Krompholz, 2006. Conduction and Breakdown Mechanisms in Transformer Oil, *IEEE Trans. on Plasma Science*, **34**, 467-475.
- [19] Carey F.A., 2000. *Organic Chemistry*, Fourth Edition, McGraw Hill Higher Education, Boston.
- [20] Cai C., H. Dai, R. Chen, C. Su, X. Xu, S Zhang, and L. Yang, 2008. Studies on the Kinetics of in situ Epoxidation of Vegetable Oils, *Eur. J. Lipid Sci. Technol.* **110**, 341–346.
- [21] Campanella A., C. Fontanini and M.A. Baltanas, 2008. High yield Epoxidation of Fatty Acid Methyl Esters with Performic Acid Generated in situ, *Chem. Eng. J.*, **144**, 466–475.
- [22] Chattopadhyay S., 2005. *Pressure Vessels: Design and Practice*, CRC Press.
- [23] Christie W.W., 2011. Mass Spectrometry of Fatty Acid Derivatives, *Lipid Library*, American Oil Chemists' Society. Available: [lipidlibrary.aocs.org](http://lipidlibrary.aocs.org) [26 Nov 2011]
- [24] Cloete J.H., J. van der Merwe, 1998. The Breakdown Electric Field Strength Between Two Conducting Spheres by the Method of Images, *IEEE Trans. on Education*, **41**, 141-145.
- [25] Dai J. and Z. D. Wang, 2008. A Comparison of the Impregnation of Cellulose Insulation by Ester and Mineral oil, *IEEE Transactions on Dielectrics and Electrical Insulation* **15**, 374 – 381.
- [26] Degeneff B.C, 2004. Power Transformers in *The Electrical Engineering Handbook*, Chen W. (Ed.), Elsevier Academic Press, 715-720.
- [27] Dervos C.T., C.D. Paraskevas, P. Skafidas, & P. Vassiliou, 2005. Dielectric Characterization of Power Oils as a Diagnostic life Prediction Method, *IEEE Insulation Magazine*, **21**, 11-19.
- [28] Dijkstra A. J. and M. V. Opstal, 1987. The Total Degumming Process, *Journal of American Oil chemists' Society*, **66**, 1002-1009.

- [29] Dissado L.A., J.C. Fothergill, 1992. *Electrical Degradation and Breakdown in Polymers*, IEE.
- [30] Dissado L.A. and R.M. Hill, 1983. A Cluster Approach to the Structure of Imperfect Materials and Their Relaxation Spectroscopy, *Proc. R. Soc. Lond. A*, **390**, 131-180, doi: 10.1098/rspa.1983.0125.
- [31] Dissado L.A. and R.M. Hill, 1984. Anomalous Low-frequency Dispersion, *J. Chem. Soc., Faraday Trans. 2*, **80**, 291-319.
- [32] Dunn R.O., 2005. Oxidative Stability of Soybean Oil Fatty Acid Methyl Esters by Oil Stability Index (OSI), *Journal of American Oil chemists' Society*, **82**, 381-387.
- [33] Dunn R.O., 2005. Effect of antioxidants on the oxidative stability of methyl soyate (biodiesel), *Fuel Processing Technology*, **86**, 1071-1085.
- [34] Duy C.T., O. Lesaint, N. Bonifaci, A. Denat, and Y. Bertrand, 2007. High Voltage Breakdown and Pre-Breakdown Properties in Rape-seed Insulating Oil, *Proceedings of the Annual Report Conference on Electrical Insulation and Dielectric Phenomena*, CEIDP.
- [35] Ekanayake C., 2006. Diagnosis of Moisture in Transformer Insulation, *PhD Thesis*, Chalmers University of Technology.
- [36] El-Refaie M.M.E., M.R. Salem, and W.A. Ahmed, 2009. Prediction of the Characteristics of Transformer Oil under Different Operation Conditions, *World Academy of Science, Engineering and Technology*, **53**, 764-768.
- [37] Erhan S. Z., T. Adhryu, and Z. Liu, 2002. Chemically Modified Vegetable Oil-based Industrial Fluid, *United States Patent* 6,583,302 B1.
- [38] Fofana I., H. Hemmatjou1, F. Meghnefi, M. Farzaneh, A. Setayeshmehr, H. Borsi, E. Gockenbach, 2010. On the Frequency Domain Dielectric Response of Oil-paper Insulation at Low Temperatures, *IEEE Transactions on Dielectrics and Electrical Insulation*, **17**, 799-807.
- [39] Fofana I., V. Wasserberg, H. Borsi and E. Gockenbach, 2001. Retrofilling Condition of HV transformers, *IEEE Electrical Insulation Magazine*, **17**, 17-30.
- [40] Forster E.O., 1999. "Electrical Breakdown in Dielectric Liquid" in *Engineering Dielectrics*, Vol. III, Electrical Insulating Liquids, Bartnikas R. (Ed.), 262-309, ASTM Publication.
- [41] Foubert, K. Dewettinck, D. Van de Walle, A. J. Dijkstra & P. J. Quinn, 2007. Physical Properties: Structural and physical Characteristics, in: *The Lipid Handbook*, F.D. Gunstone, J.L. Harwood, A. J. Dijkstra (Ed.), 3rd Edition, CRC Press, 471-534.
- [42] Frimpong G.K., T. V. Oommen, R. Asano, 2011. A Survey of Aging Characteristics of Cellulose Insulation in Natural Ester and Mineral Oil, *IEEE Electrical Insulation Magazine*, **27**, 36-48.

- [43] Goud V. V., A. V. Patwardhan, and N. C. Pradhan, 2006, Epoxidation of Mahua Oil (*Madhumica indica*) by Hydrogen Peroxide, *Biores. Tech.* **97**, 1365-1371.
- [44] Goud V.V., A.V. Patwardhan, and N.C. Pradhan, 2007. Kinetics of in situ Epoxidation of natural Unsaturated Triglycerides catalysed by Acidic Ion Exchange Resin, *Ind. Eng. Chem. Res.* **46**, 3078-3085.
- [45] Goud V. V., A. V. Patwardhan, S. Dinda and N. C. Pradhan, 2007. Epoxidation of Karanja (*Pongamia globra*) oil catalysed by acidic exchange resin, *Eur. J. Lipid Sci. Technol.* **109**, 575-584.
- [46] Gunstone F.D., J. Alander, S. Z. Erhan, B. K. Sharma, T.A. McKeon and J.T. Lin, 2007. "Nonfood Uses of Oils and Fats" in *The Lipid Handbook*, F.D. Gunstone, J.L. Harwood, A. J. Dijkstra (Ed.), 3rd Edition, CRC Press, 591-635.
- [47] Gunstone F.D., 2011. Oils and Fats in the Market Place; Commodity Oils and Fats - Palmkernel and Coconut (Lauric) Oils, *Lipid Library*, American Oil Chemists' Society. Available: lipidlibrary.aocs.org [26 Dec 2011].
- [48] Hameed S.F. and M.A. Allam, 2006. Application of FTIR Spectroscopy in the Determination of Antioxidant Efficiency in Sunflower Oil, *Journal of Applied Sciences Research*, **2**, 27-33.
- [49] Hao J., R. Liao, G. Chen and C. Ma, 2011. Influence of Copper on the By-Products of Different Oil-Paper Insulations, *Journal of Physics: Conference Series* **310** 012007 doi:10.1088/1742-6596/310/1/012007.
- [50] Heathcote, M. J., 2007. *J & P Transformer BookBook: A Practical technology of the Power transformer*, Newnes.
- [51] Hill D.J., T.T. Le, M. Darvenizab & T. Sahab, 1996. A study of the degradation of cellulosic insulation materials in a power transformer. Part III: Degradation products of cellulose insulation paper, *Polymer Degradation and Stability*, **51**, 211-218.
- [52] Hinton A.J., B. Sayers, 1998. *Beyond the Limits: 1296 Dielectric Interface*, Solartron, Hampshire.
- [53] Hinz H.J. and F. P. Schwarz, 2001. IUPAC, *Pure and Applied Chemistry* **73**, 745-759.
- [54] Holser R.A., 2008. Transesterification of Epoxidized Soybean to Prepare Epoxy Methyl Esters, *Ind. Crop. Prod.* **27**, 130-132.
- [55] Hwang H.S. and S.Z. Erhan, 2001, Modification of Epoxidized Soybean Oil for Lubricant Formulation with Improved Oxidative Stability and Low Pour point, *J. American Oil Chem. Soc.*, **78**, 1179-1184.
- [56] IEEE Std 930-2004, 2005. *IEEE Guide for the Statistical Analysis of Electrical Insulation Breakdown Data*, IEEE.

- [57] IEEE Std C57.147-2008, 2008. *IEEE Guide for Acceptance and Maintenance of Natural Ester Fluids in Transformers*, IEEE.
- [58] Ikhuoria E. U., R. O. Obuleke, & F. E. Okieimen, 2007. Studies on the Kinetics of Epoxidation of the Methyl Esters of Perkoa Biglobosa Seed Oil, *Pure App. Chem. Part A*, **44**, 235–238.
- [59] Incropera F.P., D.P. Dewitt, T.L. Bergman, A.S. Lavine, 2007. *Fundamental of Heat and Mass Transfer*, 6th Edition, John Wiley and Sons.
- [60] International Monetary Fund, IMF Primary Commodity Prices, 2012. Available: <http://www.imf.org/external/np/res/commod/index.aspx> [27 Jan 2012]
- [61] Iskender I, A. Mamizadeh, 2011. An improved nonlinear thermal model for MV/LV prefabricated oil-immersed power transformer substations, *Electr Eng*, **93**, 9-22.
- [62] IUPAC. Compendium of Chemical Terminology, 2nd ed. (the "Gold Book"). Compiled by A. D. McNaught and A. Wilkinson. Blackwell Scientific Publications, Oxford (1997).
- [63] James Walker, 2006. 'O' Rings, James Walker Co. Ltd.
- [64] Jayadasa N.H., and K. Prabhakaran Nairb, 2006. Coconut oil as base oil for industrial lubricants-evaluation and modification of thermal, oxidative and low temperature properties, *Tribology International*, **39**, 873–878.
- [65] Jian Li, S. Grzybowski, Y. Sun, and X. Chen, 2007. Dielectric Properties of Rapeseed Oil Paper Insulation, *Proceedings of the Annual Report Conference on Electrical Insulation and Dielectric Phenomena*, IEEE CEIDP.
- [66] Joanes D.N. and C.A. Gill, 1998. Comparing Measures of Sample Skewness and Kurtosis, *The Statistician*, 47, Part 1, 183-189.
- [67] Jonscher A.K., 1983. *Dielectric relaxation in solids*, Chelsea Dielectric Press, London.
- [68] Jonscher A.K., 1990. The "Universal" Dielectric Response: Part II, *IEEE Electrical Insulation Magazine*, **6**, 24-28.
- [69] Jonscher A.K., 1996. *Universal Relaxation Law*, Chelsea Dielectric Press Ltd, London.
- [70] Kanoh T., H. Iwabuchi, Y. Hoshida, J. Yamada, T. Hikosaka, A. Yamazaki, Y. Hatta, H. Koide, 2008. Analyses of Electro-chemical Characteristics of Palm Acid Esters as Insulating Oil, *Proceedings of the International Conference on Dielectric Liquid*, IEEE ICDL.
- [71] Kitson F.G., B.S. Larsen, C.N. McEwen, 1996. *Gas Chromatography and Mass Spectrometry; A Practical Guide*, Academic Press, San Diego.

- [72] Kuffel E., W.S. Zaengl, J.Kuffel, 2000. *High Voltage Engineering; Fundamentals*, Newnes, 390-391.
- [73] Liu Q. and Z. D. Wang, 2011. Streamer Characteristic and Breakdown in Synthetic and Natural Ester Transformer Liquids under Standard Lightning Impulse Voltage, *IEEE Transactions on Dielectrics and Electrical Insulation* **18**, 285-294.
- [74] Lusas E. W., 2007. "Animal and Vegetable Fats, Oils, and Waxes" in *Kent and Riegel's Handbook of Industrial Chemistry and Biotechnology*, Kent J.A., (Ed.) 11<sup>th</sup> Edition, Springer, 1546-1569.
- [75] Martin D., Z.D. Wang, P. Dyer, A.W. Darwin, I.R. James, 2007. A Comparative Study of the Dielectric Strength of Ester Impregnated Cellulose for Use in Large Power Transformers, 2007 *International Conference on Solid Dielectrics*. IEEE ICSD.
- [76] Martin D. and Z.D. Wang, 2008. Statistical Analysis of the AC Breakdown Voltages of Ester Based Transformer Oils, *IEEE Transactions on Dielectrics and Electrical Insulation*, **15**, 1044-1050.
- [77] Massey B., Ward-Smith J., 2006. *Mechanics of Fluids*, 8th Edition, Taylor and Francis.
- [78] McNutt W.J., 1992. Insulation Thermal Life Considerations for Transformer Loading Guides, *IEEE Transactions on Power Delivery*, **7**, 392-401.
- [79] McMurry J., 2000. *Organic Chemistry*, Brooks/Cole, USA.
- [80] McShane C. P., 2001. Relative Properties of the New Combustion-Resistant Vegetable-Oil-Based Dielectric Coolants for Distribution and Power Transformers, *IEEE Transaction on Industry Applications*, **37**, 1132-1139.
- [81] McShane C.P., K.J. Rapp, J.L. Corkran, G.A. Gauger, J. Luksich, 2001. Aging of Paper Insulation in Natural Ester Dielectric Fluid, 2001 *IEEE/PES Transmission & Distribution Conference & Exposition*.
- [82] McShane C. P., K. J. Rapp, J. L. Corkran, G. A. Gauger, J. Luksich, 2002. Aging of Kraft Paper in Natural Ester Dielectric Fluid, *Proceedings of the 14<sup>th</sup> International Conference on Dielectric Liquids (ICDL 2002)*, Graz, Austria, 173-177.
- [83] McShane C.P., 2002. Vegetable-Oil-Based Dielectric Coolants, *IEEE Industry Applications magazine*, **8**, 34-41.
- [84] Money W. M., 2005. Development of a High Dielectric Constant Insulating Oil, *Proceedings of the IEEE International Pulse Power Conference*, 114-1142.
- [85] Moser B.R., 2009. Comparative Oxidative Stability of Fatty Acid Alkyl Esters by Accelerated Methods, *J. Am Oil Chem Soc.*, **86**, 699–706.

- [86] Moser B.R., B.K. Sharma, K. M. Doll, S. Z. Erhan, 2007. Diester from Oleic Acid: Synthesis, Low Temperature Properties, and oxidation Stability, *J. America Oil Chem. Soc.*, **84**, 675-680.
- [87] Mungroo R., N.C. Pradhan, V.V. Goud & A.K. Dalai, 2008. Epoxidation of Canola Oil with Hydrogen Peroxide Catalysed by Acidic Ion Exchange Resin, *J. America Oil Chem. Soc.*, **85**, 887–896.
- [88] Nynas, 2010. *Transformer Oil Handbook*, Nynas AB, Sweden.
- [89] Oommen T.V., 2002. Vegetable Oil for Liquid-Filled Transformers, *IEEE Electrical Insulation Magazine*, **18**, 6-11.
- [90] Oommen T. V., C.C. Clairborne, E. J. Walsh, J. P. Baker, 2000. A New Vegetable Oil Based Transformer Fluid; Development and Verification, *Proceedings of the 2000 IEEE Conference on Electrical Insulation and Dielectric Phenomena*, 308-313.
- [91] Oommen T.V., T.A. Prevost, 2006. Cellulose Insulation in Oil-Filled Power Transformers: Part II – Maintaining Insulation Integrity and Life, *IEEE Electrical Insulation Magazine*, **22**, 5-14.
- [92] O’Brien R. D., 2004. *Fats and oils: formulating and processing for applications*, CRC Press.
- [93] Obi A.L., S.A. Jonah, I. Umar, 2001. Determination of Trace Elements in Some Nigerian Vegetable Base Oils by Neutron Activation Analysis, *Journal of Radioanalytical and Nuclear Chemistry*, **249**, 669-671.
- [94] Park S.J., F.L. Jin and J.R. Lee, 2004. Synthesis and Thermal Properties of Epoxidized Vegetable Oil, *Macromol. Rapid Comm.* **25**, 724–727.
- [95] Pearmain A.J. and H. Haddad, 2003. “Insulation” in *Electrical Engineering Reference Book*, Laughton D.F., and D.F. Warne (Ed.), Sixteenth Edition, Elsevier Science, 7/1 – 7/36.
- [96] Raju G.G., 2003. *Dielectrics in Electric Fields*, Marcel Dekker, Inc.
- [97] Rapp K.J., C.P. McShane, and J. Luksich, 2005. Interaction Mechanisms of Natural Ester Dielectric Fluid and Kraft Paper, *Proceedings of 15th IEEE International Conference on Dielectric Liquids (ICDL)*, Coimbra (Portugal).
- [98] Raw Materials Research and Development Council (RMRDC), 2004. *Report on Survey of Agro Raw Materials in Nigeria on Oil Palm*, Abuja, Nigeria.
- [99] Ryu K., 2009, Effect of antioxidants on the oxidative stability and combustion characteristics of biodiesel fuels in an indirect-injection (IDI) diesel engine, *Journal of Mechanical Science and Technology*, **23**, 3105-3113.
- [100] Saito H., H. Okubo, K. Kato, H. Kojima, N. Hayakawa, K. Kawanishi, H. Koide, 2011. Charge Behavior in Palm Fatty Acid Ester Oil (PFAE) / Pressboard Composite

- Insulation System with Charged Oil Flow, *2011 IEEE International Conference on Dielectric Liquids*, Trondheim, Norway. DOI: 10.1109/ICDL.2011.6015445.
- [101] Sarin A., R. Arora, N.P. Singh, R. Sarin, and R.K. Malhotra, 2010. Oxidation Stability of Palm Methyl Ester: Effect of Metal Contaminants and Antioxidants, *Energy Fuels*, **24**, 2652–2656.
- [102] Shablakh, M., L. A. Dissado and R. M. Hill, 1984. Nonconductive Long-Range Charge in Hydrated Biopolymers, *Journal of Biological Physics*, **12**, 63-78.
- [103] Sharma B.K., A. Adhvaryu, Z. Liu, and S. Erhan, 2006. Chemical Modification of Vegetable oils for Lubricant Applications, *J. Am. Oil Chem. Soc.*, **83**, 129-136.
- [104] Sharma B.K., Z. Liu, A. Adhvaryu, and S.Z. Erhan, 2008. One-Pot Synthesis of Chemically Modified Vegetable Oils, *J. Ag. Food Chem.*, **56**, 3049-3056.
- [105] Schmidt W.F., 1994. Conduction Mechanism in Liquids in Engineering Dielectric, Vol. III, *Electrical Insulating Liquids*, Bartnikas R., (Ed.), 147-260, ASTM Publication.
- [106] Shroff D.H., 1985. A review of paper aging in power transformers, *IEE proceedings*, **132**, Pt. C.
- [107] Silverstein R.M., F.X. Webster & D.J. Kiemle, 2005. *Spectrometric Identification of organic Compounds*, John Wiley & Sons Inc.
- [108] Simon P., and J. Cvengros, 2010. Thermooxidative stability of vegetable oils refined by steam vacuum distillation and by molecular distillation, *Eur. J. Lipid Sci. Technol.*, **112**, 1236–1240.
- [109] Stachowiak G.W., A.W. Batchelor, 2001. *Engineering Tribology*, Butterworth Heinemann.
- [110] Stockton D. P., J. R. Bland, JR., T. McClanahan, J. Wilson, D. L. Harris, and P. McShane, 2009. Seed-Oil-Based Coolants for Transformers, *IEEE Industry Applications Magazine*, 68-74.
- [111] Suwarmo, F.S, I. Suhariadi, L. Imsak, 2003. Study on the Characteristics of Palm Oil and its Derivatives, *Proceedings of the 7<sup>th</sup> International Conference on Properties and Applications of Dielectric Materials*, Nagoya, 495-498.
- [112] Suzuki T., R. Oba, A. Kanetani, T. Kano, T. Tamura, M. Kato, S. Watanabe, Y. Kasahara, M. Iwahashi, 2011. Consideration on the Relationship between Dielectric Breakdown Voltage and Water Content in Fatty Acid Esters, *IEEE International Conference on Dielectric Liquids*, Trondheim, Norway. DOI: 10.1109/ICDL.2011.6015424.
- [113] Tenbohlen S., D. Vukovic, J. Harthun, S. Barker and R. Frotscher, 2008. Application of vegetable oil-based insulating fluids to hermetically sealed power transformers, *Cigre session*, paper A2-102.

- [114] The World Bank, 2012. Commodity Prices, Available <http://data.worldbank.org/data-catalog/commodity-price-data> [27 Jan 2012]
- [115] Thomas P., S. Sridhar, K.R. Krishnaswamy, 1995. Dielectric Liquid from Vegetable Origin-Indian Beech Oil, *International Symposium on Electrical Insulating Materials Proceedings*, Tokyo, Japan, 507-510.
- [116] Tobazeon R., J.C. Filippini and C. Marteau, 1994. On the Measurement of the Conductivity of Highly Insulating Liquids, *IEEE Transactions on Dielectrics and Electrical Insulation* **1**, 1000-1004.
- [117] Umemura T., K. Akiyama, T. Kawasaki & T. Kashiwazaki, 1982. Electrical conduction in synthetic insulating liquid, *IEEE Trans. on Electrical Insulation*, **EI-17**, 533-538.
- [118] Vassilikou-Dova A. & I.M. Kalogeras, 2009. Dielectric Analysis in *Thermal Analysis of Polymers, Fundamental and Application*, Menczel J. D. & R. Bruce Prime, John Wiley and Sons, New Jersey.
- [119] Von Hippel A.R., 1954. Theory in *Dielectric Materials and Applications*, Von Hippel A. R., (Ed.), The MIT Press, Massachusetts, 3-46.
- [120] Wasserberg V., B. Dolata , H. Borsi, E. Gockenbach, H. Baehr; 2005. Ecological Friendly Alternative to Mineral Based Transformer Oils with Superior Properties, *Proceedings of the XIVth International Symposium on High Voltage Engineering*, Tsinghua University, Beijing, China.
- [121] Wadhwa C.L., 2007. *High Voltage Engineering*, Second Edition, New Age International (P) Ltd., Publishers.
- [122] Walpole R.E., R.H. Myers, S.L. Myers, K. Ye, 2007. *Probability & Statistics for Engineers & Scientists*, 8th Edition, Pearson Education, Inc., Pearson Prentice Hall.
- [123] Weidmann, Electrical Technology, 2011. Paper, Wicor Holding AG. Available: <http://www.weidmann-electrical.com/en/markets-a-products/paper/cellulose-based/presspaper-in-reels>. [25 Jan 2012].
- [124] WLP, 2011. Soybean Based Transformer Oil, Waverly Light and Power, Soybean Based Transformer Oil at Waverly Light and Power, 1002 Adam Parkway, Waverly, Iowa, U.S.A. Available: <http://wlp.waverlyia.com/environment/soybean-based-transformer-oil.aspx>. [30 Oct 2011].
- [125] Wohlfarth, Ch., 2008. Dielectric constant of 1,1,2-trichloroethene. Lechner, M.D. (ed.). *SpringerMaterials - The Landolt-Börnstein Database* (<http://www.springermaterials.com>). Springer-Verlag Berlin Heidelberg. DOI: 10.1007/978-3-540-75506-7\_41
- [126] Zaengl W.S., 2003. Dielectric Spectroscopy in Time and Frequency Domain for HV Power Equipment, Part I: Theoretical Considerations, *IEEE Electrical Insulation Magazine*, **19**, 5-19.

